THE APPLICATION OF GEOPHYSICS TO NICKEL LATERITE RESOURCE EVALUATION

Jan C. Francké, BSc., P.Geoph.

A thesis submitted in partial fulfilment of the requirements for the degree of

Master of Science in Engineering Geology

University of Canterbury

Christchurch, New Zealand

2000

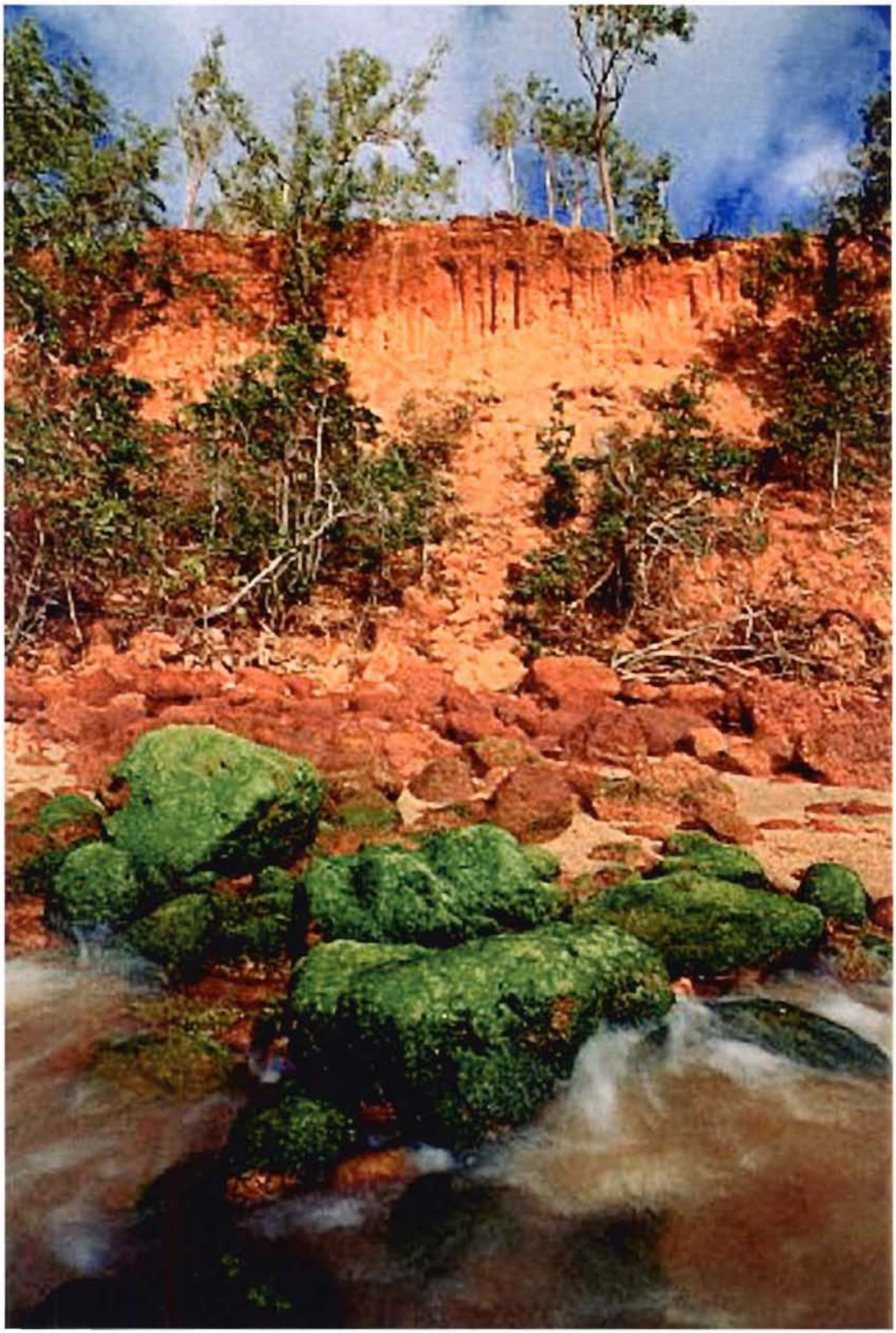

Laterite profile at Gunner's Quoin, Gurig National Park, Northern Territory, Australia.

ABSTRACT

THE APPLICATION OF GEOPHYSICS TO NICKEL LATERITE RESOURCE EVALUATION

With the dramatic growth of interest in nickel laterite resource exploitation, fueled by increasing demand and new processing technologies, the need for accurate resource delineation and careful mine planning becomes paramount. The traditional use of borehole grids to calculate mineral resources has proven to be neither sufficiently accurate nor cost-effective at many sites due to the complexity of tropical weathering profiles. Although an unconventional approach to laterite mine planning and resource delineation, emerging near-surface geophysical methods, particularly ground penetrating radar (GPR), hold tremendous potential for addressing project geology, resource delineation, and mine planning issues.

GPR acquisition and processing techniques have been developed specifically for laterite applications and have been successfully utilized in the field. Preliminary test work has been performed at varied sites in Papua New Guinea, Indonesia, Venezuela, Guatemala, the Philippines, and Brazil. Two projects in New Caledonia were selected as comprehensive test sites for experimentation with GPR. Test surveys with GPR were performed at these sites to determine the effectiveness of the method in mapping the lateritic weathering profile. A description of the geology of various humid laterite deposits and the geophysical consequences of their complex nature is discussed, as well as the correlation of the acquired geophysical data to geological borehole information.

Geophysics in general, and GPR in specific, has been proven to increase the database of knowledge with respect to project geology, as well as provide invaluable assistance in mine planning by high resolution imaging of the bedrock depth and texture as well as the accurate location of subsurface pinnacle structures at many sites.

TABLE OF CONTENTS

LIST OF FIGURES

LIST OF PLATES

1 INTRODUCTION

1.1 Sources of Nickel

Nickel is one of the more common elements in the composition of the earth, but it is sparingly distributed in the earth's crust. The current world demand for nickel is growing at a rate that surpasses that of most other base metals. Nickel is currently used chiefly in the form of alloys, by imparting great strength and corrosion resistance to carbon steel. Common uses of nickel steel, which contains 2% to 4% nickel, are automobile parts, household appliances, aviation, and most machined products. The nickel coins used for currency are an alloy of 25% nickel and 75% copper. Nickel is also a key component of nickel-cadmium batteries, as well as the nickel-metal-hydride batteries, which are increasing in popularity. Powdered nickel absorbs 17 times its own volume of hydrogen and is used as a catalyst in many processes, including the hydrogenation of oils.

Today nickel is mined from either sulphides or laterites. Sulphide base metal ores, which account for only approximately 30% of the world's nickel reserves, are typically found at depths of hundreds of metres in highly structured, hard rock geological environments (Osborne, 1996). Nickel bearing sulphides deposits which are economic to mine occur in grades of 1.5% or more, often in combination with cobalt, and usually with copper, gold and platinum group metals.

Nickel laterites are residual products derived from chemical weathering of olivine-rich cumulate rocks and their metamorphic derivatives, which have primary initial nickel contents of 0.2% to 0.4%. The process of lateritisation can increase the nickel concentration to over 1.5%.

Although approximately two-thirds of the world's known nickel reserves are found in the form of laterites, the overwhelming source of production has historically been from sulphides. This disproportion has primarily been due to the economics of nickel mining and processing. Laterite ores enjoy the potential for lower mining costs when compared to the underground or open pit operations required by sulphide deposits. However, these savings were commonly offset by the significantly higher energy costs associated

with the traditional pyrometallurgical processing of laterites when compared to the smelting of sulphide ores, which can take advantage of sulphur credits (Robson, 1998).

Recent advances in hydrometallurgical processes, which place the nickel and cobalt directly into solution using leaching under high temperature and pressure, have greatly improved the economics of tropical laterite exploitation. The high-pressure acid leach (HPAL) process, when combined with technologies such as solvent extraction and electro-winning (SXEW) to remove the nickel and cobalt from the acid solution, offer a number of advantages over traditional methods. Along with lower capital and operating costs per tonne of capacity, HPAL yields higher metallurgical recoveries, and hence maximises the economic benefits of the orebodies (Brand *et al.* 1998). These, along with many other factors such as a continued growth in world nickel consumption, currently provide strong incentives for the growth in laterite exploration and exploitation.

A major economic factor that determines the development of any laterite project is the significant capital cost associated with their shear size. Developing laterite nickel prospects often requires large investment in infrastructure due to the remote tropical locations and the HPAL process' heavy reliance on large-scale materials handling. Justifying these large expenditures requires precise resource information to garner investor confidence in an industry that is currently seen as reliant on immerging technologies. Initial exploration costs, such as the saturation drilling needed to define a laterite nickel resource entail significant expense and may prevent a project from proceeding due to the higher cost of the speculative financing needed at the project's onset. Mapping the extent of the potentially mineralised layers using geophysics changes this balance and may allow much smaller companies to successfully bring laterite properties to production.

Certain geophysical methods have the ability to image the details of the top of the rocky saprolite layer, which is the horizon that defines the maximum depth of economic resources in most laterite nickel deposits. These geophysical methods, particularly ground penetrating radar, show that the boundaries of the laterite layering are surprisingly variable between boreholes. The abrupt changes in horizon configurations are completely undetectable by drilling at any economic spacing (Francké and Parkinson 1999). Conventional estimates of resource volumes based on the point

sampling provided by boreholes at commonly employed drill spacings of 200 m, 100 m, and 25 m in saturation coverage borehole grids often do not converge upon a single reliable estimate (Parkinson 1998). This situation occurs whenever the borehole spacing is greater than the spatial frequency of the lateral variations in the geology of the deposit. Overcoming this limitation of drill-based laterite exploration requires an undesirable and mainly inferential statistical approach to mineral resource estimation. By using geophysics to accurately map the volume of the deposit, coupled with sparser drilling to confirm the layer identification and grade, a geoscientifically sound and measured resource estimate may be made quickly and economically.

1.2 Literature Review

Knowledge of nickeliferous laterites began with the discovery of nickel deposits in New Caledonia by Jules Garnier in 1863. These deposits have been mined and studied steadily since that time. Literature concerning the New Caledonian laterites has been reviewed in a modern context by Trescases (1975, 1979) and Troly *et al.* (1979). Exploration of nickel laterite deposits elsewhere in the world occurred during the middle part of this century, and most of the literature on these deposits was written after 1950.

Modern scientific data relating to nickel laterites consists generally of mineralogical and geochemical data for individual weathering profiles written by property owners. They occasionally include qualitative descriptions of the structural and topographic control of nickel enrichment at individual sites, e.g. Burger (1979), Halderman (1979), Harju (1979), and Hellsten (1998). A discussion of the quantitative theory of profile evolution and ore control is given by Golightly (1978, 1979). Data relating directly to the age and rate of development of laterite deposits is available only on the Soroako site in Indonesia (Golightly, 1979).

The application of geophysics to lateritic environments is scarcely covered in the literature. The first known paper concerned a United Nations-sponsored project in Burundi at the Musangati deposit (Peric, 1981). Since then, brief mention of ground electromagnetics methods have been made in various papers discussing the arid laterites of Western Australia (Robson, 1998; Fazakerley and Monti, 1998; Casmuti and Riel, 1996). Queen *et al.* (1998) were the first to discuss the application of large-scale geophysical programs to nickel laterite exploration. The paper discussed the

application of ground penetrating radar (GPR) at the Ramu deposit in Papua New Guinea. A number of subsequent papers on the application of GPR at a variety of sites around the world have been published since by Parkinson (1998), Francké and Parkinson (1999), and Francké and Nobes (2000). No further published discussions specific to the application of geophysics to nickel laterite exploration have been located.

1.3 Research rationale

The motivation for this research was primarily the lack of published information on the geophysical characteristics of laterite deposits, or the potential applications of geophysics in laterite resource evaluation. A number of test surveys have shown that laterite deposits are widely variable in not only their geological composition, but also their geophysical signature (Francké and Parkinson 1999; Francké and Nobes 2000). These test surveys indicated that GPR is the most suitable geophysical method for mapping the weathering profile in most humid laterites. The objective of this research was to examine and quantify the radar response at a variety of laterite sites. This research has concentrated on humid laterite deposits due to their relative complexity and geologic variability as compared to the arid laterites found in Western Australia.

In Chapter 2, the geology and geological processes involved in the formation of laterites is outlined. These processes affect the geological and geochemical properties, which in turn determine their geophysical signatures. Chapter 3 discusses the accuracy and cost-effectiveness of a range of possible geophysical methods. Chapter 4 covers the basic principles of the GPR technique, including system configuration, survey methodology, and data processing. A number of example sites from previous GPR surveys in lateritic conditions discussed in Chapter 5 illustrate the range of the GPR response to specific geological environments. The results of comprehensive test surveys at the Goro and Koniambo deposits of New Caledonia are discussed in detail in Chapters 6 and 7, respectively, and the strengths and weaknesses of the GPR method and methodology are highlighted. Chapter 8 discusses the GPR response to specific physical and geochemical properties that appear to have the greatest influence on the radar response, using the results presented in Chapters 5, 6 and 7. These findings help guide the development of a more general conceptual model for the GPR response, survey design and interpretation in lateritic environments. Finally, Chapter 9 summarises the main conclusions and recommendations for further work on the subject.

GPR data acquisition in the dense jungles of Papua New Guinea.

2 GEOLOGY OF NICKEL LATERITES

The term "laterite" (from Latin for brick-rock) is thought to have been originally coined in 1807 by Major Francis Hamilton Buchanan in reference to the red clay used for building blocks in southern India. Although these clays were in fact weathered basalts, the term is now applied to weathering profiles developed upon a wide range of bedrock types.

2.1 Global distribution of laterite resources

Although laterites are generally distributed throughout the tropical and sub-tropical regions, they may exist anywhere between 53°N (Ireland) to 41°S (Tasmania). However, a common feature of laterite deposits is that they are all situated in regions that were not subject to glaciation during the Pleistocene era. With minor exceptions, deposits are characterised by high seasonal rainfall and solar heating.

If the laterites are developed by the weathering of nickel-bearing parent rocks, a potentially economic deposit of nickel may be produced in the weathering profile. Nickel laterite deposits are located and exploited on every inhabited continent. The largest concentrations of nickel laterite deposits occur in active island arc tectonic settings, such as the south-west Pacific, and the Caribbean. Figure 2.1 illustrates the distribution of the world's nickel laterite resources. Deposits shown in yellow were the subjects of this research project.

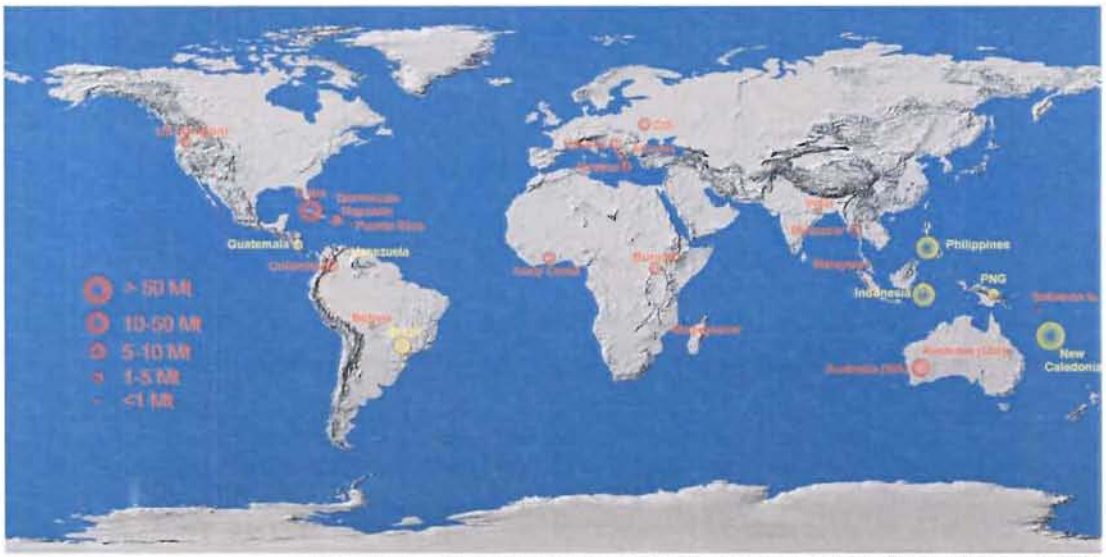

Figure 2.1 - World distribution of laterite resource (adapted from Osborne 1996).

Cuba, New Caledonia, Indonesia, and the Philippines alone account for over 75% of the total nickel laterite resource. There is now evidence that both the Cuban and the New Caledonian total laterite resources are significantly greater than presently reported.

The estimated world resource of nickel laterite is on the order of 8 billion tones grading 1.4% nickel and containing some 118 million tones of nickel. Of this resource, approximately 4.6 billion tones are classed as proven and probable reserves grading over 1.4% nickel containing about 70 million tones of nickel. At the present annual market demand, these proven and probable reserves alone would provide approximately 70 years of the total world demand for the metal (Osborne 1996).

Figure 2.2 illustrates the range of sizes and grades of the world's major laterite reserves. It is noted that the largest deposits are the low-grade limonite ores of Cuba, whilst some of the highest grades are found at the Cerro Matoso mine in Colombia and the extensive deposits in New Caledonia.

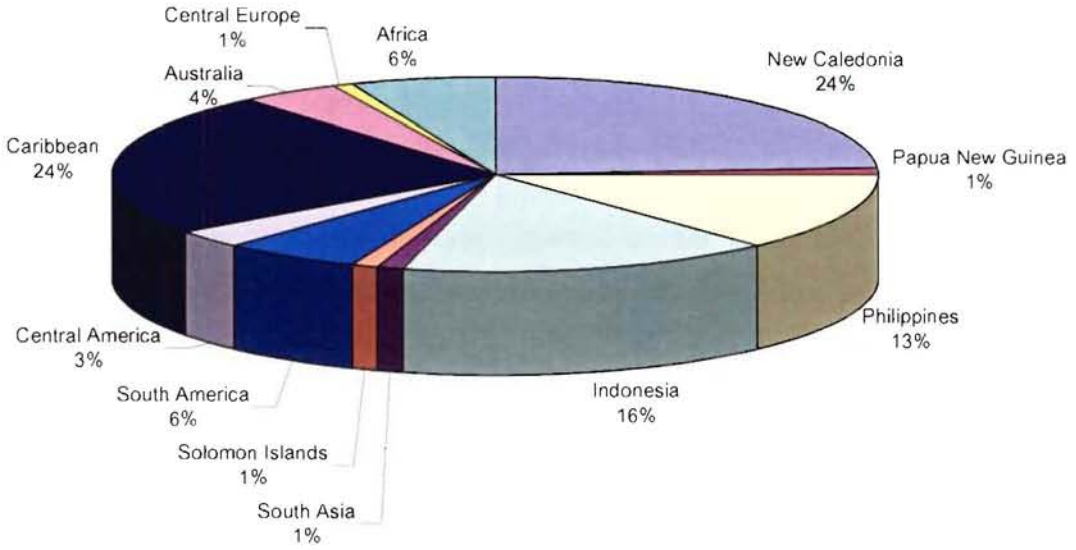

Figure 2.2 - Laterite reserves per country (Osborne 1996).

2.2 Geologic Setting

The majority of nickel laterite resources are developed in the weathered zone of Miocene and Pliocene ophiolite complexes. These harzburgite-dunite olivine cumulates can be extensive and are generally characterised by significant topographic relief. Typical deposits of this type are those in Cuba, Colombia, New Caledonia, the Philippines, Indonesia, the Dominican Republic, and the Western USA.

The remaining laterite resources are located in stable kratonic platforms, developed on komatites and layered complexes in Archean and Proterozoic greenstone belts (Golightly 1979). The komatiitic lithologies, dominated by peridotites and dunites, typically have a moderate or subdued relief. Examples of deposits developed in komatiitic lithologies include the Yilgarn Craton of Western Australia and parts of Brazil, West Africa and the Ukraine. This research project concentrates on the peridotitic laterites.

2.3 Laterite Formation

Ultramafic rocks originate as magmas from sub-crustal depths and are characterised by MgO and NiO contents substantially higher than crustal rocks. In these ultramafic magmas, nickel fractionates into the lattice of olivine $[MgFe]_2SiO_4$. The host olivine contains nickel grades averaging 0.3%. Cobalt, an important byproduct of some laterite ores, fractionates into the pyroxene lattice. Thus, nickel-cobalt ratios are higher in dunites and olivinites than in pyroxenites.

Ultramafic rocks, in general, are serpentinised. The degree of sepentinisation ranges from minor alteration adjacent to fractures to complete metasomatism. Ultramafic rocks are by nature alkaline, with pH values ranging from 8 to 9.

The oxidation and solution processes imparted on the ultramafic source rocks are complex and ongoing. Soil waters acquire acidity primarily from humic acids leached from decomposing vegetation, as well as from dissolved atmospheric gases. The soil waters readily react with the alkaline ultramafic rocks in a process that may be assisted by subsurface microbial activity.

With time, the SiO_2 and MgO are progressively leached form the serpentine mineral lattice. The relatively insoluble components, Fe, Al, Ni, Co, and Cr, accumulate within the developing residual oxidation zone.

The degree of lateritisation is determined by a complex combination of the mineralogy of the parent rock and its tectonic setting, the climate and topography. Significant accumulation of laterites, from tens of metres to over a hundred metres, occurs in areas characterised by free drainage and where the rate of erosion is significantly slower than the rate of weathering. Figure 2.3 illustrates the variation in laterite profiles produced

from both serpentinised and unserpentinised dunite and peridotite parent rocks (adapted from Alcock 1988).

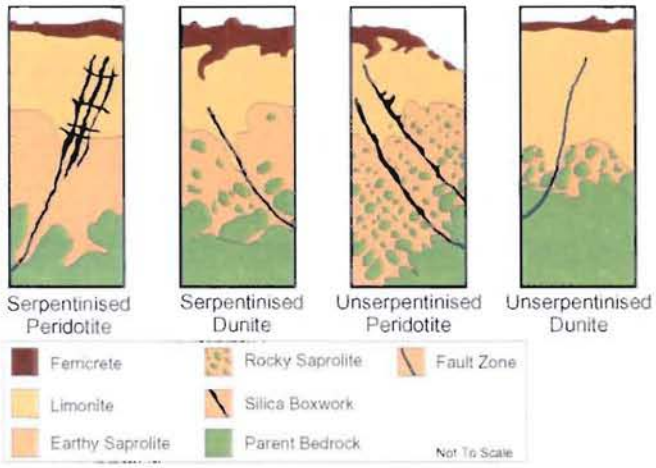

Figure 2.3 – Variable weathering profiles from serpentinised and unserpentinised dunite and peridotite.

There are a number of factors that affect the types of weathering profiles developed in tropical environments. The amount of rainfall in an area has a significant influence on the specific types of clays formed and the structure of the weathering profile created. An additional factor controlling the ultimate characteristics of the materials found in a lateritic profile is the nature of the parent material of the underlying bedrock. Variations in the amounts of felsic and mafic mineral components in crystalline rocks affect the electrical characteristics of residual soils that are produced from these rocks (Palacky 1979). Lateritic profiles from source rocks that contain more mafic minerals generally show higher electrical conductivities than do those from more felsic or silica rich parent rocks. This is due to the higher conductivity of montmorillonite clays that form during weathering of basic rocks in a humid environment. The presence of any organics in the original sedimentary parent rocks also greatly increases the conductivity of the resulting weathering profile (Parkinson 1998). The conductivity of the laterite profile is important in determining suitable geophysical methods.

Over geologic time, the conditions of oxidation, nurtured by intense solar heating and heavy rainfalls, break down the ultramafic rocks to create surface layers of residual soils. A normal, *in situ* profile may include the following units from the top down:

- Ferricrete
- Transported limonite
- *In situ* limonite
- Earthy saprolite
- Rocky saprolite
- Parent bedrock

The contacts between the horizons are transitional and the degree to which the respective horizons develop is dependent upon local conditions. Due to the process of residual enrichment, the profile is best described from the bottom upwards.

2.3.1 Bedrock

The bedrock topography tends to be highly irregular, with numerous peaks and troughs. In deposits such as Gag Island in Indonesia, Ramu in Papua New Guinea, and Celestial in the Philippines, pinnacles formed by bedrock resistive to weathering extend tens of metres above the adjacent bedrock topography and frequently outcrop. Preferential weathering within the bedrock along joints and fractures produces narrow weathered zones that extend deep into the bedrock. These narrow weathered zones are generally composed of saprolite and are known to commonly contain high nickel grades (Golightly 1979). An understanding of the frequency and amplitude of these pinnacles and troughs is critical to resource estimation and mine planning, and is the principal objective of most geophysical surveys.

Figure 2.4 – Silica boxwork within jointing.

2.3.2 Rocky Saprolite

The topography of the transition from bedrock to saprolite is also highly variable. A region of rocky saprolite exists as a transition zone, and may be in excess of ten metres thick. The term saprolite comes from Greek (*sapros*: rotten rock). The rocky saprolite is comprised of ultramafic boulders contained within a matrix of earthy saprolite. With increasing depth, the proportion of rock in the rocky saprolite increases until the cobbles and boulders merge into jointed bedrock. The rocky saprolite zone may consist of material varying in size from large boulders to gravels, where most of the parent rock minerals are present and the original structures and textures are well preserved. Partly decomposed joint blocks in fracture zones may be separated by cracks or voids containing silica boxwork or nickel-rich garnierite (Figure 2.4).

Figure 2.5 – Interstitial saprolite amidst jointed rocky saprolite blocks.

The typical appearance of this material and the interstitial nature of the rock-saprolite to earthy saprolite / limonite contact is seen in a photo from the Koniambo deposit in New Caledonia (Figure 2.5). A model for laterite development from jointed blocks of peridotite is shown in Figure 2.6 (from Golightly 1981). The saprolitic crust on the blocks increases in thickness exponentially upward toward the surface until a point that the rock core is completely dissolved just below the base of limonite. An excellent example of the serpentinisation of a corestone in shown in Figure 2.7.A greater thickness of limonite develops over rocky saprolite with closely spaced jointing.

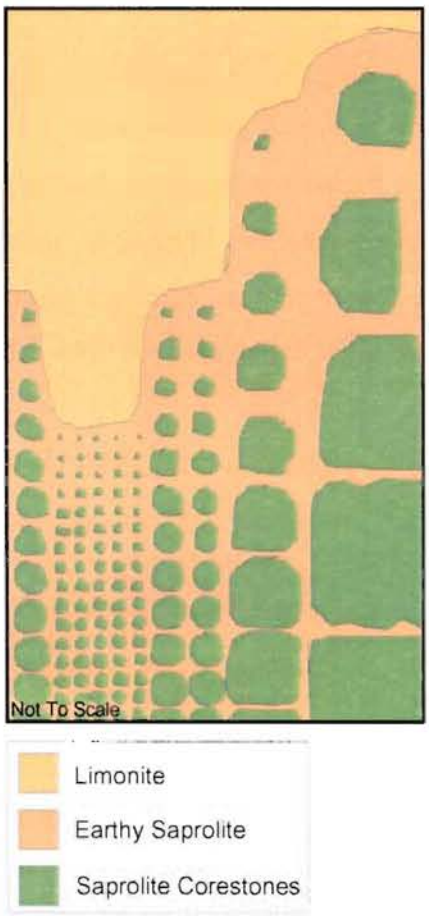

Figure 2.6 – Idealised weathering of rocky saprolite blocks.

The accurate determination of the composition and thickness of the transition from bedrock to saprolite is important during both exploration and mining phases. Large zones of boulders may cause drilling and sampling difficulties. They may also promote rapid wear of mining equipment or require blasting during mining operations. The weathered shell around rocky saprolite rocks and boulders has practical significance. Mined ore may be upgraded by tumbling these unserpentinised corestone boulders to remove the nickeliferous rims (Burger 1996).

2.3.3 Earthy Saprolite

The alteration of rock to saprolite is isovolumetic as the leaching process removes silica from the matrix without affecting the volume. The resulting earthy saprolite zone atop the rocky saprolite is

Figure 2.7 – Saprolite corestone showing serpentinisation around edges.

significantly porous and has, on average, bulk densities of 1.4 to 1.0 tonnes/m^3. However, the density of the earthy saprolite at some deposits maybe as low as 0.5 tonnes/m^3. Although it superficially resembles a clay due to its high bound water content, it is actually an open grain supported boxwork. In addition to preserving rock textures, the earthy saprolite exhibits well preserved jointing which commonly may be traced downwards into the rocky saprolite and bedrock zones. The earthy and rocky saprolite units typically mark the zones of highest nickel concentration in the laterite profile. However, the intensity of weathering is not always an indication of nickel grade, even within the same deposit (Pelletier 1996).

2.3.4 Limonite

The zone atop the earthy saprolite is referred to as limonite. Limonite is generally depleted in nickel and cobalt as compared to the saprolite zones. The *in situ* limonite zone consists of fine-grained nickeliferous goethite and ferric hydroxides. Some talc and chlorite occur as residuals from the parent rock structure. Silica boxwork extends into this zone from below, as well as stringers and nodules of asbolite, which occur at the basal part of the limonite zone. Although the structures and textures of the parent rock may remain visible, they have been completely flattened as the weathered limonitic soil has collapsed (Golighty 1981; Troly *et al.* 1979).

The locally transported limonite has a rubbly, conglomeratic appearance, and exhibits a generally reddish color that results from the occurrence of hematite. Talc and chromian spinel are the only parent rock constituents that persist in this zone (Trescases 1973).

2.3.5 Ferricrete

In the very near surface, the limonite zone may grade into a ferricrete crust, consisting of colloform goethite tubes or pisolites of goethite. The ferricrete is formed by the mobilization and recrystallisation of surficial limonite in surface acid conditions. This ferricrete cap, which is particularly present on the deposits of southern New Caledonia

(e.g. Goro), is extremely hard and exhibits high porosity, parched of bound water, and is known to be highly electrically resistive (Peric 1981).

The residual concentration of nickel in the limonite zone is generally lower in grade than in the underlying saprolite, and rarely attains a grade of greater than 2%. The nickel grade increases fairly uniformly with depth in the limonite zone. Prior to the implementation of HPAL technology, the upper, generally transported, limonite zone was disposed of as overburden, and the lower limonite and the silicate ores from the saprolite zone were exploited. With HPAL, the extraction and processing of both the limonite and saprolite units has become reasonably economic (Ried 1996).

2.4 Resource Estimate Considerations

According to the widely accepted Australian Joint Ore Reserves Committee (JORC 1999) code, a series of criteria must be met for the valid incorporation of geoscientific information in a resource estimate. These criteria include the ability to interpret the data consistently, that the interpretation can be related to a significant feature of the resource, and that the interpretation enhances the reliability of the resource estimate. The Committee has also regulated the use of the certain terminology in reports on mineral resources submitted to the Australian Stock Exchange (JORC 1999), which are summarised below for the purposes of this research project.

> **'Inferred mineral resource'** denotes a mineral resource "inferred from geological evidence and assumed, but not verified, geological and / or grade continuity."

> **'Indicated mineral resource'** denotes a mineral resource in which geological and / or sampling locations are "too widely or inappropriately spaced to confirm geological and / or grade continuity but are spaced closely enough for continuity to be assumed."

> **'Measured mineral resource'** is based on "detailed and reliable exploration, sampling and testing information gathered through appropriate techniques from locations such as outcrops, trenches, pits, workings and boreholes."

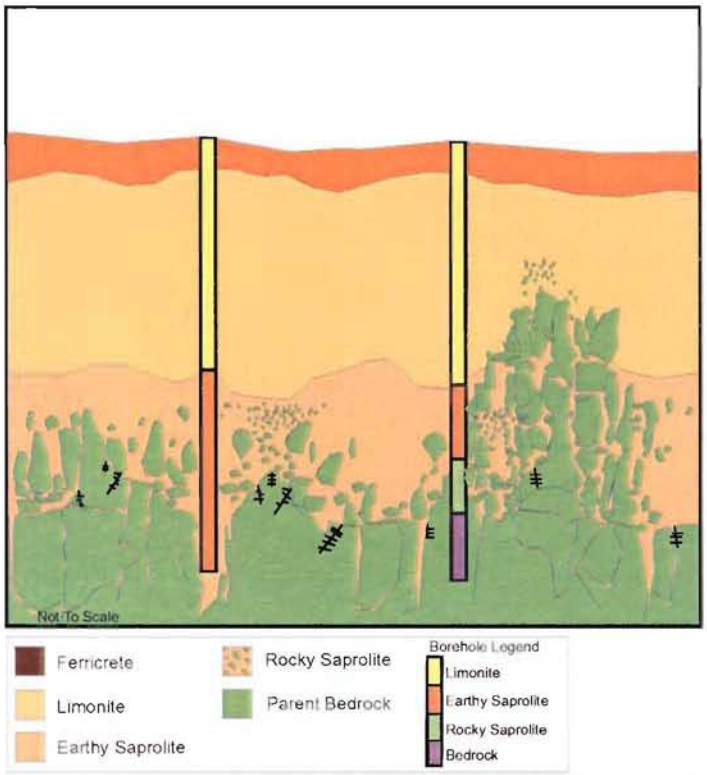

Figure 2.8 – Schematic showing variability in weathering profile.

These definitions are relevant to the description of laterite deposits especially in that they address and stress the issue of continuity. In laterite deposits, continuity of layer thickness is difficult to prove with drilling, as demonstrated in Figure 2.8. This example shows two common scenarios where a regularly spaced borehole grid may be insufficient for an accurate resource estimate. The borehole to the left has been placed within a deep fracture zone within the bedrock, possibly caused by preferential water migration down fault plains. In this case, the borehole would indicate a thicker section of saprolite than exists in reality. Conversely, the borehole to the right was placed adjacent to a large pinnacle structure of unweathered bedrock. Pinnacles such as this are common to most lateritic environments and may impact on resource estimates. Some of the limitations of conventional borehole grids may be minimised by the use of geophysics.

The widespread nature of lateritisation generally precludes any need for geophysical exploration to determine the extents of mineralisation. Although it may not be economically viable, lateritisation over any ultramafic rock adjacent to a known deposit usually contains appreciable nickel grades. Therefore, rather than locating additional mineralisation, the task of geophysics is to assist the geologist in determining the amount of resource known to be present. Thus, geophysics must be directed towards the imaging of the physical dimensions of the weathering layers.

Guerioum historic laterite mining site near the Koniambo deposit, New Caledonia

3 SUITABLE GEOPHYSICAL METHODS

Extensive investigations involving geophysics at a variety of laterite sites have enabled an evaluation of the effectiveness of different geophysical methods in mapping the weathering profile. The rules of thumb often applied for predicting the success of a geophysical survey in temperate regions can be inappropriate for use in a tropical setting (Parkinson 1998; Francké and Parkinson 1999).

Economic deposits of laterite ore vary from several metres to over 100 m in thickness. For the purposes of mine planning, the highest resolution method that can penetrate the deposit's depth is required. The widespread nature of laterite deposits dictates the use of a method that can ideally be linked with a global positioning system (GPS), and which operates in a "continuous" profiling mode.

Geophysical techniques useful for lateritic nickel exploration must exploit the fundamental differences in physical properties of the weathering profile:

Ferricrete:	Very resistive, hard and dense, high in iron and low in water content.
Limonite:	Moderately resistive, soft and porous, uniform soil-like properties and a moderate water content.
Saprolite:	Moderately conductive, low porosity, firm and clay-like with high water content, relic structures.
Rocky Saprolite:	Boulders resistive but with conductive weathered skins, low overall water content.
Bedrock:	Usually relatively dense and resistive with low water content relative to saprolite.

3.1 Seismic Refraction

Seismic refraction surveying utilises seismic energy that is imparted into the ground by a mechanical source and returns to the surface after travelling through the ground along refracted ray paths (Hatherly and Tayton1983). Seismic refraction with compression waves has had a long history of application in laterite exploration despite the extremely slow velocities in limonite, high-energy absorption in laterite and the method's inherently lower resolution when compared to many other ground geophysical techniques. Velocity differences at the gradational contact between weathered and unaltered material may be much less significant than the increase in velocity at the

water table, which would result only in arrivals from the water table. Typical clay velocities are only marginally higher than the velocity of water-saturated unconsolidated sediments (Chandola *et al.* 1997).

Ray paths in areas of heavily weathered soft rocks are either not well defined or curve across gradational contacts. If the change in velocity between weathered and competent material occurs over a distance greater than one wavelength (about 3-5 m), no coherent refracted arrivals will be seen. In effect, compression wave seismic refraction profiling becomes a one-sided tomography problem once the simplification of sharp interfaces is no longer valid (Parkinson 1998; Docherty 1992).

However, moderately successful refraction seismic in limonite has been performed with geophone spacings from 2 to 10 m (Francké and Parkinson 1999). Seismic refraction surveying using sledgehammer or shotgun shell sources allows investigation to between 10 m and 40 m in depth, however interpretation is labour intensive. Seismic refraction using dynamite is generally found to be unsatisfactory for mapping depths of limonite in shallow areas (i.e. less than 20 m – 30 m) due to the slow acquisition and insufficient resolution. The extreme topography of the pillars and crevices along the bedrock interface may violate the assumptions made in standard refraction data processing software.

An alternative to the standard compression wave refraction profiling is investigations using shear waves. There are several advantages to using shear wave refraction profiling in lateritic environments. Since the water table arrival is not significant, the absence of this arrival allows discrimination of other more subtle interfaces in the data. Due to the slower velocities of the shear waves, which are typically one-third of that of the compression waves, the wavelengths of the shear waves (2 m – 3 m) are only one-third of that of the compression waves, resulting in potentially higher spatial resolution. In addition, the shear modulus of the layers can be estimated using the existing relations based on the ratios of the shear and compression wave velocities.

Shear wave refraction interpretation proceeds similarly to compression wave interpretation except that more care is required in picking arrivals since the shear arrival is not necessarily the first arrival. The recent research by the petroleum industry into shear wave and compression wave relationships has resulted in increasing use of shear

reflection surveying for characterizing rock properties (Mavko and Jizba 1994; Norminton 1990). The portable vibratory sources used for shallow seismic surveys could be used to provide energy for refraction / reflection profiling in a combined profiling / physical parameter testing system.

3.2 Seismic Reflection

In seismic reflection surveys the travel times are measured of arrivals reflected from subsurface interfaces between media of different acoustic impedance. Seismic reflection is generally a higher resolution method than refraction and has proved useful for delineating the details of laterite deposits deeper than 50 m (Miller and Xia 1997). The resolution of a seismic survey is proportional to the wavelengths of the imparted acoustic signal. The use of small gun sources and higher frequency geophones (100 Hz) in shallow surveys can result in higher resolutions than with dynamite sources, due to the generally loose surface soils. The use of either horizontal impact shear hammers or small portable swept frequency shear sources can also enhance the resolution of seismic surveying. A factor that may limit the resolution of seismic reflection is the poor geophone and shot coupling in loose lateritic soils.

A variation of seismic reflection profiling, spectral analysis of surface waves (SASW) is an *in situ* seismic method used for determining shear wave velocity profiles. The basis of the SASW method is the dispersive characteristics of Rayleigh waves when travelling through a layered medium. Rayleigh wave velocity is determined by primarily the shear wave velocity, but also the compression wave velocity and material density of the subsurface. The resolution of SASW varies inversely with frequency and thus it can be used to derive the shear strength structure as a function of depth (Bates *et al.* 1996)

Recent developments in compact computer-controlled SASW methods may be of use in lateritic weathering profiles due to the homogeneity of the upper layers and ease of generating surface waves in plastic materials such as limonite. Although the depths of effective investigation for shear-stiffness profiling are quoted at between 10 m and 30 m, the application may be of use in providing more detailed and accurate field predictions of settlement in weathering profiles for foundation engineering at laterite processing plant sites.

3.3 Direct Current Resistivity

In the DC resistivity method, artificially generated electric currents are introduced into the ground and the resulting potential differences are measured at the surface. Deviations from the pattern of potential differences expected from homogeneous ground provide information on the form and electrical properties of subsurface stratigraphy (Coen and Yu 1981). The results of a DC resistivity survey are typically plotted in the form of a pseudosection, which gives an approximate but distorted view of the subsurface geology. Interpreting resistivity data requires an appropriate inversion technique to be applied to correct for electrode array and topography effects and present results in true depths.

DC resistivity has been found to be a very useful technique for characterizing tropical alluvial and colluvial materials in humid environments, but the technique lacks sufficient resolution at economic spacings to be useful in resource estimation (Parkinson 1998; Francké and Parkinson 1999). However, the method has a definite place in initial prospecting for mineral resources due to its low cost and simplicity in the field, although standard Schlumberger depth soundings are likely to be distorted by lateral changes in laterite thickness.

In small-scale resistivity studies along pit walls, typical laterite resistivities have been found to be of the order of 400 ohm-m in limonites and 150 ohm-m in saprolites (Francké and Parkinson 1999). Rinds on corestones are much more conductive than the parent rock due to actively leaching minerals, whereas the very resistive crystalline ultramafic bedrock offers a good resistivity contrast against weathered materials.

3.4 Electromagnetics

Electromagnetic surveying methods make use of the response of the ground to the propagation of electromagnetic fields, which are comprised of an alternating electric intensity and magnetising force. Primary electromagnetic fields are generated by passing alternating currents through a transmitter made of wire coils. The response of the ground is the generation of secondary electromagnetic fields which are detected by the alternating currents that they induce to flow in a receiver coil by the process of electromagnetic induction (Geonics Ltd. 1980).

Electromagnetic methods are fast and relatively unaffected by near-surface conductivity variabilities or ferricrete caps. However some areas of ferricrete caps have large iron contents (up to 70%), which can cause erratic EM readings in some cases. EM instruments are divided into FEM (frequency domain, such as EM-31 and EM-34) and TEM (transient methods such as NanoTEM or TEM47). FEM methods are typically employed in a profiling mode, which can be used mainly for the crude detection of rock ribs and areas of subcropping weathering profile. At a recent project in Costa Rica, Parkinson (1998) noted that the silicification from hydrothermal alteration in the bedrock noted in boreholes correlated well with resistivity highs in the overlying saprolite. This example illustrates the remnant texture of the parent rock that is common in the saprolites, in that a higher fraction of silica sometimes remains in the saprolite after extensive weathering.

In arid laterite deposits, such as those found in Western Australia, the surface layer is often either electrically conductive due to salts left behind by evaporation or may form a hard resistive crust over a more conductive layer (Hellsten *et al.* 1998; Monti and Fazakerley 1996). Conductivities in the underlying saprolite are generally significantly higher than those found in humid profiles.

Due to the salts that typically concentrate in the arid weathering profile, FEM methods are not recommended. Difficulties are often encountered with resistivity methods as well.

TEM sounding or imaging has a wider application in ground-based laterite mapping since small multiturn loop (5-20 m loop sizes) soundings systems can achieve useful resolutions of 15 m to 30 m and still penetrate as much as 30 m to 100 m through the weathering profile (Cooper and Maliotis 1991). TEM soundings operate on the principal of radiating a circulating eddy current into the ground and as a result horizontal resolution decreases rapidly with depth. TEM systems may also be appropriate for mapping depth to shallow bedrock in arid laterite environments. Electrical mapping of soil parameters within the laterite profile in arid environments becomes difficult due to the unrelated background variations in salt content (Peric 1981; Palacky and Kadekaru 1979).

Several new instruments employing a technique known as capacitively coupled conductivity have recently become available. This method combines GPS positioning and the profiling advantages of FEM with a data type more similar to DC dipole-dipole resistivity. The variable separations of the dipole antennas allow a ready inversion of the data into images of lateral and depth variations for electrical profiling in laterite deposits. It operates by towing a transmit and a receive dipole over the ground surface which exchange a 16 kHz signal that is influenced by ground conductivity at various depths. This method requires no electrode contact with the ground and thus is practical in arid areas where other geophysical methods work less effectively and inserting electrodes for DC resistivity is difficult due to ferricrete caps.

Little information is available on the application of airborne electromagnetics to laterite exploration. It is thought that any successful survey would depend on the presence a distinct mineralogical contrast between the laterite and the surrounding region. In theory, it may be possible to use airborne methods to determine the thickness of the weathering profile at certain types of laterite deposits (Choudhury and Kalpan 1982).

3.5 Ground Penetrating Radar

The ground penetrating radar (GPR) method involves the radiation of short pulses of high-frequency electromagnetic energy into the ground from a transmitting antenna. The electromagnetic wave propagates into the ground at a velocity that is related to the electrical properties of the subsurface materials (specifically, the relative dielectric permittivity of the material). When the wave encounters an interface of two materials having difference dielectric properties, a portion of the energy is reflected back to the surface, where it is detected by a receiver antenna and transmitted to a control unit for processing and storage (Davis and Annan 1989).

Radar is the method of choice if the laterite thickness is less than approximately 50 m. To some extent, radar requires damp residual soils and preferably an open level surface to attain its maximum capability. It is interesting to note that alluvial tropical soils that superficially resemble laterites are often nearly opaque to radar due to their high organic and clay contents. However, reworked and transported limonite is still transparent to radar energy. Radar can be used either in a step and measure mode in extremely rough terrain for first exploration or in a continuously reading mode from GPS equipped vehicles to acquire data for detailed mining panel layout (Balde and Aiken 1997).

Borehole radar has also been employed in this research project to characterise electromagnetic velocities and to map the thickness of ferricrete.

Due to its high-resolution and ease of acquisition, GPR appears to be one geophysical technique with the potential to delineate the targets of interest in laterite deposits cost effectively. The application of GPR to lateritic environments the focus of this research project and is discussed in detail in Chapter 4.

GPS data acquisition in New Caledonia.

4 OVERVIEW OF THE GROUND PENETRATING RADAR TECHNIQUE

The concept of applying radio waves to penetrate and map the subsurface is not new. The most successful early work with GPR was the use of standard military radar systems and radio echo sounders to map the thickness of ice sheets in the Arctic and Antarctic. Pioneering research was conducted by the Royal British Antarctic Survey in the 1960's (Harrison 1970). Work with GPR in non-ice environments began in the early 1970's, focusing on permafrost soil applications (Annan *et al.* 1994). As understanding of the strengths and limitations of the technique became more apparent, the possible applications dramatically broadened.

The greatest historical inhibitor to the maturing of GPR as a recognised geophysical method was the inherent need for precise timing of sub-microsecond events. Computers that could capture and display such fleeting pulses of electromagnetic energy as radar reflections were extremely large and usually not portable (Davis *et al.*. 1985). With the advent of the high-speed laptop computer in the early 1990's, the ability to be able to capture, digitise, and store large volumes of radar data was realised. Although the technique has been successfully used for a myriad of applications around the world, it is still in its infancy. Today, typical commercial applications of GPR include engineering and environmental site evaluations (Annan *et al.* 1990), fracture mapping (Davis and Annan 1989), stratigraphic mapping (Jol and Smith 1991), void detection (Campbell *et al.* 1993), pipeline river crossings (Francké 1997), forensic studies (Nobes 1999), glaciology and permafrost engineering (Moorman and Frederick 1998), as well as archaeological studies (Conyers and Goodman 1997).

4.1 Principles of GPR

GPR uses some of the same principles as the reflection seismic method commonly used in petroleum exploration. The two methods are often complementary since the radar waves generally do not penetrate to depths greater than 50 m, and seismic reflection exploration is often very difficult at depths of less than 25 m due, in part, to the effects of surface waves.

4.1.1 The GPR Method

The GPR method employs a high-frequency electromagnetic (radio wave) pulse transmitted into the ground. The elapsed time is measured between the transmission and the reception at the surface of the energy reflected from a subsurface discontinuity. The discontinuities where reflections occur are usually created by changes in electrical properties of the ground, variations in water content, lithologic changes, or variations in bulk density at stratigraphic interfaces.

The receiving antenna is electrically matched to the transmitting antenna, and the signal is recorded as a time-varying voltage. These signals are relayed to a control unit, amplified, and recorded as a function of time since the transmission of the pulse. In order to improve the signal-to-noise ratio of the recorded data, multiple transmissions are made at the same location and the received signals are "stacked" by averaging. Data may be stacked 32, 64, or even 128 times at the same location to improve data quality. The entire system (i.e., the transmitting antenna, receiving antenna, and control unit) is then advanced a set step size along the survey line and the process is repeated.

The reflected data recorded at each step is displayed adjacent to the ones recorded before it to create a radar profile. A series of returned signals that, when placed adjacent to each other, produce a coherent feature across the profile is referred to as a "reflection." Distinct reflections usually occur from stratigraphic boundaries or other physical discontinuities. As the radar system records received signals as a function of the time since transmission, reflections recorded later in time are received from deeper in the ground.

The primary objective of GPR in laterite exploration is to differentiate lithologic interfaces. The strongest radar reflections in the ground occur at the interface between two thick units with greatly varying electrical properties. The degree to which radar reflections can be recorded by the system is related to the amplitude of the reflected waves. The higher the amplitude, the more visible the reflections. Lower-amplitude reflections usually occur when there are only small variations in the electrical properties between layers, or when the subsurface is relatively homogeneous.

Radar energy undergoes dispersion and attenuation as it radiates into the ground. When portions of the original transmitted signal are reflected back to the surface, they undergo

additional attenuation by the media through which they propagate before finally reaching the receiving antenna on the surface. To enable detection, subsurface interfaces must have a sufficient electrical contrast at their boundary as well as be located shallow enough so that sufficient radar energy is still available for reflection back to the surface. Due to dispersion and attenuation, the radar energy that is propagated to increasing depths becomes weaker and more spread out over a greater surface area, leaving little energy to be reflected. Thus, by the time the radar energy has returned to the surface, only very low amplitude signals may be recorded.

4.1.2 Parameters Affecting Radar Transmission

At each site the maximum depth from which signals can be recorded varies with the geological conditions and the equipment being used. Specifically, the maximum depth of effective penetration is a function of the frequency of the electromagnetic waves that are propagated into the ground, the ground conductivity, and the magnetic permeability (Annan *et al.* 1975). Subsurface media that are highly dielectric will permit the propagation of the most electromagnetic energy without attenuation. The more electrically conductive a material is, the less dielectric it is. An ideal radar environment would be a region that is highly dielectric with a low electrical conductivity.

The dielectric permittivity of a medium is a description of the material's ability to store, and then allow the propagation of, electromagnetic energy when an electromagnetic field is imparted on it. Olhoeft (1981) describes dielectric permittivity as being the ability of a material influenced by an electromagnetic field to become polarised, and therefore respond to, propagated electromagnetic waves. The dielectric permittivity of a material is determined by its composition, moisture content, bulk density, porosity, physical structure, and temperature (Olhoeft, 1981). The dielectric permittivity used in calculating the propagation of radar waves in the ground is actually a ratio of the material's electrical permittivity and the electrical permittivity of free space (= 1), and is thus a unitless coefficient. Dielectric coefficients range from one in air, through 4 – 10 in most resistive geological environments, to as high as 50 in high-conductivity clay. Fresh water has a dielectric coefficient of 80.

The dielectric coefficient not only controls the attenuation of radar waves, but also the velocity at which they propagate. The relation between the dielectric coefficient and the radar wave velocity is:

$$v = \frac{c}{\sqrt{K}} \qquad [4.1]$$

where K is the dielectric permittivity of the material, c is the speed of light in free space, and v is the velocity of the radar energy propagating through the material.

Two other parameters that affect the propagation of radar energy in the ground are the magnetic permeability and the electrical conductivity of the medium. The magnetic permeability is the ability of the medium to become magnetised when an electric field is imparted on it. The magnetic permeability of a medium is proportional to the amount radar energy that will be attenuated. Most geologic materials found in the near-surface are only slightly magnetic, and therefore have a low magnetic permeability. Media that contain magnetite minerals, iron-oxide cement, or iron-rich soils can have a high magnetic permeability and therefore attenuate and slow radar energy.

Electrical conductivity is the ability of a medium to conduct electric current. The electrical conductivity of a medium is proportional to the amount of attenuation it will impart on propagating radar energy. Since the electrical and magnetic components of electromagnetic energy are co-dependent, the total field tends to dissipate rapidly in highly conductive environments where the electrical component is essentially conducted away. Highly conductive environments will include those with a high clay fraction, particularly if the clay is wet.

4.1.3 Radar energy propagation

The radiation pattern of a dipole antenna situated in a homogeneous non-dielectric medium (air) is symmetrical and aligned perpendicular to the dipole orientation. However, when the antenna is placed at the boundary between two half spaces such as air and the ground, a significant change occurs in the radiation pattern due to ground coupling. Ground coupling is the ability of an electromagnetic field to be transformed from transmission in the air to transmission in the ground. Due to ground coupling, refraction, which occurs as the radar energy passes into the ground, causes a change in the shape of the radar beam, with most of the energy focussed into the ground in an elliptical cone whose apex is at the centre of the transmitting antenna (Figure 4.1). The angle of this cone is proportional to the dielectric permittivity of the ground (Goodman

1994). Thus, a high dielectric permittivity would produce a lower radar wave velocity with a more focussed conical transmission "illumination zone" or footprint. The subsurface radiation pattern is not only directly beneath the antenna, but also in front, behind and to the sides.

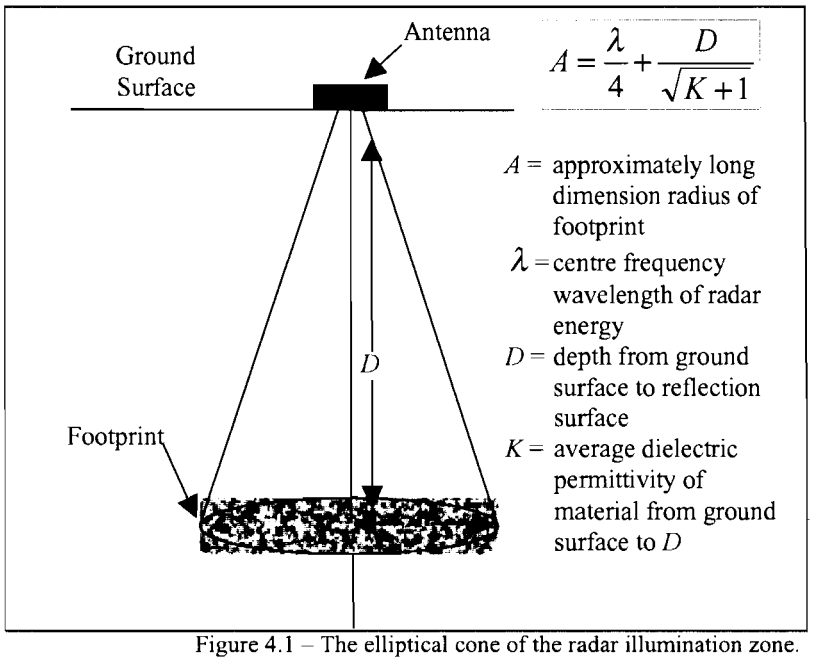

Figure 4.1 – The elliptical cone of the radar illumination zone.

The size of the illumination zone can be estimated by the area of the first Fresnel zone. The first Fresnel zone is the area of the illuminated zone for which reflected signals travel a path length less than $L + \frac{\lambda}{4}$, where L is the normal distance to the plane and λ is the wavelength of the signal in the medium. Thus the area of the first Fresnel zone is:

$$\sigma = \pi \sqrt{\left(\frac{\lambda^2}{16} + \frac{\lambda L}{2} \right)}. \qquad [4.2]$$

A significant portion of the energy transmitted by the radar system propagates into the air. This energy can reflect from aboveground objects and return to the receiver to be recorded as background clutter. This sensitivity of the system to aboveground objects located alongside survey lines requires the dipole antennas to be aligned so that the long axis of the illumination zone is parallel to the line direction. Thus the largest side lobes of the aboveground antenna radiation pattern can be kept aligned with and within the confines of the cut-line through the surrounding vegetation. This becomes essential in dense tropical jungles, where thick tree trunks abound. Although progressing along the

line in this mode is operationally inconvenient and results in the need for more line clearing, this precaution is worthwhile and prevents the geologically important subsurface signal from being lost in the clutter of diffractions that result from dense jungle foliage. In areas less heavily tree covered, the antenna orientation becomes less critical.

The concept of the illumination zone is critical when interpreting radar data. Radar data acquired in lateritic environments generally are characterised by a series of superimposed hyperbolic reflections. The apexes of these hyperbolic arches are produced by discrete reflectors, such as individual corestones and boulders, and are a result of the conical illumination angle of the down-going radar wave from the transmitter. Since the transmitted energy illuminates subsurface features before the antenna is directly over the object, the travel time to the scattering point is initially greater than when located directly over the point reflecting the energy. Similarly, when the antennas have moved past the reflector, the travel time of the wave to the reflector gradually increases again until the reflection is lost. This results in the characteristic concave downwards arches of the diffraction patterns. This concept is best illustrated in Figure 4.2, which shows the hyperbolas caused by two isolated saprolite corestones in a homogeneous limonite. The angle of the asymptotes of the hyperbolas cased by buried objects can often be used to estimate the average radar velocity between the surface and the object. Thus, the following equation may be applied:

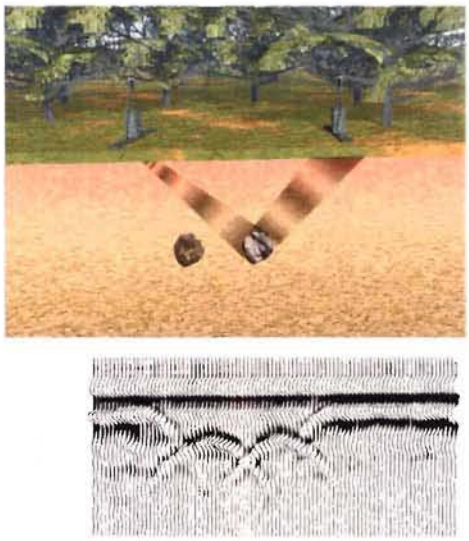

Figure 4.2 – Hyperbolas caused by two rocky saprolite corestones in homogeneous laterite.

$$\left(\frac{Vt}{2}\right)^2 = \left(\frac{Vt_0}{2}\right)^2 + x^2 \qquad [4.3]$$

where V is the desired velocity, t and t_o are the change in time along the asymptote of the hyperbola, and x is the corresponding distance along the surface.

4.1.4 Radar resolution

The ability to resolve buried features is for the most part determined by the frequency of the transmitting and receiving antennas, and therefore by the wavelengths of the radar energy. GPR is based on standard principles of electromagnetic wave propagation, and therefore the wavelength (λ) is inversely proportional to the frequency (f) of the antennas and proportional to the radar wave velocity (v):

$$\lambda = \frac{v}{f}. \qquad [4.4]$$

Thus, a 25 MHz antenna pair would generate an electromagnetic wave of about 12 m in length when transmitted in air. The wavelength of energy from the same antennas propagating through dry sands (dielectric permittivity $\approx$ 3) is reduced to 6 m. Radar reflections are generated whenever the imparted radar wave encounters a sharp change in the dielectric permittivity within the subsurface. If this change in dielectric permittivity, and thus velocity, occurs over a distance of less than one quarter of a wavelength, a coherent reflection will be returned to the surface. Thus individual objects, such as saprolite corestones, would in theory need to be on the order of $\lambda/4$ in diameter to cause a returned signal, where λ is the wavelength of the radar wave in the media traversed. In the case of a layered velocity structure, vertical variations on the order of $\lambda/8$ or even $\lambda/12$ are, in theory, resolvable given appropriate equipment and environment.

4.1.5 Signal attenuation

As previously noted, radar attenuation with depth is controlled by the dielectric permittivity, the electrical conductivity, and the magnetic permeability of the media through which the radar waves propagate. Absorptive attenuation losses of electromagnetic energy increase as the water content of the ground increases and also varies with the amount of salts in the medium. In extremely unfavourable conditions such as wet, clay-rich soils radar penetration may be limited to the first few metres of the subsurface. In ideal conditions such as the arid resistive environment of dry sands, penetration may be in excess of 50 m.

Generally, materials with lower electrical conductivity (high resistivity), allow greater electromagnetic wave propagation and have a low dielectric permittivity. Media that

have a high electrical conductivity greatly impede radar penetration. The attenuation is caused by absorption, due to the conductivity losses in the ground and geometric spreading over a larger surface area with increasing depth. Signal attenuation may be quantified by the equation:

$$\alpha[dB/m] = \left(\frac{2\pi f}{c}\right)\tan\left(\frac{\sigma}{2\pi f \varepsilon_o \varepsilon_r}\right) \qquad [4.5]$$

where f is the frequency, σ is the conductivity, and ε_r is the permittivity of free space. By examining the amplitude of the first output wavelet on the radar traces relative to the output voltage of the transmitter a relation of

$$A_{INC} = 4 \times V_{OUT} \qquad [4.6]$$

can be derived. Note that output power and not the output voltage is required in order to translate the values into signal amplitude. Combining Equations 4.6 and 4.7 yields

$$attenuation = 20\log\frac{A_{RES}}{4 \times V_{OUT}}. \qquad [4.7]$$

A decibel is defined by the relation

$$20\log\frac{A_{RES}}{A_{INC}} \qquad [4.8]$$

where A_{RES} is the residual power and A_{INC} is the incident power at time zero (t_0) in the radar trace. Since the attenuation defined in equation [4.7] is in dB/m, the value is multiplied by the travel distance at each given depth where the residual power is to be computed. Thus,

$$A_{RES} = 4 \times V_{OUT} \times 10^{-\left(\frac{attenuation}{20Depth}\right)}. \qquad [4.9]$$

Using these relations, and knowing parameters such as electrical conductivity and dielectric permittivity of the media, the suitability of different antenna frequencies and output powers can be calculated.

The penetration depth of a radar signal is proportional to the output power of the transmitting antenna and inversely proportional to the antenna frequency. The detectability of a subsurface object or horizon can be theoretically predicted using the radar range equation. A discussion of the radar range equation is outside the scope of this project. Although complex, the equation,

$$Q = 10\log\left(\frac{\varepsilon_{Tx}\cdot\varepsilon_{Rx}\cdot G_{Tx}\cdot G_{Rx}\cdot c^2\cdot g\sigma\cdot e^{-4aL}}{64\pi^4 f^2 L^4}\right) \qquad [4.10]$$

may be simplified to a ratio of minimum detectable signal power to the power input to the transmitting antenna. Thus,

$$Q = 10\log\frac{P_{MIN}}{P_S}. \qquad [4.11]$$

This relation may be used as a general guideline for determining the delectability of a target or target geological boundary.

4.1.6 Acquisition parameters

Many parameters of the radar survey geometry are dependent on the dielectric permittivity and antenna frequency being used. The selection of spacing between individual radar readings, or traces, is closely linked to the centre operating frequency of the antennas and to the dielectric properties of the subsurface media traversed. In order to ensure the ground response is not spatially under-sampled (aliased), the Nyquist sampling interval is observed. The Nyquist sampling interval is one quarter of the wavelength in the host material at the surface and is expressed by

$$n_x = \frac{c}{4f\sqrt{K}} = \frac{75}{f\sqrt{K}} \qquad [4.12]$$

where f is the antenna centre frequency (in MHz) and K is the relative dielectric permittivity. Note that, by combining equations [4.1] and [4.4], the Nyquist sampling interval is equal to one-quarter of the radar wavelength at the ground surface. If the station spacing is greater than the Nyquist sampling interval, the data will not adequately define steeply dipping reflectors.

The spacing between the transmitter and receiver antennas is determined by adhering to simple mathematical relations between target depth and antenna separation. To maximise target coupling, antennas are spaced such that the refraction-focusing peak in the transmitter and receiver antenna illumination zones point to the common depth to be investigated. Since the antenna pattern peaks at the critical angle of the air-earth interface, an estimate of the optimum antenna separation is given by the expression

$$S = \frac{2 \times Depth}{\sqrt{(K-1)}} \qquad [4.13]$$

where S is the antenna separation and K is the dielectric permittivity of the media traversed by the radar wave (Annan *et al.* 1975). Increasing the antenna separation also increases the reflectivity of relatively flat lying planar targets. Since the dielectric permittivity values of the dielectric coefficient may vary dramatically over a single survey line due to significant variations in the subsurface, an estimate is generally made to set the antenna separation to 20% of the target depth. Depth resolution of targets decreases as antenna separation increases, particularly as the antenna separation approaches half the target depth. It is generally not feasible to alter antenna separations along a survey line. However, with low frequency antennas, such as those with frequencies centred at 50 MHz, 25 MHz, and 12.5 MHz, signal saturation becomes a controlling factor when determining antenna separation. Therefore, the separation of those antennas is varied in accordance with general acquisition guidelines (Annan and Cosway 1992). Table 4.1 illustrates the variability in antenna spacing generally used for geologic mapping.

Antenna	Rx to Tx Spacing
200 MHz	1 metre
100 MHz	1 metre
50 MHz	2.5 metres
25 MHz	5 metres
12.5 MHz	8 metres

Table 4.1 – Standard antenna separations.

4.2 Application of GPR to Laterites

Penetration depths of up to 65 metres have been achieved with GPR in lateritic weathering environments (Francké and Parkinson 1999; Francké and Nobes 2000; Parkinson 1998). Conventional wisdom in the temperate regions dictates that radar surveys are usually unsuccessful in an area with a high clay fraction. This research project indicates the contrary, as the almost 100% clay-like saprolite materials found at a number of laterite sites are effectively transparent to radar energy.

The impressive depths of penetration of radar signals in humid laterites can be explained by the additive effects of three main factors: excellent target contrast; a lack of attenuation in the weathering profile possibly due to the leaching of conductive minerals and fine grained material; and good antenna coupling.

The main objective in laterite exploration is to image the contact of the weathering materials with the unaltered bedrock, which usually defines the limit of mining. Radar reflections from this boundary are thought to be primarily due to the changes in water content between materials, as discussed in Chapter 8. Both limonite and saprolite have a very high water content. Crystalline bedrock has a low water content due to its lack of porosity. Thus, the interface between the weathered material and rock produces a very strong radar reflection. The thin conductive skin that forms on weathering rock also enhances the reflectivity

A somewhat wasteful aspect of radar surveying is the fact that unshielded antennas normally radiate upwards as well as they do downwards. Fortunately, coupling of radar energy into the ground is enhanced by the effect of the relatively high water content of both saprolites and limonites, which increases their dielectric permittivities. Refractive focusing of the energy at the surface causes a greater proportion of the energy to be directed downwards than is normal in temperate soils.

As mentioned previously, radar waves will be reflected from subsurface discontinuities in dielectric permittivity. Examples of physical properties that affect dielectric permittivity are listed below in what is considered to be the order of importance in lateritic profiles:

Water content – Variation in the percentage of water is a significant controlling factor of the dielectric constant. The dielectric coefficient describes the magnitude of the electrical component of the impedance. Changes in porosity and grain size are major determinants of water content. The high dielectric coefficient of water (80) slows or impedes the passage of the radar signals, shortening their wavelength, as expressed in equations [4.1] and [4.4]. Saturated lateritic soils are often porous materials with relatively high water content and thus can have a lower radar velocity. Chalcedony, corestones, and unaltered bedrock have a low water content, and thus a higher radar velocity. Therefore, rocks embedded in the earthy saprolite scatter reflections strongly if they are larger than half a wavelength, or if they form an assemblage larger than half a wavelength.

Conductivity – Surface deposits of conductive fine-grained clays, such as alluvial or lacustrine sediments, can affect the passage of the energy into deeper materials and limit penetration due to high attenuation, as expressed in equation [4.5]. Radar energy is absorbed strongly by conductive materials such as fine-grained fresh clays, which can limit penetration to several metres (Daniels at al. 1988). Residual clays in tropical environments are typically well leached due to the removal of conductive minerals and salts by the heavy rainfalls and warm temperatures, and therefore may be less conductive than those in other environments.

Percentage Iron – High concentrations of magnetic minerals such as iron, nickel and possibly chromium, as have been found in abundance in placer environments at other nickel laterite sites, can also lead to radar reflections. However, since the variations can be gradational, these changes are not as significant a source of radar reflections as the variations in water content.

4.3 GPR Data Acquisition

The transmitter generates the radar wave by dumping a single fast pulse of high voltage into the dipole antenna. The high voltage is generated within a sealed battery-powered unit mounted on the antenna. Standard radar transmitters operate at either 400 V or 1000 V, the latter being used for deeper profiling. The transmitter is triggered through fibre optic cables connected to the control console.

Receiver units vary in their sensitivity. For deep surveying in tropical weathering profiles, a very high sensitivity is required. The soils of lateritic environments may attenuate energy faster than in other locations due to increased conductivity through inadequate leaching of conductive minerals or fine grained material. This may limit the effective depth of penetration to approximately 40 metres. Higher signal-to-noise ratios generally allow for better resolution and radar penetration.

The receiver is a small battery-powered unit attached to the antenna that is triggered by a fibre-optic cable from the console. The console unit is mounted within a backpack and carried behind the transmitter and receiver. The handheld computer is connected to the backpack by means of a heavily shielded cable, and is located a further distance behind the console unit. In this configuration, the computer is positioned as far as possible from the receiver antenna to minimise interference from the spurious emissions of the computer circuitry. The layout of the radar equipment for laterite surveying is shown in Figure 4.3. A trigger starts the receiver acquiring data for a set time window immediately after the initial transmitted pulse. A second fibre optic cable carries data containing reflections from the subsurface, after being received by the receiver, as a series of digital optical pulses from a light-emitting diode. After summing the appropriate number of stacks, the data are recorded into a handheld computer attached to a backpack carried by the operator.

Figure 4.3 – Radar system layout with Tx leading, followed by Rx, console backpack and handheld computer.

A variety of radar antenna frequencies are appropriate for the acquisition of data in lateritic environments. The most important consideration is to choose a frequency low enough to penetrate the earth materials while high enough to resolve the structures of interest. For the purpose of this research, every available antenna was employed for comprehensive experimentation. Antenna frequencies of 200 MHz, 100 MHz, 50 MHz, 25 MHz, and 12.5 MHz were utilised for

various portions of the research, with the use of lower frequencies implying larger antennas and somewhat lower resolution yet deeper penetration (Table 4.2).

Antenna Frequency	Antenna Length	Wavelength in Air (v=0.30 m/ns)	Wavelength in Typical Laterite (v=0.06 m/ns)	Estimated Penetration In Typical Laterite
12.5 MHz	9.6 m	24 m	3.4 m	40 m
25 MHz	4.8 m	12 m	1.7 m	30 m
50 MHz	2.4 m	6 m	0.8 m	20 m
100 MHz	1.2 m	3 m	0.4 m	10 m
200 MHz	0.6 m	1.5 m	0.2 m	5 m

Table 4.2 – Properties of various radar antennas.

To best meet research objectives and achieve maximum profile resolution and depth of penetration, radar traces were acquired at the research test sites at set intervals along each survey line, as opposed to a continuous "scan" along the survey lines. Continuous scans are comprised of a rapid succession of transmitted and reflected pulses. As such, continuous scans are often blurred and of poor quality since the recorded signals cannot be stacked at a single location. The set intervals used during the research project were determined by the antenna frequency in use.

Table 4.3 lists the station step sizes used with each antenna.

Antenna	Station Spacing
200 MHz	0.25 metres
100 MHz	0.5 metres
50 MHz	1 metre
25 MHz	1 metre
12.5 MHz	1 metre

Table 4.3 - Standard antenna step size.

Although a station spacing of one metre or less is not typical for surveys in lateritic environments, this close spacing did produce significantly higher quality data at the research sites. If only larger structures are of primary interest, the intervals between traces may be as much as doubled to speed data acquisition, while adhering to the Nyquist interval.

The radar antennas were generally oriented perpendicular to the line direction. This orientation allows for the best data quality by minimising the effects of above-ground reflections from trees adjacent to the cut-lines. The response is thus primarily from subsurface features that are parallel to the electric field of the dipole antennas, which is also parallel to the survey direction. Two exceptions to this were attempts to use the

12.5 MHz antennas both in-line and in parallel (akin to skis). These attempts were made in order to capitalise on the deep penetration possible with the lowest frequency antennas, whilst minimizing the logistical difficulties of moving the 9.6 metre wide antennas down cut lines.

To further increase the signal-to-noise ratio, a data-enhancing stack or cumulative average of 32 or 64 pulse repetitions were acquired at each station while the antennas were held stationary. Although a greater number of stacks may have yielded slightly higher quality results, survey production time would have at least been doubled.

The zero time of the receiver and transmitter system, that is the arrival time of the air wave that travels directly from the transmitter to the receiver, was calibrated at the start of each survey line to compensate for temperature effects on the fibre optic cables and electronic components.

4.4 GPR Data Processing

Raw data were recorded at the test sites in pulseEKKO™ *.DT1 binary format files with an accompanying ASCII *.HD header. The *.DT1 files contain both the digital stacked data as well as comments regarding survey markers and borehole locations.

During the test surveys, initial data analysis was performed daily to ensure data quality. Also on a daily basis, profiles were corrected for proper orientation, individual traces were edited to account for minor variations in antenna separation, duplicate traces were deleted and missing traces were inserted using a cubic-spline interpolation technique. This ensured that the data acquired each day was entirely edited and prepared for subsequent processing. Daily editing and preparation of the data were essential to ensure that minor variations in parameters and any anomalies in acquisition are immediately accounted for. This process may be particularly time consuming if large volumes of data have been acquired.

Upon return from the test projects, the corrected and edited *.DT1 and *.HD files were imported into the GRADIX™ software package. This advanced software represents an adaptation of specialised workstation-based petroleum seismic reflection processing programs to the PC platform with specific adaptations for radar signal processing.

A generalised outline of the processing steps applied to the GPR profiles acquired at laterite sites includes:

Spatial resampling – Among the most critical editing steps, this process utilises software to compensate for variations in the step size between individual traces. This is accomplished by correlating the noted positions and trace numbers of each survey picket and/or borehole marker with the actual co-ordinates as provided by a survey crew. Once the position in a Cartesian co-ordinate plane is fixed for each known landmark point, the intervening data may be "rubber-sheeted" using a two-dimensional cubic-spline interpolation. This results in a marked improvement in survey accuracy along each line.

Declipping – Data are interpolated to remove inductive effects and compensate for truncation of high-amplitude signals due to the single-precision nature of the raw data format. Declipping also somewhat reduces the effect of receiver saturation at early time (Figure 4.4).

Dewowing – Depending on the proximity of the transmitter and receiver, as well as the electrical properties of the ground, the transmitted signal may induce a slowly decaying low-frequency "wow" on the trace, which is superimposed on the higher-frequency reflections. The removal of this effect is accomplished by transforming the data from the time domain into the frequency domain using a fast Fourier transform (FFT). A cut frequency is then assigned to the point of inflection that defines the change from the spectral peak of the antenna centre frequency and the wow effect. The data are then high-pass filtered to remove the effects of the signal wow, which allows better resolution of geological features. An example of a raw trace and a de-wowed trace is shown in

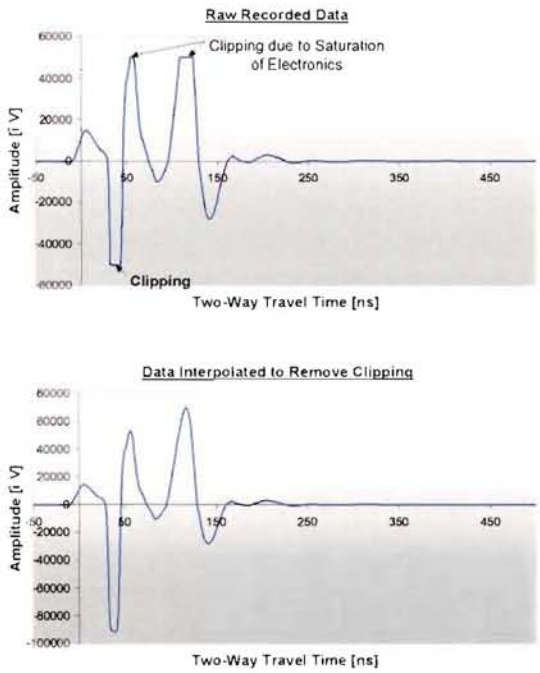

Figure 4.4 – Effects of declipping on raw radar data.

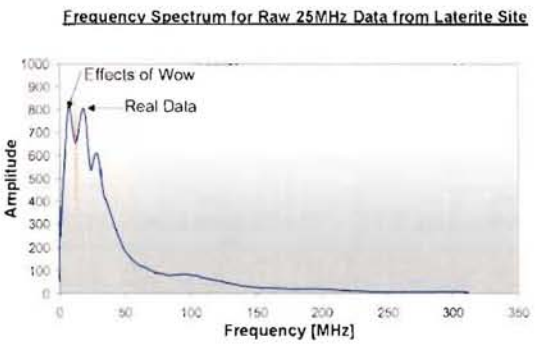

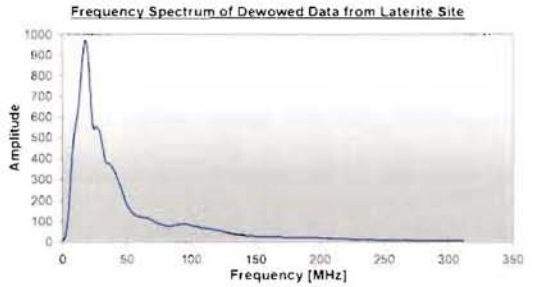

Figure 4.5 – Effect of dewow on frequency spectrum of radar data.

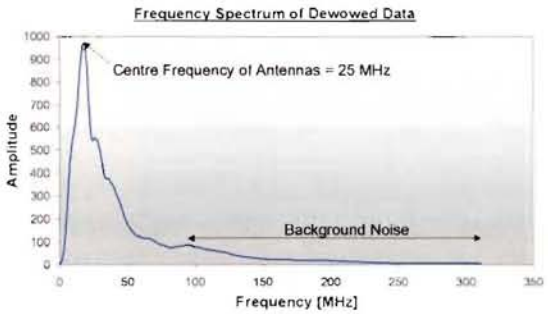

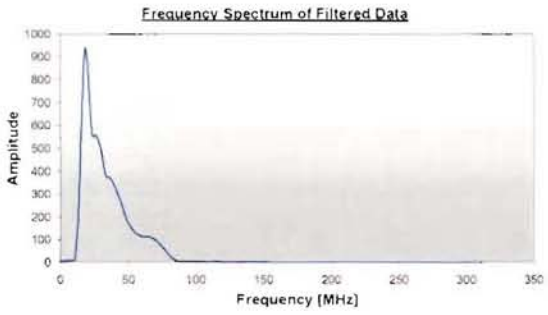

Figure 4.6 – Effects of filtering on frequency spectrum of radar data.

Figure 4.5. Occasionally, a small portion of remnant wow is visible on standard radar amplitude plots as slight background colour shifts.

Zero-time correction – This involves the compensation for jitter from trace to trace of the first arrival peak caused by small variations in antenna separation and surface ground conditions. The zero-time correction is accomplished by a cross-power correlation in the frequency domain. Time zero is also assigned to the profiles to define the zero depth level.

Filtering – Each radar profile undergoes an analysis to determine the parameters best suited for signal filtering. It is generally insufficient to apply a standard filter to all profiles acquired in lateritic environments due to the dramatic variations in subsurface media. In general, the highest quality results have been found with a Butterworth bandpass filter with a passband centred around the transmitting frequency of the antenna, and a variable stopband dependent on the type of sub-surface media. A frequency plot of a sample filter is shown in Figure 4.6. A number of parameters are experimented for each line to determine the optimum filter settings.

Spectral balance – Lateritic weathering profiles are known to act as effective high-cut filters for radar data, thus attenuating the high-frequency components of the return signals. Spectral balancing strives to balance the amplitude spectra of the data by

dividing the data into overlapping, equal-energy Gaussian filters in the frequency domain. The data are transformed back into the time domain for further processing and display after filtering.

Velocity determination – The conversion of a time scale to a depth scale, generally requires the accurate determination of a single averaged velocity for the profile. Whereas for common civil and military radar applications this velocity is simply the speed of light in air (0.30 m/ns), GPR requires the determination of an electromagnetic propagation velocity within the sub-surface. Most applications use a statistically averaged radar wave velocity through a medium similar to that found *in situ*. It has been found that a reasonably accurate determination of velocities is from the analysis of hyperbolic reflections in the data caused by discrete subsurface objects such as corestones and boulders (Francké and Parkinson 1999; Annan and Cosway 1992). The angle of the asymptotes of these hyperbolae gives an accurate indication of the RMS radar velocity at the location of the object. At the Goro site in New Caledonia, a series of vertical radar profiles (VRPs) were acquired to carefully examine the velocity distribution with depth at that site (Section 6.4).

***fk* migration** – In regions of closely spaced corestone and boulders, hyperbolic diffraction patterns merge and become a complex texture when such diffractions are superimposed. To minimise or eliminate this effect, a process of data migration is used. Migration is a process that collapses hyperbolic diffractions by summing the reflection energy of the hyperbolae into a single point or region at the apex of the original hyperbola. Using migration, individual corestones and boulders are better resolved, and an indication of the density of corestone occurrence as well as the general texture and depth of weathering of the bedrock is also better indicated. In theory, *fk* migration also moves dipping reflections to their proper spatial position. *fk* migration is a fast, effective migration algorithm that is performed in the *fk* (frequency-wavenumber) domain. The velocity profile for each line is used in the migration routine.

Depth conversion – The conversion of the radar data profiles from a time scale to an approximate depth scale, using velocity profiles, is particularly difficult. Commercial software does not compensate for vertical and lateral variations in radar velocity, for example between regions of chalcedony and weathered dunite. Although a number of attempts were made to construct software specifically for this research to compensate

for lateral variabilities in the radar velocities, none were stable upon execution. Thus, a constant velocity was utilised for depth conversion of the radar data. This velocity was based on the correlation of the weathering limits as noted in the radar data to those indicated by boreholes. An estimate of velocity was also made based on the hyperbolic diffractions of isolated corestones within the weathered dunite. The two methods of velocity estimation agreed to within ±15%. However, it is noted that the values used for the radar wave velocities are estimates at best. It is believed that these values are sufficiently accurate for the purposes of the research. At the Goro site in New Caledonia, vertical radar profiles surveys were conducted within boreholes to provide a direct measurement of the radar velocities at that site. A discussion of this method is covered in Section 6.4.

Editing and application of elevation static corrections – Surveyed elevations of the radar lines were provided by survey crews. From this information, slices were made of the topographic grid along survey lines to provide *x y z* coordinates at various points along each line. The elevation data were then extracted by cubic spline interpolation to produce an elevation at every radar trace. Individual traces were then shifted upwards or downwards to match the topography.

Grid conversion and transference to display software – Each radar profile is effectively a two-dimensional grid of discrete values which each corresponds to a trace sample point. Once processing is complete, profile grids are then translated into commercial plotting and data display packages using conversion software written for this research project. For this project, Surfer® from Golden Software of Colorado was used for interpretation purposes. Using Surfer®, data sections were generally created at a horizontal scale of 1:1000, with no vertical exaggeration. Once the radar data were transferred into the Surfer® package, a colour scale was used for each type of data. The colours for the radar data were selected so as to best enhance interpretability. Alterations in the colour scale would not, however, affect the final interpretation.

Final presentation of the GPR datasets was performed utilising the CorelDRAW® 9 software package. CorelDRAW® contains a number of features that simplify presentation of radar data, and allows the plotting of large, custom-length pages.

4.5 GPR Data Interpretation

The first phase of processing GPR data from a laterite site is generally culling the voluminous borehole and interpolated geology information provided by the property owner to contain succinct information pertinent to the GPR data.

When the GPR data are viewed in real amplitude, a "surface down" interpretation approach is used in the interpretation, in which the real reflections and artefacts are identified consecutively downwards from the first event. The primary objective of this interpretation is to map the weathering profile of the laterite.

The first events visible in the section are usually artefacts, which result from the unfiltered remnants of the prominent antenna ringing and also from direct arrival air wave bands occurring in the first few metres. In areas with sufficiently strong reflections from shallow rock (less than 3 - 5 m) the reflections are strong enough to overcome the interfering bands and show as distinct reflections.

In general, the region below the horizontal banding is a relatively featureless zone of low amplitude and low frequency radar reflections that occurs in the part of the section interpreted to represent laterite or weathered peridotite.

Immediately beneath the laterite and weathered saprolite region is an area that, on the raw data profiles, is represented as a strong pattern of superimposed arches. Once the data are migrated, these arches collapse into point sources. This zone is interpreted to represent the region of corestones and boulders atop unaltered bedrock. This interpretation has been confirmed by correlation of these "speckles" to exposed rocky saprolite at selected test sites, such as the Loma de Níquel deposit in Venezuela and the Celestial Property in the Philippines.

The radar data usually clearly indicate the zone above the unaltered bedrock contact, as well as the general texture of the bedrock. Relatively unaltered bedrock is generally displayed as a featureless zone of low amplitude, high frequency data near the bottom of the profiles. The precise basis for interpretations made on radar data acquired at each site studied is outlined in Chapters 5 through 7.

Generally, there are more features visible in the radar data than can be easily interpreted using digitised lines. The richness of the information in the radar profiles can be distracting. In particular, although the region of bedrock weathering is clearly defined, it is difficult to assign it a line-interpretation. A single digitised line that best represented the transition zone between the interpreted weathered material and the unaltered bedrock is placed on each profile. The colour of this line is selected so as to not bias the view, while maintaining visibility. It should be emphasised that this interpretation is strictly an indication of the occurrence of objects (corestones and/or weathered bedrock) that are on a scale similar to the minimum resolution of the antennas utilised. That is, a discrete object is required to have a reflecting length in the order of the Fresnel zone to be imaged by the radar antennas. Fortunately, corestones in most lateritic environments are not generally greatly disseminated, and commonly occur in somewhat cohesive units.

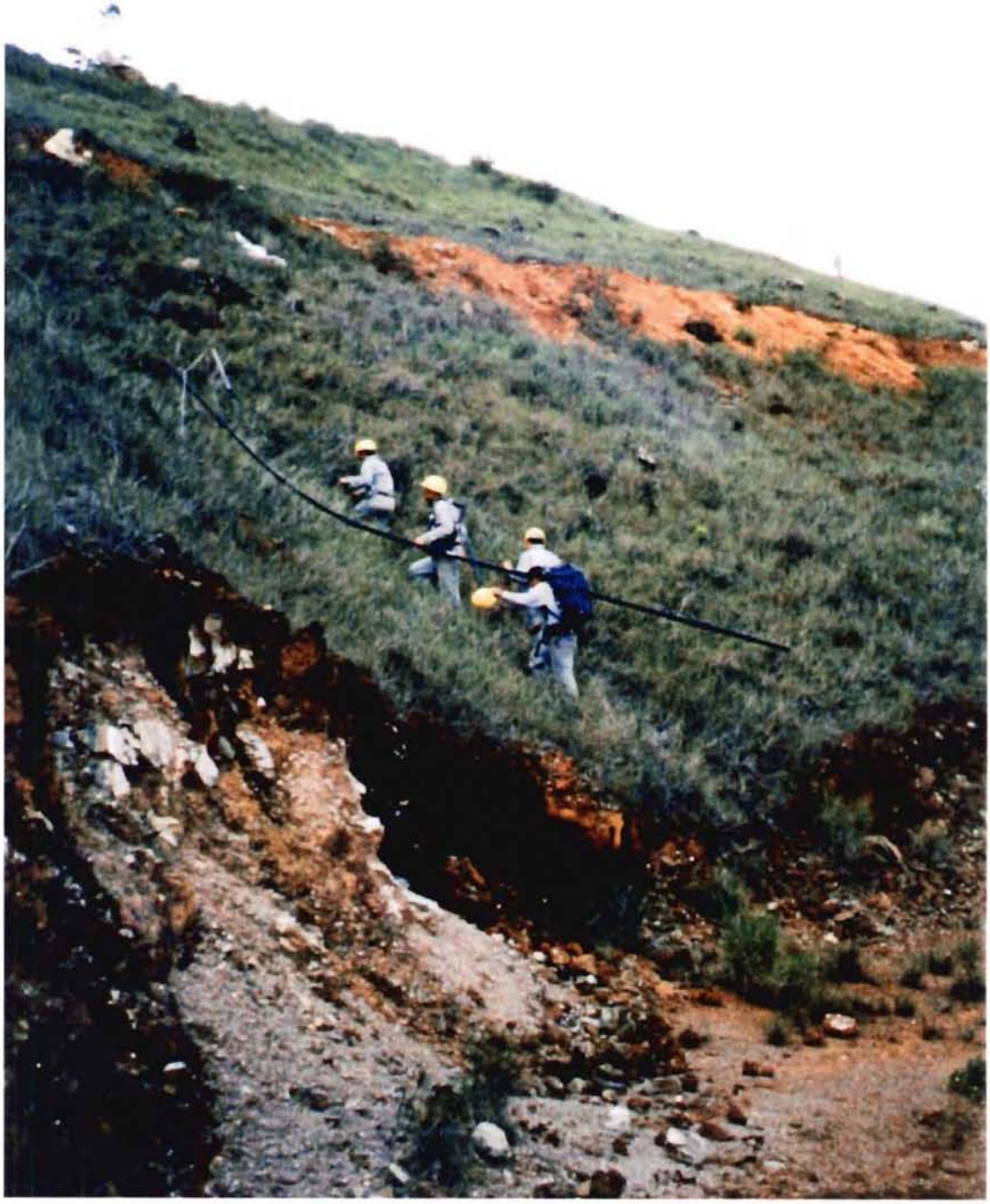

Deep radar profiling with the 12.5 MHz antennas in Venezuela.

5 PRELIMINARY GPR TEST SURVEYS

Based on the theoretical suitability of GPR in lateritic environments, a series of test surveys were performed at a number of laterite sites. These surveys determined the viability of the technique in a wide variety of humid lateritic conditions. The following examples are arranged to illustrate the utility of GPR for delineating specific geological features and targets.

5.1 Mapping of Rocky Saprolite Interface: Ramu (Papua New Guinea)

The first GPR survey in laterites was performed on a commercial basis for Highlands Pacific Limited of Brisbane, Australia at their Ramu Nickel Laterite Prospect in the Madang Province of Papua New Guinea.

Figure 5.1 – Location of Ramu.

5.1.1 Geological Setting

The Ramu nickel laterite deposit is located in the foothills of the Bismarck Range of Papua New Guinea (Figure 5.1). The deposit lies within the Marum Basic Belt, a Miocene ophiolite complex consisting predominantly of gabbros and dunites with lesser amounts of pyroxenites and harzburgites. Ramu is underlain by variably serpentinised and weathered dunite and peridotite that has been strongly uplifted and extensively tectonically faulted to form plateaus, ridges and valley systems. Weathering of the dunite and peridotite produces a profile typically comprising of red limonite, yellow limonite, rock-free (earthy) saprolite, rocky saprolite, and bedrock (Figure 5.2). Locally any or all of the layers, excepting bedrock, may be absent.

As in most wet tropical laterites, one of the principal difficulties in producing a reasonable resource / reserve estimate for the Ramu deposit is the short-range variability of the ore thickness. Local 25 m by 25 m drilling grids demonstrated that nickel, and to a lesser

Figure 5.2 – Ramu weathering profile.

degree cobalt, could be adequately measured by a 100 m by 100 m drilling grid. However, the project's Resource Geologist determined that at this grid spacing, estimates of the mineralisation thickness (and thus tonnage) would not be acceptable for classification of the resource in the measured category.

5.1.2 GPR Exploration

To address the problem of variability in the thickness of the laterite cover, a seismic refraction test survey was performed by a previous property owner at Ramu during the 1970's. The results of this survey were inconclusive, and yielded little additional information beyond that garnered from test pits and boreholes. Possible reasons for the unsuitability of the seismic technique at Ramu include the frequently occurring steeply dipping rocky saprolite interfaces within the weathering profile that may violate the principles of seismic refraction. Additionally, seismic refraction data often produce inconclusive results in regions of gradational lithological interfaces, such as the poorly defined bedrock interface at Ramu (Parkinson 1998). Highlands Pacific subsequently conducted a review of several geophysical methods, and suggested that ground penetrating radar was the method most likely to provide results suitable for use in a resource estimate (Queen *et al.* 1998).

Two large GPR surveys were undertaken at Ramu. A number of antennas were tested, including 100 MHz, 50 MHz, and 25 MHz. Although suitable for the application, 12.5 MHz antennas were not tested due to their extreme length and the associated logistical difficulties of production surveying in dense tropical jungles. Based on a number of criteria, namely ease of acquisition, profile resolution and adequate depth penetration, the 25 MHz antennas were selected for production surveying.

An initial test survey was performed on six lines at Ramu with the 25 MHz antennas. The data from these lines were examined using the traditional wiggle-trace display, as has historically been standard for radar data. These data (Figure 5.3), demonstrate the difficulty in interpreting the raw profiles. Although there are subtle changes in the amplitude and frequency of the raw data, distinct interfaces that may be correlated to the rocky saprolite or the bedrock are absent.

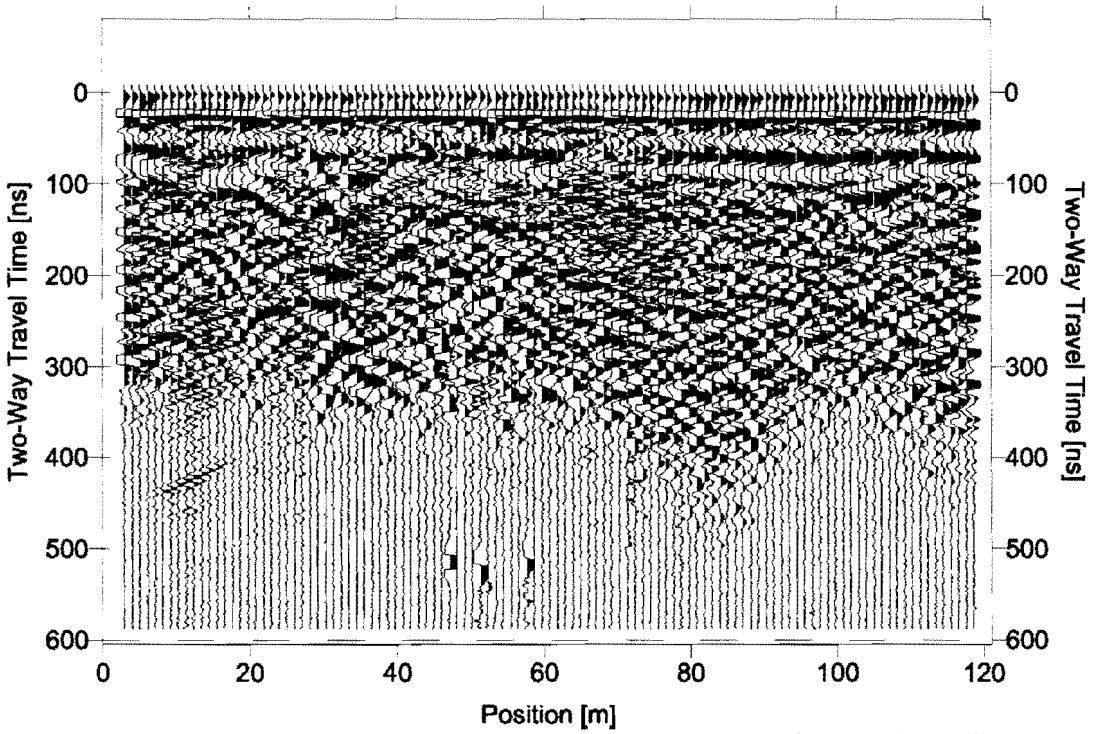

Figure 5.3 – Raw radar data from Ramu.

The processing applied to the Ramu data was relatively unsophisticated, and involved editing, position correction, and a large AGC window. As discussed in Section 4.4, with AGC, each sample in a trace is gained according to the average absolute amplitude of a moving window centred about the sample. The size of the moving window is defined by the size of the AGC window, which may be fine-tuned to enhance the interpretability of a radar dataset.

By using a large AGC window of approximately 400 ns, a number of features became apparent. The same data as shown above are displayed after processing in Figure 5.4. A region of high amplitude data is evident as two pinnacle structures that are particularly

evident to the left of the profile. The upper limit of this region correlates nearly perfectly with the occurrence of rocky saprolite in the drill cores. In addition, regions of the data where this feature is seen to approach the surface between positions 80m and 120m correlate with obvious outcroppings from site observations.

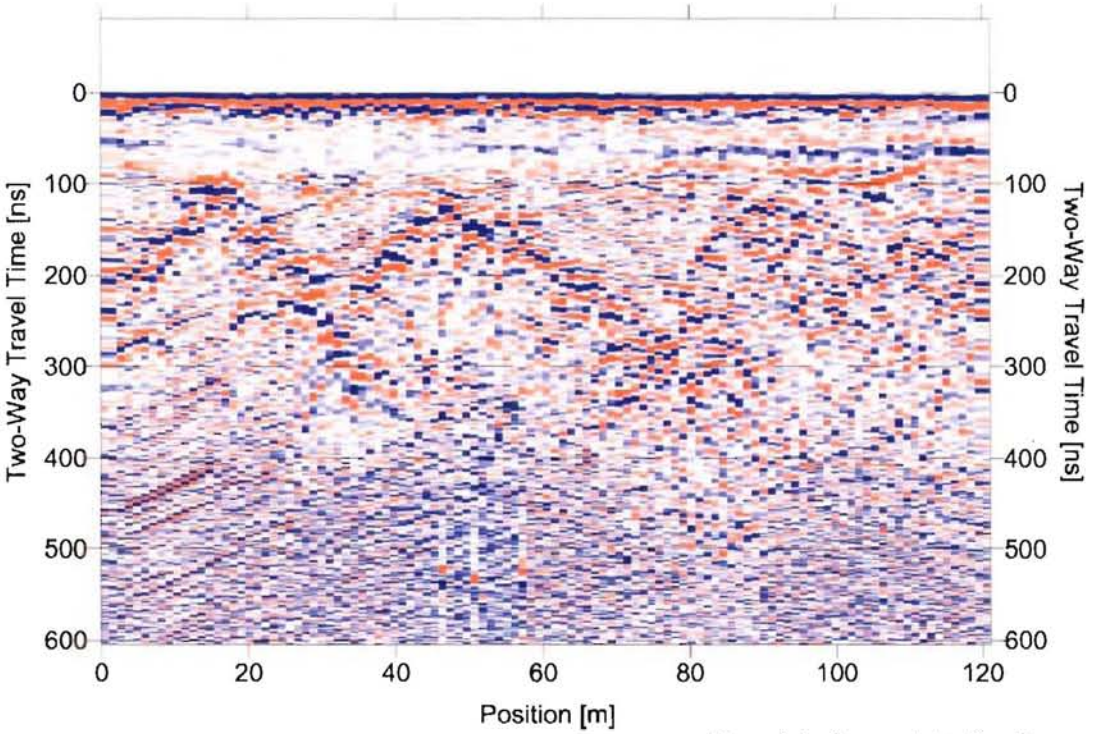

Figure 5.4 – Processed data from Ramu.

An analysis of the six lines acquired during the test survey indicated that as predicted, the primary geological properties which were found to most significantly affect electrical impedance in the weathering profile were those associated with changes in water saturation, along with variations in media porosity and permeability. Water content has a strong effect on the dielectric coefficient of soils, affecting the electrical component of impedance. Variations in porosity and grain size may be also contributors to this effect. The red and yellow limonite overburden are porous media with high water content, and are thus characterised by relatively low radar wave velocities. Rocky saprolite generally has a very low water content, and therefore has significantly different electrical properties than the earthy saprolite. As a result, the rocky saprolite horizon provides an ideal reflector for radar waves.

The top of the rocky saprolite is marked by a sharp rise in the unweathered rock content. The red and yellow limonite, as well as the rock-free saprolite, contains only rare isolated cobbles. Once the rocky saprolite is encountered, the rock content rapidly rises to roughly 30% by volume. It is the contrast between the rock-free material and rocky material that the GPR has proved most able to map at Ramu.

These data have demonstrated that once appropriate processing steps are applied, the GPR data can be used to define the top of the rocky saprolite. Examination of the GPR data indicates that 95% of the GPR depth interpretations agree within 7% of the depths found by drill holes. Of the holes where the GPR shows the top of rocky saprolite to be significantly shallower than the drill results, over half of these discrepancies can be attributed to remnant siliceous water-excluding breccias occurring in the saprolite at the depths picked from the GPR profile (Figure 5.5).

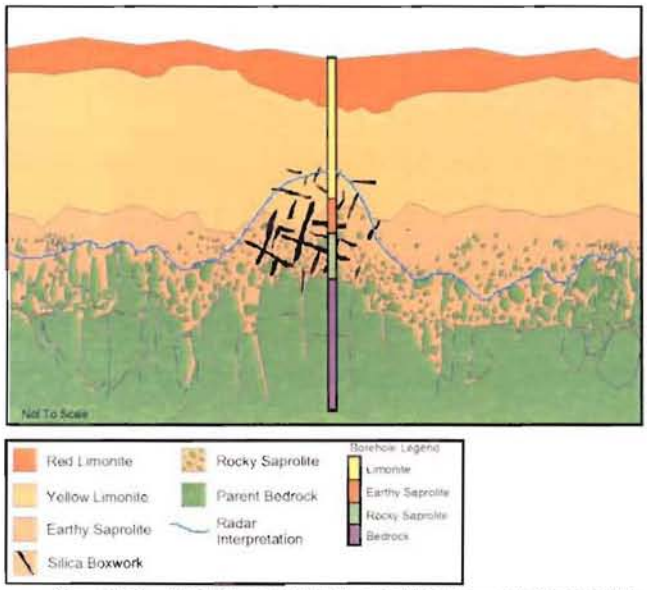

Figure 5.5 – Misinterpretation due to silica boxwork in saprolite.

A second condition known to cause interpretation problems exists in small portions of the deposit where the rock-free laterite thickness is greater than 35 m. Beyond this depth, insufficient radar energy is usually reflected from the rocky saprolite boundary to produce a coherent reflection (Figure 5.6). However, this second condition has little consequential impact on the reserve estimate, as an estimate based solely on the geophysical data would be prone to underestimation of the laterite depth in regions where the depth of weathering exceeded the penetrability of the radar.

The success of GPR in mapping the rocky saprolite boundary may be attributed to the homogeneity of the overlying limonite. Another factor contributing to the deep GPR penetration seen at Ramu is that the high permeability of the limonite allows it to be well leached of any conductive salts by the region's high rainfall.

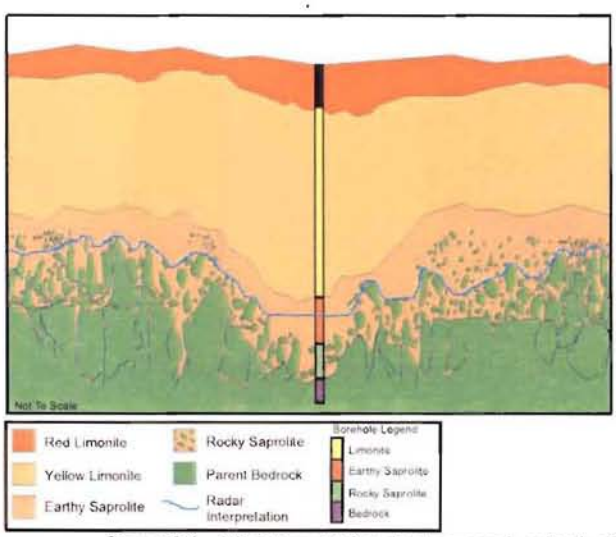

Figure 5.6 – Misinterpretation due to excessive depth of weathering profile.

Despite some limitations, it is evident that GPR is a more effective method of defining the top of rocky saprolite than a linearly interpolated model derived from drill hole data alone. Due to the accuracy in the definition of the top of the rocky saprolite, and the excellent horizontal control over surface variability given by the one-metre sample interval of the radar along the survey lines, Highlands Pacific felt sufficiently confident to classify the yellow limonite and rock-free saprolite in areas defined by the 100 m by 100 m drilling and covered by 100 m spaced GPR lines within the measured category of mineral resource. Based on the interpreted GPR data and the information derived from boreholes, a detailed isopach map was created for a mining block of the Ramu prospect. This isopach map is shown in Figure 5.7, where areas of red indicate shallow regions of the laterite, and blue indicates deeper weathering. This map illustrates that regions of deeper weathering are not always linear, as would be expected by preferential weathering along fault zones.

The GPR data acquired at Ramu were inadequate at determining the depth of the entire weathering profile to the bedrock interface. This may be due to a high attenuation within the rocky saprolite layer.

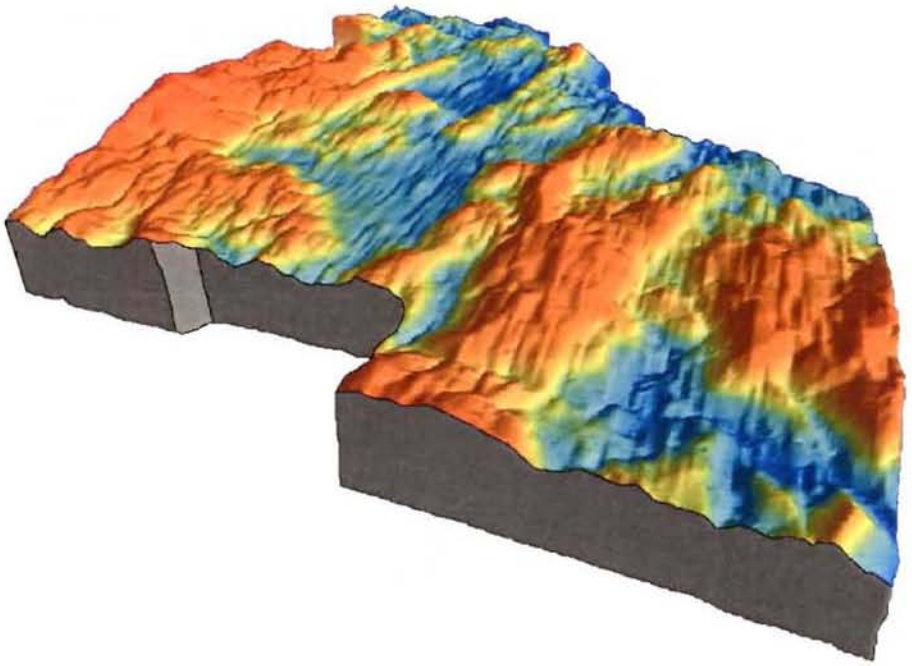

Figure 5.7 – Isopach map produced entirely from GPR data interpretation.

Three example radar profiles from Ramu are shown on Plates 5.1 through 5.3. Plate 5.1, shows the results of a carefully controlled experiment using three different antenna frequencies over the same portion of survey line. This portion of line was selected for its relatively shallow weathering profile, which permitted a direct comparison of the attributes of each antenna frequency. The maximum depth of the rocky saprolite interface on this section of line is of the order of 13 - 15 metres. As is illustrated by the radar data, the higher frequency antennas do appear to provide somewhat enhanced resolution. Due to the relative shallowness of the weathering profile along this survey line, the results are inconclusive regarding the maximum penetration depths of each antenna. It appears that the 100 MHz antennas penetrated the 13 m profile with comparable success to the 25 MHz antennas. As this line was aligned oblique to the borehole grid, no borehole information is available for correlation purposes.

The second example, Plate 5.2, shows a section of acquired line that traverses two pre-existing boreholes. The colour codes for the borehole information have been simplified so that yellow indicates yellow limonite, red indicates red limonite, green indicates saprolite, and blue indicates bedrock. The borehole located near position 30600m shows that the

rocky saprolite interface is encountered at a depth of approximately 8 metres. Similarly, the borehole located near position 30700m indicates rocky saprolite near 12 metres deep. Prior to the inclusion of the geophysical data, the original resource estimate interpolated a linear connection between the rocky saprolite occurrences in each borehole. However, as is clearly evident in the radar data, as well as from cursory surface observation, a wide outcrop of rocky saprolite exists between approximately positions 30660m to 30680m.

The excellent depth of investigation of radar energy achieved in the areas of the undisturbed weathering profile contrasts dramatically with an almost complete lack of depth penetration in areas of alluvial and lacustrine materials located at specific areas within Ramu, as illustrated in Plate 5.3. The difference in results is attributable in part to the presence of fine silts in the alluvial materials that absorb radar energy. Part of the reason for the relative transparency of saprolite and limonite is their featureless aspect. Little energy is scattered out of the radar beam traversing the limonite enroute to the rocky layer since the materials are quite uniform compared to the often poorly sorted alluvial and lacustrine deposits.

5.2 Mapping of Bedrock Depth and Corestone Distribution: Weda Bay (Indonesia)

It was initially assumed that the shear volume of data acquired at Ramu would provide an excellent insight on the suitability of GPR at laterite sites. However, as proceeding projects would prove, each laterite site, and even individual regions within a laterite site, can often produce highly variable geophysical signatures.

Based on the success of the Ramu project in PNG, a test survey was conducted at Weda Bay Minerals' prospect on Halmahera Island in Eastern Indonesia.

5.2.1 Geological Setting

The Weda Bay deposit is located on the sparsely populated island of Halmahera in the Moluccas Province of Indonesia, 2500 km east of Jakarta (Figure 5.8).

Figure 5.8 – Location of Weda Bay.

The ultramafic rocks in the Weda Bay area are dominated by harzburgite with lesser dunite, displaying a range of textures from massive fine-grained varieties to strongly brecciated and re-cemented types. Serpentinisation is widespread but patchy. The serpentinisation process is very important in the lateritisation of the primary bedrock at Weda Bay because regular and pervasive serpentinisation leads to increased permeability and promotes weathering, whilst bedrock pinnacles and strong corestone development will occur where serpentinisation is less advanced. The intensity of serpentinisation is controlled by the distribution of fractures in the parent ultramafic rock that allows hydrous fluids access to the olivine-rich bodies of the rock

Figure 5.9 illustrates a typical profile of the Weda Bay laterite occurrences. A unique feature of the Weda Bay deposits is the occurrence of saprolitic corestones throughout the weathering profile. These corestones represent less altered and weathered ultramafic rocks, which range in size from small pebbles to boulders several metres in size. They occur at all levels throughout the profile and their presence is largely structurally controlled. Areas of less intense fracturing and jointing will generally display less pervasive serpentinisation with the consequence that the rocks in these regions are less permeable and therefore less susceptible to the weathering process involved in laterite formation. The numerous corestones throughout the weathering profile at Weda Bay are in contrast with the relatively "clean" red and yellow limonites of Ramu.

5.2.2 GPR Exploration

Weda Bay Minerals' primary objective for the test GPR survey was to be able to map the bedrock interface between boreholes during the initial exploration program. The boreholes indicated a highly variable and thus unpredictable bedrock topography.

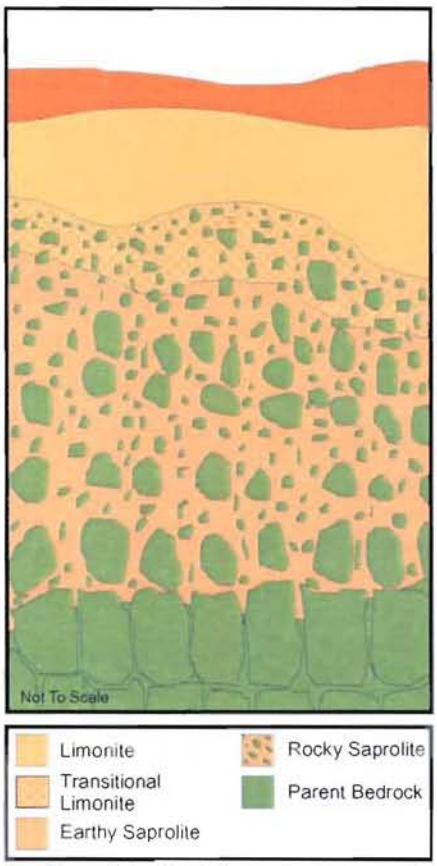

Figure 5.9 - Weda Bay weathering profile.

The Weda Bay borehole information contained information on the percentage of rock found in the core at intervals as small as 30 cm. As expected based on the unique lateritisation profile, corestones ranging in size from cobbles to boulders cause local variations in the rock content of the recovered core. As the boreholes approach the unweathered bedrock interface, the rock content approaches 100%. Based on these data, a rough estimate of the relative distribution of corestones may be made. However, the variability in corestone distribution was too sparsely sampled by the 100 m by 100 m exploration borehole grid to have validity in a reserve estimate. Due to this problem, a secondary objective of the GPR survey was to attempt to classify the relative concentration of corestones on a gross scale along the survey lines.

Approximately 25 km of radar data were subsequently acquired at a number of individual deposits within the Weda Bay prospect. As predicted based on a comparison of geological profiles between Weda Bay and Ramu, the radar data exhibited a significantly different signature. By applying normal AGC gains with a time window of approximately 200 ns, textural changes became evident at varied depths in the radar profiles.

The most pronounced textural change in the data occurred at depths that, once a CMP-derived velocity of 0.075 m/ns for limonite was applied, appeared to coincide with the occurrence of the unweathered bedrock in the boreholes. It was thus interpreted that this textural change was related to the bedrock interface. Although reasonably obvious along most of the radar profiles, in many areas this subtle change in texture became very difficult to interpret.

A more subtle change in the texture of the data was evident in certain areas of the deposit, in the data signature of the weathered laterite zone. It was assumed that regions of larger corestones, or denser concentrations of corestones, would cause more scattering hyperbolas in the radar data, and thus a coarser texture. The lack of strong return signals from the unweathered zone is attributed to the lack of reflecting features once the radar energy encounters the relatively homogeneous parched bedrock.

When compared to the borehole information, the regions of strong reflections correlated well to boreholes that encountered large rocky saprolite corestones. The low-amplitude data at the bottom of the radar sections also correlated well to the bedrock interfaces encountered in the boreholes. However, the subtlety of these textural changes made a comprehensive interpretation impossible.

The example GPR profiles from Weda Bay are included on Plates 5.4 and 5.5. Borehole data have been included that describe the occurrence of rocky material (white black scale) and the associated nickel grades (white green scale). The nickel grade data are included in an attempt to correlate the radar signature with grade variations.

Plate 5.4 illustrates the complexity in geology that can exist between boreholes in lateritic environments. The two bedrock pinnacles imaged on the radar section were undetected by the nearby boreholes A2010 and A2002. Features such as these have direct impact on bench design. Mining benches are created by progressively removing layers of the weathering profile to form a large pit with stepped edges.

Plate 5.4 also shows the variation in texture of the radar data in areas of sparse and dense corestone distribution. A number of isolated sections have been crosshatched on the radar profile to indicate what are interpreted to be regions of denser concentrations of larger corestones. These areas are characterised by stronger reflections that are less horizontally coherent. The interpretation of these areas was greatly assisted by comparison with borehole information, as the textural changes are quite subtle.

Of note on many of the Weda Bay datasets is the presence of a high-amplitude horizontal banding that occurs along the top of the profiles. This banding is not continuous across profiles, but is generally at a constant depth. It is also noted that this banding is loosely coincident with the region of highest nickel concentration. As nickel can be concentrated at or immediately below the active water table, which is known to be at approximately the depth shown on the data sections, it is hypothesised that this coherent reflection is caused by the radar waves encountering groundwater. This reflection is interpreted with a yellow line on the profiles.

A second example from Weda Bay, shown in Plate 5.5, demonstrates the importance of examining the texture of the radar data rather than actual reflectors as is commonly done with GPR data at other sites. The correlation of the radar profile and the borehole information is excellent on this example. A region between northings 54410N and 54450N is clearly shown on the radar to consist of bedrock to surface. Field observations indicate that this area was indeed a bedrock outcrop flanked by laterite.

As seen on the previous example, a strong reflector is shown to undulate at varied depths, close to the surface. Again, this reflector, interpreted with a yellow line, appears to correlate well with the region of highest nickel grades.

5.3 Instantaneous Frequency to Map Bedrock: Loma de Níquel (Venezuela)

It was evident from the Weda Bay results that the most important consideration when interpreting radar data acquired in lateritic environments is not always the real amplitude reflections, but often the subtle changes in texture of the data. These textural changes are only valid if careful controls are maintained during the acquisition of the original data. For example, variations in antenna spacing, the presence of interfering radio signals or nearby reflecting objects, and even ground coupling of the antennas would create changes in the data texture. It was also determined from the Weda Bay data that an objective and consistent interpretation of the texture of radar data is extremely difficult.

Following the Weda Bay project, substantial effort was made to quantify the textural variations seen in the data in order to obtain of a more robust interpretation model. This

was performed as part of the preliminary work of this research project. Textural variations may be quantified by analysing the frequency content of the data. A literature review produced a number of relevant articles on complex seismic trace attribute processing (Tanner *et al.* 1973).

Historically, the standard display for GPR data has been black and white wiggle traces or a common seismic red-white-blue variable amplitude scale. In the latter scheme, areas of large amplitude positive reflections appear red, large amplitude negative reflections appear blue, and low amplitude reflections appear white. To compensate for the dissipation in radar reflection amplitude with depth, an automatic gain control (AGC) function is commonly applied to radar data. AGC attempts to equalise all signals by applying a gain that is inversely proportional to the signal strength. It is important to consider that AGC does not preserve signal strength. Hence, once the data have undergone AGC compensation, reliable deductions can no longer be made concerning the strength of any particular reflector relative to other reflectors.

Previous projects involving laterite sites relied on standard data display and signal gain functions. After much careful observation of historical data, it was realised that far more information may be gleaned from the radar data by analysing the frequency content within small set time windows down each trace, rather than by viewing the AGC amplitudes. Although normal amplitude displays are theoretically superior in imaging individual reflections such as fault planes within the unaltered bedrock, the watertable, or reflections within corestone-free laterite, the transition from saprolite to unaltered bedrock as well as the degree of weathering within the bedrock is somewhat difficult to define. Therefore, a complex trace attribute software package was developed specifically for laterite applications involving GPR data, which examines the instantaneous frequency of the data in two dimensions.

This is accomplished by treating the radar trace $f(t)$ as the real part of the complex trace

$$F(t) = f(t) + f^*(t)i \qquad [5.1]$$

The imaginary part of the complex trace, $f^*(t)i$, can then be obtained by the Hilbert transform of the real part. The weighted instantaneous frequency can then be defined as

$$w(t) = \frac{\int A(t-\tau)w(t-\tau)L(\tau)d\tau}{\int A(t-\tau)L(\tau)d\tau} \qquad [5.2]$$

where $L(\tau)$ is a low-cut filter (Tanner et al. 1973).

In order to utilise the technique and to best adjust individual parameters, a programme was written to rapidly convert real-amplitude radar data to instantaneous frequency data. The results of this program are similar to those achieved with the GRADIX™ software, although there is more control over individual parameters.

The new processing scheme was tested on the Weda Bay data and dramatically improved their interpretability, a new test site was sought which would provide ideal radar acquisition conditions. An ideal site would have featured open planes with few or no trees to provide spurious interference, ample borehole control with a host of geological and geochemical data, and perfect antenna ground coupling due to a lack of jungle undergrowth. After much searching and negotiations with property owners, such a site was found in northern Venezuela.

5.3.1 Geological Setting

The Loma de Níquel deposit is situated in the north of Venezuela, approximately 80 km from Caracas (Figure 5.10). The deposit is located at the top of a mountain ridge. The surrounding hillsides are steep, with slopes averaging between 30% and 70%. The elevation difference between the mine site and the surrounding area is an average of 300 m. The deposit is a mass of serpentitic peridotites with a N70E strike

Figure 5.10 – Location of Loma de Níquel.

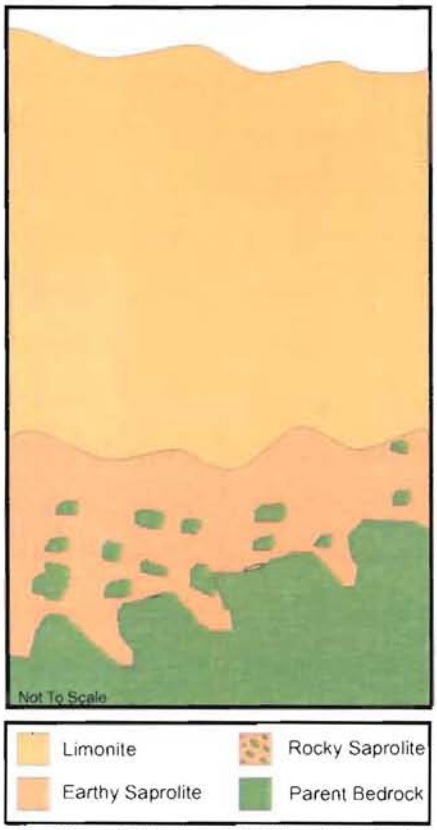

Figure 5.11 - Loma de Níquel weathering profile.

and variable width ranging from 0.7 to 1.2 km.

Boulders and corestones occur in the weathered materials atop the bedrock surface. Structural geology and topographic features control the occurrence of these corestones. The region of corestone occurrence is an average of 1 m thick, and is restricted to the zone immediately above the bedrock interface. A generalised weathering profile at Loma de Níquel is shown in Figure 5.11.

The nickel resource at Loma de Níquel is located within the limonite and saprolite and includes corestones. A significant factor in the mine planning is the bedrock topography, which forms the base layer of the mining benches.

The property owner, Anglo American South America, determined that additional interstitial information was required between their 50 m by 50 m borehole grid for a more complete reserve estimate. The finely-spaced borehole grid shows significant variations in the laterite thickness, as is seen in other deposits. The site was ideal for trials with GPR using the new processing scheme due to the lack of any trees, perfect ground coupling on the smooth surface, and a wealth of borehole information made readily available by Anglo American.

5.3.2 GPR Exploration

A comprehensive survey consisting of 26 km of 25 MHz data acquired at one metre station spacing, along with an additional 6 km of 12.5 MHz data at one metre spacing was completed. Extreme care was exercised during the survey to ensure alignment with the borehole grid and perfect acquisition parameters such as ground coupling and antenna separation

The GPR data acquired at the Loma de Níquel site are generally of exemplary quality. An initial inspection of the data acquired with the 25 MHz antennas during the early stages of the field operation indicated that the estimated maximum depth of penetration was of the order of 35 – 40 metres. To overcome this potential limitation, 12.5 MHz antennas were employed for short profiles along seven lines. However, upon further analysis, it is evident that the maximum penetration of the 25 MHz antennas at the Loma de Níquel site is somewhat greater than was initially estimated, and is possibly in the range of 45 metres. However, the data from the 12.5 MHz antennas served to provide a lower resolution view of areas of deep weathering, which often facilitated interpretation. It is noted that in these areas, the boundary between saprolite and unaltered bedrock consists of a large transition zone. Interpretation of these areas based solely on the 25 MHz antenna data is somewhat more difficult due to the ability of these antennas to image smaller corestones and boulders than the 12.5 MHz antennas. In general, the 12.5 MHz antennas appear better at imaging deep weathering profiles due to their low resolution, which in effect filters out the reflections from smaller corestones and boulders.

Of primary concern during the processing of the radar profiles was the normalisation of the final product. That is, a significant effort was made to ensure that all profiles would be comparable to each other, including those acquired using the 12.5 MHz antennas. Standardisation of the processing scheme was ensured by following a parallel-processing regime, whereby all profiles underwent the same processing steps together.

To demonstrate the effectiveness of the instantaneous frequency method of processing the radar data acquired at Loma de Níquel, three segments of data are shown in Figures 5.12, 5.13, 5.14. The first in the series is a segment of raw GPR data from a survey line (Figure 5.12). Only basic processing has been applied to this line, which includes a dewow filter and simple filters to diminish noise spikes. An examination of the data indicates a number of near-linear horizontal radar events that exist in the first 100 ns of the profile. The first two of these are related to the direct arrivals of radar energy from the transmitting antenna to the receiving antenna through the air (v = 0.30 m/ns) and through the surface of the ground (v = 0.07 m/ ns). The velocity of the upper limonite layer at Loma de Níquel was

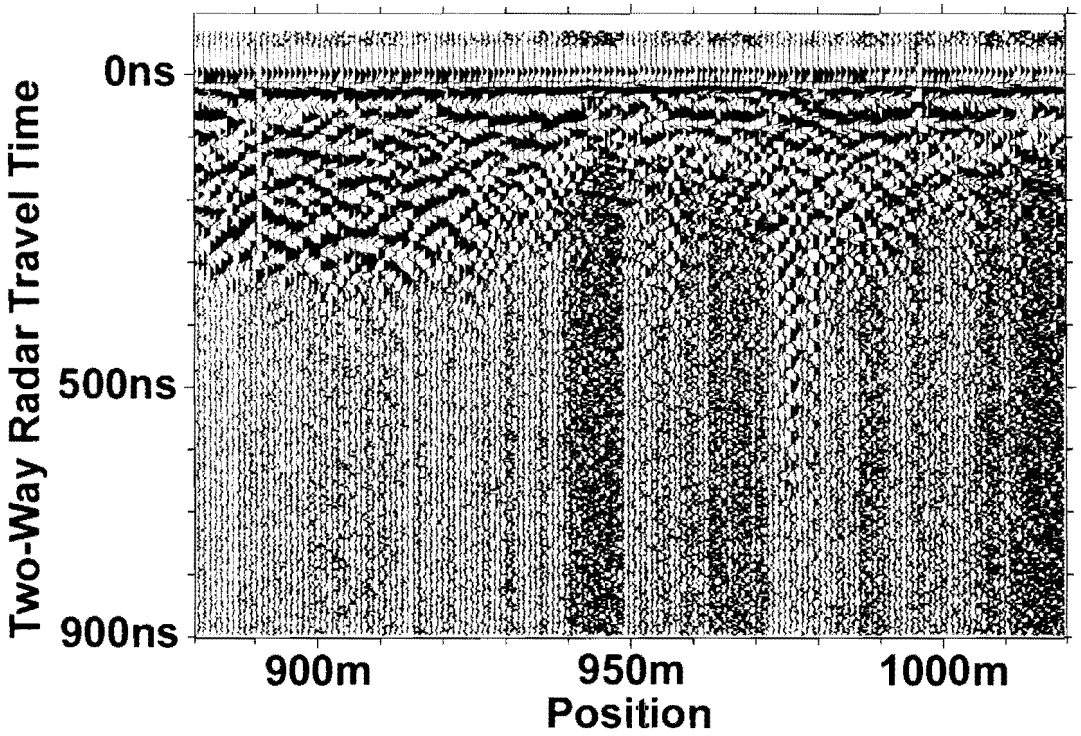

Figure 5.12 – Raw data acquired at Loma de Níquel.

derived from averaging the results of CMP surveys and the correlation of depths with boreholes. The two techniques of velocity determination were in close agreement. The subsequent banding seen in the data profile is related to reflections form the rock-free limonite, and may represent relict bedding from the original parent rock.

Beneath this zone on the raw data profile is a region of high-amplitude, low-frequency scattering with little lateral coherency. This region is interpreted to represent the primary weathered zone of limonite and earthy saprolite. Little evidence of relict structure is seen here, possibly due to the incomplete weathering in this zone, which has yet to cause the full collapse and compaction of the crystalline structure. The region of greatest interest when interpreting the data is the change from the high-amplitude low-frequency data representative of the weathered zone to the low-amplitude high-frequency data in the unweathered zone of bedrock. This feature is readily discernable, but an accurate and consistent interpretation is somewhat difficult. This is particularly the case in areas where the transition from weathered to unweathered material is gradational and extends over a great depth.

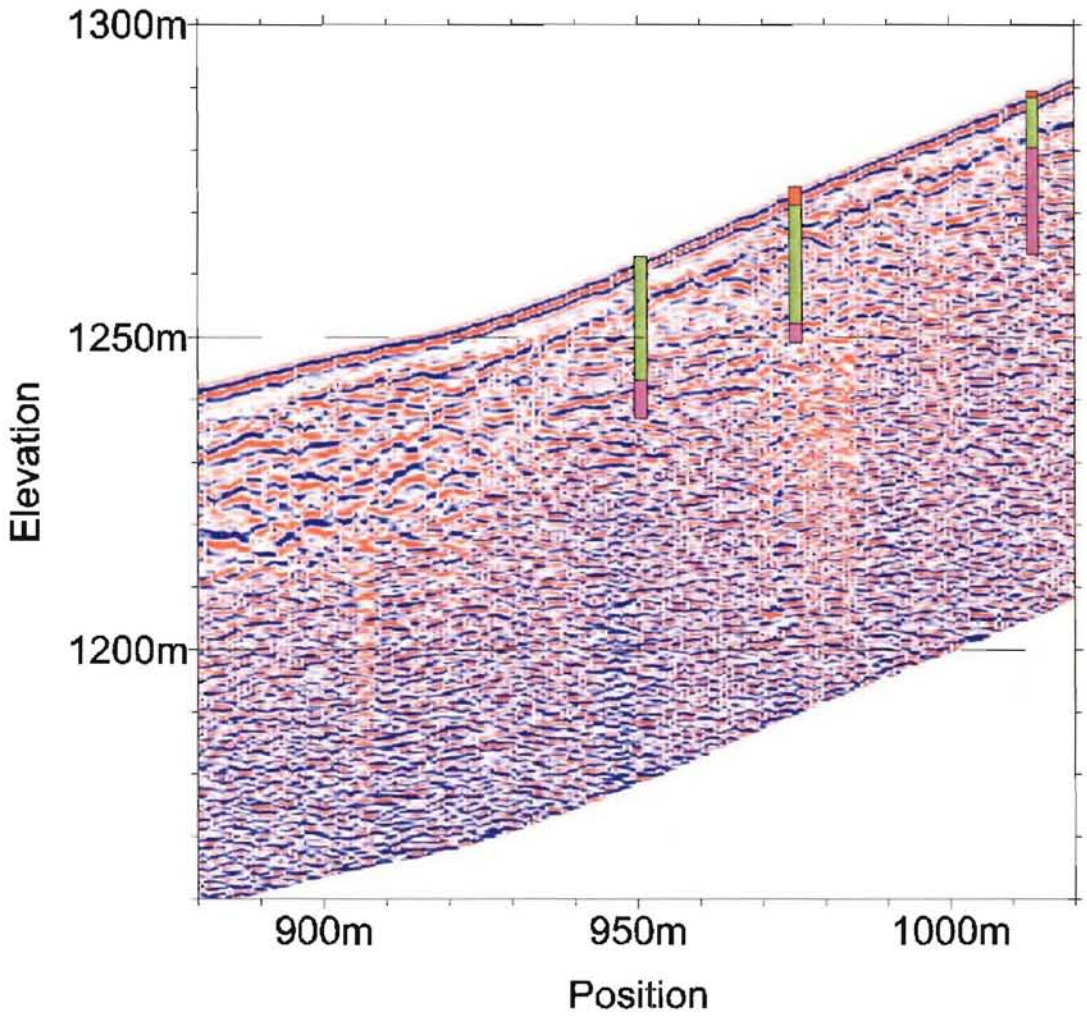

Figure 5.13 – Processed GPR data from Loma de Niquel.

Figure 5.13 shows the same segment of data after depth and topographic correction, using the full processing regime outlined in Chapter 4, and the standard display parameters of a variable amplitude plot. This type of data display is common to the seismic industry and portrays locally high positive amplitude data as being red, and locally high negative amplitude data as being blue.

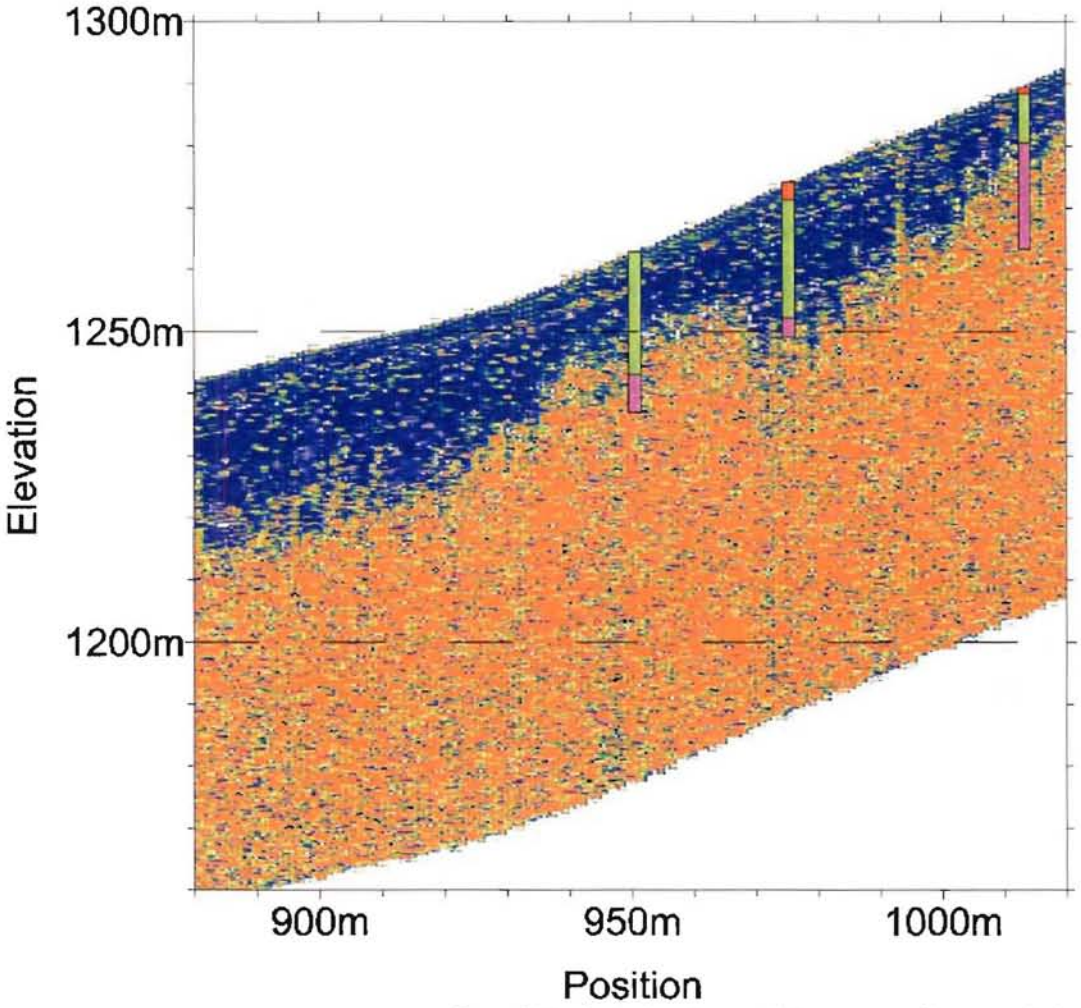

Figure 5.14 – Radar data shown with instantaneous frequency display.

This was the method used in the display of the processed radar data from the two previous test sites at Ramu and Weda Bay. As is shown on the section, the near-linear features close to the surface are still evident, as is the now subtler shift from the high-amplitude data in the weathered zone to the low amplitude data in the unweathered zone.

A simplified log of the boreholes located on this survey line is displayed on Figure 5.13. The red indicates limonite, green earthy saprolite, and purple and bedrock. In effect, the purple zone represents the base of mining at Loma de Niquel. Although there is a correlation evident between the textural change in the data with the bedrock encountered in the data, a comprehensive interpretation is difficult.

When the new processing scheme involving instantaneous frequency analysis is applied to the data acquired at Loma de Níquel, the transition between the saprolite / boulder region and unaltered bedrock becomes well defined (Figure 5.14). Also visible on the instantaneous frequency display are regions of green speckles near the base of the weathered zone. By comparing the real amplitude data with the instantaneous frequency display, a loose correlation may be made between the regions of green speckles and isolated high amplitude events on the original data. Most of these isolated high amplitude events are the processed remnants of strong diffraction hyperbolas, thought to be caused by large isolated rocky saprolite corestones.

The *fk* migration step in processing attempts to collapse these hyperbolas into a discrete point. Thus, a theoretical correlation may be made between the occurrence and density of the green speckled zone in the instantaneous frequency data and regions of large corestones near the base of the weathering profile. This hypothesis was confirmed by examining the incidence of corestones in boreholes, as well as along deep road cuts which penetrated the full weathering profile.

It is evident that the effective use of the instantaneous frequency processing is dependent on the acquisition of data being as consistent as possible. The processing steps preceding this, although enhancing data interpretability, also serve to standardise data profiles in frequency content. Thus little, if any, bias is introduced on a line-by-line basis when interpreting the instantaneous frequency data.

A discussion of the correlation of the GPR data to borehole information should be predicated by mentioning the inherent differences in the material properties identified by each technique. The definitions of rock types (i.e., laterite, saprolite, and bedrock) identified in boreholes are the result of a combination of mining economic criteria and geologic concepts. The geochemical parameters applied to the drill samples are primarily relevant to the percentage iron and nickel concentration in the sample. Laterite is defined in the boreholes as containing greater than 35% iron, and saprolite as containing less than 35%

iron but with a nickel concentration of greater than 0.8%. Bedrock is then defined as the region where the nickel concentration drops below 0.8%.

Nevertheless, the correlation to borehole data was excellent. The radar data correlated to within 10% of the bedrock depth in 93% of the 360 boreholes that encountered bedrock. Due to the volume of geological and geochemical information available at Loma de Níquel, an extensive statistical analysis of their correlation to the radar data is given in Chapter 8.

Four sample profiles acquired at Loma de Níquel are shown on Plates 5.6 through 5.9. Plate 5.6 is one of the most interesting lines acquired. The 25 MHz data indicate a highly variable bedrock topography. To the south of the profile (<740m), the transition zone consisting of corestones and boulders appears to exist from the surface to a depth of approximately 18 metres. The downwards-increasing frequency of corestones is possibly indicated in the radar data by the green speckles in this region of the data. A precise definition of unaltered bedrock is somewhat difficult in this area, as well as in a similar region between positions 980m and 1045m. Between positions 740m and 960m, a region of deep laterite / saprolite cover is shown on the radar profiles. This correlates well with the information from five relevant boreholes in this region, one of which encountered bedrock at approximately 33 metres.

The most interesting feature of this line occurs at position 1060m, where an extremely deep zone of weathering is shown on the radar profile to penetrate into the bedrock. The depth of this preferential weathering cannot be determined, as it appears to be greater than the depth of the radar section (46 m). A borehole immediately adjacent to this feature indicates bedrock at 14 m, although it appears that the placement of this borehole was considerably offset from the centre of the radar anomaly. It was confirmed that this anomaly was not caused by interference or spurious noise, as the segment of line was repeated in both directions many times with the same results. Additionally, adjacent lines indicated a similar feature, although less deep, extending up to 200 metres in a linear alignment. Based on the Fresnel zone minimum-resolution stipulations described in Chapter 4, the detection of a feature as narrow as that shown on Plate 5.6 by 25 MHz antennas is somewhat dubious.

However, the Fresnel zone equations also indicate that the relatively slow velocity of the limonite at Loma de Níquel may have the effect of focusing the illumination zone of the antennas, possibly allowing features such as this to be detected. This anomaly has since been drilled and a deep zone of weathered laterite was encountered. Narrow zones such as these may be exploited during mining as they commonly contain higher nickel grades due to their preferential accumulation of the nickel (Golightly 1979).

The second example from Loma de Níquel is shown on Plate 5.7. While correlation of the radar data from this profile with available borehole information is excellent, of note is a pinnacle feature near position 1062m. This pinnacle rises approximately 17 m and outcrops near an adjacent borehole. This borehole appears to have been offset 10 m from the pinnacle, and thus encountered bedrock at the depth of the surrounding region. Surface observation in the region of position 1062m showed an unusual concentration of rocks in linear arrangement surrounded by rock-free limonite. A second, smaller, pinnacle is visible near position 994m, but does not appear on the radar data or by surface observation to outcrop. Many such features were encountered at Loma de Níquel, and were often confirmed by simple surface examination of the otherwise barren limonite ground. Pinnacles such as these impact on mine planning by both degrading the reliability of the reserve estimate, and, more importantly, affecting the traficability of the site during mining. Relatively subdued bedrock topography is obviously desirable. Mine engineers and planners would determine if these pinnacles can, or need, be removed by mining equipment or blasting, or rather simply mined around.

Perhaps one of the best data sets acquired on the Loma de Níquel project, Plate 5.8 clearly illustrates the extreme variability in bedrock depth as well as the degree of weathering of the bedrock surface. Between positions 750m and 885m, the bedrock appears more weathered with a thicker transition zone. The bedrock signature becomes more homogeneous to the north of position 900m, and deepens to nearly 36 m at the base of the northern ridge. North of this point, the bedrock interface is interpreted to dramatically rise and visibly outcrops at the peak of the ridge. A deep cut made through the ridge approximately 50 m from this line clearly shows a thick transition zone of rocky saprolite that increases in density from the

surface to the interface of the parent bedrock at an approximate depth of 5 m. No borehole information was available to confirm the interpretation of this line.

The next example confirms the correlation of the data acquired with the 25 MHz antennas and those acquired with the 12.5 MHz antennas. Two versions of the same profile are shown in Plate 5.9. The upper profile illustrates the instantaneous frequency plot of the 25 MHz data, while the bottom illustrates the 12.5 MHz data.

The 25 MHz data set correlates well with the available borehole information, although a number of individual boreholes were positioned off-line or were not recorded during acquisition. Along with a more prominent transition between laterite / saprolite and bedrock south of position 820m, a significant shallowing of bedrock is well imaged beneath the top of a surface hill.

The 12.5 MHz data correlate well with those for the 25 MHz antennas from the same line. The data are in general agreement with the relevant borehole information, although none of these boreholes encountered bedrock. The 12.5 MHz data indicate a bedrock contact at or very near the bottom of these boreholes.

The final example from Loma de Níquel illustrates one of the possible shortcomings of the instantaneous frequency method when analysing radar data from lateritic sites. The same 25 MHz data profile as in Plate 5.9 is shown at the top of Plate 5.10 using the instantaneous frequency method. Beneath are the same data using the real amplitude method utilised at Ramu and Weda Bay. A linear feature is clearly evident dipping northwards near the south end of the real amplitude line. This feature is absent on the processed instantaneous frequency data. Using the limonite / earthy saprolite velocity of 0.073 m/ns, this feature is theoretically imaged to depths exceeding 50 m. In actuality, the feature may be significantly deeper, as the velocity of the parched bedrock would be significantly higher than the overlying weathered profile. A number of boreholes in the region have penetrated a fault structure that is coincident with the linear feature seen in the radar data. Although the detection of bedrock faulting is of little consequence for mine planning, such information is important in constructing the geological model of the deposit.

5.4 Laterite Weathering on Extreme Topography at Sechol (Guatemala)

Based on the success of the Loma de Níquel project in Venezuela, a number of other sites were subsequently attempted using similar acquisition and processing methods. One of the more interesting sites examined for a test survey was Chesbar Resources' Sechol prospect. The Sechol prospect occurs in eastern Guatemala near the Caribbean Sea, and approximately 140 km northeast of Guatemala City (Figure 5.15).

Figure 5.15 – Location of Sechol.

5.4.1 Geological Setting

The laterite deposits occur on elongated terraces and summit areas along a belt of ultramafic rocks in the Sierra de Santa Cruz and the Sierra de Las Minas on the north shore of Lake Izabal. The deposits comprise a residual mantle of limonitic soil and saprolite formed through tropical weathering of the ultramafic bedrock in areas where the rate of chemical weathering exceeds the rate of erosion. The extreme topography at the Sechol prospect affects the lateritisation process. The steep slopes appear to promote the weathering of the laterite at rates faster than the lateritisation process, as is evidenced by the near complete lack of laterite on the slope faces.

Throughout most of the deposit, outcrops are scarce and are mostly restricted to roadcuts and major streams, with the exception of the steep slopes on the edges of the survey zone as mentioned above. The degree of serpentinisation and shearing in particular are thought to have a pronounced effect on the rate and nature of laterite development at the Sechol prospect (Harju 1979). A schematic of the lateritic profile at Sechol is shown in Figure 5.16.

5.4.2 GPR Exploration

A comprehensive survey was conducted with lines spaced at 100 m increments. Due to the relative shallowness of the Sechol prospect (average depth 12 m) as compared to Loma de

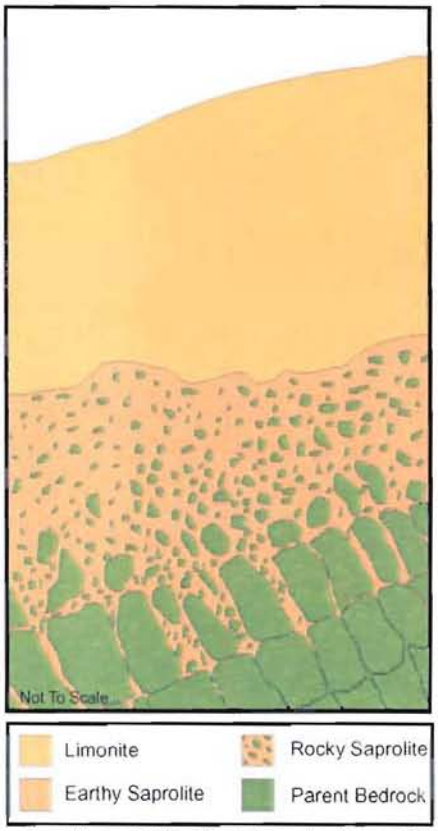

Figure 5.16 – Sechol weathering profile.

Niquel (average depth 22 m), the 50 MHz antennas were employed. Approximately 28 km of data were acquired at one-metre step size across the main part of the prospect. Due to the preliminary stage of exploration, no borehole data and very limited test pit information was available. The radar data were to be used to strategically place new test pits and boreholes in regions of greatest interest or variability in the weathering thickness.

An analysis of the interpreted profiles from the GPR survey indicates a highly variable bedrock topography. The spatial scale of these variations is often on the order of tens of metres. Due to the relatively coarse radar line spacing of 100 metres contour plots based on the GPR interpretation and created using standard gridding algorithms are somewhat mathematically and practically invalid. However, a contour map of the region surveyed showing depth to the interpreted unaltered bedrock was created (Figure 5.17).

The unaltered bedrock isopach map was created by first concatenating the digitised data for the interpreted unaltered bedrock interface from each survey line at Sechol. These data were then gridded using a standard Kriging method with a search radius of 200 metres. The grid created was re-interpolated to a 20 m by 20 m cell size, which is identical to a grid previously created based on the surface elevation contours. By taking the difference between two grids, an isopach map of the calculated depth to the interpreted unaltered bedrock may be made.

A number of interesting features are readily visible on the isopach map. It is evident that the thickest areas of lateritisation occur on the crests of ridges and in the low valleys

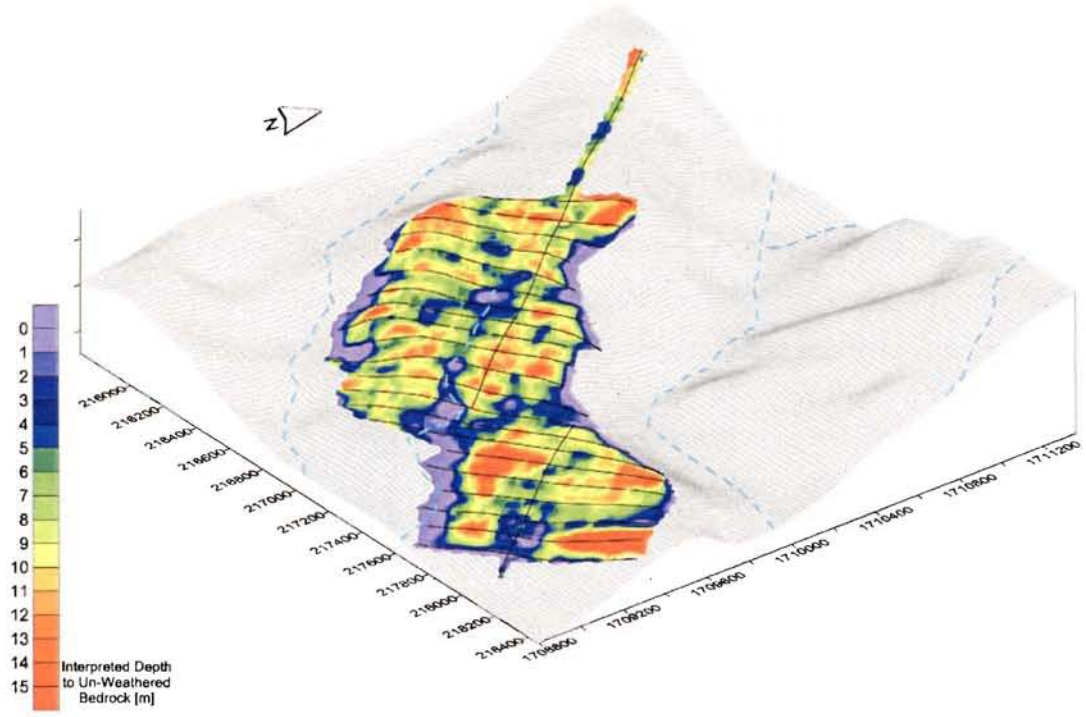

Figure 5.17 – Isopach map created based on radar data showing depth of weathering.

between ridges. The edges of the isopach map, where there are steep slopes, show little or no laterite cover. In addition, a band of thin laterite cover is shown aligned perpendicular to the cross lines. This band is related to a creek that runs through the survey area that has been incised into and eroded away any adjacent laterite. Most importantly, the isopach map illustrates the variability of the laterite thickness throughout the deposit.

A sample of GPR data acquired at the Sechol prospect is shown on Plate 5.11, which illustrates well the dynamics of laterite profiles encountered in steep terrain. As with all lines at Sechol, and indeed most laterite sites with extreme topography, the weathering and transportation process exceeds the lateritisation process on slopes generally greater than 30°. The steep slopes on either side of this example profile have caused any developed laterite to be eroded and transported. The abrupt changes in laterite thickness at 9120E and 9890E indicate the points at which the laterite profile is controlled more by the lateritisation process than erosion. In the field, these points coincided with noticeable breaks in slope. However, the topographic information available was insufficient to resolve this change.

5.5 Mapping Regions of Thick Transitional Zone: Celestial Prospect (Philippines)

5.5.1 Geological Setting

Another site of note where a test survey was conducted is Mighty Beaut Minerals' Celestial prospect. The Celestial nickel prospect is situated in south central Palawan Island, in the southwest of the Philippine archipelago (Figure 5.18). It is located approximately 175 km south of Puerto Princesa. The deposit covers approximately 2,800 hectares, with a variable lateritic weathering thickness. The deposit topography is moderate to rugged. The region of the deposit relevant to this project features gently sloping ridges and mini-plateaus.

Figure 5.18 – Location of Celestial.

5.5.2 GPR Exploration

On review of the geologic information available, the Celestial prospect appeared similar in nature to the Sechol prospect. Both contain a relatively shallow weathering profile with rock outcropping along steep slopes. Based on these similarities, the 50 MHz antennas were utilised.

Again, due to the preliminary stage of exploration, no borehole information was available at the Celestial prospect. However, an extensive grid of test pits had been installed by Might Beaut Minerals. The radar profiles were aligned with this grid and traversed as many pits as possible.

In reviewing the acquired radar data and the provided test pit information, an interesting feature becomes immediately apparent. Whereas on previous sites (with the exception of Weda Bay) the transitional zone of rocky saprolite was somewhat restricted to a thin zone above the unweathered bedrock, the transition zone at Celestial appears to be significantly thicker (Figure 5.19). Although they are much more cost-effective for base level exploration programs, one of the drawbacks of test pits in lateritic environments is that they often fail to reach the base of the weathering profile when they encounter large, immobile rocky saprolite corestones. Particularly in a case like Celestial, these corestones may overlie areas of greater lateritisation beneath. Regions of dense rocky saprolite are indicative of

Figure 5.19 – Celestial weathering profile.

localised zones of parent rock that were resistant to the weathering process and / or of zones of less jointing in the parent rock. Preferential water migration along sub-vertical joints can often weather substantial areas beneath less decomposed zones above.

This thick transitional area of rocky saprolite complicated the interpretation of the radar data acquired at Celestial. Many of the data profiles are dominated by large regions of "green speckles", which have in other projects indicated the presence of large corestones.

Plate 5.12 contains an example of radar data acquired at Celestial. This profile is typical of the radar data acquired at sites exhibiting relatively thick transitional zones. The interpreted bedrock interface is highly variable in depth, with a number of pinnacle structures. Although no topographic information was available to apply to the radar data, the southern end of Plate 5.12 commences near the top of a steep slope, and is shown on the radar data to contain near-surface bedrock. Ten test pits were available for correlation with the radar data along this line. The GPR data indicates that test pits A1, A2, and A3 were each dug insufficiently deep to properly yield an estimate of the volume of weathered material. These pits appear to extend approximately half as deep as the weathering profile shown in the GPR data.

Test pit A4 extended to a depth of 15 m, and was terminated in saprolite. This correlates well with the radar profile, which indicates that this pit reached within a few metres of the unaltered bedrock interface.

Further to the north, test pits A5 through A8 are all in agreement with the radar data, and each was terminated in laterite. Some of these pits appear to have been placed between bedrock pinnacles. Of note is test pit A9, which was terminated in saprolite, yet is shown on the radar data to extend into bedrock. A brief comparison of the radar signature of the bedrock in this region as compared to that along other portions of the profile clearly indicates that the area surrounding A9 has undergone a higher degree of weathering. The geophysical interpretation was made relatively conservative by placing the line signifying the base of the weathered zone atop the interpreted partially altered regions.

An interesting feature rarely seen in lateritic environments is visible near 350N at a depth of approximately 3 metres and dipping to the south. It appears that a linear feature of weathered material is wedged between the corestones of the less-weathered material above, and the unweathered bedrock below. This is most probably caused by preferential weathering down jointing or a fracture plane in the paleo-bedrock surface.

5.6 Mapping of Chalcedony Ribs: Brazil

A final test site bears discussion due to its unique characteristics. A deposit studied in Brazil is unusual due to the occurrence of frequent and thick chalcedonic ridges that traverse a region of the site. A primary objective of the test survey was to determine the location, orientation and thickness of these ridges, as well as the interstitial laterite weathering depths. A specific processing routine was developed in order to best image the chalcedony ribs.

5.6.1 Geological Setting

The deposit is located in central Brazil and is developed over a ridge consisting of peridotite and serpentinised peridotite. The deposit topography is moderate to rugged, and features steeply sloping ridges and mini-plateaus.

The East Zone is situated along the eastern edge of the ridge. The East Zone is similar in nature to that found at many other humid lateritic environments such as Loma de Níquel in Venezuela. The ore forms a blanket parallel to a gently sloping surface, and is covered by a

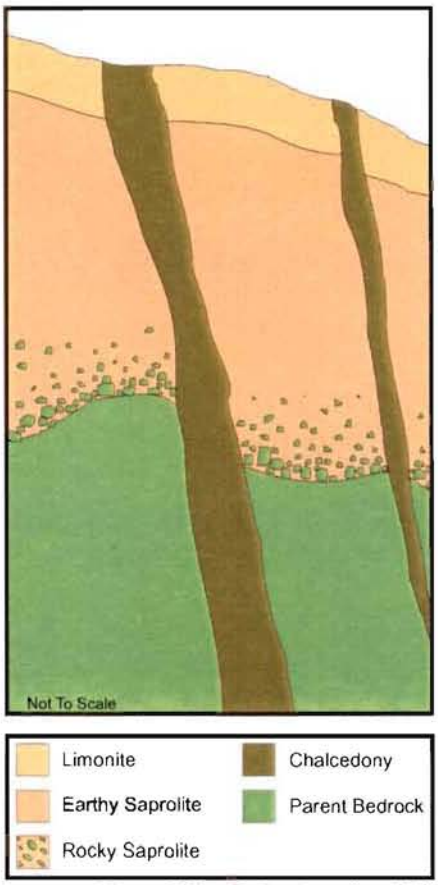

Figure 5.20 – Chalcedony ribs within weathering profile.

few metres of iron-rich overburden. The ore layer varies in thickness from 2 m to 10 m, and grades from a clay-rich top to a rocky bottom.

The West Zone covers the upper portions of the ridge, and is marked by parallel steeply dipping fault zones, which form parallel crests. Silicification follows the fault planes, and each crest is formed by silicified serpentinites in the form of chalcedony (Figure 5.20). The chalcedony is non-nickel bearing. The faulting allows greater fracturing of the serpentinites, while the silicification provides protection against erosion. These factors create favourable conditions for the intense and deep weathering of the dunites with significant accumulation of high-grade nickel.

The weathered dunites situated amongst adjacent zones of chalcedony sheets reach depths varying from 10 m to over 50 m. The widths of the weathered zones vary greatly from a few metres to over 60 m. The ore is fine grained, but contains centimetre to metre masses of silicification and chalcedony.

5.6.2 GPR Exploration

A GPR survey was conducted using the 25 MHz antennas at the site along a series of survey lines that each traversed both the East and West Zones. An initial inspection of the data immediately revealed that although the depth of the weathering profile was easily imaged using the instantaneous frequency display in the East Zone, neither the real amplitude display nor the instantaneous frequency data gave an immediate indication of the location of the chalcedony ribs in the West Zone.

Figure 5.21 – Exposed chalcedony rib.

It was expected that the chalcedony ribs would exhibit sufficiently different dielectric properties than the surrounding laterite to produce a strong radar signature. The chalcedony has a significantly greater porosity than the laterite, but is known to exhibit low permeability, and much of the pore space of the chalcedony is air. Thus, it was expected that the chalcedony would be more resistive than the surrounding laterite.

The best indication of the ability of the radar to detect the chalcedony ribs was given by collecting a series of short test survey lines directly over a 5 m high rib that had been exposed by test mining (Figure 5.21). The raw data from this exercise clearly indicated that the chalcedony had produced a high-amplitude, low frequency response when the antennas were directly atop the rib (Figure 5.22). The response of the surrounding laterite was somewhat opposite to that of other sites, and even the East Zone located a few hundred metres away, in that it was characterised by a generally low-amplitude, high frequency signature. The strong scattering

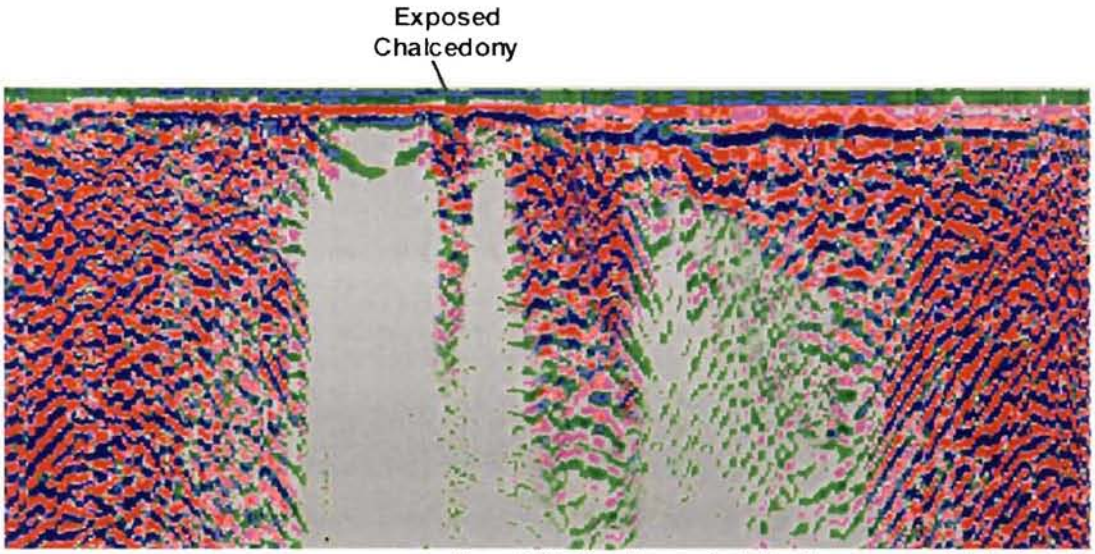

Figure 5.22 – Raw data acquired directly atop exposed chalcedony rib.

seen at other laterite sites and in the East Zone was not evident in the West Zone laterites.

The nature of the near-vertical anomaly produced by the chalcedony ribs on the test line was unexpected. Due to the wave nature of the radar energy and its dispersion patterns, it was assumed that hyperbolic diffraction curves would be recorded as the radar antennas approached and receded from the rib. However, the raw data indicate that the only the actual rib was imaged. This is thought to be, in part, due to the relatively slow laterite velocities found at the site (0.055 m/ns) and their effect on the focusing of the radar illumination zone (Section 4.1).

Upon completion of the acquisition, extensive research was conducted to determine a processing scheme that would enhance the interpretability of the chalcedony occurrences, whilst imaging the weathering profile in the East Zone. A number of discussions with geophysicists involved in the petroleum industry suggested the use of a trace normalising function (Robillard, pers.comm. 2000).

As previously noted, common radar processing techniques involve the application of an AGC gain function to the data. AGC attempts to equalise all signals by applying a gain that is inversely proportional to the signal strength. The AGC gain functions are applied on a trace-by-trace basis, resulting in a normalised dataset with individual traces gained to a pre-set limit. This method often emphasises the coherency and continuity of lateral reflecting events, as is necessary for such projects as alluvial exploration. Laterite environments however, require a gain function that highlights the lateral variability of vertical and near-vertical structures.

A normalised dataset that results from AGC compensation would effectively suppress the lateral variability of the data and inhibit the interpretation of vertical structures. Therefore, a "true relative amplitude" function was devised for the Brazilian data, which considers the average decay curve of the reflection energy for the entire data profile. The gain is calculated by taking the inverse of the average rectified signal amplitude. Since the signal amplitude tends to drop off exponentially, the calculated gain function is usually an increasing exponential curve. The average trace is decimated to a certain number of points

(in this case from 750 points to a more computationally-manageable 500) that provides sufficient smoothing for the inverse operation. The compensating gain is then applied to every trace in the profile, maintaining relative amplitudes, and highlighting vertical structures.

This gain function appears to have been successful in delineating the chalcedony. Due to the resistive nature of the chalcedony, the reflected energy returned to the receiver was stronger than is possible in a lateritised peridotite. It is noted that TRA is ineffective at delineating the depth of dunite weathering, and conversely the instantaneous frequency plots fail to detect regions of chalcedony. Therefore, each radar dataset underwent both processing steps.

The plots of the TRA radar data proved difficult to interpret. To ensure mathematical validity, the application of the TRA process to the raw radar data was performed prior to correcting for topography. The application of TRA to radar data was developed specifically for these data, and some research remains to determine the optimal parameters to best enhance the interpretation. The results of the TRA often yield subtle changes in trace amplitudes that correlate well with the interpolated location of chalcedony as indicated by boreholes. These subtle changes are well imaged in data displayed without topographic correction. However, once the data were draped over topography, the interpretability of the profiles was severely diminished. Therefore, interpretations were performed using both the flat and topographically corrected datasets.

The interpretation methodology for the TRA data involved locating regions that displayed strong positive or negative amplitude reflections, in contrast with the surrounding low amplitude data. The strong positive and negative amplitude regions are shown as bright red and white zones amidst the light blue low amplitude region.

Interpretation of the instantaneous frequency data to map the thickness of the dunite weathering was difficult in areas where a clear distinction between weathered material and unaltered bedrock is absent. In these regions, a conservative approach was used where the

boundary between weathered and unweathered material was placed atop any region of uncertainty.

The instantaneous frequency data were ineffective for mapping the occurrence of chalcedony. Large bodies of chalcedony appear on the instantaneous frequency plots as regions of weathered materials. Using the instantaneous frequency alone leads to ambiguity in the interpretation of the data. It is also noted that due to the effects of processing artefacts on the instantaneous frequency data, accurate interpretations may be impossible within the first four metres of the subsurface.

It is recognised that due to the wave characteristics of radar energy, near-vertical dips are not well resolved in the data. However, the correlation of the radar data with TRA showing the chalcedony occurrences are coincident with 92% of those mapped by the boreholes

The interpretations of the instantaneous frequency and TRA were combined into a separate profile, with borehole information and interpolated geology overlain. This approach to data presentation was made to minimise confusion between different types of processing and the unique features each is able to image.

The example profile shown on Plates 5.13 through 5.16 is amongst the most complex processed for this site. A total of six distinct chalcedony occurrences are imaged on the TRA plot of the radar data. This example profile illustrates well the variability in the geometries of individual chalcedony bodies. The occurrence between positions 5m to 40m appears to be near vertical, whereas that between positions 65m and 125m appears to taper at depth. A similar variability is shown on the remaining three chalcedony bodies.

The depth to unweathered peridotite is shown in the instantaneous frequency as being highly variable. Due to the considerable separation between chalcedony bodies, the depth of weathered material is relatively well mapped. Similar to other lines, the instantaneous frequency plot shown in Plate 5.15 appears to indicate a zone of deep weathering in regions which are known to represent chalcedony as indicated on the TRA profile.

An analysis of the borehole information in comparison to the geophysical profiles indicates an excellent correlation. From the uphill side of the line, BH1 indicates a chalcedony occurrence between positions 10m and 45m. The radar data corroborate this interpolation, but indicate the chalcedony to be somewhat offset from the position shown on the geological profile. It is also noted that a thin (< 2 m) region of weathered peridotite indicated by the borehole was not imaged in the radar section.

A zone of weathered material as shown on the geological profile between positions 80m and 120m is indicated on the combined interpreted radar data as actually consisting of chalcedony. This geometry of the interpreted chalcedony body is consistent with the findings of boreholes BH2 and BH3. Similar to boreholes BH1, a thin region of weathered material shown on BH2is not imaged by the radar.

A chalcedony occurrence interpreted on the geological profile between positions 170m and 190m is shown on the radar interpretations as occurring between 170m and 205m. This interpretation is in approximate agreement with the findings of borehole BH4. A similar interpretation is made regarding the interpolated chalcedony between positions 265m and 300m, where the radar interpretation indicates the body to be somewhat larger than the geological profile.

A minor discrepancy exists at borehole BH8, which is not shown to have encountered chalcedony. The radar interpretations from this region indicate that the borehole was installed near the edge of a 28 m wide chalcedony body.

These initial test surveys showed that the GPR technique can be an effective tool for imaging the weathering profile in a variety of different laterite geologies. However, due to the requirement of these foregoing projects for large acquisition over large areas, further experimentation was required with different radar antennas and parameters in order to better understand the relationship between laterite geology and radar signature.

Mine access roads on a massif in New Caledonia

6 GORO (NEW CALEDONIA)

Two sites were selected to examine in greater detail, the suitability of GPR exploration in lateritic environments. As the utility of GPR has been demonstrated for relatively shallow deposits, as discussed in Chapter 5, two additional sites were selected primarily for their substantial depth of weathering, as well as for their geologic complexity. These sites were surveyed solely for this research project, which permitted experimentation with different acquisition parameters and new techniques of velocity determination. Both sites, INCO's Goro (this chapter) and Falconbridge's Koniambo (Chapter 7), are located on New Caledonia.

6.1 Geological Setting

New Caledonia is an Overseas Territory of France located in the southwest Pacific Ocean. The island stretches approximately 410 km northwest to southeast, and is situated approximately 1300 km northeast of Brisbane, Australia and 1800 km northwest of Auckland, New Zealand. New Caledonia lies near a ridge between the Indo-Australian Plate and the Fiji Plate on an active island arc, and is situated amongst the ultramafic belts of Australasia (Figure 6.1).

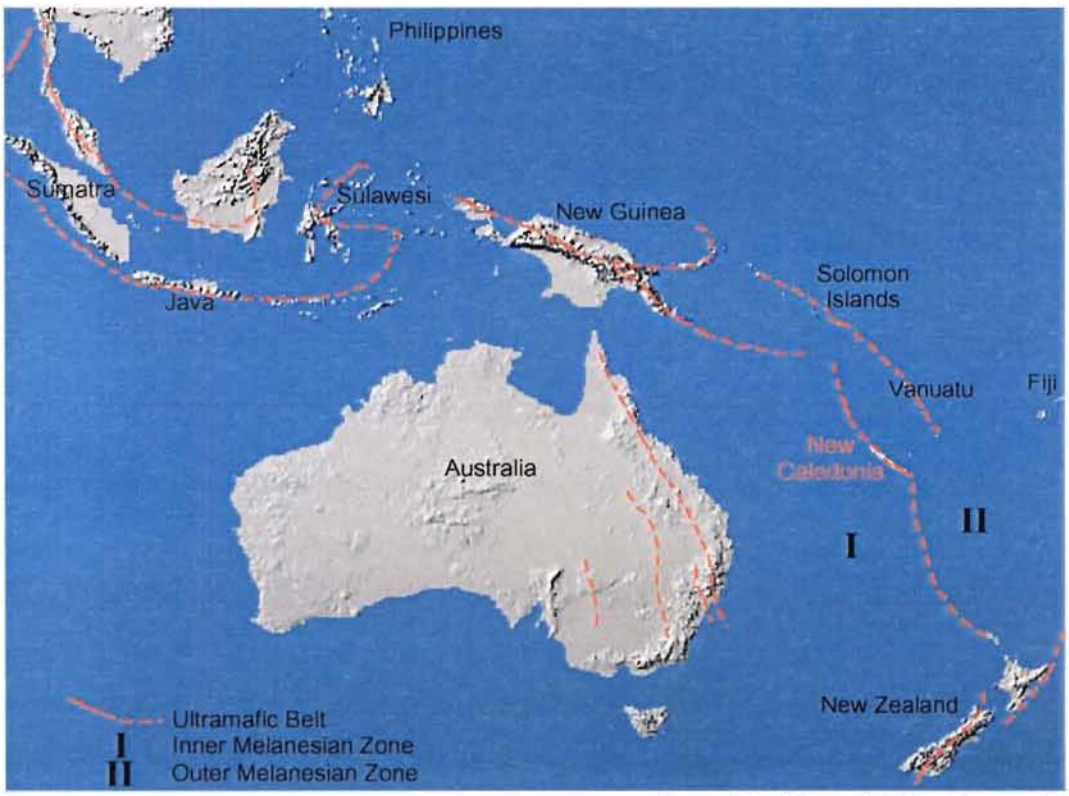

Figure 6.1 – Ultramafic belts of Australasia.

The mineral garnierite, a nickel-bearing magnesia silica, was discovered on New Caledonia by French mining engineer Jules Garnier in 1865. Mining of the garnierite began in 1875. Since that time, New Caledonia has held a prominent role in the world's nickel production. Prior to the discovery of the Sudbury district in Ontario, New Caledonia dominated the world's nickel production. There are more than 300 individual nickeliferous laterite deposits in New Caledonia, which are well distributed throughout the island (Figure 6.2).

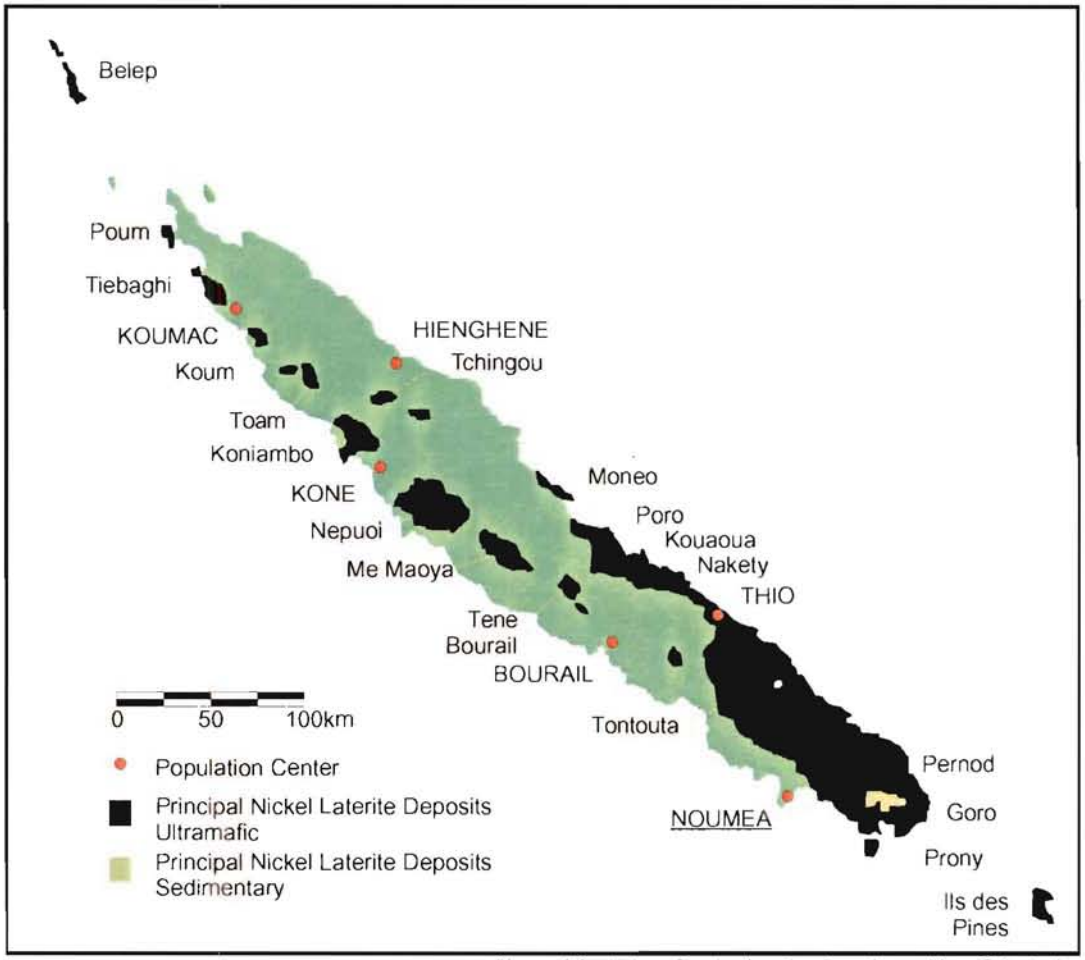

Figure 6.2 – Map of major laterite deposits on New Caledonia.

Nickel laterites on New Caledonia are derived from ultramafic masses that were emplaced in the Oligocene by westward thrusting of peridotites over variable strata. The ultramafic formations extend over approximately one-third of the island. The Southern Massif covers an extensive portion of the southern end of the island. INCO's Goro deposit is situated within this Southern Massif, near the southern tip of the island at 21° 59' S, 166° 32' E (Figure 6.3).

Figure 6.3 – Location of Goro

The weathering process at Goro initiates at the joints and fractures that exist within the near-surface regions of the peridotite bodies. As the alteration process continues, rocky and earthy saprolite is formed when boulders of jointed peridotite are surrounded by the weathered product, which progressively replaces the fresh rock until it has completely dissolved.

The overlying limonite is formed after considerable leaching of the silica and magnesia from the saprolite. The alteration profile is thus divided over time into two primary groups consisting of limonitic material composed of remnant iron hydroxide, and saprolitic material in which the silica and magnesia are the main constituents.

At Goro, the two primary facies may be further subdivided into different horizons. From the surface downwards, the limonitic material is divided into:

- Ferricrete (known locally as *cuisse de fer*)
- Red laterite (*laterite rouge*, a mixture of haematite, goethite, limonite, with pisolites beneath the ferricrete)
- Yellow laterite (*laterite jaune*, primarily limonite)

The saprolitic regions are divided into:

- Earthy saprolites
- Rocky saprolites (a mixture of all proportions of partially decomposed fresh rock and peridotitic boulders)

Underlying the entire weathering sequence is a basement of unaltered peridotite. A schematic representation of the weathering sequence at Goro is shown in Figure 6.4.

The weathering process is primarily controlled by water drainage along joints and fractures in the parent rock. The degree of drainage controls the development of the saprolitic and limonitic zones. In areas where significant drainage occurs, the limonitic zone predominates the profile, with a thin or nonexistent saprolitic zone. Conversely, in areas of low drainage, the saprolitic zone predominates. For the purposes of the test

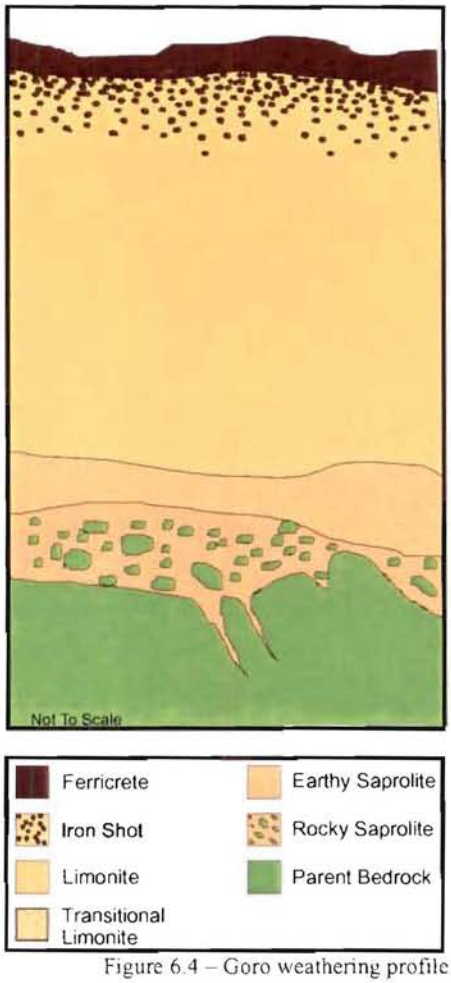

Figure 6.4 – Goro weathering profile

GPR surveys, regions of the deposit with relatively thick limonitic zones were examined. A schematic of a theoretical section of a well-drained plateau at Goro is shown in Figure 6.5.

6.2 Previous Geophysical Investigations at Goro

In recent years, INCO tested a number of geophysical methods for mapping the base of the weathering profile, and the thickness and distribution of the surficial ferricrete layer. The methods used have included transient electromagnetics (TEM), ground and borehole frequency-domain electromagnetics (FEM), seismic refraction and reflection, magnetometrics, as well as ground penetrating radar. From discussions with INCO (King, pers.comm. 1999, 2000), it is evident that GPR and seismic refraction were the most promising methods employed. FEM data were acquired down boreholes with an EM39 system, which yielded information on the electrical conductivities of various facies in the weathering profile. Magnetometrics was not successful, but may have somewhat shown areas of general mineralisation. The work with GPR used 200 MHz antennas to map the thickness of the ferricrete layer. The GPR data acquired were difficult to interpret, but did exhibit some correlation with the known thickness of ferricrete shown in boreholes. Much of the previous work conducted at Goro is of a confidential nature and is not available for discussion in this research project.

Seismic refraction proved the most successful geophysical method to map the base of the alteration zone at Goro. However, seismic refraction is prohibitively expensive, and requires the drilling of shot holes to accommodate explosive seismic sources. The drilling of these blast holes and the employment of a local licensed blaster added to the cost of the seismic survey. Traditional impact sources were ineffective in lateritic conditions due to surface absorption of transmitted waves.

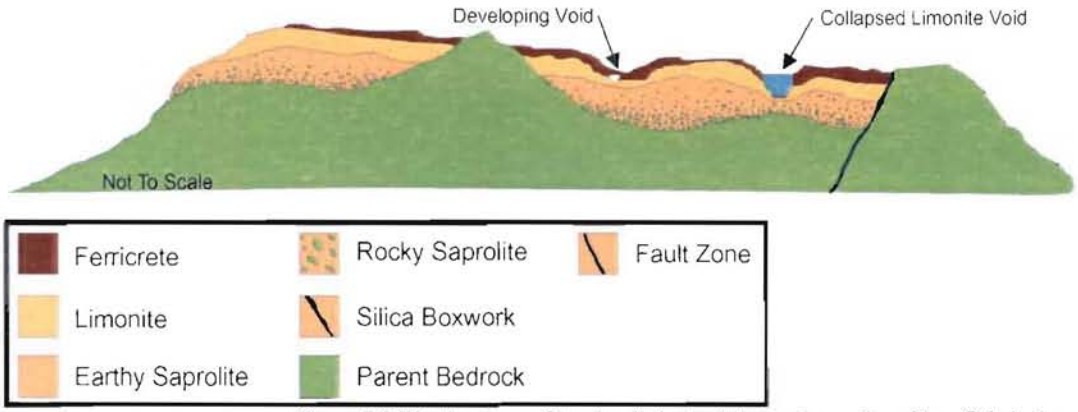

Figure 6.5 Weathering profile of well-drained plateau in southern New Caledonia.

A second series of trials were recently performed using compressional wave seismic surveys at Goro. The seismic refraction survey was reasonably effective in mapping a two layered structure (King, pers.comm. 2000). The deepest layer mapped was generally consistent with the depth to bedrock measured by boreholes. However, in some parts of the survey lines, the deepest layer corresponded to a dense unit within the saprolite zone. Boreholes indicate that these dense units were most probably conglomerations of rocky saprolite suspended within earthy saprolite.

6.3 GPR Survey Line Coverage

During the research project GPR survey, a wide variety of radar antenna centre frequencies were evaluated at the Goro deposit. Antenna frequencies of 200 MHz, 100 MHz, 50 MHz, 25 MHz, and 12.5 MHz were utilised for various portions of the project, with the use of lower frequencies implying larger antennas with somewhat lower resolution but deeper penetration (Table 6.1).

Antenna Frequency	Antenna Length	Wavelength in Air (v=0.30 m/nanosecond)	Wavelength in Goro Laterites (v=0.042 m/nanosecond)	Estimated Penetration at Goro
12.5 MHz	9.6 m	24 m	3.4 m	30 m
25 MHz	4.8 m	12 m	1.7 m	20 m
50 MHz	2.4 m	6 m	0.8 m	15 m
100 MHz	1.2 m	3 m	0.4 m	10 m
200 MHz	0.6 m	1.5 m	0.2 m	5 m

Table 6.1 – Properties of GPR antennas used at Goro.

The GPR lines used for this project followed pre-existing roads, established by INCO for access to rows of boreholes (Figure 6.6). Radar acquisition rates varied widely, according to the antennas used. In general, with the 25 MHz antennas, GPR survey acquisition rates averaged 1.8 – 2.0 km/day. The subdued terrain in the region of the

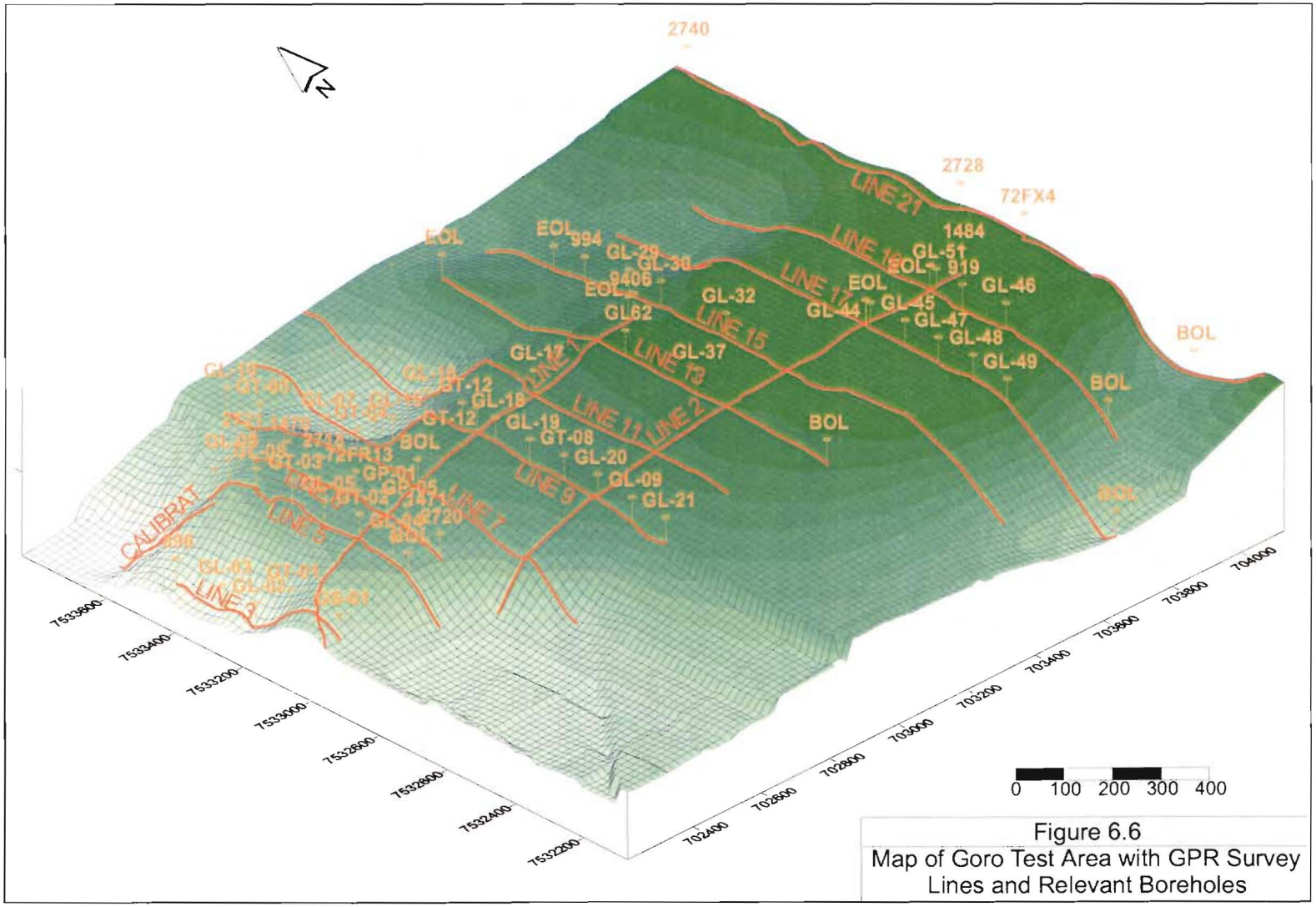

Figure 6.6
Map of Goro Test Area with GPR Survey Lines and Relevant Boreholes

test survey contributed to acquisition rates somewhat faster than usually anticipated at laterite deposits.

Table 6.2 is a summary of the line locations, names, and distances, along with antenna parameters used for each survey line.

6.4 Velocity Determination Using Vertical Radar Profiles

At the Goro site, a relatively uncommon method of accurate velocity determination was used which employs a specially designed borehole antenna. Four vertical radar profiles (VRPs) were acquired at boreholes GL-31, GP-01, GT-10, and GP-49. A VRP involves fixing a standard transmitting antenna at a certain position on the surface and collecting data as a special receiving antenna is lowered down the borehole at known steps. The transmitting antenna is then moved a pre-determined step size away from the borehole, the receiving antenna is hoisted back up the borehole, and the process is repeated. The maximum depth which may be surveyed to is dictated by either the maximum length of the borehole antenna cable (25 metres) or the maximum depth of the borehole. A schematic diagram of the borehole radar acquisition is shown in Figure 6.7. In this way, a "half tomogram" of the velocity structure of the intermediate media between the surface and the borehole maybe constructed and information on radar velocity, attenuation, and dispersion may be produced.

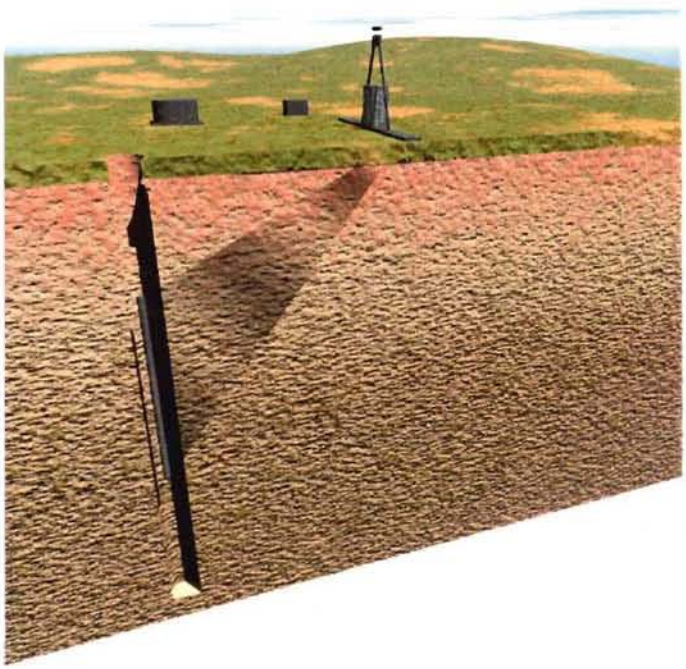

Figure 6.7 – Layout of equipment for VRP acquisition.

The four boreholes surveyed by VRP, GL-31, GP-01, GT-10, and GP-49, were selected because they penetrated the primary units of interest where the radar velocities were anticipated to be most variable: ferricrete, limonite, and earthy saprolite. In each instance, the receiving antenna was lowered at 0.5 metre intervals down the hole while

Line #	Line Name	Frequency	Antennas	From	To	Distance	Comments
1	Mainroad	12.5 MHz	Perpendicular	897	GL90	300	Test 12.5 MHz for mapping bedrock
2	Mainroad	12.5 MHz	In-line	897	GL90	300	Test 12.5 MHz for mapping bedrock
3	Line 6	200 MHz	Perpendicular	GP1	1475	100	Map ferricrete
4	Line 6	50 MHz	Perpendicular	bh1492 – 50m	bh1470 + 100m	500	Compare 50 MHz and 25 MHz
5	Line 6	50 MHz	Perpendicular	bh1492 – 50m	bh1470 + 100m	500	Compare 50 MHz and 25 MHz
6	Line 6	25 MHz	Perpendicular	bh1492 – 50m	bh1470 + 100m	500	Profile rocky saprolite
7	Line 5	100 MHz	Perpendicular	GL04	GT03	600	Map ferricrete
8	Line 5	25 MHz	Perpendicular	GL04	GT03	600	Profile rocky saprolite
9	Line 3	25 MHz	Perpendicular	GS01	896	500	Contains no or little ferricrete
10	Line 7	25 MHz	Perpendicular	1046	997	500	Profile rocky saprolite
11	Line 7	25 MHz	Perpendicular	GL10	997	560	Profile rocky saprolite
12	Line1	25 MHz	Perpendicular	GT12	9406	460	Profile rocky saprolite
13	Line2	25 MHz	Perpendicular	FX4	Line17	400	Test antenna orientation
14	Line 15	25 MHz	Perpendicular	GL32	994	500	Profile rocky saprolite
15	Line 17	50 MHz	Perpendicular		GL48	700	Profile rocky saprolite
16	Line 17	25 MHz	Perpendicular		GL44	700	Profile rocky saprolite
17	Line 17	25 MHz	Parallel		GL48	700	Profile rocky saprolite
18	Line 19	25 MHz	Perpendicular		Line2	500	Profile rocky saprolite
19	Line 21	25 MHz	Perpendicular		Line2	1600	Profile rocky saprolite
20	CALIBRAT	25 MHz	Perpendicular			200	Map bedrock deepening
21	TESTMINE	50 MHz	Perpendicular			50	Map ferricrete
22	BULKSAM	100 MHz	Perpendicular			100	Map ferricrete
23	BULKSAMP	50 MHz	Perpendicular			100	Map ferricrete
24	Line 9	25 MHz	Perpendicular		Line2	400	Profile rocky saprolite
25	Line 17	25 MHz	Perpendicular	Line 2			Profile rocky saprolite
26	Line 2	25 MHz	Perpendicular				Profile rocky saprolite

Table 6.2 – GPR lines acquired at Goro.

the transmitting antenna was moved at one or two metre intervals away from the hole for each spread. The recording geometry at each hole is shown in Table 6.3. The velocity records are presented in Plate 6.11. The data for hole GP-49 contains a horizontal low-frequency signal which appears to have travelled through the air and was possibly caused by a surface reflection. It is also possible to generate critical refraction at the air-ground boundary due to the high velocity in the air.

Borehole Name	Tx Range from BH (m)	Rx Depth (m)	Rx Spacing (m)	No. of Raypaths
GL-31	2.0, 3.0, 5.0, 7.0	1.0-28.5	0.5	228
GP-01	1.0-11.0,15.0,20.0	1.5-28.5	0.5	364
GP-49	2.0,3.0,5.0,7.0	1.0-28.5	0.5	228
GT-10	2.0,3.0,5.0,7.0	1.0-28.5	0.5	228

Table 6.3 - VRP parameters used at individual boreholes.

As is standard procedure for vertical seismic profiles (VSP) used extensively in the oil industry, the first break of the VRP data is plotted against receiver-transmitter separation to obtain velocity information. The first break corresponds to the transit time of the direct arrival of the radar signal propagating through the ground. The results are shown in Appendix A. These time-distance plots are accurate indicators of the velocity structure of the media directly adjacent to the boreholes surveyed. From the results, there appear to be two primary interpretable velocities (Robillard and King 2000):

1. A near-surface velocity of approximately 0.11 m/ns that corresponds to the ferricrete cap, which is generally arid. The ferricrete ranges in thickness from 3-8 m at the borehole locations.

2. A deeper velocity of .042 m/ns that corresponds to the limonite section containing high moisture content.

It is noted that the measured velocity for the limonite section is exceptionally slow as compared to other laterite sites, and is near to that of pure water. A review of borehole information made available indicates that the water saturation of the Goro profile is not exceptional when compared to other laterite deposits.

A parameter of interest when evaluating the radar wave velocity (and thus penetration of the radar energy) is the iron concentration in the ferricrete and limonite. At Goro, the iron fraction in the ferricrete often exceeds 70% (Tessarolo, pers.comm. 1999). While

this is value is not exceptional for laterite sites, iron concentration does have a direct relation to radar wave velocity. Grant and West (1965) suggest that magnetic permeability is proportional to the degree of hydrous alteration (serpentinisation), oxidation state, as well as a number of other parameters. As stated in Section 4.1.2, radar wave velocity and attenuation are inversely proportional to magnetic permeability. A similar effect was observed at an ironsand deposit in New Zealand by Beeching (1999), where the radar velocity in the highly resistive and arid titanomagnetite was unusually low (0.06 m/ns). Resistive and arid media would be expected to exhibit a relatively high radar velocity. Beeching suggested that the high magnetic permeability of the ironsands had caused the low velocity values recorded. No information is available on the relative degree of serpentinisation or oxidation, and thus magnetic permeability, of the upper portions of the Goro profile as compared to other laterite deposits. However, it is hypothesised these parameters may have a significant affect on the radar velocities and penetration at Goro.

To corroborate these velocity data, an analysis of the hyperbolas contained in the GPR profiles was performed using the GRADIX software package. Although not as accurate as the VRP method, this method applied to a number of hyperbolas on different GPR lines appears to substantiate the extremely low velocity of the limonite as determined by the VRPs.

6.5 Radar Penetration Depths

Regardless of the transmitter voltage used, it was noted that the recording time window of 1200 ns used during field acquisition would provide at most 29 m of depth penetration, based on the velocities determined using the VRP technique. However, as stated above, the deepest coherent reflections on the radar data are of the order of 900 ns, or 19 m. In either case, these depths are generally far shallower than required to image the top of the rocky saprolite layer.

An analysis of the parameters necessary to theoretically achieve the penetration sufficient to image the rocky saprolite interface at Goro may be made using generalised principles of the radar range equation, as introduced in Chapter 4. As the penetration depth is directly proportional to output voltage of the transmitter and inversely proportional to antenna frequency, the attenuation curve of the radar system in a specific environment may be found by plotting the signal strength as a function of

Line No	Antenna Frequency	TX Voltage	Maximum time with 25 MHz *T*max*25*	Maximum time with indicated antennas *T*max *f*	Voltage [V] / Frequency [MHz]	$\frac{T\max f}{T\max 25}$
6	200 MHz	400 V	340 ns	130 ns	2	38.2
5	100 MHz	400 V	350 ns	200 ns	4	57.1
6	50 MHz	1000 V	340 ns	250 ns	20	73.5
5	25 MHz	1000 V	350 ns	same	40	100
6	25 MHz	1000 V	340 ns	same	40	100
6	200 MHz	400 V	410 ns	120 ns	2	29.3
5	100 MHz	400 V	350 ns	170 ns	4	48.6
6	50 MHz	1000 V	410 ns	350 ns	20	85.4
5	25 MHz	1000 V	350 ns	same	40	100
6	25 MHz	1000 V	410 ns	same	40	100

Table 6.4 – Maximum penetration (in time) with 25 MHz, 50 MHz, and 100 MHz antennas.

voltage over frequency. In this case, signal strength was plotted as a percentage of the penetration depths achieved with the 25 MHz antennas. Because a wide variety of antennas were used for the same survey lines at Goro to evaluate the effectiveness of GPR, a number of data points may be plotted related to the maximum penetration (latest reflected event detected by each antenna frequency in the datasets) versus the ratio of voltage to frequency. The maximum time picked was based on the maximum depth of penetration for each survey line examined. The last coherent reflection is best imaged in the frequency domain, using the instantaneous frequency conversion discussed in Section 5.3. In the frequency domain, the time at which the frequency spectrum becomes "white", indicating the prevalence of background noise, was picked. This procedure was repeated for each individual data set listed in Table 6.4.

A graph of the relative penetration depth (as a percentage of that achieved at the same point using the 25 MHz antennas) versus antenna frequency is shown in Figure 6.8 for the data listed in Table 6.4. This graph illustrates the exponentially decreasing penetrability of the radar waves generated by higher frequency antennas.

The curve of the ratio of maximum time recorded with 25 MHz antennas to the maximum time recorded with the indicated antennas (as a percentage of the 25 MHz maximum time) versus the ratio of transmitter voltage to antenna frequency is shown in Figure 6.9. As stated above, the 25 MHz antennas and the 1000 V transmitter were selected to represent 100%. The extrapolated values are shown to approach a maximal penetration of approximately 180% of the depth achieved with the 25 MHz antennas, regardless of the antenna frequency or transmitter voltage

.Based on the logarithmic nature of the radar range equation, [4.10], it is reasonable to attempt to fit a logarithmic curve to the plot of signal strengths versus penetration depths at Goro. This logarithmic curve may be then extrapolated to greater depths, again based on the 25 MHz antennas with 1000 V transmitter being 100% (Figure 6.10). This graph indicates that depths greater than 200% of the current depth reached would be difficult using the 25 MHz antennas and 1000 V transmitter. It appears that to achieve the necessary penetration, a voltage-to-frequency ratio of the order of 5000 is required. Due to the logistical constrains of moving antennas longer than the 25 MHz (4.8 metres) along cut lines, as well as the dramatic decrease in resolution with lower signal strength of the order of 100,000 V must be used to reach the rocky saprolite at Goro. As this is not practical using a single 25 MHz antenna, the use of an array of high-power antennas is suggested. For example, such an array may consist of eight 25 MHz antennas placed at half wavelength (approximately 2 metre) separations each radiating 10,000 V.

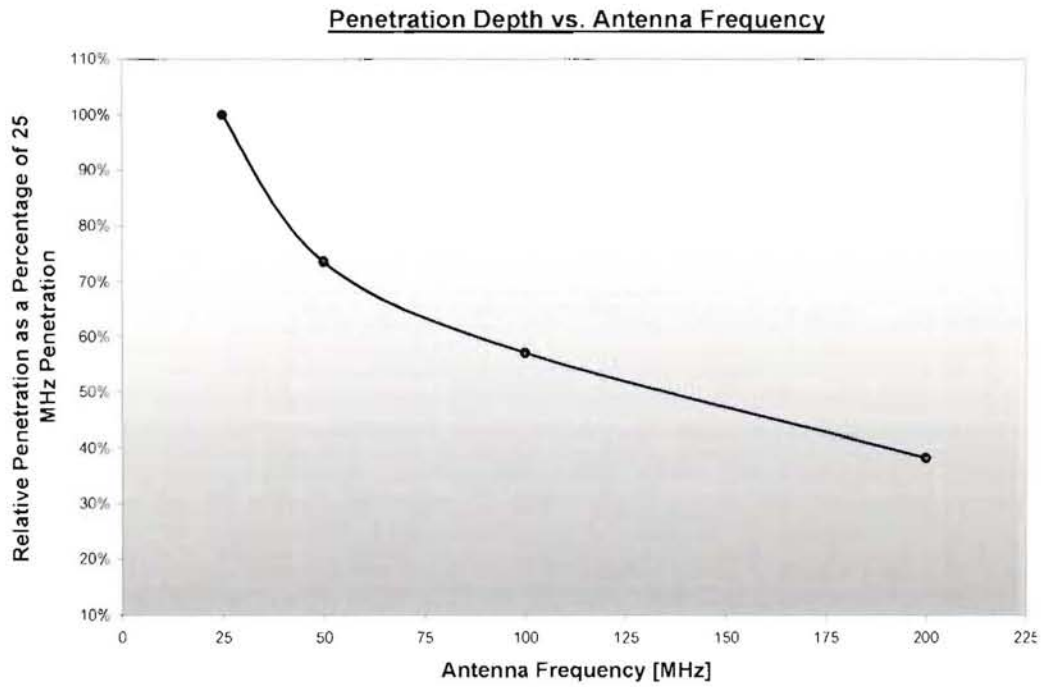

Figure 6.8 – Penetration depth vs. antenna frequency.

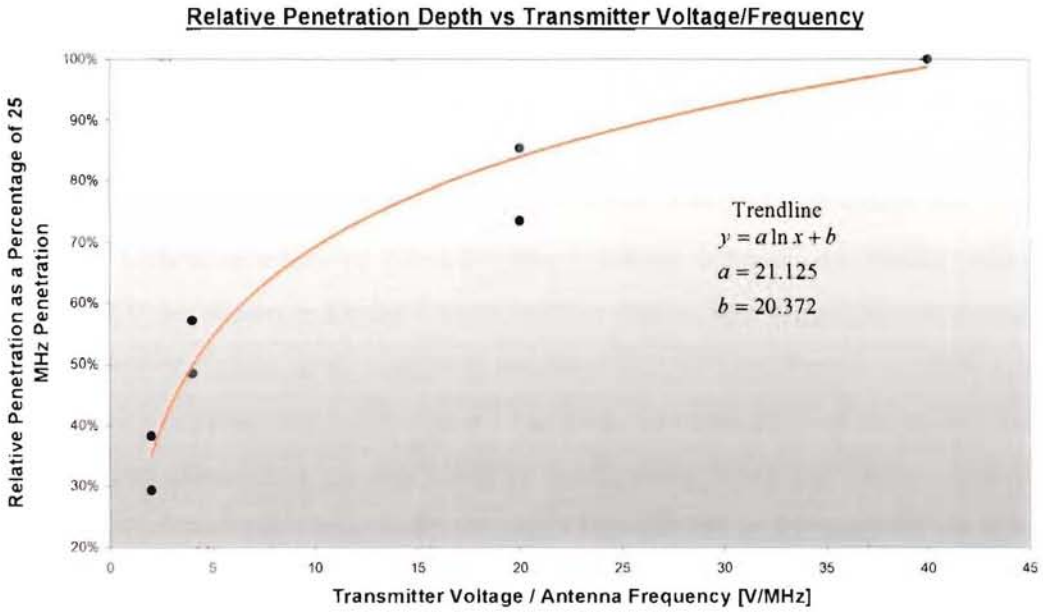

Figure 6.9 – Relative penetration depth vs. transmitter voltage/frequency..

To further explore the limitations of the equipment utilised at Goro, additional calculations may be made using alternative methods. A method commonly used in calculating GPR performance at specific sites is a relation of amplitude versus depth. Electrical conductivity profiles were measured by INCO during previous geophysical test work. Using an EM39 borehole probe, a conductivity of 10 mS/m in the limonite

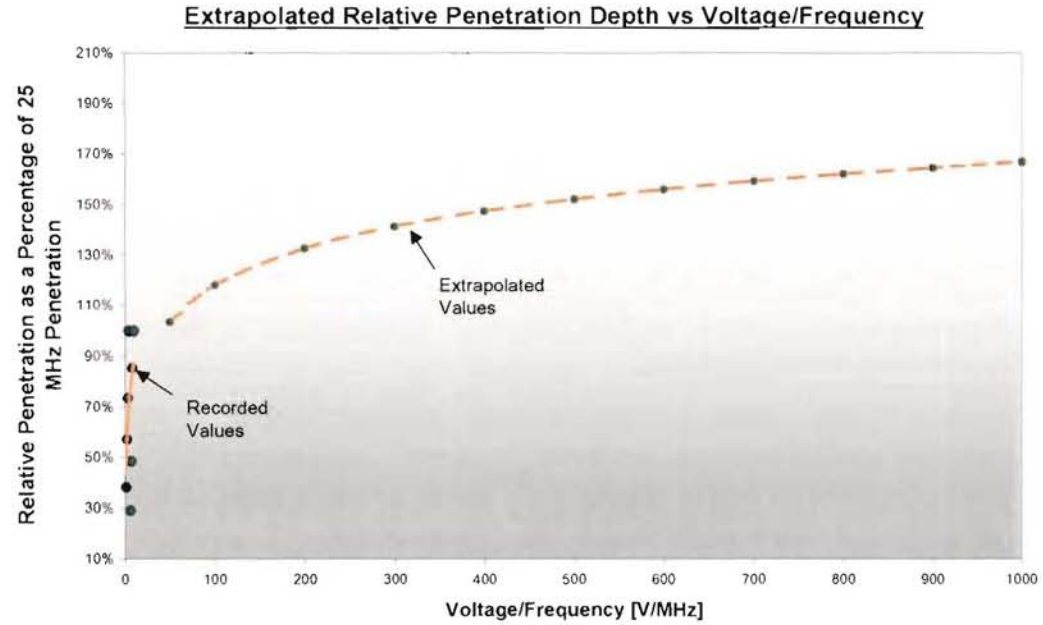

Figure 6.10 – Extrapolated relative penetration depth vs. voltage/frequency..

was recorded. Knowing the radar wave velocity at Goro, and thus the dielectric permittivity, the attenuation for the 25 MHz antennas is calculated using equation [4.9] as 2 - 3 dB/m.

Using equations 4.5 through 4.9, which relate attenuation to input power, the curves associated with attenuations of 2 and 3 dB/m, and input voltages of 1,000V, 10,000V, and 20,000V are shown in Figure 6.11. On these curves, 100 is used as representative of the sensitivity limits of the receiving antenna. For an input power of 1000 V, the penetration is expected to reach between 17 to 24 m for attenuations of between 2 and 3 dB/m. These calculations are confirmed by examination of the field data. The power versus depth curves also serve to demonstrate the difficulty of attaining depths greater than 30 m with a single antenna even with 20 times the power used in the present survey.

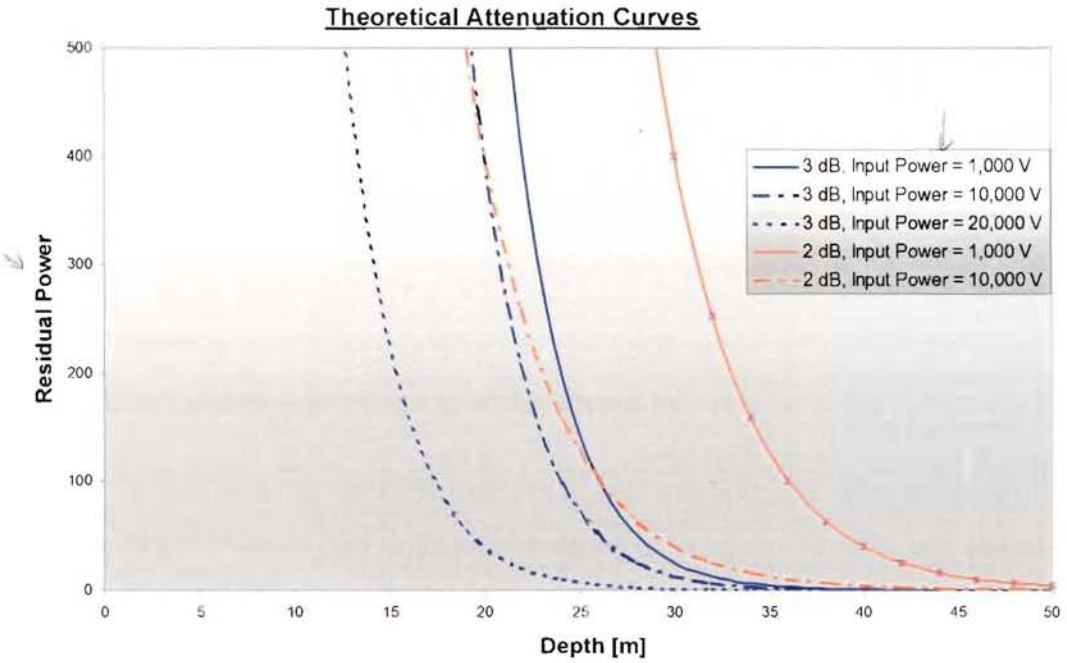

Figure 6.11 – Theoretical attenuation curves.

6.6 GPR Results

The GPR data acquired at the Goro site are generally of poor to average quality. As stated in the INCO internal report (Robillard and King 2000), GPR lines where the data were not stacked 64 times are of generally lower quality, and thus the interpretation is more dubious, than for those lines where the data were stacked 32 times. It is noted that at all other laterite sites surveyed using GPR world-wide, 32 stacks has proven to be

sufficient for imaging the base of the weathered zone to depths in excess of 70 metres. As stacking is used to increase the signal to noise ratio, the need for greater stacking at Goro illustrates the geophysical uniqueness of the deposit as compared to other deposits surveyed previously.

During data acquisition some equipment problems were encountered with the 1000V transmitter. In lieu of the 1000 V transmitter, the 400 V transmitter unit was employed for acquisition along Lines 2 and 21. Data from these two lines appear to be of lower quality than those acquired with the 1000 V transmitter.

The interpretations shown on Plates 6.1 through 6.13, as well as the descriptions below, are in no way meant to be exhaustive. Exemplary anomalous features are highlighted on the radar profiles and detailed below. Significantly more interpretation may be possible given the richness of the radar datasets. However, the mapping of individual boulders and small collapsed karsts is outside the scope of this project. The "Position" axes on the data profiles indicate distance along the radar survey line and are relative only to the BOL (beginning of line). As previously stated, no borehole lithology information was made available for the interpretation of the radar data. Thus interpretations were based solely on data characteristics in relation to those acquired at a number of other laterite sites worldwide, and observations made in the INCO internal report.

Line Along Road at Test Mine - 50 MHz (Plate 6.1)

One of the best examples of GPR data from Goro was acquired along a roadway into the Test Mine. A short 30m segment was surveyed using the 50 MHz antennas along the top of a cut bank adjacent to the roadway. The initial premise for this test line was an attempt to image any subsurface voids that were apparent along the cut bank by water seepage. Analysis of the data acquired indicates a strong reflective layer at a depth of approximately 7 to 8 metres. Careful examination reveals that this layer is in fact a conglomeration of super-imposed reflection hyperbolas such as would be caused by an abrupt layer of large boulders. Unfortunately, no borehole information is available from this region to confirm the geophysical interpretation.

Line 1 - 25 MHz (Plate 6.2)

Line 1 is typical of radar data acquired at Goro. The data are surprisingly rich in features considering the limited depth of penetration allowed by the slow radar velocities. Between positions 0m to 120m, a strong reflective event is evident at a depth of about 7 metres. This feature appears to dip to greater depths as it approaches position 120m, and possibly continues beyond the range of the radar penetration. Based on the data acquired along other lines, particularly at the Test Mine, this feature is interpreted to represent a layer of large boulders.

A number of obvious features characteristic of isolated boulders or blocks of ferricrete within a relatively homogeneous limonite are evident on all GPR lines acquired at Goro, particularly on Line 1. Examples of these are indicated near positions 195m and 470m. Much of Line 1, as is the case with all GPR lines acquired at Goro, contains regions of strong scattering features. The interpretation of GPR data from lateritic environments relies strongly on an analysis of the "texture" of the data. Thus, regions such as these are generally indicative of the presence of scattered corestones, broken and submerged ferricrete, and perhaps rocky saprolite. Conversely, homogenous "smooth" regions are generally characteristic of "clean" limonitic material with few inclusions.

Of greatest interest on Line 1 is a region between positions 220m and 320m, where what appears to be a collapsed karstic feature as much as 10 m deep is evident. The base of the feature appears to be comprised of broken ferricrete blocks or boulders, as is evidenced by the numerous hyperbolae. The material within the concave feature appears to be relatively homogeneous and layered. This is thought to be transported limonitic material, which has in-filled the collapsed karst. Data such as these may also be characteristic of a paleochannel. Air photos and geological mapping viewed on site appeared to indicate a lineament present in this general region, which may be indicative of faulting.

Line 2 - 25 MHz (Plate 6.3)

Line 2 contains a number of features not commonly seen in lateritic weathering environments. Between positions 400m and 700m exists a thick region of undulating

banding within a homogeneous material. It is thought that this region is too extensive to be caused by the in-fill of transported limonite into a collapsed karst, or by alluvial action. A possible explanation offered by INCO's site geologist (Tessarolo, pers. comm. 1999) is that these features, seen on other lines, may represent relict parent rock strata. Although the literature suggests that limonite has undergone sufficient collapse to destroy relict structure in most lateritic environments (Golightly 1979; Brand *et al.* 1998; Troly *et al* 1979), evidence to the contrary is commonly seen in borehole cores from Goro (Tessarolo, pers. comm. 1999).

A number of features evident on Line 2 between positions 750m and 950m are interpreted to be boulder layers. The possibility of relict parent structures in the limonite as well as submerged ferricrete and boulder layers greatly complicates the interpretation. A linear dipping feature within a layer that is interpreted to be limonite is clearly evident between positions 1000m and 1060m. This feature may be a discontinuity in the limonite or saprolite (such as a fault), which has permitted the migration of surficial ferricrete into the weathering profile. This feature may also be indicative of a layer of large boulders, although the lack of visible hyperbolas suggests otherwise.

Line 5 - 25 MHz (Plate 6.4)

A region of large boulders is evident near position 20m on Line 5. This reflecting layer is comprised of superimposed hyperbolas characteristic of an abrupt layer of rocky saprolite.

An anomaly present on most GPR lines from Goro is best exemplified on Line 5 near position 280m. The anomaly is similar in character to features interpreted as boulders, but the profile is however lacking the strong hyperbolic signatures common to large objects. A possible explanation for this anomaly is the occurrence of submerged ferricrete, commonly seen in borehole cores at depths beyond 30 metres (Tessarolo, pers. comm. 1999). Surficial ferricrete may be transported to great depths by migration due to preferential water movement down faults and fractures in the weathering profile.

An example of what is interpreted to be a subsurface void in the limonite or earthy saprolite is evident near position 580m. Voids are typically represented on the data

profiles differently than isolated boulders in that the hyperbolas caused by air or water-filled voids generally are repeated many times beneath the actual location of the anomaly (i.e. as "multiples").

A region between positions 480m and 580m is an example of the importance of careful application of depth and elevation corrections to radar data. On the flat profiles prior to the application of elevation statics, this feature appears as a concave layering, possibly caused by the in-fill of a collapsed karst. However, upon topographic correction, these layers appear linear and nearly parallel. Thus, it is thought that this feature is in fact evidence of relict parent rock structure in the limonite.

Line 6 - 200 MHz (Plate 6.5)

The 200 MHz antennas were utilised along a segment of Line 6 in an attempt to determine the best acquisition parameters to map the surficial ferricrete layer. It was later determined that the ideal antenna configuration for this task appeared to be the 50 MHz or 100 MHz antennas. The 50 MHz antennas are of sufficient resolution to detect the change in dielectric properties between the surficial ferricrete and the underlying limonite, whilst not over-resolving the extreme near-surface layers (< 2 m), making interpretation difficult (as is the case with the 200 MHz antennas). However, the 200 MHz data do yield some excellent examples of near-surface voids. At positions 140m and 160m, multiple vertically-stacked hyperbolas are clearly evident down the data profile. Such anomalies in the data are generally characteristic of air or water filled voids.

Line 9 - 25 MHz (Plate 6.6)

Two good examples of what are thought to represent collapsed karsts are shown near positions 475m and 625m on Line 9. The strong basal reflections are possibly indicative of broken ferricrete, while the near-horizontal banding contained within the concave features may represent transported limonite.

Also visible on Line 9 is possibly an abrupt layer of large boulders in the weathering profile located between positions 250m and 350m.

Line 13 - 25 MHz (Plate 6.7)

As with most other GPR lines at Goro, a region of large boulders is present throughout Line 13. These layers are particularly evident between the start of the line to position 550m, beyond which point the layer becomes less distinct and difficult to interpret.

As was seen in Line 2, an extensive region of undulating banding in the GPR data is clearly evident over the first two-thirds of the profile for Line 13. Again, a possible explanation for this banding is the existence of relict parent rock structures in the limonite. This zone appears to disintegrate north of borehole GL-42, and dissolves into a region of strong scattering events. A number of isolated boulders are evident between positions 760m and 850m. Beyond this position, the profile becomes difficult to interpret due to the lack of textural change in the data.

Line 15 - 25 MHz (Plate 6.8)

Line 15 was included in this review to illustrate data typical of an extensive region of distributed boulders. A large number of discrete hyperbola may be mapped along Line 15, each of which indicates the presence of a scattering object. These objects may be large boulders or submerged ferricrete, or in some instances, void spaces. Along some parts of Line 15, these boulders appear to form cohesive layers, such as between positions 450m and 600m, and between positions 850m and 925m. An anomaly between positions 1125m and 1200m may be misinterpreted as a collapsed karstic feature. However, the material contained with the concave feature is not horizontally layered, but scattered in a similar manner as the rest for the line. Thus this anomaly is interpreted to be another layer of large boulders.

Line 17 - 25 MHz and 50 MHz (Plates 9, 10, and 11)

Most GPR lines studied during the test surveys at Goro were acquired with multiple frequencies to determine the optimum antenna parameters. Although most lines were interpreted based on the 25 MHz data, the 50 MHz data from Line 17 are also shown on Plates 6.10 and 6.11. Line 17 exhibits exemplary data over a segment that extends north from a stream near the start of the GPR line to borehole GL-45. Across this region, a strong reflecting layer is clearly visible in both the 25 MHz data and the 50

MHz data. Examination of this layer indicates that as noted on other GPR lines, it is comprised of a superimposed series of hyperbolae, each representative of a large boulder.

Due to the extreme changes in topography on this line, both the 25 MHz and 50 MHz data from Line 17 are shown with only 2X vertical exaggeration in Plate 6.9 and 6.10. However, a third plot of Line 17 has been added which shows the 50 MHz data prior to the topographic correction (Plate 6.11). The boulder layer in the uncorrected dataset appears quite visible on this flat section.

Although no geological information is available for those located along Line 17, borehole GL-49 does indicate the occurrence of large boulders at a depth that closely matches that shown on the radar profiles (Tessarolo, pers.comm. 1999). To the north of borehole GL-48, the interpreted boulder layer becomes disseminated and more difficult to interpret.

Line 19 - 25 MHz (Plate 12)

Line 19 is similar to previous GPR lines at Goro and contains examples of boulders, layers of boulders and possible in-filled collapsed karsts. Near position 20m, a number of well-formed hyperbolas are present, which are indicative of isolated large boulders. Between positions 40m and 120m, is an area that may be interpreted as broken zones of larger boulders.

Between positions 360m and 420m, a region similar to the interpreted collapsed and in-filled karsts mentioned in previous lines is present on Line 17. Again, the in-fill material appears to be relatively flat-layered, thus indicating transported and re-deposited limonitic material.

The relatively poor results at Goro are attributed to a number of factors. The most significant is the thought to be the low velocity of the radar waves at the site. As stated in Chapter 4, the velocity of radar waves is dependant on factors such as water content ground conductivity, and magnetic permeability. From a review of moisture logs from a number of Goro boreholes, it would appear that the water content is similar, if not somewhat higher, that that found at other humid laterite sites. The conductivities of the

laterite profile as measured during a previous EM39 borehole electromagnetics survey appear consistent with those measured at other sites (Peric 1981). It is thus theorised that the magnetic permeability of the profile may be significantly greater than elsewhere. Higher magnetic permeability may be the result of greater serpentinisation or oxidation in the upper portions of the weathering profile.

Another factor that acts against the suitability of GPR at Goro is the shear complexity of the deposit. The presence of the surficial ferricrete, as well as ferricrete that may have migrated downwards in the weathering profile often complicates the interpretation of the general texture of the data. The addition of frequent voids in the limonite and saprolite, as well as greatly disseminated corestone boulders is a further complication.

Thick ferricrete cover shown along GPR survey line at Goro.

7 KONIAMBO (NEW CALEDONIA)

7.1 Geological Setting

The Koniambo nickel-cobalt laterite deposit is located in the Province Nord of New Caledonia, 270 km northwest of Nouméa (Figure 7.1). The Koniambo massif is irregular in shape, and generally oriented NW-SE. The massif measures 20 km long by 6 km to 10 km wide, and extends from sea level along a narrow coastal plain to a maximum elevation of 856 m. The area of the massif is 144 km^2. A series of elevated plateaus and terraces have developed along the axis of the massif over its entire length, with frequent stepped terraces extending from the main ridge. Significant laterite mineralisation covers an estimated 45 km^2 of the Koniambo massif.

Figure 7.1 – Location of Koniambo.

Ferricrete and limonite cover are principally developed over the axial ridge of the massif, with sporadic cover over a number of isolated terraces that lie to the west. With the exception of four main limonite plateaus that occur along the ridge, limonite cover is generally less than 5 m thick and ore-grade saprolite is often exposed at the surface.

The primary limonitic facies of the weathering profile are generally as discussed for Goro in Chapter 6. Briefly, they consist of:

- Ferricrete
- Red limonite
- Yellow limonite
- Transitional limonite

However, at Koniambo, the saprolitic regions are further divided into:

- *Facies superior* (0% - 10% serpentinite)
- *Facies intermediate* (10% - 40% serpentinite)
- *Facies normal* (40% - 70% serpentinite)
- *Facies basal* (70% - 95% serpentinite)
- Serpentinite (> 95% serpentinite)

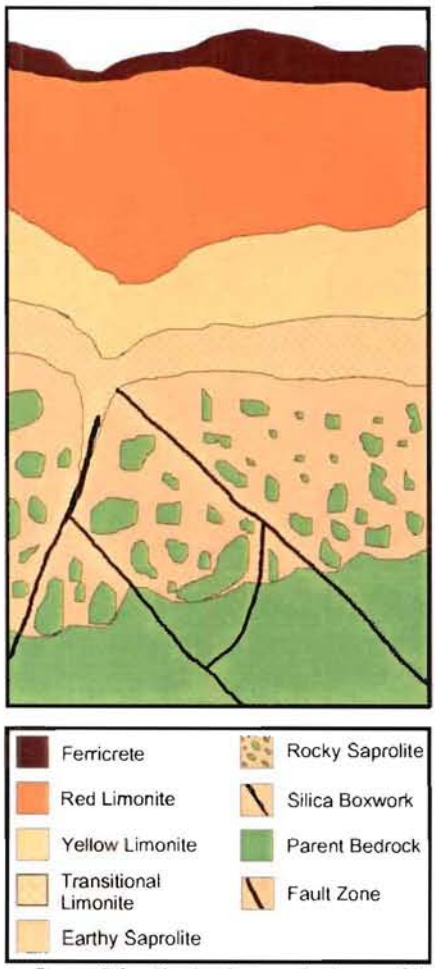

Figure 7.2 – Koniambo weathering profile.

A schematic representation of the weathering sequence at Koniambo is shown in Figure 7.2.

The schematic representation does not, however, adequately portray the complexity of the Koniambo deposit. An extensive geological and alteration mapping program has been carried out by Falconbridge across the massif (Audet, pers.comm., 1999). The findings of this program indicated that the regions of significant alteration in the saprolite were coincident with major structural features. Structural mapping undertaken by Falconbridge along historical mining benches in the Koniambo region indicates that there are significant faults that have developed in the Koniambo massif. The faults can extend from tens to hundreds of metres in length. As seen in many other humid lateritic environments, these zones generally indicate regions of significant preferential weathering down the fault zones. The alteration zone within fault planes may be up to 12 m wide, and tens of metres deep. These zones often feature increased nickel enrichment, particularly at intersecting fault planes. The structural mapping has also indicated that the fault patterns are complex but display local symmetry in relation to major lineaments (Audet pers.comms., 1999).

7.2 GPR Survey Line Coverage

The following table is a summary of the line locations, names, and distances, along with antenna parameters used for each GPR survey line acquired during the research project. The arrangement of the survey lines is best illustrated in Figures 7.3 and 7.4, which show the Test Zone and Trazy regions respectively. Information from boreholes shown in orange was provided by Falconbridge as part of this research project.

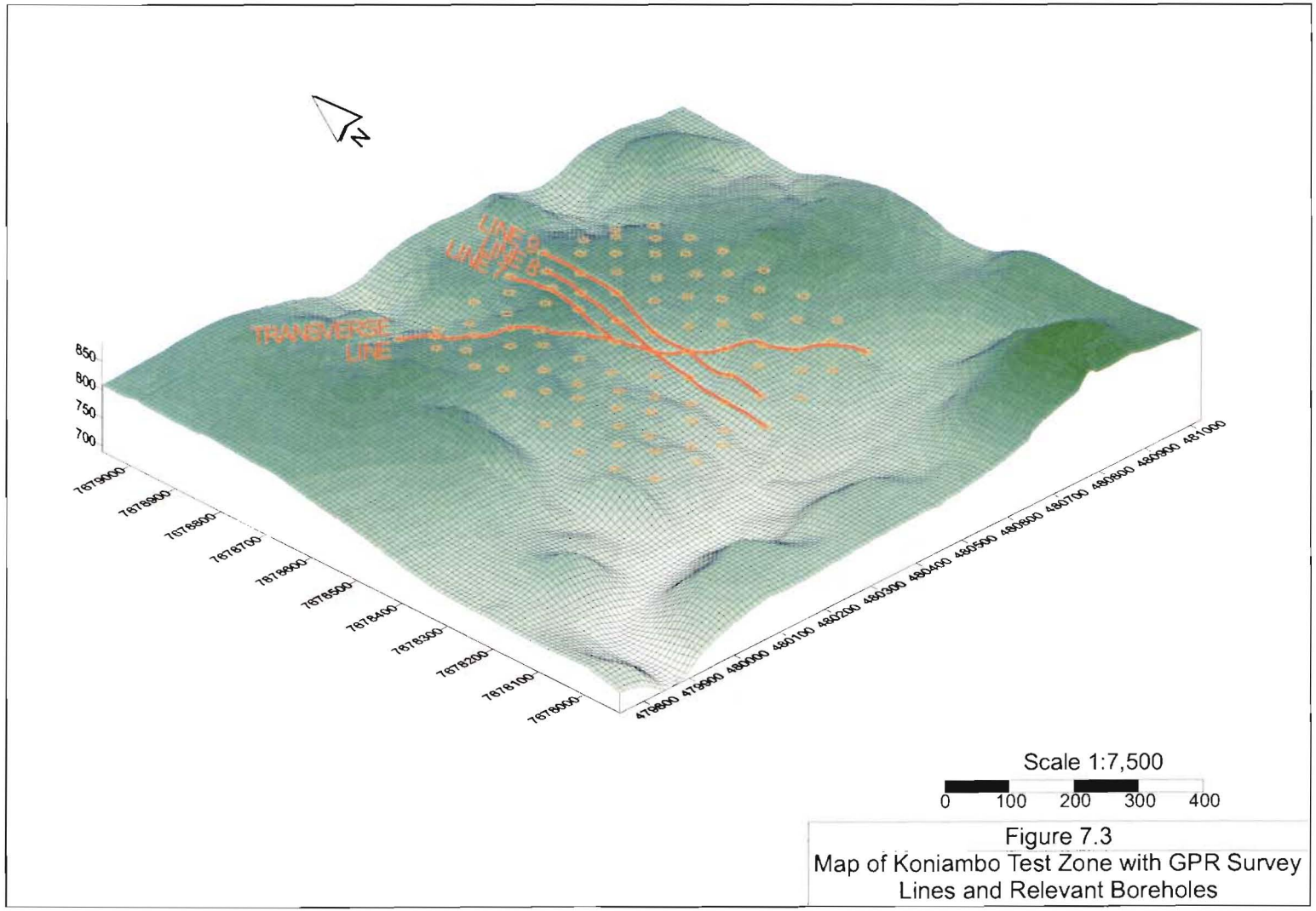

Figure 7.3
Map of Koniambo Test Zone with GPR Survey Lines and Relevant Boreholes

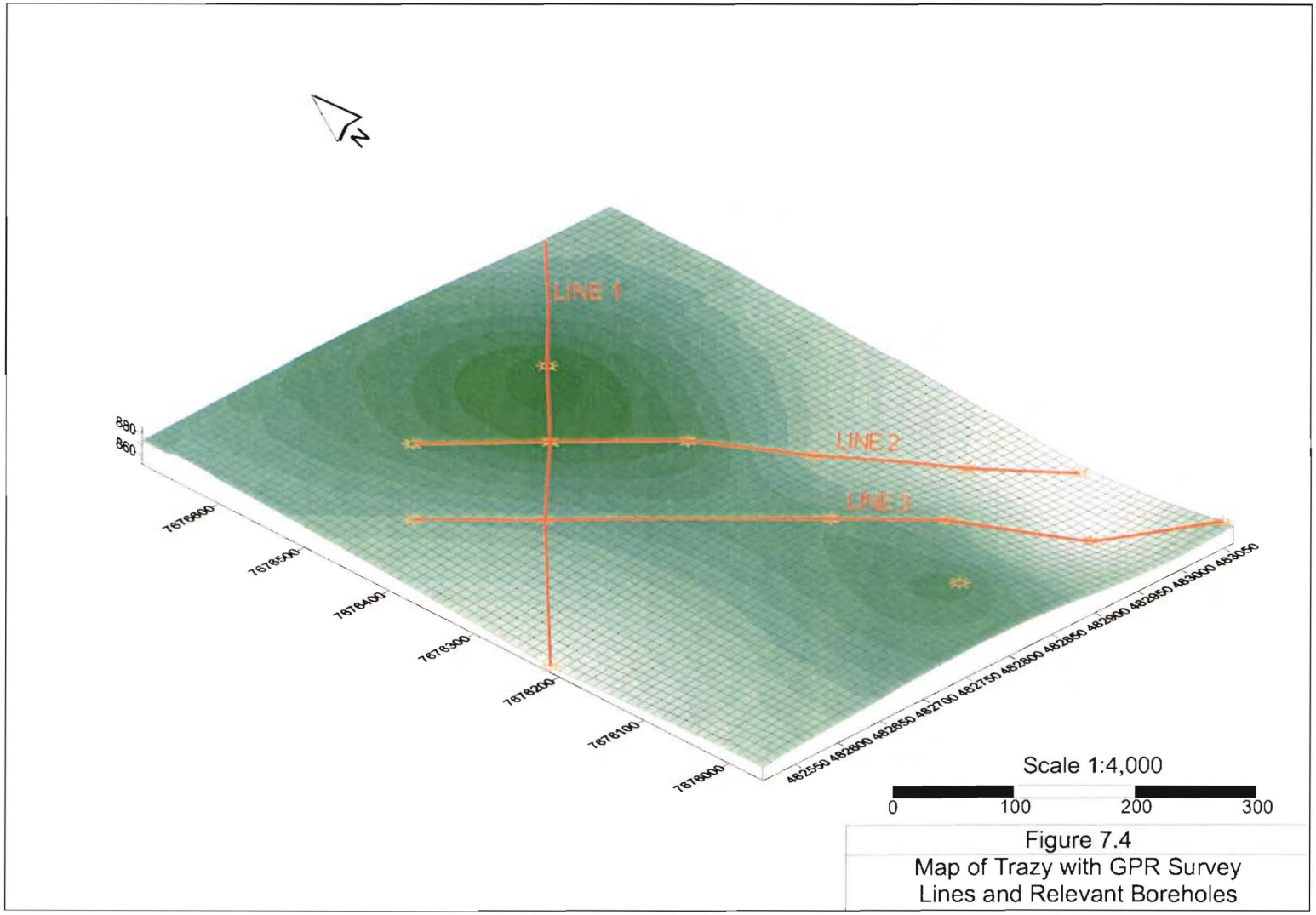

Figure 7.4
Map of Trazy with GPR Survey Lines and Relevant Boreholes

Location	Line Name	Frequency	From	To	Distance	Comments
Test Zone	Line 7	25 MHz	E4740	E4710	236	
Test Zone	Line 8	25 MHz	E4775	E4715	488	
Test Zone	Line 9	25 MHz	E4871	E4811	487	
Test Zone	Transverse 1	25 MHz	F4075	E4410	732	
Test Zone	Cross 1	25 MHz	1	18	192	Lack of borehole data
Test Zone	Cross 1	50 MHz	1	18	224	Lack of borehole data
Test Zone	Cross 1	100 MHz	1	18	208	Lack of borehole data
Test Zone	Cross 2	25 MHz	24	36	160	Lack of borehole data
Test Zone	Cross 2	50 MHz	24	36	160	Lack of borehole data
Test Zone	Cross 2	100 MHz	24	36	160	Lack of borehole data
Trazy	Line 1	25 MHz	Y5340	I5980	671	Poor data quality due to instrumentation
Trazy	Line 2	25 MHz	Y5320	Y5871	671	Not analyzed due to lack of borehole data
Trazy	Line 3	25 MHz	Y5410	Z5070	671	
Trazy	Line 4	25 MHz	Y5601	Z5051	553	

Table 7.1 List of GPR acquired at Koniambo.

7.3 Analysis of GPR data

7.3.1 General Discussion

The GPR data acquired at the Koniambo site are generally of average quality. The data acquired during the research project were submitted to Falconbridge geophysicists for review. A cursory assessment indicated a possible correlation of the radar data processed using rudimentary schemes with the limonite / saprolite interface (Stevens pers.comm., 1999). This finding is interesting in that there is not expected to be a sufficient difference in the dielectric properties of the lower limonite zones and the earthy saprolite to impart radar reflections. The changes in dielectric properties that are sufficient to cause radar reflections are generally associated with changes in the water content at different depths in the weathering profile. The greatest change in water content generally occurs at the earthy saprolite / rocky saprolite interface or at the interface with unweathered parent rock. These regions represent transitions from humid weathered material to arid unweathered corestones and bedrock. However, each laterite site exhibits widely different geophysical signatures and any theoretical relationship between radar reflections (or the frequency of the reflected radar signals) and geology / mineralogy should be examined. Unfortunately, all boreholes at Koniambo are drilled using reverse circulation, and consequently no water content information is available from within the profile. Also, no geochemical analyses were made available for the

research project. An analysis of the correlation of the GPR data to the available borehole information is made in Section 7.4.

The correlation of the radar data to the provided borehole information is closely dependant on the selection of an appropriate radar velocity to apply to the data. The primary method of radar velocity determination used at Koniambo was the analysis of discrete hyperbolae in the radar data. Using the GRADIX™ software package, an average velocity of 0.075 m/ns was derived from 83 individual hyperbolae. A number of CMP surveys were also acquired with 50 MHz antennas at boreholes E4660, E4665, and E4010 in the Test Zone. An example of the CMP data along with an interpretation is shown in Figure 7.5 for borehole E4665. As illustrated by the CMP, the velocity estimate of 0.051 m/ns is significantly slower than those measured using the hyperbola method.

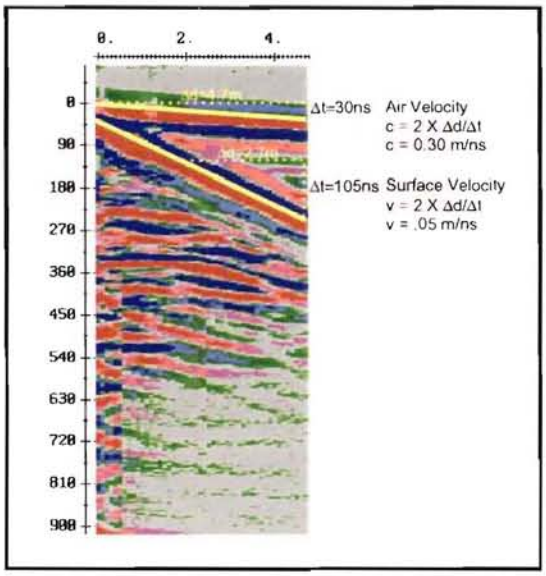

Figure 7.5 – CMP from borehole E4665.

It has been determined from the prior work in similar environments that CMP data are usually erroneous in determining the velocity of the bulk limonite (Parkinson 2000; Queen *et al.* 1998). The CMP data in laterites often is only indicative of the very near surface velocity, which at Koniambo may be primarily ferricrete. Based on this knowledge, the radar data from Koniambo were correlated to borehole information using the velocity of 0.075 m/ns as indicated by the hyperbolae. The borehole antennas used at Goro were not available for the research at Koniambo.

It is thus noted that the recording time window of 1200 ns used during field acquisition would provide at most 40 m of depth penetration. This depth should thus be generally sufficient to map the weathering profile over most of the deposit as indicated on the borehole logs provided by Falconbridge.

7.3.2 Borehole Correlation

Prior to a discussion on the correlation of the GPR data to borehole information provided at Koniambo, it is important to note the inherent differences in the material properties identified by each technique. As in the case of Loma de Níquel, the definitions of rock types (i.e., limonite, saprolite, and bedrock) identified in boreholes are the result of a combination of mining economic criteria and geologic concepts. The geochemical parameters applied to the drill samples are primarily relevant to the percentage of serpentinite concentration in the sample (Audet pers.comm., 1999).

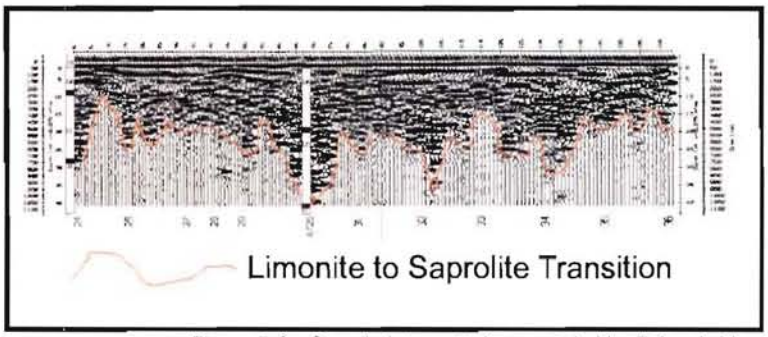

Figure 7.6 – Sample interpretation provided by Falconbridge.

In contrast to the borehole core logging scheme for horizon definition, GPR responds to significantly different rock properties that would likely produce coherent reflections. These properties were outlined in Section 4.2, but may be summarised in an approximate order of importance as: water content, conductivity, and the percentage of iron.

As previously mentioned, Falconbridge geophysicists had noted a possible correlation between limonite / saprolite boundary from the boreholes and the radar data (Stevens pers.comm., 2000). The correlation was based on the shift in the data from high-amplitude, low-frequency data in what is assumed to be the limonitic material, to the low-amplitude, high-frequency data in the saprolitic zones. A sample of the simplified interpretation is shown in Figure 7.6. The shift in the frequency content of the data is occasionally difficult to interpret in the raw radar sections. The instantaneous frequency processing scheme developed for other laterite sites aims to enhance the interpretability of this shift. However, at most other sites, this shift has been indicative of the transition from weathered (humid) to unweathered (arid) portions of the weathering profile.

Nevertheless, the correlation of the GPR data to the limonite / saprolite boundary, as well as to the weathered / unweathered boundary were analysed. The most accurate and unbiased analysis is to compare the frequency content of the GPR data using the instantaneous frequency display to the depth of the weathering profile as taken to be most obvious first consistent occurrence of partially-altered rocky saprolite encountered in the boreholes. Also, a comparison was made between the instantaneous frequency data and the depth of the interface from transitional limonite to intermediary saprolite (*facies intermediate*) as indicated in the borehole analyses. The differences in depths derived from the GPR surveys and those determined from boreholes were normalised by expressing the differences as a percentage of the boreholes depth. Thus, if *dGPR* was the depth estimated from the GPR survey and *dBH* was the depth estimated from the borehole, then the difference, ä, is expressed as:

$$\delta = 100 \times \frac{dGPR}{dBH}. \qquad [7.1]$$

It is noted that the shift from the fully altered material to the partially altered rocky material is generally coincident with the transition from limonitic material to saprolitic facies.

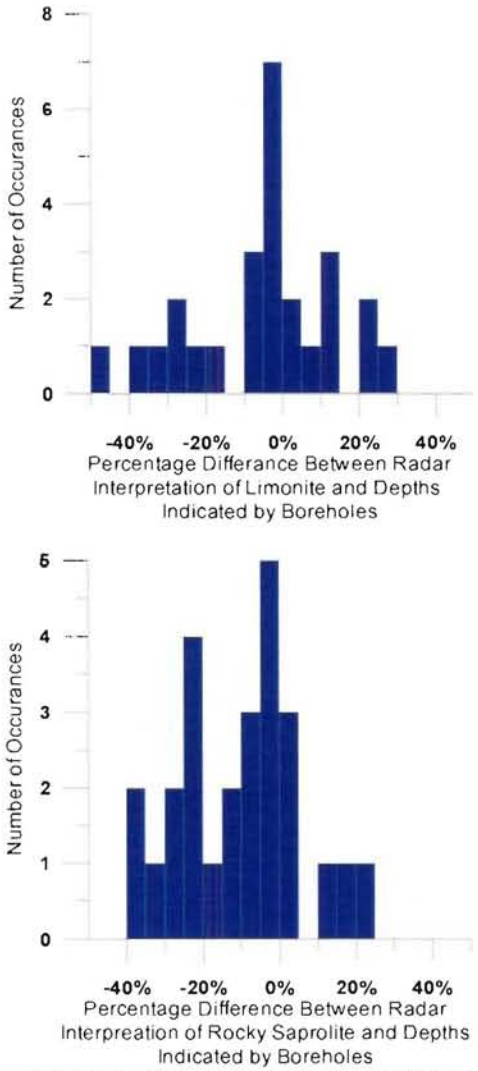

Figure 7.7 – Histograms of percentage difference between borehole logs and GPR data.

The histogram plots of the percentage difference between the borehole logs and the GPR data are shown in Figure 7.7, where negative differences indicate that the geophysical response detected the target zone at shallower depths than the borehole logs. These plots indicate that a slightly more robust correlation exists between the limonite / saprolite transition and the radar data than with the occurrence of unweathered rocks. This observation is consistent with the initial interpretation provided by Falconbridge geophysicists. On previous projects, borehole

data have not indicated a significant change in water content between the limonitic and earthy saprolite zones. However, the formation geology of the limonite and earthy saprolite indicates that the collapsed structure of the limonite may be less porous and permeable than the open structure of the saprolite, which may affect the radar response.

It is noted that a reliance on the analysis of the frequency content of the data may be misleading in certain circumstances. Where the frequency content of the dataset changes usually indicates the deepest coherent reflector that returns radar energy. The signal essentially "dies out" due to the lack of further significant reflectors at deeper depths. However, in an environment where the conductivity of the weathering profile is sufficiently high, or where the weathering profile exceeds the maximum penetration of the radar system, a similar change in frequency will still be recorded. Thus, without borehole control, the loss of signal may be also interpreted as attenuation due to ground conductivity or as loss of signal reflection due to an excessive depth to the target layer. Based on the data acquired at deposits such as Ramu (Section 5.1) and Loma de Níquel (Section 5.3), situations where the depth of the weathering profile exceeds the penetration of the radar signals are exemplified by a more gradual change in frequency content as the signal reduces in return strength. Abrupt changes (shown as changes from blue to orange in the dataset displays) are usually geologically significant.

Each dataset shown in Plates 7.1 through 7.8 includes the real amplitude data as well as the instantaneous frequency data. The real amplitude profiles were plotted using a standard seismic color scheme of red-white-blue to indicate relative reflection strengths after application of the AGC gain.

7.4 GPR Results

7.4.1 Test Zone

Line 7 – 25 MHz (Plate 7.1)

Line 7 is an ideal example of typical instantaneous frequency data from lateritic environments. The frequency change throughout the profile is abrupt from blue (low frequency) to orange (high frequency). In nearly any other laterite deposit, this transition would mark the zone of boulders at least a wavelength (in this case 2.8 m) in diameter, or the transition to unweathered bedrock. However, when compared to the borehole information provided for the three boreholes (E4740, E4730, E4710), little

correlation is evident. Results from boreholes E4740 and E4730 indicate that large saprolitic boulders are present at shallow depths in the profile, whereas the radar data indicate deep weathering. The correlation of the transition from limonite to saprolite in borehole E4710 to the radar information is somewhat better. However, the borehole indicates the occurrence of large saprolitic boulders, whereas the radar indicates a relatively coherent unweathered zone at the same depth. In this situation, an analysis of the moisture content in the profile would have aided the analysis and interpretation.

Line 8 – 25 MHz (Plate 7.2)

A relatively good correlation can be made along Line 8 between the geology mapped by boreholes and the radar frequency content. With the exception of the information from the southern-most borehole, E4775, which is significantly different than the radar interpretation, most boreholes match the geophysical interpretation of the transition from limonite to earthy saprolite to within 10%. Additionally, there appears to be a better correlation at boreholes where there is an absence of transitional limonitic material. A change from earthy limonite to intermediate saprolite evidently produces the best correlations at Koniambo.

Line 9 – 25 MHz (Plate 7.3)

Line 9 exhibits some of the best correlations between the geological and geophysical data acquired at Koniambo. Most of the six boreholes located along the line match well with the radar interpretation. The southernmost borehole, E4871, indicates saprolitic boulders at depths somewhat deeper than those shown at the coincident point on the radar profile. However, the remaining five boreholes indicate the depth to rocky saprolite to be within 10% of that detected on the interpreted radar response. Borehole E4851 appears to have been placed adjacent to a small pinnacle that exists near chainage 170m. The slight discrepancy at this point between the radar data and the depths inferred from the borehole data may be explained by small surveying inaccuracies during radar acquisition. A deviation of a few metres from the survey line in a region of a pinnacle may produce the differences observed between the radar and borehole results.

Transverse Line 1 – 25 MHz (Plate 7.4)

Transverse Line 1 shows a good correlation with the borehole information, but may somewhat contradict the previous assumption that the best correlation is to the limonite / saprolite transition. The correlation of the degree of alteration of the saprolite to the radar data interpretation appears to be more robust than that of the limonite / saprolite transition. This is apparent at boreholes F4075, E4965, E4855, and to a lesser extent at E4410. A significant discrepancy is noted at borehole E6535 which indicates that unaltered saprolite exists at a depth much shallower than that shown on the radar data.

A number of small pinnacle structures are also observed in the Transverse Line 1 profile. These pinnacles are common to lateritic environments and are generally indicative of small regions of parent rock that were resistive to the weathering process.

Variogram Cross Lines 1 and 2 – 25 MHz, 50 MHz, 100 MHz (Plate 7.5)

No naming convention was available to differentiate the two radar profiles acquired along the variogram cross at the Test Zone. Thus, Cross Line 1 was referred to as the radar line coincident with the boreholes numbered 1 through 18. Cross Line 2 referred to the radar line coincident with the boreholes numbered 24 through 36. Unfortunately, no adequate topographic or borehole information was available from Falconbridge to facilitate the correlation of the geophysical data to the borehole information for these cross lines. However, general observations may be made regarding the nature of the datasets in comparing the three different antenna centre frequencies utilised. The best comparison of these data is to examine the instantaneous frequency plots.

From an overview of the three datasets from each Cross Line, it appears that the transition from the low frequency high amplitude orange data to the high frequency low amplitude blue data is much more abrupt, and thus interpretable, at higher frequencies. Working from the hypothesis that the frequency shift in the data is correlated with the base of the humid altered zone, as is found with most other laterite sites, the above observation that higher frequencies produce more interpretable instantaneous frequency data may be then explained by the mathematics of wave propagation. The higher frequency signals have a smaller wavelength (the 100MHz signal would have ¼ the wavelength of the 25 MHz signal). Since objects, or transitional zones, are only

detected when they occur over a region on the order of a wavelength, it is expected that the 100 MHz data will be more detailed than for the 25 MHz data. In contrast, the 25 MHz data appear to be very difficult to interpret in certain regions, particularly between boreholes 1 through 9 on Cross Line 1, and between boreholes 24 and 28 on Cross Line 2. The interpretations shown on the GPR profiles with the instantaneous frequency display are based on a visible shift in frequency content of the radar data. They are not meant to necessarily indicate a geological contact, but may be related to a geochemical or other material property change (i.e. humidity, %Fe, etc.). At Loma de Níquel the lower frequency 12.5 MHz data appeared easier to interpret than the 25 MHz data. This contradiction is hypothesised to be due to the thickness of the partially-weathered rocky saprolite zone, which was significantly thinner at Loma de Níquel than at Koniambo.

The interpretation of the radar frequency content for the three antennas utilised is variable. As previously stated, this result is expected due to the ability of the higher frequency antennas to image smaller changes in dielectric properties, such as would occur with smaller rocky saprolite corestones (Section 4.3.3). Corestones progressively increase in size with increased depth in the weathering profile. Thus, the 100 MHz antennas are expected to detect a dielectric boundary at a level somewhat shallower in the profile than the 50 MHz and the 25 MHz antennas, as was the case at Loma de Níquel.

7.4.2 Trazy

Trazy Line 1 – 25 MHz (Plate 7.6)

Both equipment and weather problems plagued data acquisition along Trazy Line 1. A malfunctioning transmitter caused large amplitude spikes at the bottom of most radar traces. Although no feasible rectification was available on site, subsequent processing effectively removed these offending noise spikes. An undesirable but unavoidable artefact of this processing was a slight alteration in the frequency content of the data. This caused the transition from the low frequency high amplitude data in the weathered zone to the high frequency low amplitude data in the unweathered zone to be somewhat obscured and less interpretable. However, a relatively good correlation may be made to the borehole information provided. It is noted that no information was provided for borehole I5890. As for previous radar profiles discussed, the best correlation is at boreholes where an abrupt transition from limonitic material to intermediate saprolite

occurs. Examples of such boreholes on Trazy Line 1 were Y5340, Y5520, and I5980. Data in the region of Y5611 are difficult to interpret due to the aforementioned acquisition problems. It appears that the radar data indicate the base of the weathering profile to be substantially shallower than that mapped by the borehole.

Trazy Line 3 – (Plate 7.7)

Although the problems encountered on Trazy Line 1 with the equipment were intermittently apparent on Trazy Line 3, the correlation of the data to the borehole information is generally good. The most significant discrepancy exists at Z5070, where the borehole information indicates an extremely deep weathering profile. The radar data at this location are excellent examples of the potential for ambiguity in the interpretation of significantly deep radar information. The subtle change in frequency content in this region occurs very deep in the radar profile (at long reflection times). Thus, this change may also indicate simply a loss of signal return due to attenuation at depth. This suggestion is substantiated by examining the gradual transition from the weathered zone to the unweathered zone as interpreted in the radar data. In this region, the change appears to be much less defined – another indication that the signal may have simply "died out".

The data acquired at Koniambo indicate that the correlation of the radar interpretation to the geological information provided by boreholes has been reasonably good, although significant variations do exist. An analysis of the percentage difference between the interpreted radar profiles and the borehole information indicates that a correlation is best made with the radar frequency and the limonite / saprolite boundary rather than with the depth of the physical alteration zone. In general, the best correlation between the geophysical data and the borehole information appears to occur at boreholes where an abrupt transition from limonite to intermediate saprolite exists without an interstitial transitional limonite.

View from Koniambo Massif

8 INFLUENCE OF WATER SATURATION AND MINERAL CONTENT ON RADAR RESPONSE

8.1 Radar Frequency vs. Percent Humidity

The hypothesis used for most of the interpretations of radar data acquired at the six test sites and two project sites discussed in this research has been that the water content of the laterite profile has the greatest impact on the radar data. The relative strength of a GPR reflection is proportional to the contrast in dielectric coefficients between two media. The *in situ* dielectric coefficient of soil (between 5 and 15) is highly sensitive to the degree of saturation by pore water (dielectric coefficient of 81). The relationship between the level of water saturation in a porous soil and its dielectric coefficient have been widely studied (Knight and Nur 1987; Knight and Endres 1990), and many formulae have been derived. However, each formula is related to the individual dielectric coefficient of the components of the water-soil matrix. For humid soils such as in the weathered section of a laterite profile, the high water content will produce high dielectric coefficients, and thus generate strong reflective events. The strongest reflection events are generally characterised by a frequency content near the antenna central frequency and are associated with the humid weathered zones of the laterite profile. Conversely, the arid bedrock zone of the profile tends to produce a significantly higher frequency radar response.

Evidence in support of this theory is particularly well illustrated at sites such as Loma de Níquel in Venezuela (Section 5.3), where the correlation made between the lithologies mapped in the boreholes and the radar data was excellent. As previously discussed (Sections 2.3 and 4.1), the gross lithology of a lateritic weathering profile is closely related to the water content, in that the weathered zone (limonite and saprolite), which is generally the portion of the profile to be mined, is characterised by a very high water content. The rocky saprolite and bedrock portions of the profile have a low water content. This change is normally abrupt, and is hypothesised to be the primary cause of the frequency shift in the radar data frequently observed at the weathering boundary.

The validity of this theory is best demonstrated by a statistical analysis of the radar data as compared to the water content of the weathering profile at various points. The only data concerning the water content of the profile available is located within boreholes. There are a number of methods used for drilling boreholes for laterite resource

determination. One of the least expensive is a reverse circulation (RC) method. Unfortunately, due to the nature of the RC drilling technique, the original moisture content of the profile is not recovered. The Koniambo deposit in New Caledonia used this type of drilling. Coring by diamond drilling provides perhaps the best method of mapping the variations in the profile humidity, but is a much more expensive technique. Sites such as Ramu in PNG and Loma de Níquel in Venezuela used this method of drilling in establishing their borehole grids.

A statistical analysis of the correlation of the radar data with borehole data requires the best possible radar data acquired at an ideal site, along with ample borehole information that covers the entire weathering profile and penetrates into fresh parent rock. When compared to the other sites investigated, the location that offered the best radar data along with the most abundant borehole information was at Loma de Níquel in Venezuela (Section 5.3).

In order to correlate radar data to borehole information, the radar data must first undergo the general processing flow described in Section 4.3. As the processing steps discussed are completely one-dimensional, i.e. they do not take into consideration the horizontal coherency of the data, processing schemes may be applied to any single trace, or groups of traces within a profile. Thus, a program was written to extract from the 89 profiles acquired at Loma de Níquel, only those traces with which a comment related to a borehole was associated. Borehole comments were attached to individual traces as the location of a borehole was directly encountered during acquisition.

A hybrid data file was thus created that contained only the traces associated with boreholes. The file consisted of 91 traces that corresponded to 91 boreholes scattered throughout the site. Due to the confidentiality of the borehole data, no map can be presented which shows their spatial distribution.

This hybrid file underwent most of the processing steps described in Section 4.3 (namely declipping, dewowing, zero time correction, filtering and depth conversion). The instantaneous frequency display developed for the Loma de Níquel project (Section 5.3) was also used on this group of traces. The vertical scale of the resulting dataset was converted from two-way travel time of the radar waves to a depth scale using the radar velocity determined for the Loma de Níquel site, derived from comparisons to

borehole information as well as from CMP surveys taken at a number of points on the site (0.07 m/ns). In the analysis of the original radar data acquired at Loma de Níquel, this velocity produced depth sections that correlated very well to the borehole lithologies.

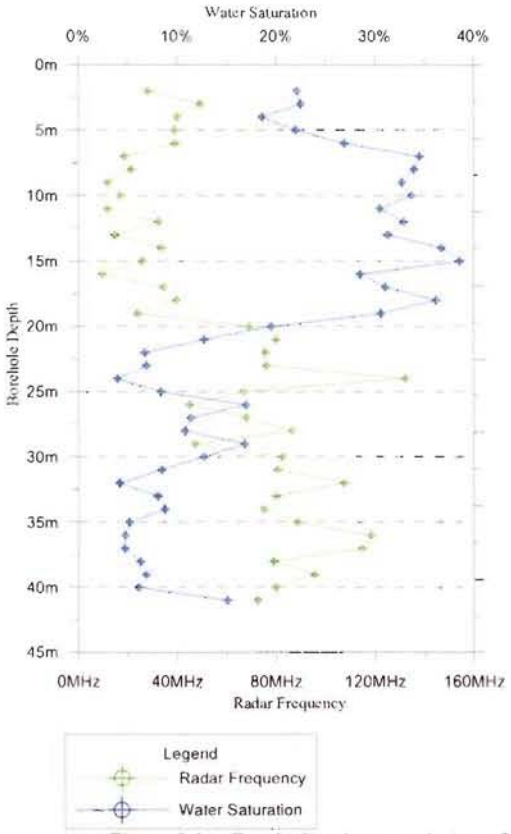

Figure 8.1 – Graph showing correlation of instantaneous radar frequency to water saturation.

The instantaneous frequency data output from this final step in processing of the hybrid file contained 625 data points over a depth range of 41 metres. The borehole information provided on spreadsheets was sampled at one-metre increments down each borehole. Thus the radar data needed to be interpolated and re-sampled at the same one-metre intervals. A number of methods were attempted using the standard computer spreadsheet programs. The most reliable method involved writing a program that, in effect, examined the instantaneous frequency data every metre, discarded any positive and negative value spikes (deemed as noise), and averaged the remaining values. A relatively smooth instantaneous frequency response vs. depth curve was thus obtained for each radar trace associated with a borehole. An example of such a graph for one borehole is shown in Figure 8.1, along with the associated water saturation values. It is noted that the abrupt change from low-frequency to high-frequency radar data occurs at nearly the exact depth as the equally abrupt change from a high water content to low water content in the weathering profile. This transition also marks the bottom of the weathering profile as detected by the borehole.

Thus a total of 1,399 metres of borehole data, at one-metre intervals, could be easily correlated to the instantaneous frequency content of radar data at the exact same points in the weathering profile.

The borehole information available from the specific holes used in this study included detailed mineralogical and geochemical analysis as well as humidity data. The mineralogical and geochemical data were derived from XRD and XRF analyses, whereas the humidity was based on sample weights before and after drying. It is noted that these test were undertaken by an internationally recognised geochemistry laboratory, and crosschecked by other independent tests (Alvez pers.comm., 1999). These borehole data should be sufficiently accurate for the purposes of this discussion.

The graph of radar frequency vs. water content is shown in Figure 8.2 for all 1,399 data points. A correlation is clearly evident in the region between 0% and 25% humidity. At a water content greater than 25%, the correlation is somewhat less evident. As is expected, a small number of scattered data points are present on the graph that show no correlation between the radar frequency and water content.

The software package CurveExpert (Hyams, 1997) was used in an attempt to generate the best fit mathematical equation for the data shown in Figure 8.2. CurveExpert attempts to fit the data points on a graph to a mathematical model. The available models are divided into different regression families: exponential, power, yield-density, growth, sigmoidal, as well as sinusoidal, Gaussian, hyperbolic, and rational function models. Each family contains up to ten sub-sets of base models. Polynomial equations

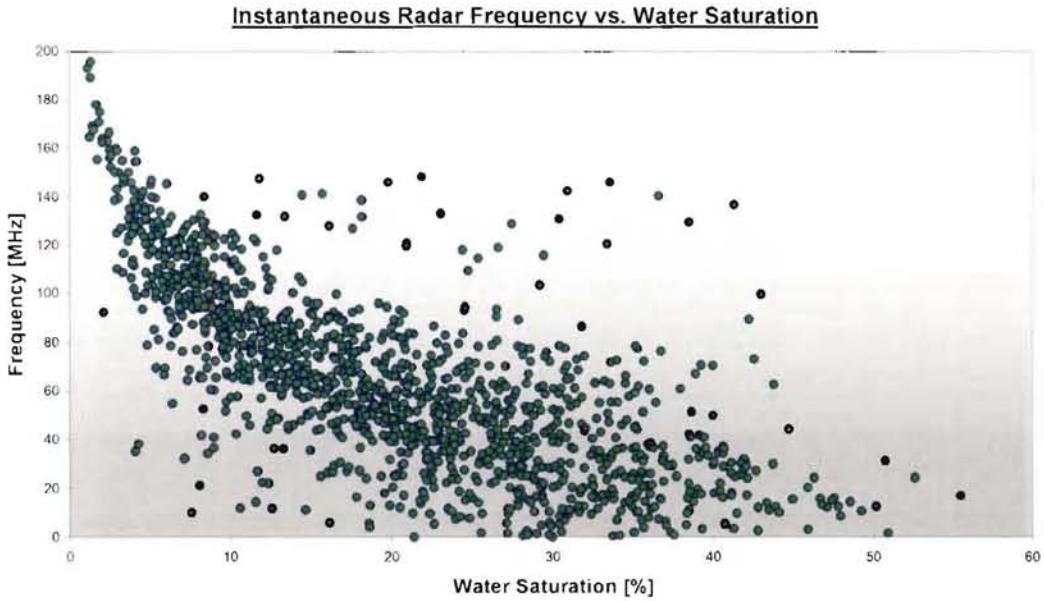

Figure 8.2 – Instantaneous radar frequency vs. water saturation.

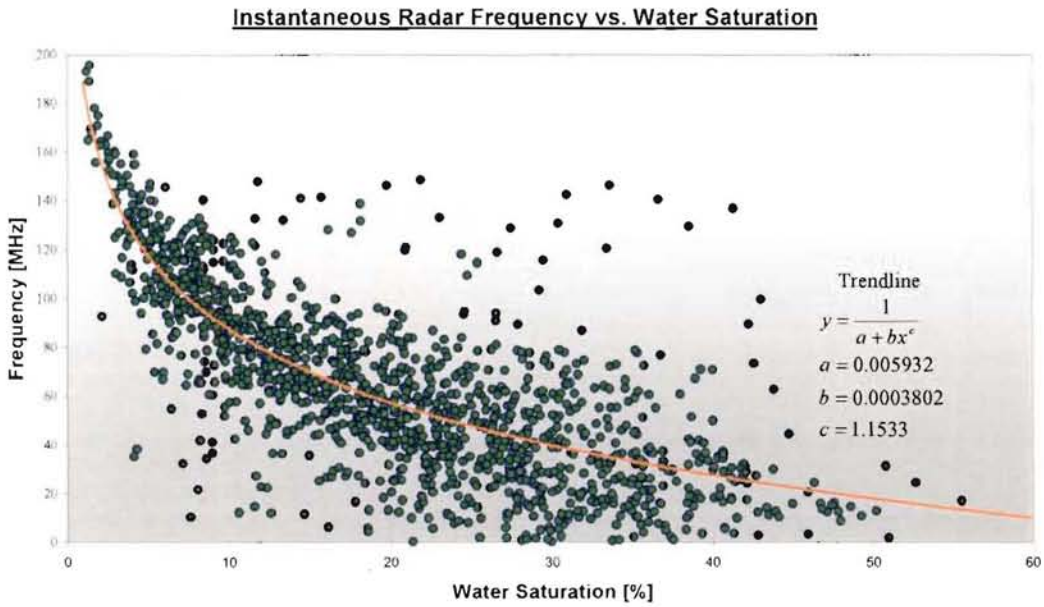

Figure 8.3 – Instantaneous radar frequency vs. water saturation with trendline.

can be matched up to the 14th order. As no previous research has been conducted on the correlation of the frequency content of GPR data to the humidity of a lateritic weathering profile there was no *a priori* indication of the nature of the mathematical model to use. Thus all model families were tested for the initial analysis. The best-fit model is of the yield-density type, and is known as a Harris model (Hyams, 1997). A Harris model has the form:

$$y = \frac{1}{a + bx^c} \qquad [8.1]$$

The yield-density models are widely used in scientific applications, especially in agricultural modelling. These models have historically been used to represent the relationship between the yield of a crop and the spacing or density or planting. The curve related to this equation, as well as the coefficients for a, b, and c, are shown in Figure 8.3. The best-fit model was reached after 39 iterations. The software generates two useful error analyses of the curve fit performance: the correlation coefficient and the standard error of the estimate. The correlation coefficient ranges from -1 to 1, where -1 indicates a perfectly decreasing (usually linear) trend, and +1 indicates a perfect increasing (usually linear) trend. The standard error is a unitless positive number that represents the relative misfit between the model and the data; a smaller standard error represents a better fit between the model curve and the data. The Harris model used to match the radar frequency with the humidity data has a correlation coefficient of 0.76 and a standard error of 23.7.

8.2 Percent Humidity vs. Percent Ni

In examining the borehole data from Loma de Níquel, a rough correlation became evident between the water content and the nickel grades. Indeed, examination of borehole data available from other laterite sites indicated a similar correlation. Borehole EM39 electromagnetic data from a previous test survey at Goro showed a marginal correlation between nickel grades and electrical conductivity of the soil (King pers.comm. 2000).

Based on the correlation of the radar data to the water content discussed above, further analysis of the dependence of mineralogical grades, most importantly nickel, on water saturation appear to be warranted.

When examined on an individual borehole basis, the correlation between the nickel grade and the water content appears to be good. In general, changes in the water content large enough to potentially yield a frequency shift in the radar data also approximately correspond to changes in the nickel grades. However, when the entire database of 1,399 points is plotted, little correlation is evident between the humidity of the weathering profile and the nickel grades (Figure 8.4). This is particularly so above a humidity of 10% or nickel grades of 0.5%, which describe the weathered zone of the laterite profile. Using the same criteria as those discussed in the previous section, the correlation coefficient of the best fit to these points is 0.64, with a standard error of 46.

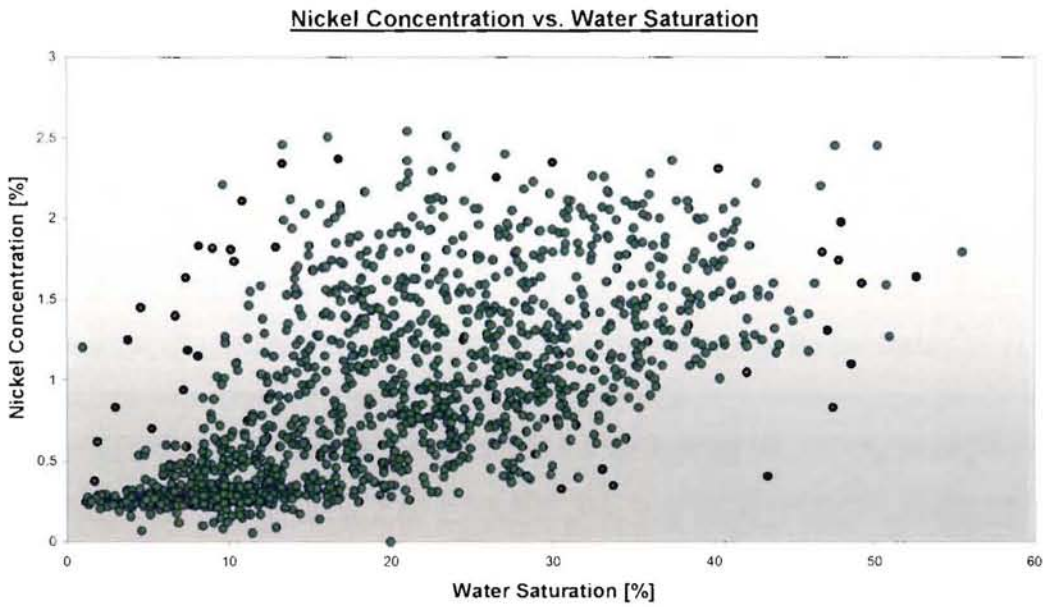

Figure 8.4 – Nickel concentration vs. water saturation.

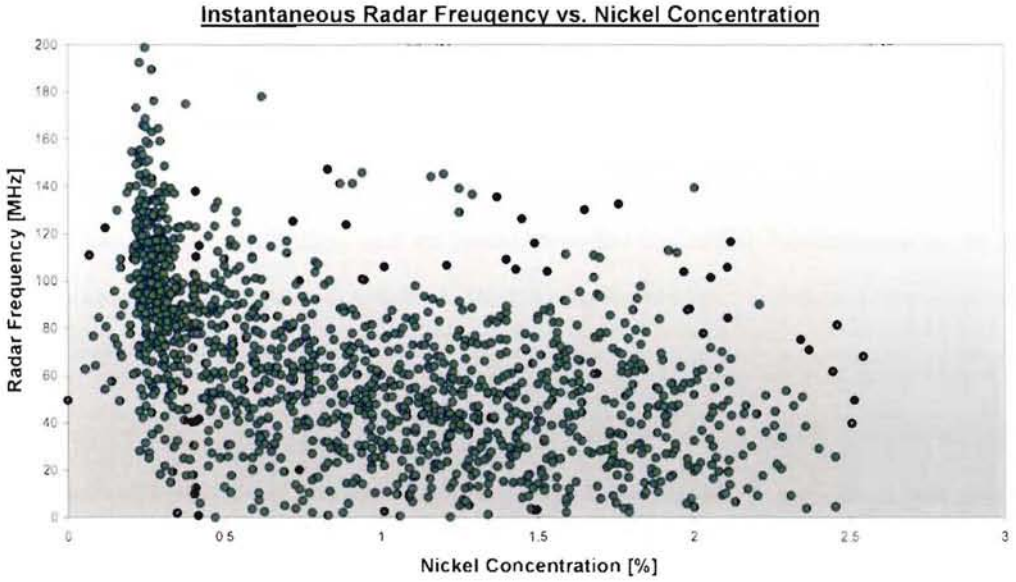

Figure 8.5 – Instantaneous radar frequency vs. nickel concentration

These values indicate that there is little correlation between the nickel grades and the humidity of the weathering profile at Loma de Níquel. Discussions with a number of laterite specialists have indicated that the best correlation between these two variables would be seen at a site where the lateritisation process is presently active, such as at Goro (Tessarolo pers.comm. 1999). At Loma de Níquel, the process is has for the most part ceased (Alvez pers.comm. 1999).

An attempt to correlate the radar frequency response to the nickel grades measured in the boreholes is shown in Figure 8.5. As expected based on the lack of good correlation between the humidity and the nickel grade, there is nearly no correlation between the radar data and the nickel grades. It is again noted that these data are relevant only for the Loma de Níquel site, and may not be representative of correlations found in other, developing, laterite sites.

8.3 General Correlation of Geochemistry and Mineralogy to Radar Data

Although not economically significant, another parameter of possible consequence to the radar signature is the iron concentration in the weathering profile. As described in the Chapter 2, iron oxide largely remains after the decomposition of the parent rock. Thus, the concentration of the iron decreases with depth in the profile. Using the same techniques as above, Figure 8.6 shows the correlation of the iron grade vs. humidity.

The best-fit curve for this relation is a 4th order polynomial expression, which provides a correlation coefficient of 0.82 and a standard error of 7.5. The correlation of iron grade to humidity is particularly good at iron grades less than 35%. A comparison of the radar frequency response to the %Fe is shown in Figure 8.7. A similar polynomial expression as above yielded a correlation coefficient of 0.78 and a standard error of 29.2. Thus, some correlation can be made between the radar frequency and the iron grade, although this argument is not as compelling as that for the correlation of the radar data and the humidity.

A number of other interesting correlations were attempted. A good correlation can be made between the radar frequency and the concentration of cobalt in the profile, particularly for Co concentrations under 250 ppm (Figure 8.8). This correlation is directly related to the correlation of the humidity to cobalt concentration (Figure 8.9). A similar correlation can be made between the radar data and the concentration of magnesium oxide in the profile (Figure 8.10). As MgO is the primary ionic component found in leachate in the lateritisation process (Golightly 1979), it is expected that its concentration increases greatly with depth, and thus is inversely proportional to the water saturation (Figure 8.11).

An analysis of the mineralogical correlations with the radar frequency indicates that any perceived relationship can be more easily explained by position of the data points within the weathering profile, and the associated humidity.. Therefore, no distinct correlation of the radar frequency data and the mineralogical constituents of the Loma de Níquel weathering profile was found that was independent of the water content.

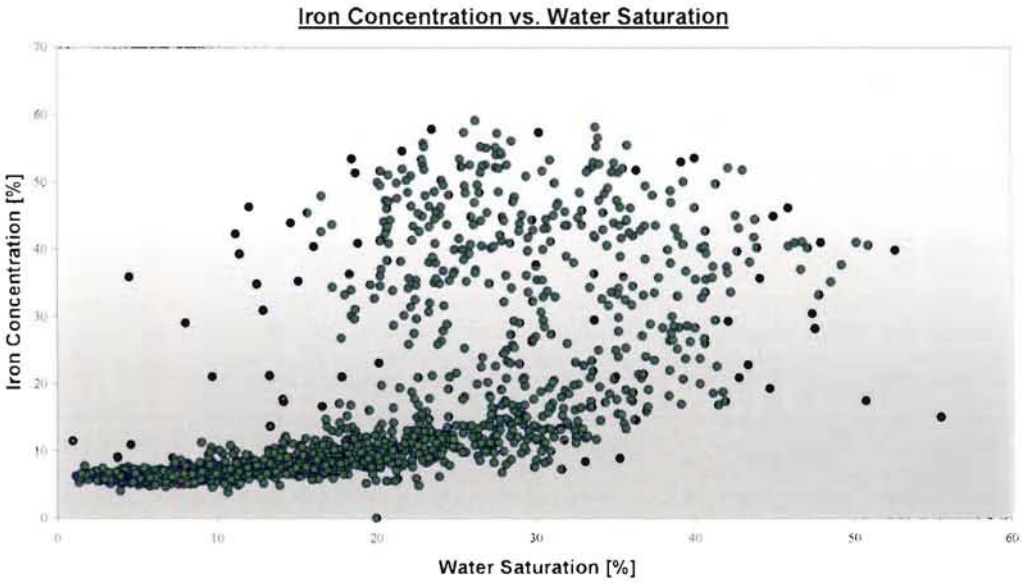

Figure 8.7 – Iron concentration vs. water saturation.

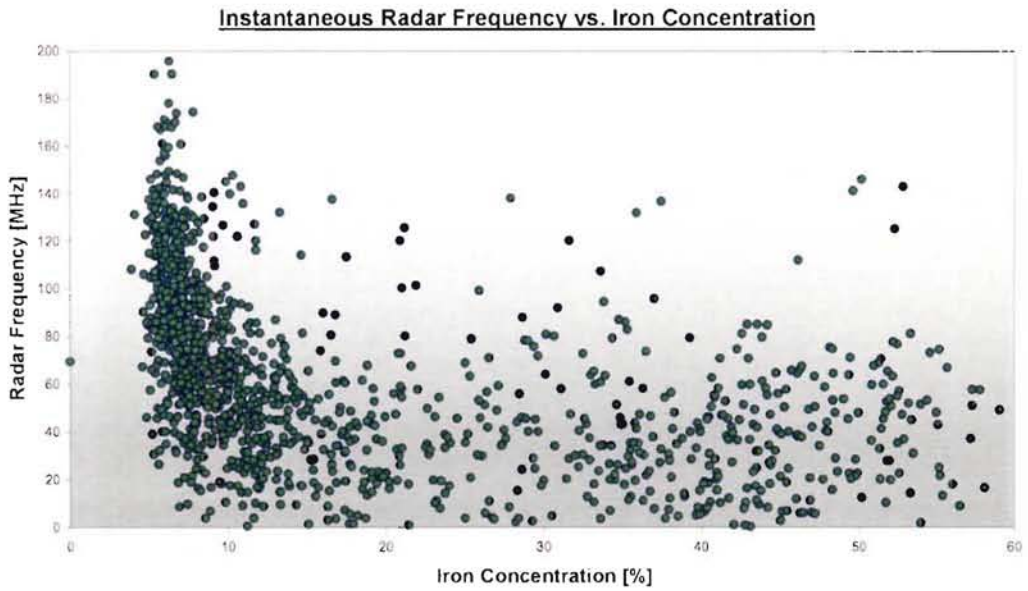

Figure 8.6 – Instantaneous radar frequency vs. iron concentration.

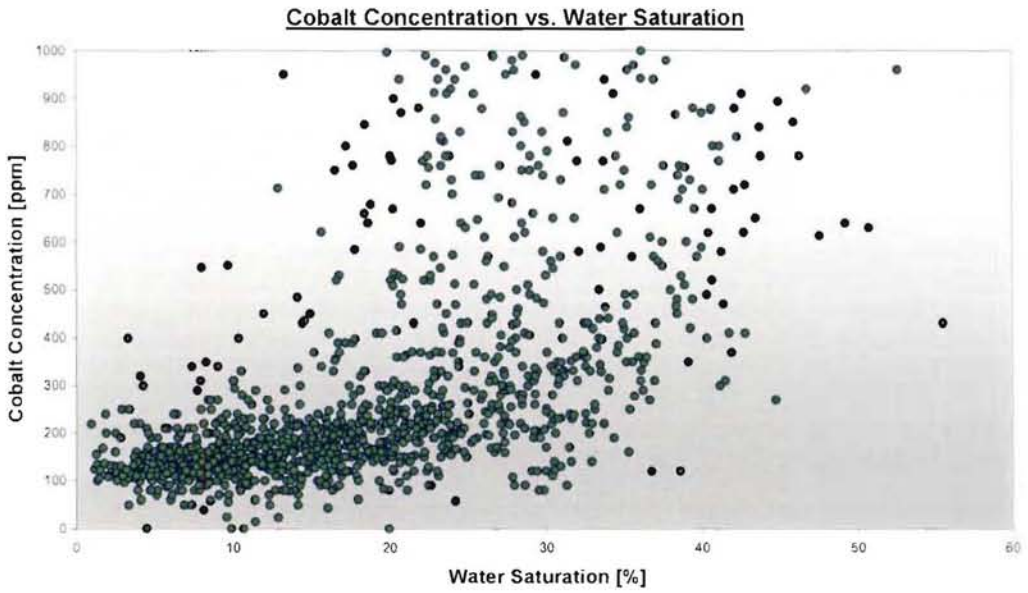

Figure 8.8 – Cobalt concentration vs. water saturation.

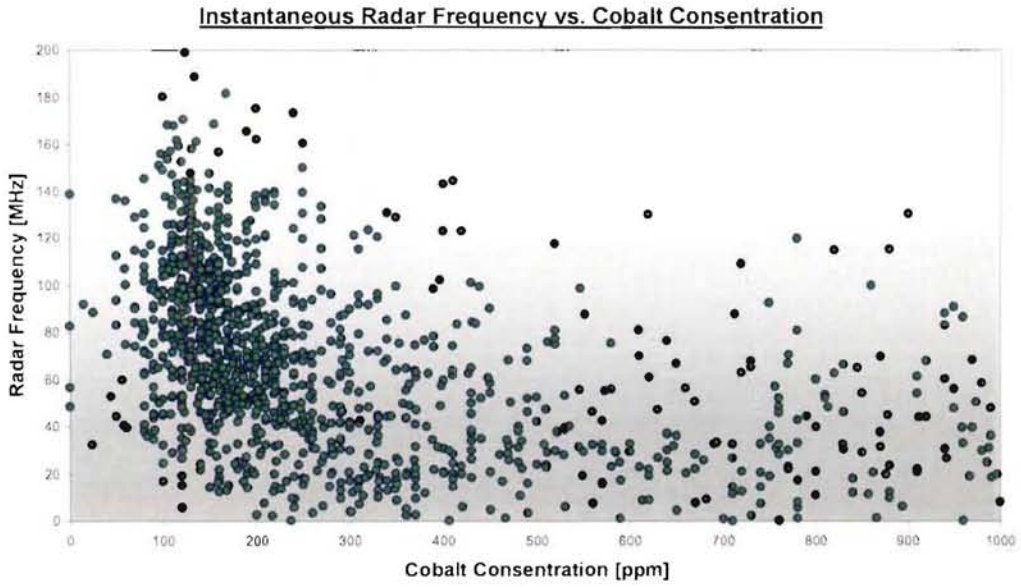

Figure 8.9 - Instantaneous radar frequency vs. cobalt concentration

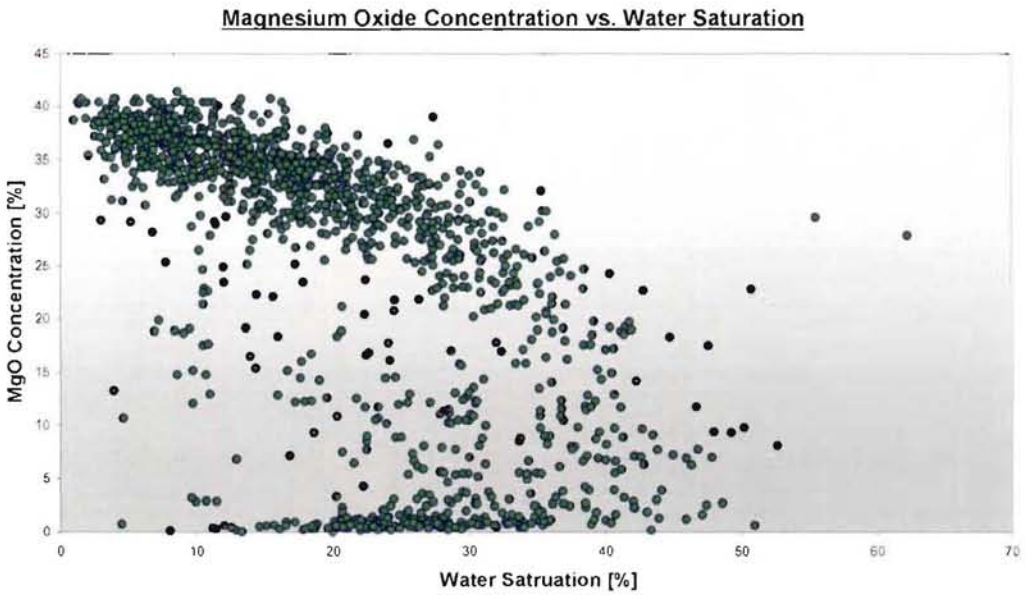

Figure 8.10 - Magnesium oxide concentration vs. water saturation.

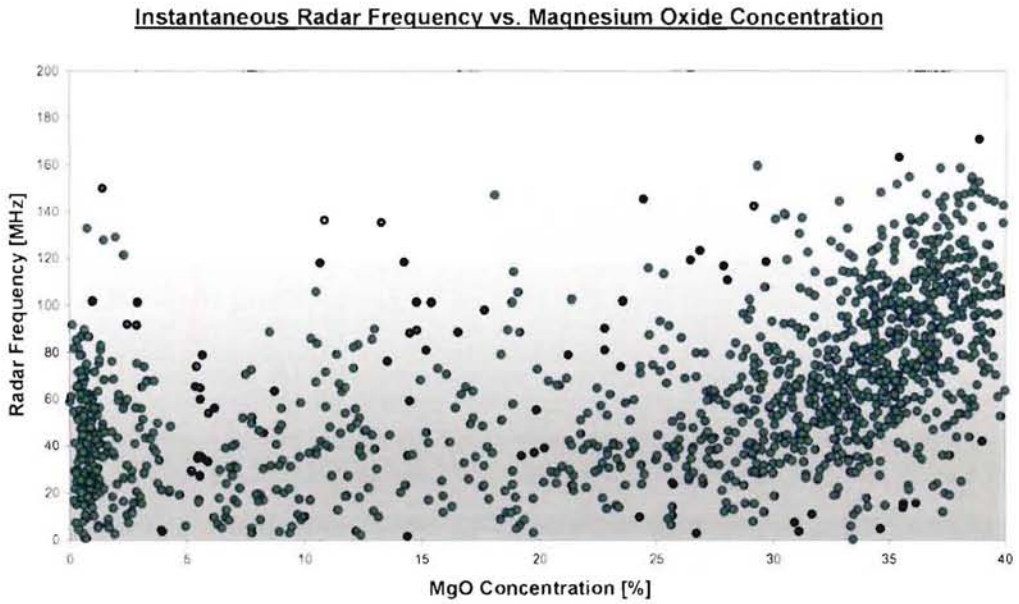

Figure 8.11 – Instantaneous radar frequency vs. magnesium oxide concentration.

Laterite cliff in Brazil showing exposed bedrock pinnacle and rocky saprolite corestones.

9 CONCLUSIONS AND RECOMMENDATIONS

9.1 Summary and Conclusions

Based on the geologic complexity of humid laterite deposits, a number of near-surface geophysical methods may be appropriate. Of these, GPR has been shown to be the most promising. Extensive tests have demonstrated that GPR can be highly effective in imaging the complex subsurface structures of humid laterite deposits, thereby increasing the understanding of the geology of a deposit. It is evident that GPR is a more effective method of defining the gross lateritisation sequence in some deposits than a linearly interpolated model derived from borehole or test pit data alone. Although borehole grids remain necessary for grade control, a coarser hole spacing based on geophysical information may result in a significant cost savings.

An analysis of the correlation of the radar data acquired at a site in South America to the geological information derived from boreholes indicates a strong relation between radar frequency and humidity in the profile. This analysis, along with data acquired at a variety of other sites suggests that the most important feature of a lateritic profile that impacts radar signatures is the water content. The water content tends to drop sharply at the transition between the earthy saprolite and rocky saprolite or bedrock. This zone also marks the transition from high-amplitude, low-frequency radar data to low-amplitude, high-frequency data. This change in radar frequency content is well delineated at most sites using the instantaneous frequency processing developed as part of this research. Although effective at imaging the gross features of the weathering profile, instantaneous frequency processing tends to mask linear features of possible importance, such as faults within the parent bedrock.

At the two sites in New Caledonia where GPR was tested extensively, radar signals were attenuated at shallower depths than in any other site previously studied. The poor results at Goro may be attributable to a possibly greater degree of serpentinisation and / or oxidation of the upper, iron-rich, sections of the weathering profile as compared to other laterite deposits. Greater serpentinisation or oxidation would lead to a higher magnetic permeability, and thus lower radar wave velocities with more attenuation.

The shortcomings of the GPR method in thick laterite profiles such as at Goro (> 40 m) may be overcome by the use of seismic refraction. Although significantly more costly that GPR, seismic survey techniques have shown some potential to delineate the gross weathering profile at depths well beyond the penetrability of radar.

Radar data acquired at Koniambo were difficult to correlate to borehole information, primarily because of the geological complexity of the deposit. A statistical analysis indicates the best correlation can be made between the radar data and the limonite / saprolite boundary. The correlation is greatest at boreholes where an abrupt transition from limonite to intermediate saprolite exists without an interstitial transitional limonite. This finding is contradictory to the results from the other test sites, where excellent correlations were made to the depth of the physical alteration zone, which generally is the earthy saprolite / rocky saprolite or bedrock transition.

The success of GPR in most humid laterites is unexpected given the high clay fraction in the weathering profile. It appears that laterites are exceptional circumstances because the clays have been leached of their conductive mineralogy, thereby lowering their dielectric permittivity and electrical conductivity (Section 4.1.2). The high water content of laterites may also assist in achieving deeper penetration of the radar energy due to refractive focussing (Section 4.1.3).

Caution must be exercised when evaluating a lateritic resource for the suitability of GPR. This research has demonstrated that there are dramatic variations in the geophysical response to tropical weathering profiles between different sites. For example, data from Ramu were easily able to map the top of rocky saprolite to depths of over 55 metres. However, it was ineffective at penetrating through saprolite into the unaltered bedrock. Conversely, data from Weda Bay and Sechol were able to profile the bedrock topography and texture, while not providing significant information on the limonite to saprolite boundary. It is hypothesised that the remnant electrical properties of the parent rocks have a significant affect on the radar signature and its penetration though weathering profiles.

Although no test work has been performed as part of this research on arid lateritic deposits, it is anticipated that high frequency electromagnetic methods such as GPR would be ineffective because the surface layer is often either electrically conductive due to salts left behind by evaporation or may form a hard resistive crust over a more conductive layer (Brand *et al.* 1996). Conductivities in the underlying saprolite are generally higher than those found in humid profiles (Parkinson 1998).

9.2 Recommendations

The richness of information provided by a carefully controlled geophysical survey in a lateritic environment may provide additional information beyond the gross weathering features. In theory, discrimination between laterite and earthy saprolite could be expected based, for example, on GPR reflections at horizons where differing water and mineral contents of the two materials exist, if the boundary is not gradational (i.e. greater than the Fresnel zone). More geological control and testing of the specific materials found at individual sites would be required to give confidence in extending the geophysical interpretation to this application. The interpretation of this transition would be significantly more difficult than that of the transition from weathered lateritic material to un-weathered rocky saprolite corestones and bedrock as was the primarily objective of most of the test surveys.

The refinement of the software created for this research and used to process the GPR data from many of the project sites is by no means complete to date. Further improvements in interpretability and accuracy may be accomplished by the integration of geophysical modelling or an iterative process for matching borehole and test pit information by locally varying radar velocities to account for small variations in material properties across individual profiles. That is, a more site-specific approach may be indicated.

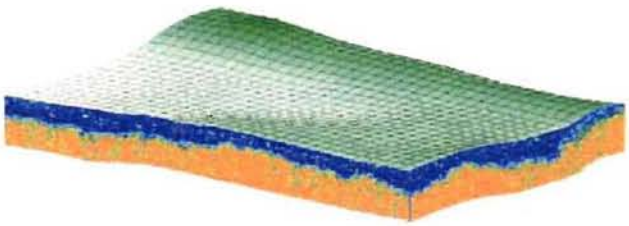

Figure 9.1 – Fence diagram of two-dimensional GPR lines from Loma de Niquel.

Due to the relative ease and speed of acquisition of GPR data, it may be possible to construct a 2½-dimensional data cube by interpolating between a grid of closely-spaced 2-dimensional profiles. However, the volume of data acquired may be prohibitively large. A less costly alternative may be to acquire a grid of GPR data with line spacings of the order of 100 m. Although this spacing would not image small individual pinnacles, fence diagrams may be created to assist in the geological understanding of the deposit. Such an exercise was undertaken using test data from the Loma de Niquel site in Venezuela (Figure 9.1). New software packages utilising the

virtual reality mark-up language (VRML) to image and manipulate data cubes and fence diagrams are readily available and would be of use in this application.

Despite significant advances in recent years, ground penetrating radar technology is still in its infancy. As diverse new applications are developed for the method, the understanding for its capabilities and limitations grow. The recent success of GPR in lateritic weathering environments disputes common assumptions that radar is ineffective in clay or iron-rich environments.

ACKNOWLEDGEMENTS

Sincere appreciation is extended to the large number of individuals and corporations who have lent invaluable support and financial assistance to this project. The principal sponsors of this project were INCO Ltd. and Falconbridge (Australia) Pty Ltd. The author wishes to thank Alan King, Claude Robillard, and Christian Tessarolo of INCO, Marc-Antoine Audet of Falconbridge, as well as Larry Queen of Highlands Pacific, Wilson Scarpelli, José Andre Alvez, and Romero Queiroz of Anglo American South America, and Bruce McMullin of Mighty Beaut Minerals for their geological insight.

Gratitude is also extended to INCO Ltd, Falconbridge (Australia), Highlands Pacific Ltd., Anglo American Base Metals, Weda Bay Minerals, Mighty Beaut Minerals, and Chesbar Resources for their permission to publish the respective datasets.

Appreciation is also given to the project's academic supervisor, Dr. David Nobes, who has contributed a great amount of time, insight and guidance.

The author's company, Associated Mining Consultants Ltd (AMCL), has contributed greatly to this project by providing much of the GPR instrumentation used for the research work. More importantly, AMCL donated the gift of time by granting the author considerable leave from professional obligations in order to complete the research work.

Finally, the author wishes to thank Graham Parkinson of Klohn Crippen Consultants, without whom none of this would have been possible.

REFERENCES

Alcock, R.A., 1988, The character and occurrence of primary resources available to the nickel industry. In: Tyroler, G.P. & Landolt, C.A. (editors), Extractive metallurgy of copper, nickel, and cobalt: The Metallurgical Society, 67-89

Allnor, R., Caiti, A. and Arntsen, B., 1997, Inversion of seismic surface waves for shear wave velocities: Annual Meeting Abstracts, Society Of Exploration Geophysicists, 1921-1924.

Annan, A.P. and Cosway, S.W., 1992, Simplified GPR beam model for survey design: Annual Meeting Abstracts, Society of Exploration Geophysicists, 747-760.

Annan, A.P., Cosway, S.W. and Sigurdsson, T.S., 1994, GPR for snow pack water content: 5th Int. Conf. On Ground Penetrating Radar, Proceedings.

Annan, A.P., Scaife, J.E. and Giarnou, P., 1990, Mapping buried barrels with magnetics and ground penetrating radar: Annual Meeting Abstracts, Society of Exploration Geophysicists, 422-423.

Annan, A.P., Waller, W.M., Strangway, D.W., Rossiter, J.R., Redman, J.D. and Watts, R.D., 1975, The electromagnetic response of a low-loss, 2-layer, dielectric earth for horizontal electric dipole excitation: Geophysics, **40**, no. 3, 285-298

Balde, M. and Aiken, C. L. V., 1997, Global positioning system (GPS) elevations and geoid corrections in geophysical surveys with examples in Nevada, North Dakota and Ecuador: Annual Meeting Abstracts, Society Of Exploration Geophysicists, 535-538.

Barnes, A. E., 1992, The calculation of instantaneous frequency and instantaneous bandwidth (short note): Geophysics, **57,** no. 11, 1520-1524.

Barongo, J. O. and Palacky, G. J., 1991, Investigations of electrical properties of weathered layers in the Yala area, western Kenya, using resistivity soundings: Geophysics, **56,** no. 01, 133-138.

Bates, C.B., Phillips, D., Lavely, E and Lynn, H.B., 1996, Near surface variability in shear wave velocity anisotropy: Annual Meeting Abstracts, Society of Exploration Geophysicists, 739-742.

Beeching, A., 1999, The potential of ground penetrating radar and other geophysical methods for delineating subsurface clay layers at the Taharoa ironsand mine. Unpublished B.Sc. (Honours) project, Department of Geological Sciences, University of Canerbury.

Besset, F., Coudray, J., 1978, Le comportement du nickel dans les processus d'alteration, des peridotites de Nouvelle Caledonie: Bur. Récherches Geol. Min. Bull., ser **2**, sec. 2, no. 3, 207-223.

Brand, N.W., Butt, C.R.M., Elias, M., 1998, Nickel laterites: classification and features: AGSO J. of Austral. Geol. & Geoph., **17**(4), 81-88.

Brand, N.W., Butt, C.R.M., Hellsten, K.J., 1996, Structural and lithological controls in the formation of the Cawse nickel laterite deposits, Western Australia – implications for supergene ore formation and exploration in deeply weathered terrains: Nickel'96 Conf., Proceedings, 185-190.

Buland, A., 1998, Relative Amplitude Processing - a Contractor Evaluation : 61st Mtg. Eur. Assoc. Expl Geophys., Extended Abstracts, European Association Of Geophysical Exploration, Session:P004.

Burger, P.A., 1996, Origins and characteristics of lateritic nickel deposits: Nickel'96 Conf., Proceedings, 179-183.

Cambell, T., Tealby, J.M. and Giannopoulos, A., 1993, Signal analysis of GPR data of voids in archaeology: 61st Mtd. Eur. Assoc. Expl. Geophys., Extended Abstracts, European Association of Geophysical Exploration, Session: P039.

Chandola, S. K., Singh, V., Singh, J. N. and Chaturvedi, R. K., 1997, Weathering configuration of Ariyalur - Pondicherry depression and its impact on seismic data: Annual Meeting Abstracts, Society Of Exploration Geophysicists, 126-129.

Choudhury, Kalpan, 1982, Statistical analysis of airborne electromagnetic signatures of different conductor groups in tropical terrain of Karnataka India: Geophys. Prosp., **30,** no. 02, 217-231.

Coen, S. and Yu, M.W.H., 1981, The inverse problem of the direct current conductivity profile of a layered earth: Geophysics, **46**, no. 12, 1702-1713.

Conyers, L.B. and Goodman, D., 1997, Ground penetrating radar – an introduction for archaeologists: AltaMira Press Inc.

Cooper, N.J. and Maliotis, G., 1991, The application of transient electromagnetics to an integrated mineral exploration program: 61st Mtg. Eur. Assoc. Expl. Geophys., Extended Abstracts, European Association of Geophysical Exploration, 334-335.

Daniels, D.J., Gunton, D.J. and Scott, H.F., 1998, Introduction to subsurface radar: IEEE Proceedings, Vol. 135, Pt. F, No. 4, 278-320.

Davis, J.L. and Annan, A.P., 1989, Ground penetrating radar for high-resolution mapping of soil and rock stratigraphy: Geophys. Prosp., **37**, no. 05, 531-552.

Davis, J.L., Annan, A.P., Black, G. and Leggatt, C.D., 1985, Geologic sounding using low-frequency radar: Annual Meeting Abstracts, Society of Exploration Geophysicists, Session: AG.4.

Docherty, P., 1992, Solving for the thickness and velocity of the weathering layer using 2-D refraction tomography: Geophysics, **57**, no. 10, 1307-1318.

Fazakerley, V.W., Monti, R., 1998, Murrin Murrin nickel – cobalt deposits, in Berkman, D. A., Mackenzie, D.H.: Geology of Australian and Papua New Guinean Mineral Deposits, Austral. Ins. Min. Metall., 329-334.

Francké, J.C., 2000, Ground penetrating radar survey of the Sechol Nickel Prospect, Guatemala: Confidential report submitted to Chesbar Resources Ltd. by Assoc. Min. Consul. Ltd.

Francké, J.C., 1999, Ground penetrating radar survey of the Loma de Niquel Prospect, Venezuela: Confidential report submitted to Minorco SA by Assoc. Min. Consul. Ltd.

Francké, J.C., 1999, Ground penetrating radar survey of the Celestial Nickel Prospect, Philippines: Confidential report submitted to Mighty Beaut Minerals Inc. by Assoc. Min. Consul. Ltd.

Francké, J.C., 1999, Ground penetrating radar survey of the Barro Alto Nickel Prospect, Brazil: Confidential report submitted to Anglo American Base Metals by Assoc. Min. Consul. Ltd.

Francké, J.C., 1997, The role of ground penetrating radar in a pipeline river crossing – a case history from the jungles of Ecuador: 3rd Meeting Environmental and Engineering Geophysical Society European Section, Proceedings, 279-282.

Francké, J.C., Nobes, D.C., 2000, A preliminary evaluation of GPR for nickel laterite exploration: In Noon, D.A., Stickley, G.F. and Longstaff, D. (eds), GPR 2000: Proceedings of the 8th Int. Conf. On Ground Penetrating Radar, Proceedings, 7-13.

Francké, J.C., Parkinson, J.G., 1999, The new role of geophysics in nickel laterite exploration and development: Mining Millennium / PDAC 2000 Conf., Proceedings.

Geonics Ltd., 1980, Electromagnetic terrain conductivity measurement at low induction numbers: Geonics Technical Notes.

Golightly, J.P., 1979, Geology of Soroako nickeliferous laterite deposits: International Laterite Symposium, Proceedings, 38-57.

Golightly, J.P., 1979, Nickeliferous laterites: a general description: International Laterite Symposium, Proceedings, 3-23.

Golightly, J.P., 1981, Nickeliferous laterite deposits: Economic Geology, 75th Ann. Vol., 710-718.

Gomez, R., Ogryzlo, C.T. and Dor, A.A., 1979, The Cerro Matoso nickel project: International Laterite Symposium, Proceedings, 412-458.

Goodman, D., 1994, Ground penetrating radar simulation in engineering and archaeology: Geophysics, **59**, no. 5, 224-232.

Grant, F.S. and West, G.F., 1965, Interpretation theory in applied geophysics: McGraw Fill Book Company, 345-350.

Gurevich, B., 1999, Effect of fluid viscosity on elastic wave attenuation in porous rocks: Annual Meeting Abstracts, Society Of Exploration Geophysicists, 17-21.

Harrison, C.H., 1970, Reconstruction of subglacial relief from radio echo sounding records: Geophysics, **35**, no. 06, 1099-1115.

Hatherly, P.J. and Tayton, J.W., 1983, The shallow refraction seismogram: Proceedings of the ASEG 13th Geophysical Conference, Australian Society of Exploration Geophysicists, 37-39.

Haldemann, E.G., Buchan, R., Blowes, J.H., Chandler, T., 1979, Geology of lateritic nickel deposits, Dominican Republic: International Laterite Symposium, Proceedings, 57-84.

Harju, H.O., 1979, Exploration of Exmibal's nickel laterite deposits in Guatemala: International Laterite Symposium, Proceedings, 245-251.

Harju, H.O., 1979, Exploration of PT INCO's nickel laterite deposits in Sulawesi, Indonesia: International Laterite Symposium, Proceedings, 292-299.

Havryluk, I., Huff, V.R., 1979, The current status of the Gag Island nickel laterite project: International Laterite Symposium, Proceedings, 382-394.

Hellsten, K., Lewis, C.R., Denn, S., 1998, Cawse nickel-cobalt deposit, in Berkman, D. A., Mackenzie, D.H.: Geology of Australian and Papua New Guinean Mineral Deposits, Austral. Ins. Min. Metall., 335-338.

Jol, H.M. and Smith, D.G., 1991, Ground penetrating radar investigation of northern lacustrine deltas, Can. J. Earth Sci., 28, 1939-1947.

Knight, R. and Endres, A., 1990, A new concept in modeling the dielectric response of sandstones. Defining a wetted rock and bulk water system: Geophysics, **55**, no. 05, 586-594.

Knight, R. and Nur, A., 1987, The dielectric constant of sandstones 60 kHz to 4 MHz: Geophysics, **52**, no. 05, 644-654.

Langer, E., 1979, Ferronickel production at Marro do Niquel, Minas Gerias, Brazil: International Laterite Symposium, Proceedings, 397-411.

Lillie, A.R., Brothers, R.N., 1970, The geology of New Caledonia: N.Z.J. Geol. Geophys. **13**, 145-183.

Linchenat, A. and Shirakova, I., 1974, Individual characteristics of the nickeliferous iron (laterite) deposits of the north eastern part of the Cuba (Pinares de Mayari, Nicaro and Moa): Int. Geol. Cong., 24th Session, pt. XIV, sect. 14, 172-187.

Malamphy, M. C. and Vallely, J. L., 1944, Geophysical survey of the Arkansas bauxite region: Geophysics, **09,** no. 03, 324-366.

Matheson, P.J., 1996, The development of nickel/cobalt laterites in the South West Pacific: Nickel'96 Conf., Proceedings, 59-60.

Mavko, G. and Jizba, D., 1994, Relation between seismic P- and S-wave velocity dispersion in saturated rocks: Geophysics, **59,** no. 01, 87-92.

Miller, R.D. and Xia, J., 1997, Near-surface velocity gradients and their effect on shallow reflection data: Annual Meeting Abstracts, Society of Exploration Geophysicists, 792-795.

Monti, R. and Fazakerley, V.W., 1996, The Murrin Murrin nickel cobalt project: Nickel'96 Conf., Proceedings, 191-195.

Moorman, B.J. and Frederick, M.A., 1998, The application of ground penetrating radar to the study of glacial hydrology, 7th Int. Conf. On Ground Penetrating Radar, Proceedings, 137-142.

Musu, R. and Bell, J.A.E., 1979, PT INCO's Indonesian nickel project: International Laterite Symposium, Proceedings, 300-322.

Nobes, D.C., 1999, Geophysical surveys of burial sites: A case study of the Oaro urupa: Geophysics, **64**, no. 2, 357-367.

Norminton, E. J., 1990, Seismic model studies of the overburden bedrock reflection: P-wave and s-wave: Annual Meeting Abstracts, Society Of Exploration Geophysicists, 376-379.

Olhoeft, G.R., 1981, Electrical properties of rocks, in Touloukain, Y.S., Judd, W.R. and Roy, R.F., Eds., Physical Properties of Rocks and Minerals: McGraw-Hill, 257-330.

Osborne, R.C., 1996, Nickel laterite – existing operations and new developments: Presented at Prospectors and Developers Assn. of Canada (PDAC) Mtg.

Palacky, G. J. and Kadekaru, K., 1979, Effect of tropical weathering on electrical and electromagnetic measurements : Geophysics, **44,** no. 01, 69-88.

Palacky, G. J. and Sena, F. O., 1979, Conductor identification in tropical terrains - Case-histories from the Itapicuru Greenstone Belt Bahia Brazil: Geophysics, **44,** no. 12, 1941-1962

Parkinson, J.G., 1998, Geophysical site characterization in tropical weathering profiles: 8th Congress of Internat. Assn. of Eng. Geol. Vol. 1, 103-110.

Pelletier, B., 1996, Serpentines in nickel silicate ore from New Caledonia: Nickel'96 Conf., Proceedings, 197-205.

Peric, M., 1981, Exploration of Burundi nickeliferous laterites by electrical methods: Geophys. Prosp., **29,** no. 02, 274-287.

Queen, L.D., Parkinson, G.J., Francké, J.C., Brown, E.A., 1998, The integration of ground penetrating radar in resource delineation for nickel laterites in Papua New Guinea: Pac. Expl. Tech. Conference, Proceedings.

Ried, J.G., 1996, Laterite ores – nickel and cobalt resources for the future: Nickel'96 Conf., Proceedings, 11-16.

Robson, T., 1998, The Australian laterite nickel revolution: Presented at Metal Bulletin's Nickel and Its Markets Seminar

Sopko, M.D., 1979, The Exmibal nickel project: International Laterite Symposium, Proceedings, 272-291.

Springer, G., 1974, Compositions and structural variations in garnierites: Can. Mineral., v. 12, 381-388.

Taner, Koehler, Sheriff, 1979, Complex seismic trace analysis, Geophysics **44,** 6 June, 1041 -1059The Australian Institute of Mining and Metallurgy, 1999, Australasian code for reporting of mineral resources and ore reserves (The JORC code).

Theimer, B.D., Nobes, D.C. and Warner, B.G., 1994, A study of the geoelectrical properties of peatlands and their influence on ground penetrating radar surveying: Geophys. Prosp., **42,** 179-209.

Trescases, J.J., 1973, Weathering and geochemical behavior of the elements of ultramafic rocks in New Caledonia: Bur. Min. Res. Austral., Bull. **141,** 149-163.

Trescasses, J.J., 1975, L'evolution geochimique supergene des roches ultrabasiques en zone tropical. Formation des gisements nickeliferes de Nouvelle Caledonie: Nim ORSTOM, #78.

Troly, G., Esterle, M., Pelletier, B.G., Reibell, W., 1979, Nickel deposits in New Caledonia – some factors influencing their formation: International Laterite Symposium, Proceedings, 85-120.

West, D. and Witherly, K., 1995, Geophysical exploration for gold in deeply weathered terrains; two tropical cases: ASEG 13th Geophysical Conference, Australian Society Of Exploration Geophysicists, **26,** 124-130.

Unremediated historic mine site in New Caledonia.

APPENDIX I - NOTES ON THE GROUND PENETRATING RADAR METHOD

The radar method is superficially similar to reflection seismic surveying as used in petroleum exploration, in that depths are plotted on profiles using interpreted velocities and the two-way travel times of a reflected pulse.

In radar, the ideal pulse is a short single oscillation at a rated frequency of the antenna such as 25 MHz. In practice, the antennas ring after the output pulse, and as a result each reflection is composed of several complex cycles, causing even simple horizons to be represented as patterns of multiple lines on the radar profiles. In theory, a process called deconvolution can combine the data with a known signature of the output pulse in order to compress the effective pulse, resulting in sharper horizons in the final profiles. For uniform surface conditions, deconvolution can visibly improve the radar section, but in practice it is difficult to perform.

The radar pulse generally travels more slowly in the ground as it passes to greater depths. Conversely, seismic waves tend to travel more quickly with increased depth. One of the major influences on radar pulse velocity is the amount of water in the formation (i.e. pore space) and the conductivity of that water. As depth increases towards the water table, the pore space begins to fill with water and the radar velocity decreases. The limiting factor on the depth penetration of radar signals is the conductivity of the formation. Highly conductive fresh clays or fine silts will reduce the penetration and the velocity. Surface waters tend to be much less conductive than groundwater and are usually transparent to radar. Groundwater tends to be more conductive due to dissolved salts leached from the earth materials, absorbing radar energy. Lower radar frequencies can penetrate deeper before being absorbed, but may give a less precise definition of the geology due to their longer wavelengths.

At an interface where the velocity changes suddenly, the radar pulse will also experience a reflection of a portion of its incident energy. This can occur at changes in the porosity or the capillary conditions, such as exist between sands and gravels or at a gravel – bedrock interface. Below the water table, fractures in the bedrock may be water filed and show a strong enough contrast to cause a strong radar reflection to

occur. Changes in the iron content of the rocks, such as weathered seams in bedrock, will also cause strong reflections.

The radar method primarily shows interfaces where the properties of the earth change, either in radar velocity, conductivity, or in magnetic susceptibility. Although the radar method delivers a very detailed structural picture of changes in the subsurface, it does not directly classify materials. Instead, the interpreter must be prepared to examine the structure and decide if it matches a reasonable geological scenario. With increasing experience, the distance between boreholes can gradually be increased up to an optimum, which results in the most efficient overall mining program.

Interpretation of the results is an iterative process in which strategically placed borehole data is essential. Most importantly, studying the radar data gives the geologist a new appreciation for how much variation occurs in the sub-surface between boreholes.

The interpreter must be able to visualise the velocity variations and allow for initial discrepancies in the match between drill holes and radar profiles. This gives the radar data the best fit to the borehole information, and thus to the actual geology itself. Unfortunately, due to the lack of sufficient test pit or borehole data, this process was not possible at the some of the sites studied in this research. However, it is believed that the velocity estimates used, and thus the depth figures derived, were sufficiently accurate for the purposes of this project.

GLOSSARY OF RADAR RELATED TERMS

Attenuation

Attenuation describes how energy is lost or dissipated by a transformation of one type of energy to another. Attenuation is also used to describe energy lost through geometric spreading, surface and volume scattering, waveguides and multipathing.

Antenna frequency

Antennas are rated by their natural center frequency of oscillation, e.g. 25 MHz. Radar antennas are designed to be critically or over-damped so that the shortest output pulse at the desired frequency is produced.

Decibel (dB)

Ratio of signals: 10 times log of (Value 1 / Value 2).

Deconvolution

Filter operator that removes distortion from pulse.

Fresnel zone

A change in radar velocity can be distinguished only if its size is greater than the Fresnel zone. The zone if one of a theoretically infinite number of concentric ellipsoids of revolution which define volumes in the radiation pattern of an antenna.

***fk* filter**

Frequency (f) – wave number (k) filtering. Allows filtering of energy in profile based upon frequency and direction.

Imaginary impedance

Response of wave to conductivity. Higher conductivity results in faster absorption and dispersion (i.e. a smearing of the pulse form in time).

Radar

Radio Detection and Ranging

Radar range equation

The radar range equation describes how electromagnetic waves propagate through a material. For GPR, the equation describes how the propagating wave is modified by the transmitter antenna properties, geometric spreading losses, exponential material dissipation losses, scattering from a change in properties, orientation, polarization, geometric

spreading, coupling, and the receiver antenna properties.

Real impedance

Amplitude response of wave to magnetic and electric properties of the earth materials. Controls velocity and wavelength in material. Derived from electrical permittivity (dielectric constant) and magnetic susceptibility.

Signal to noise ratio

Measure of data integrity arrived at by dividing the returned signal power by the background noise power. SNR is typically measured in decibels. The higher the ratio, the better the radar data.

Velocity

The velocity of a radar wave in a given medium is equal to the speed of light in that medium, which is always slower than the speed of light in free space. The factors which control electromagnetic wave velocity are the dielectric permittivity and magnetic permeability polarisation properties of the medium.

In most nonmagnetic materials, the velocity equation may be simplified as equaling the speed of light in free space, c, divided by the square root of the relative dielectric permittivity.

Wavelength

The wavelength describes the spatial distance traveled by a propagating radar wave in one period. The wavelength is the velocity of propagation in a medium divided by the frequency of the radar wave.

INDEX

Plate 5.1 – Comparison of 25 MHz, 50 MHz and 100 MHz Antennas: Papua New Guinea

25 MHz Antennas

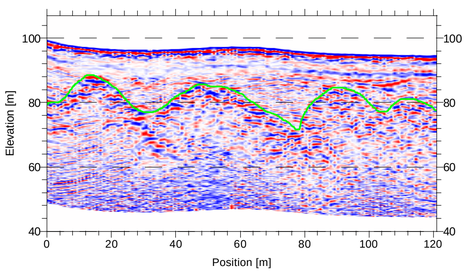

50 MHz Antennas

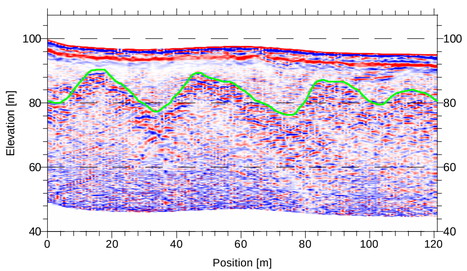

100 MHz Antennas

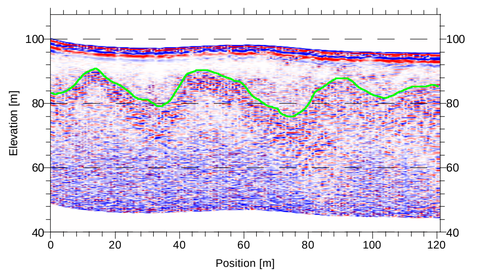

Radar Colour Amplitude Scale

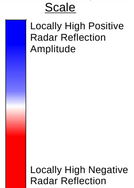

Interpretation Legend

From:
The Application of Geophysics in Nickel Laterite Resource Evaluation
by Jan Francke
MSc. Thesis - University of Canterbury
New Zealand - 2000

Scale 1:1000
No Vertical Exaggeration

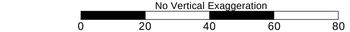

Chapter 5 - Plate 1
Comparison of 25 MHz, 50 MHz and 100 MHz Antennas
Ramu (Papua New Guinea)

Real Amplitude GPR Data
25, 50, and 100 MHz Antennas
250 ns AGC Window

Plate 5.2 – Bedrock Mapping Showing Rocky Saprolite Outcrops: Papua New Guinea

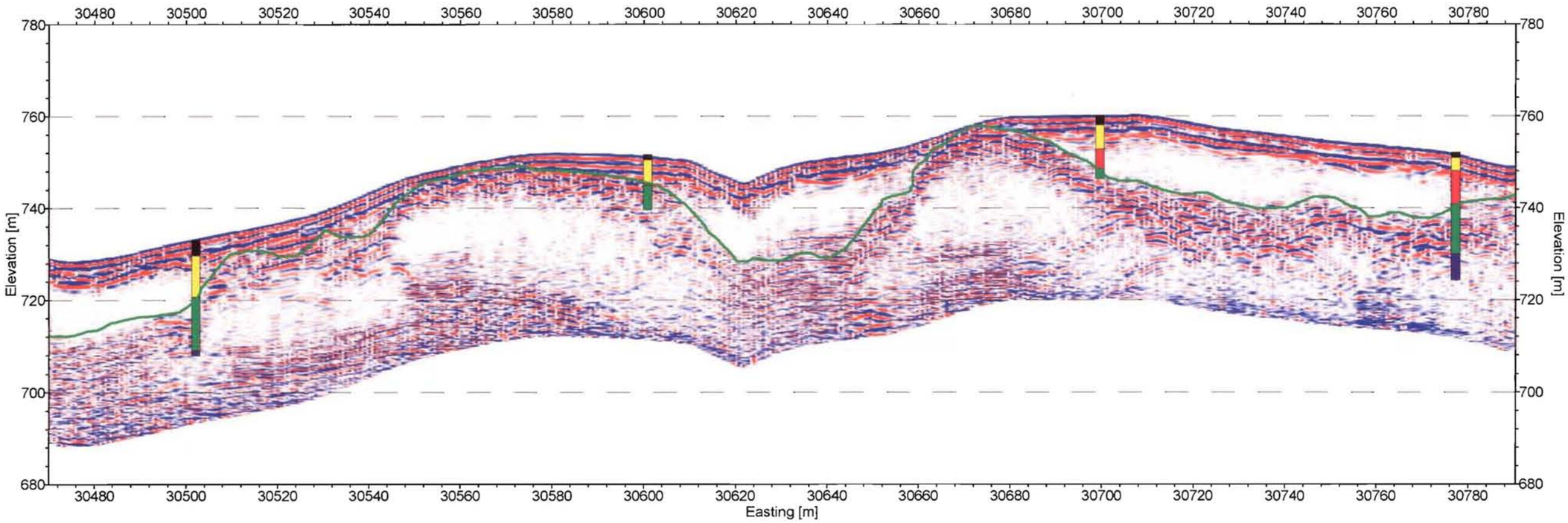

Borehole Legend

- Limonite Overburden
- Limonite
- Earthy Saprolite
- Rocky Saprolite
- Bedrock

Radar Colour Amplitude Scale

- Locally High Positive Radar Reflection Amplitude
- Locally High Negative Radar Reflection Amplitude

Interpretation Legend

- Interpreted Top of Rocky Saprolite

From:
The Application of Geophysics in Nickel Laterite Resource Evaluation
by Jan Francke
MSc. Thesis - University of Canterbury
New Zealand - 2000

Scale 1:1000
No Vertical Exaggeration

0 20 40 60 80 100 120

Chapter 5 - Plate 2
Bedrock Mapping Showing Rocky Saprolite Outcrops Ramu (Papua New Guinea)

Real Amplitude GPR Data and Interpretation
25 MHz Antennas
300 ns AGC Window

Plate 5.3 – Radar Attenuation in Lacustrine Environment: Papua New Guinea

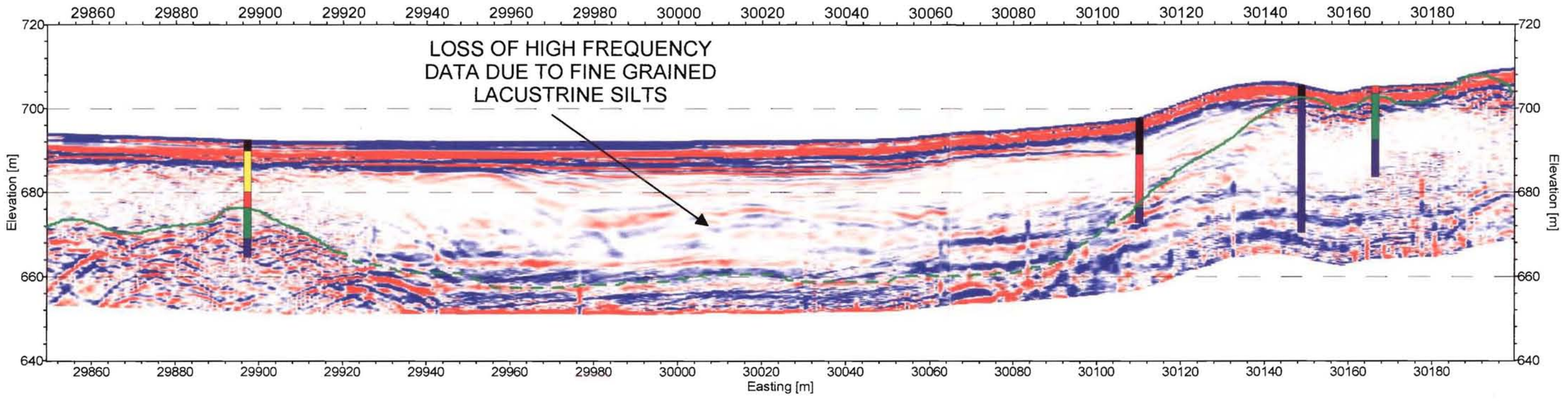

Borehole Legend

- Limonite Overburden
- Limonite
- Earthy Saprolite
- Rocky Saprolite
- Bedrock

Radar Colour Amplitude Scale

- Locally High Positive Radar Reflection Amplitude
- Locally High Negative Radar Reflection Amplitude

Interpretation Legend

- Interpreted Top of Rocky Saprolite

From:
The Application of Geophysics in Nickel Laterite Resource Evaluation
by Jan Francke
MSc. Thesis - University of Canterbury
New Zealand - 2000

Scale 1:1000
No Vertical Exaggeration

0 20 40 60 80 100 120

Chapter 5 - Plate 3
Radar Attenuation in Lucustrine Environment Ramu (Papua New Guinea)

Real Amplitude GPR Data and Interpretation
25 MHz Antennas
300 ns AGC Window

Plate 5.4 – Bedrock Mapping Showing Two Sub-cropping Pinnacles: Indonesia

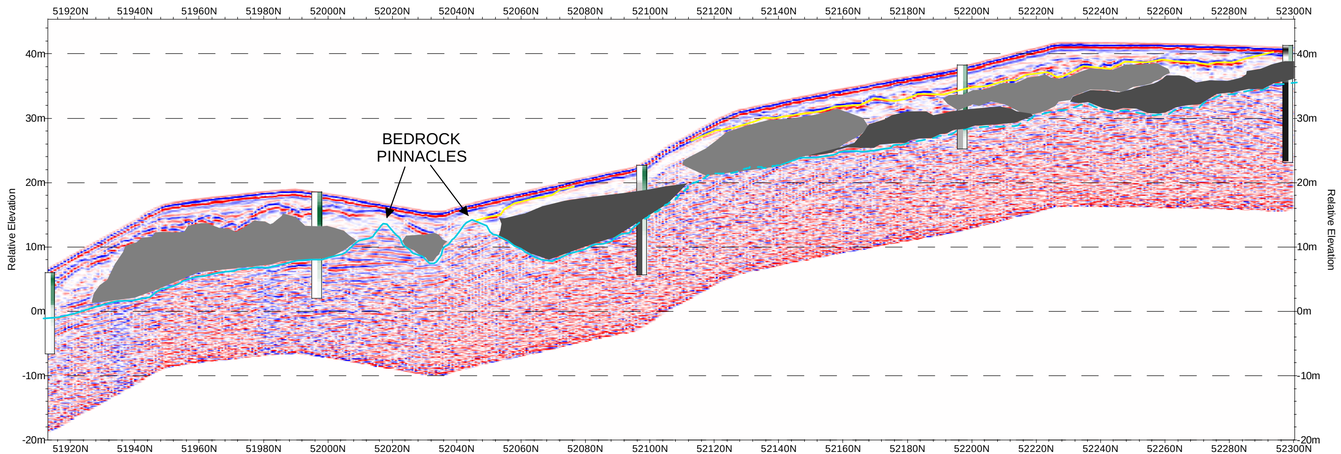

Northing

Borehole Legend

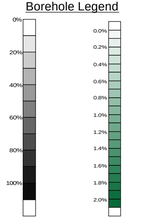

Percent Corestones/ Bedrock | Nickel Grade

Radar Colour Amplitude Scale

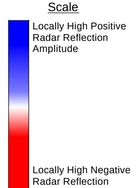

Locally High Positive Radar Reflection Amplitude

Locally High Negative Radar Reflection Amplitude

Interpretation Legend

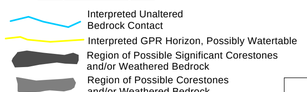

Interpreted Unaltered Bedrock Contact

Interpreted GPR Horizon, Possibly Watertable

Region of Possible Significant Corestones and/or Weathered Bedrock

Region of Possible Corestones and/or Weathered Bedrock

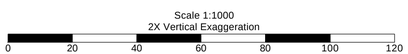

From:
The Application of Geophysics in Nickel Laterite Resource Evaluation
by Jan Francke
MSc. Thesis - University of Canterbury
New Zealand - 2000

Chapter 5 - Plate 4
Bedrock Mapping Showing Two Sub-cropping Pinnacles Weda Bay (Indonesia)

Real Amplitude GPR Data and Interpretation
50 MHz Antennas
400 ns AGC Window

Plate 5.5 – Variable Bedrock Topography with Outcrops: Indonesia

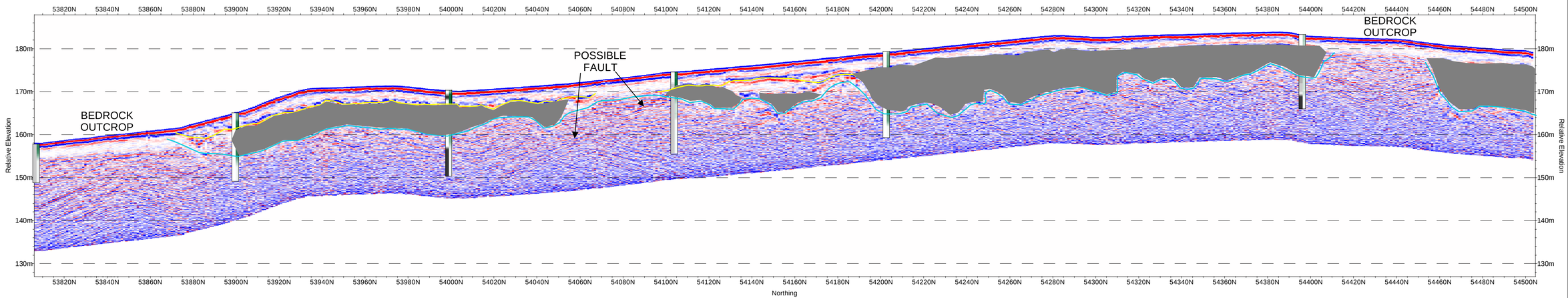

Borehole Legend

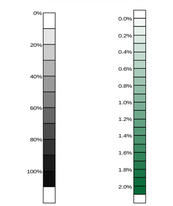

Percent Corestones/ Bedrock | Nickel Grade

Radar Colour Amplitude Scale

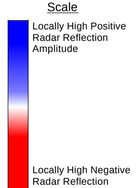

Locally High Positive Radar Reflection Amplitude

Locally High Negative Radar Reflection Amplitude

Interpretation Legend

Interpreted Unaltered Bedrock Contact

Interpreted GPR Horizon, Possibly Watertable

Region of Possible Significant Corestones and/or Weathered Bedrock

Region of Possible Corestones and/or Weathered Bedrock

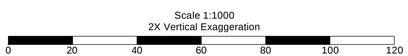

From:
The Application of Geophysics in Nickel Laterite Resource Evaluation
by Jan Francke
MSc. Thesis - University of Canterbury
New Zealand - 2000

Chapter 5 - Plate 5
Variable Bedrock Topography with Outcrops
Weda Bay (Indonesia)

Real Amplitude GPR Data and Interpretation
50 MHz Antennas
400 ns AGC Window

Plate 5.6 – Bedrock Mapping Showing Deeply Weathered Zone: Venezuela

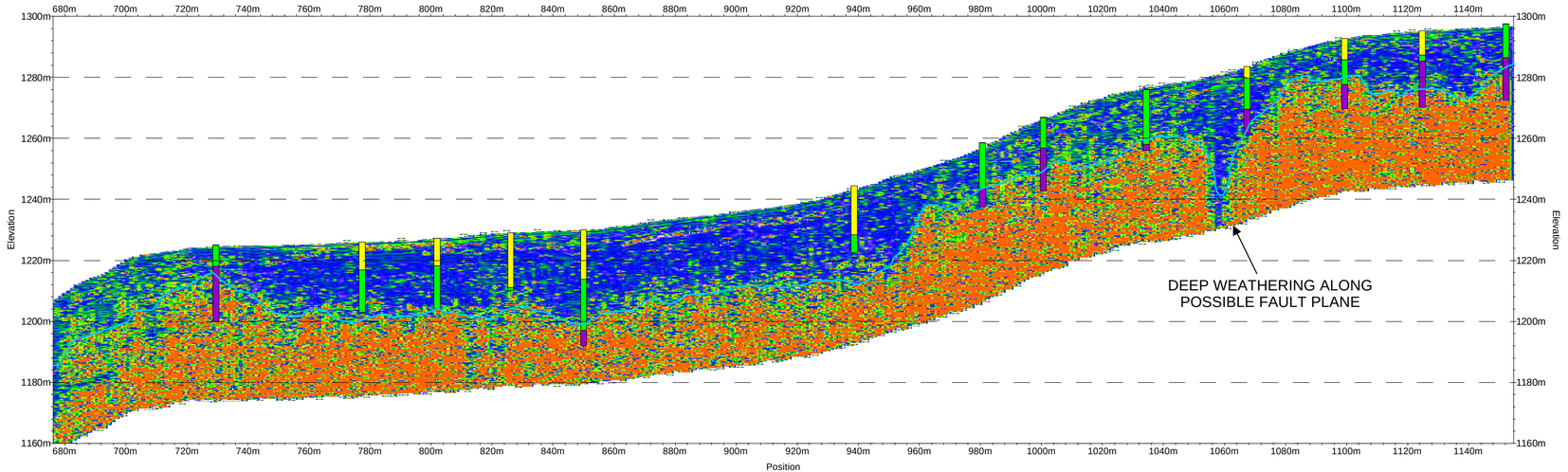

Borehole Legend

- Laterite
- Saprolite
- Un-Altered Bedrock

Radar Colour Instantaneous Frequency Scale

- Probable Weathered Laterite / Saprolite Region
- Probable Unaltered Bedrock or Corestones

Interpretation Legend

- Interpreted Unaltered Bedrock Contact

Scale 1:1000
No Vertical Exaggeration

0 20 40 60 80 100 120

From:
The Application of Geophysics in Nickel Laterite Resource Evaluation
by Jan Francke
MSc. Thesis - University of Canterbury
New Zealand - 2000

Chapter 5 - Plate 6
Bedrock Mapping Showing Deeply Weathered Zone Loma de Niquel (Venezuela)

Instantaneous Frequency GPR Data and Interpretation 25 MHz Antennas

Plate 5.7 – Bedrock Mapping Showing Pinnacle Structure: Venezuela

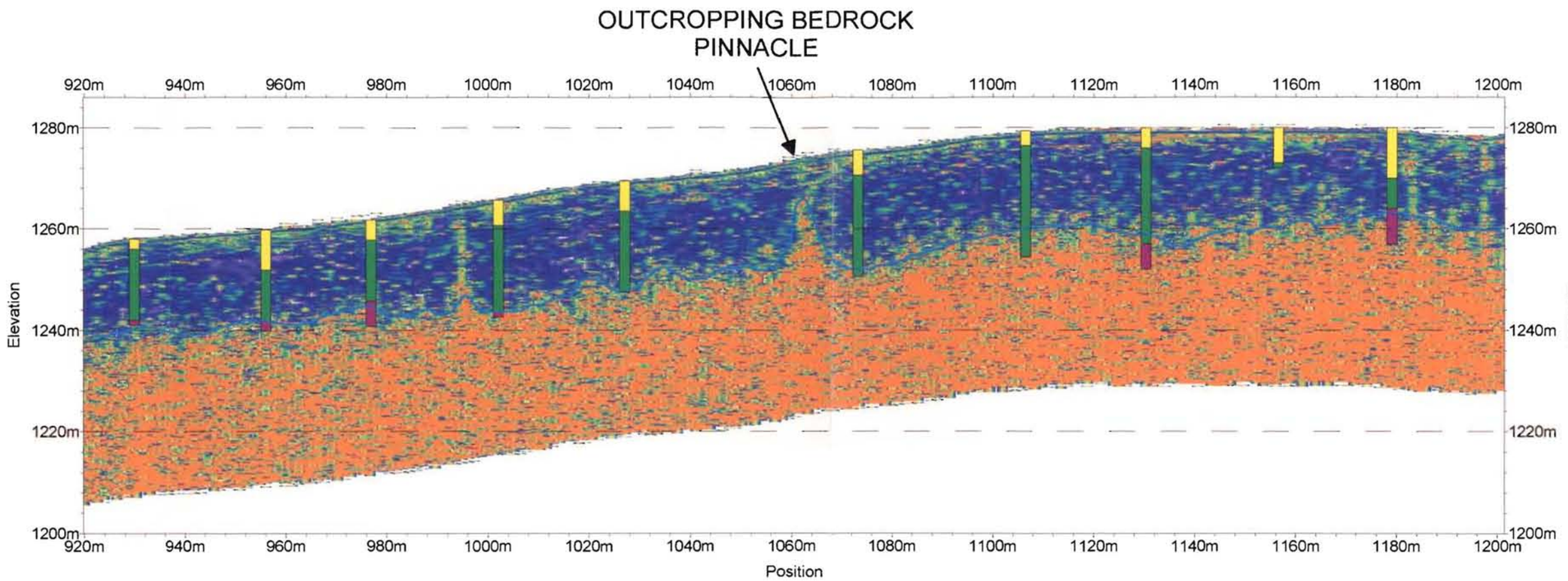

Borehole Legend

- Laterite
- Saprolite
- Un-Altered Bedrock

Radar Colour Instantaneous Frequency Scale

- Probable Weathered Laterite / Saprolite Region
- Probable Unaltered Bedrock or Corestones

Interpretation Legend

- Interpreted Unaltered Bedrock Contact

Scale 1:1000
No Vertical Exaggeration

0 20 40 60 80 100 120

From:
The Application of Geophysics in Nickel Laterite Resource Evaluation
by Jan Francke
MSc. Thesis - University of Canterbury
New Zealand - 2000

Chapter 5 - Plate 7
Bedrock Mapping Showing Pinnacle Structure Loma de Niquel (Venezuela)

Instantaneous Frequency GPR Data and Interpretation 25 MHz Antennas

Plate 5.8 – Highly Variable Bedrock Depths: Venezuela

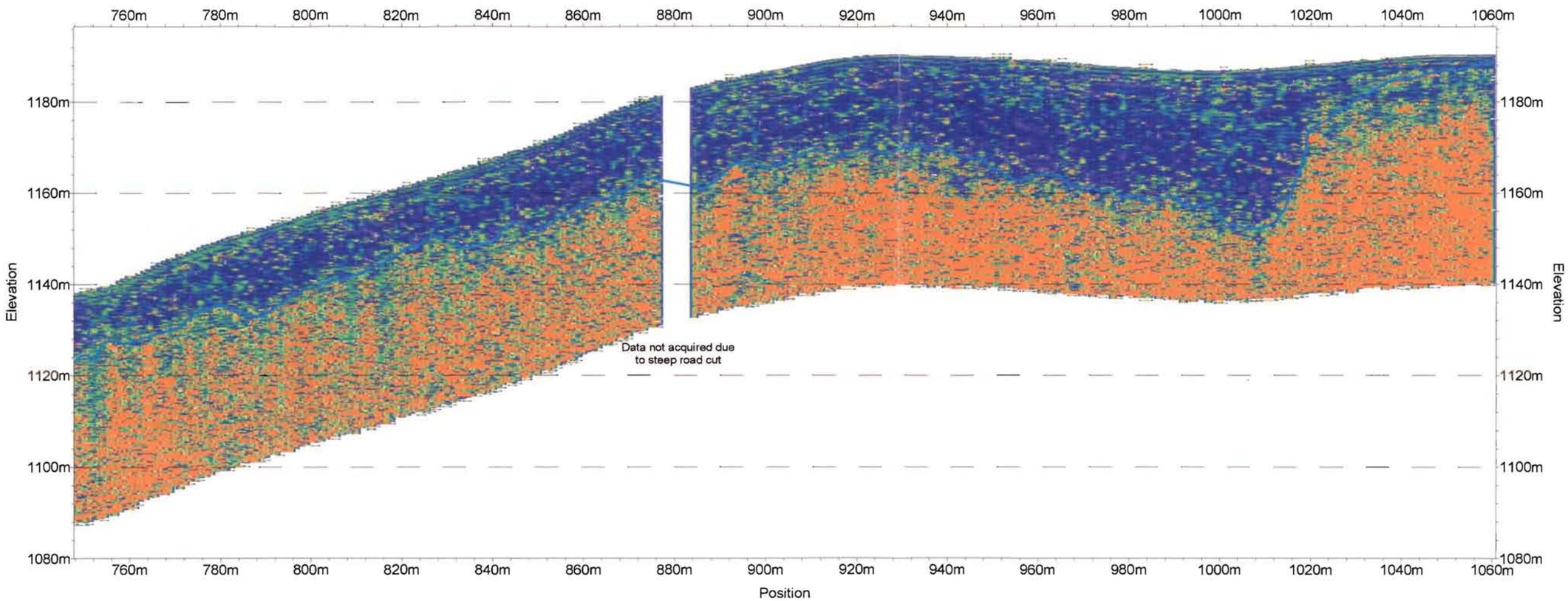

Radar Colour Instantaneous Frequency Scale

Probable Weathered Laterite / Saprolite Region

Probable Unaltered Bedrock or Corestones

Interpretation Legend

Interpreted Unaltered Bedrock Contact

From:
The Application of Geophysics in Nickel Laterite Resource Evaluation
by Jan Francke
MSc. Thesis - University of Canterbury
New Zealand - 2000

Scale 1:1000
No Vertical Exaggeration

0 20 40 60 80 100 120

Chapter 5 - Plate 8
Highly Variable Bedrock Depths
Loma de Niquel (Venezuela)

Instantaneous Frequency GPR Data and Interpretation
25 MHz Antennas

Plate 5.9 – Comparison of 12.5 MHz and 25 MHz Antennas: Venezuela

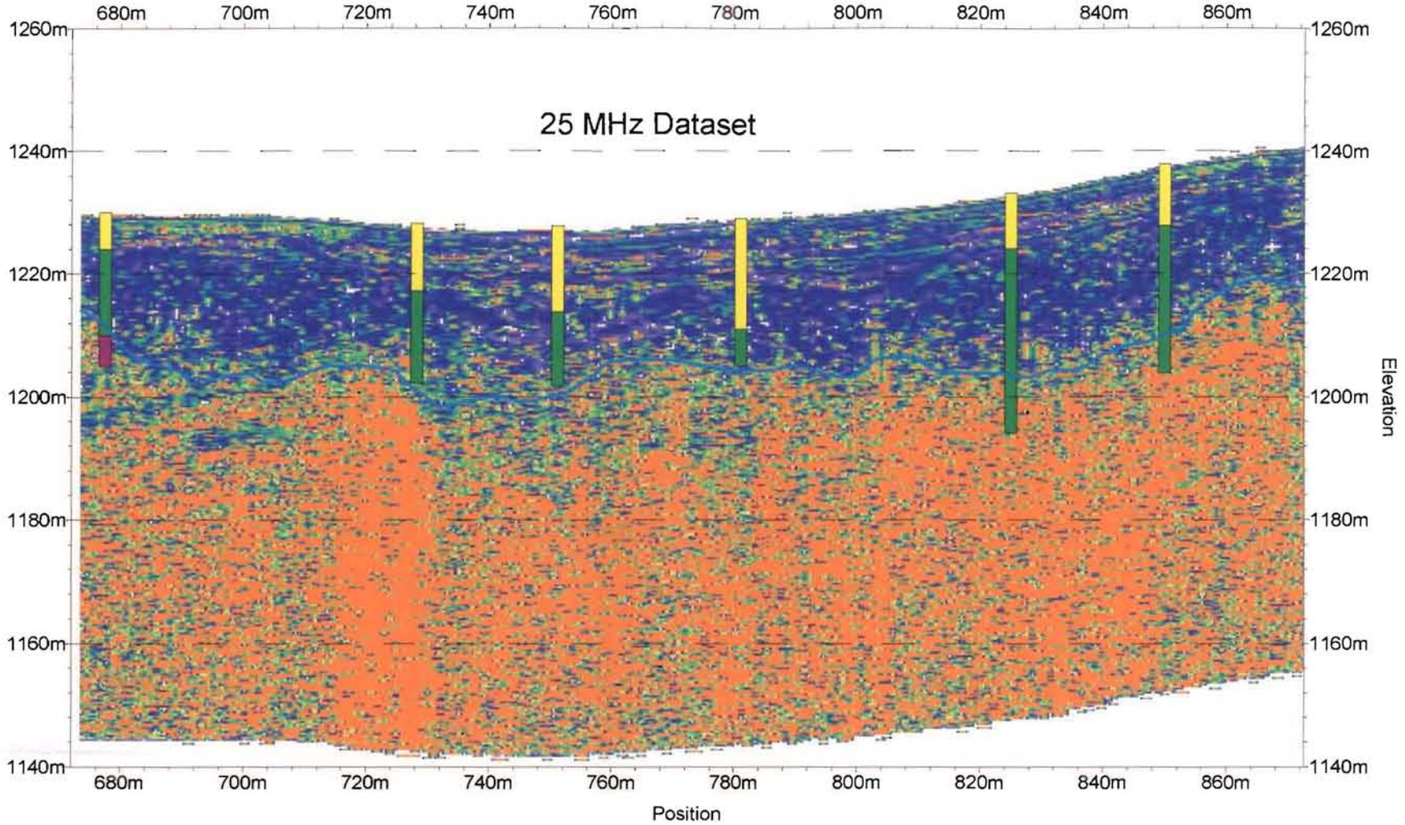

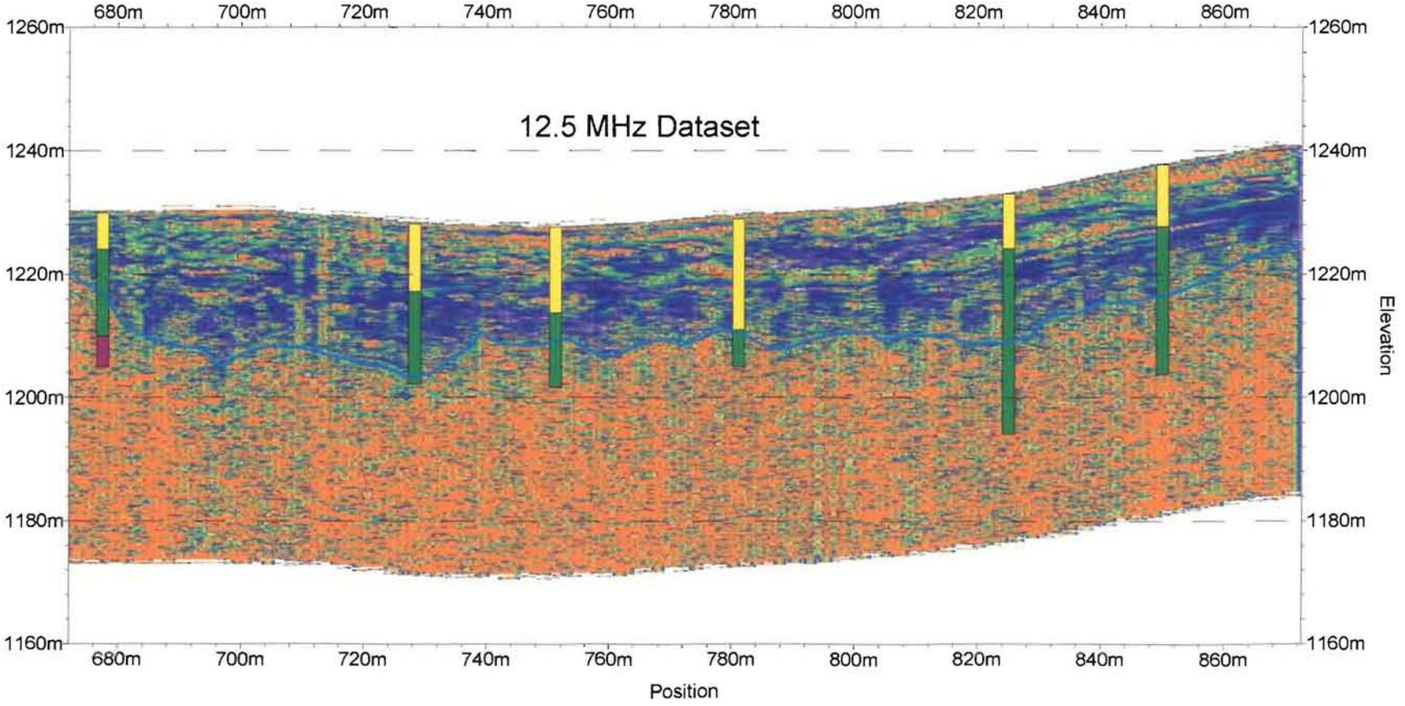

Borehole Legend

- Laterite
- Saprolite
- Un-Altered Bedrock

Radar Colour Instantaneous Frequency Scale

- Probable Weathered Laterite / Saprolite Region
- Probable Unaltered Bedrock or Corestones

Interpretation Legend

- Interpreted Unaltered Bedrock Contact

From:
The Application of Geophysics in Nickel Laterite Resource Evaluation
by Jan Francke
MSc. Thesis - University of Canterbury
New Zealand - 2000

Scale 1:1000
No Vertical Exaggeration

0 20 40 60 80 100 120

Chapter 5 - Plate 9
Comparison of 12.5 MHz and 25 MHz Antennas
Loma de Niquel (Venezuela)

Instantaneous Frequency GPR Data and Interpretation
12.5 MHz and 25 MHz Antennas

Plate 5.10 – Comparison of Fault Mapping with Real Amplitude and Instantaneous Frequency Displays: Venezuela

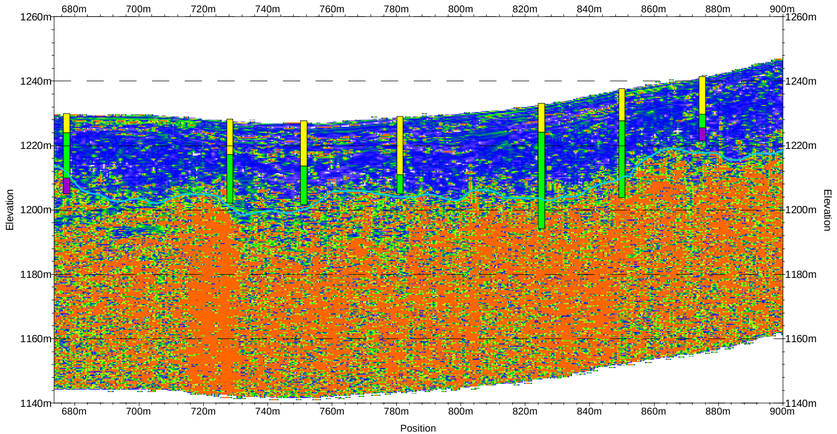

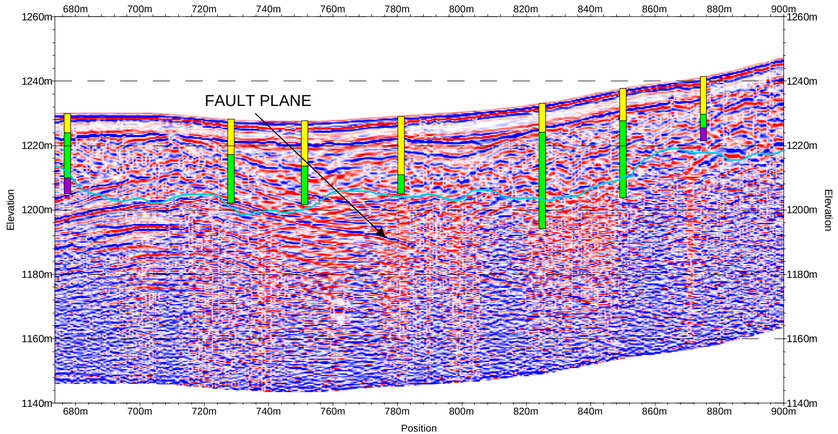

Borehole Legend

- Laterite
- Saprolite
- Un-Altered Bedrock

Radar Colour Instantaneous Frequency Scale

- Probable Weathered Laterite / Saprolite Region
- Probable Unaltered Bedrock or Corestones

Radar Colour Amplitude Scale

- Locally High Positive Radar Reflection Amplitude
- Locally High Negative Radar Reflection Amplitude

Interpretation Legend

- Interpreted Unaltered Bedrock Contact

0 20 40 60 80 100 120

Scale 1:1000
No Vertical Exaggeration

From:
The Application of Geophysics in Nickel Laterite Resource Evaluation
by Jan Francke
MSc. Thesis - University of Canterbury
New Zealand - 2000

Chapter 5 - Plate 10
Comparison of Fault Mapping with Real Amplitude and Instantaneous Frequency Displays
Loma de Niquel (Venezuela)

GPR Data and Interpretation
25 MHz Antennas

Plate 5.11 – Bedrock Mapping Showing Thin Remnant Laterite on Peripheral Slopes: Guatemala

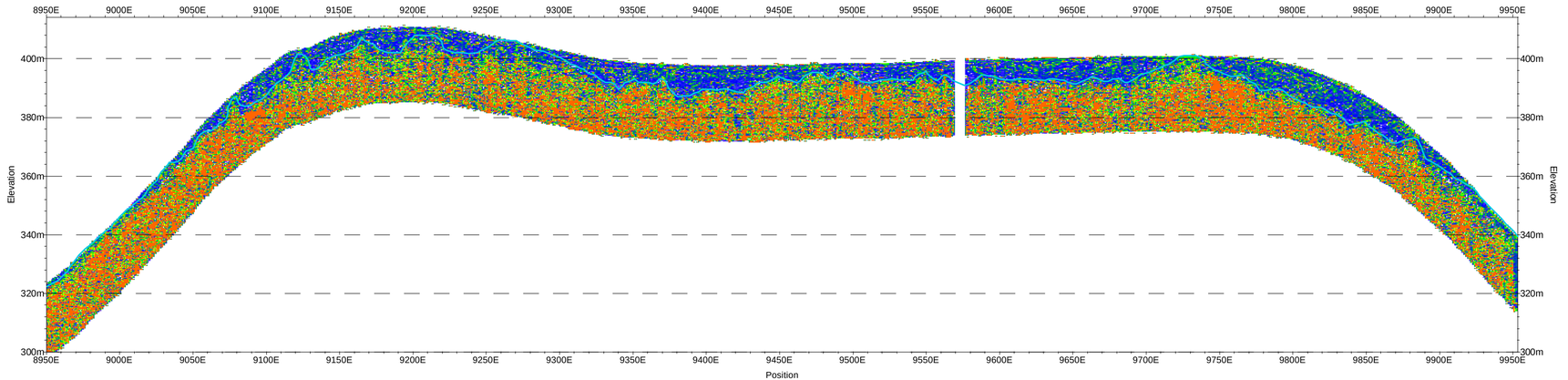

Radar Colour Instantaneous Frequency Scale

Probable Weathered Laterite / Saprolite Region

Probable Unaltered Bedrock or Corestones

Interpretation Legend

Interpreted Unaltered Bedrock Contact

Scale 1:2000
2X Vertical Exaggeration

0 40 80 120 160 200 240

From:
The Application of Geophysics in Nickel Laterite Resource Evaluation
by Jan Francke
MSc. Thesis - University of Canterbury
New Zealand - 2000

Chapter 5 - Plate 11
Bedrock Mapping Showing Thin Remnant Laterite on Peripheral Slopes Sechol (Guatemala)

Instantaneous Frequency GPR Data and Interpretation 50 MHz Antennas

Plate 5.12 – Bedrock Mapping Showing Zones of Thick Transitional Rocky Saprolite: Philippines

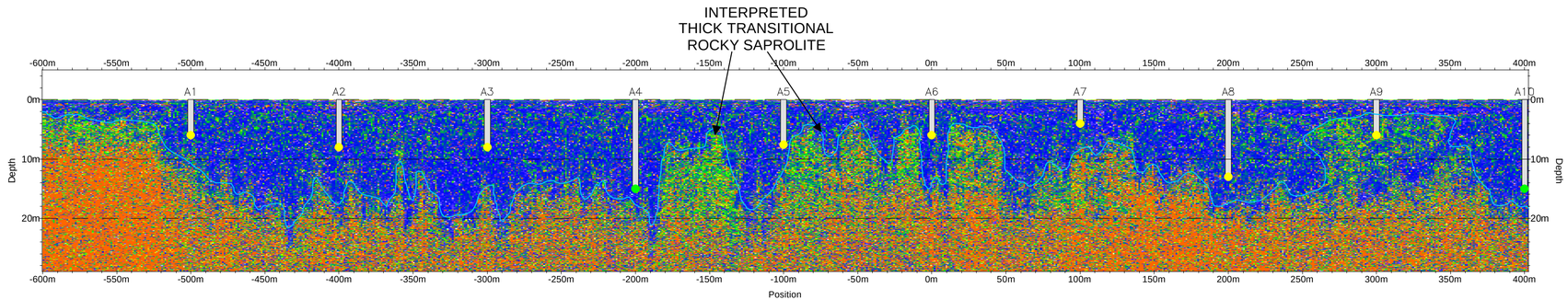

Test Pit Legend

- Testpit Terminated in Laterite
- Testpit Terminated in Saprolite

Radar Colour Instantaneous Frequency Scale

- Probable Weathered Laterite / Saprolite Region
- Probable Unaltered Bedrock or Corestones

Interpretation Legend

- Interpreted Unaltered Bedrock Contact

Scale 1:2000
4X Vertical Exaggeration
0 40 80 120 160 200 240

From:
The Application of Geophysics in Nickel Laterite Resource Evaluation
by Jan Francke
MSc. Thesis - University of Canterbury
New Zealand - 2000

Chapter 5 - Plate 12
Bedrock Mapping Showing Zones of Thick Transitional Rocky Saprolite Celestial (Philippines)

Instantaneous Frequency GPR Data and Interpretation 50 MHz Antennas

Plate 5.13 – Chalcedony Mapping with True Relative Amplitude Display: Brazil

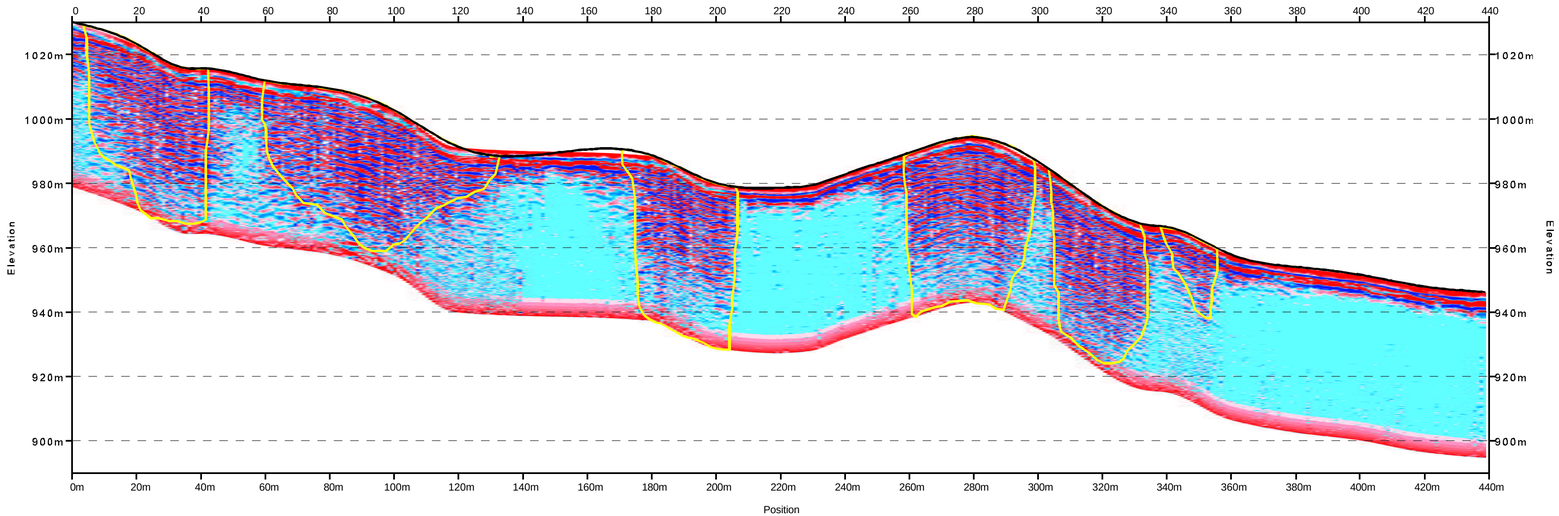

Interpretation Legend

Probable Region of Chalcedony

Radar Colour Normalized Amplitude Scale

Relative High Amplitude Radar Reflection After TRA

Relative Low Amplitude Radar Reflection After TRA

Scale1:1000
No Vertical Exaggeration

0 50 100 150 200

From:
The Application of Geophysics in Nickel Laterite Resource Evaluation
by Jan Francke
MSc. Thesis - University of Canterbury
New Zealand - 2000

Chapter 5 - Plate 13
Chalcedony Mapping
Brazil

True Relative Amplitude Display of Processed GPR Data Showing Interpreted Occurrence of Chalcedony

Plate 5.14 – Chalcedony Mapping with True Relative Amplitude (No Topography): Brazil

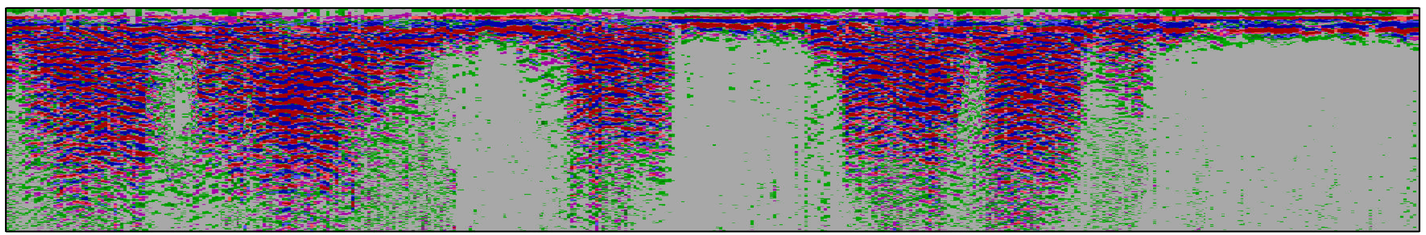

Radar Colour Normalized Amplitude Scale

Relative High Amplitude Radar Reflection

Relative Low Amplitude Radar Reflection

Horizontal Scale 1:1000

0 50 100 150 200

From:
The Application of Geophysics in Nickel Laterite Resource Evaluation
by Jan Francke
MSc. Thesis - University of Canterbury
New Zealand - 2000

Chapter 5 - Plate 14
Chalcedony Mapping
Brazil

Processed GPR Data with No Topogrphic Correction Showing Occurance of Chalcedony

Plate 5.15 – Bedrock Mapping with Instantaneous Frequency Display: Brazil

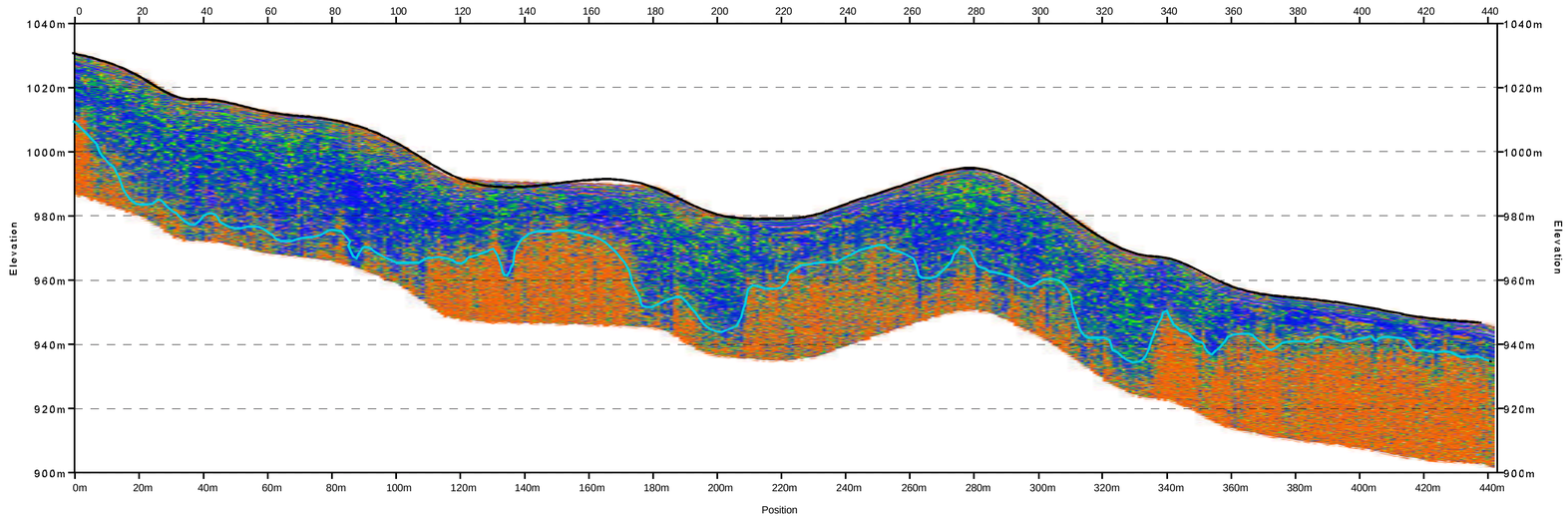

Interpretation Legend

Interpreted Depth of Unweathered Bedrock

Radar Colour Instantaneous Frequency Scale

Probable Weathered Laterite / Saprolite Region

Probable Unaltered Bedrock or Corestones

Scale 1:1000
No Vertical Exaggeration

0 50 100 150 200

From:
The Application of Geophysics in Nickel Laterite Resource Evaluation
by Jan Francke
MSc. Thesis - University of Canterbury
New Zealand - 2000

Chapter 5 - Plate 15
Bedrock Mapping
Brazil

Instantaneous Frequency Display of Processed GPR Data Showing Interpreted Depth of Weathering

Plate 5.16 – Combined Interpretation of Chalcedony Mapping: Brazil

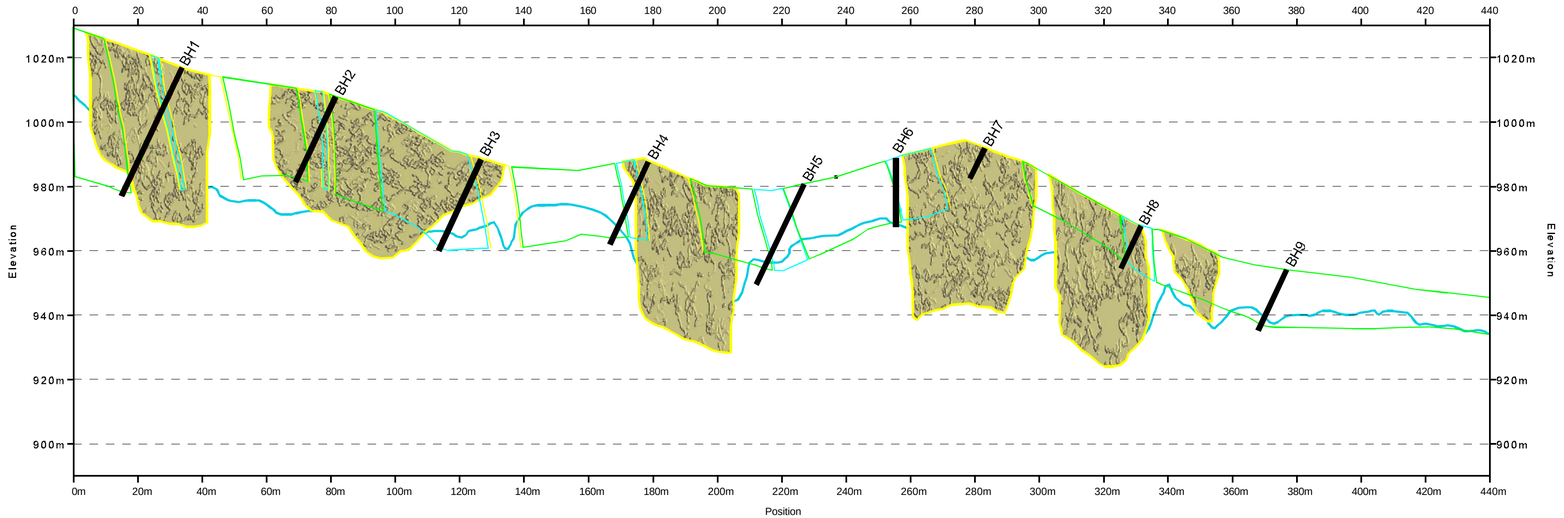

Interpolation Legend

- Laterite
- Silicified Dunite
- Serpentinized Dunite
- Chalcedony

Interpretation Legend

- Probable Region of Chalcedony
- Interpreted Depth of Unweathered Bedrock

Scale 1:1000
No Vertical Exaggeration

0 50 100 150 200

From:
The Application of Geophysics in Nickel Laterite Resource Evaluation
by Jan Francke
MSc. Thesis - University of Canterbury
New Zealand - 2000

Chapter 5 - Plate 16
Bedrock and Chalcedony Mapping
Brazil

Interpretation of GPR Data with Interpolated Borehole Information

Plate 6.1 – Test Mine

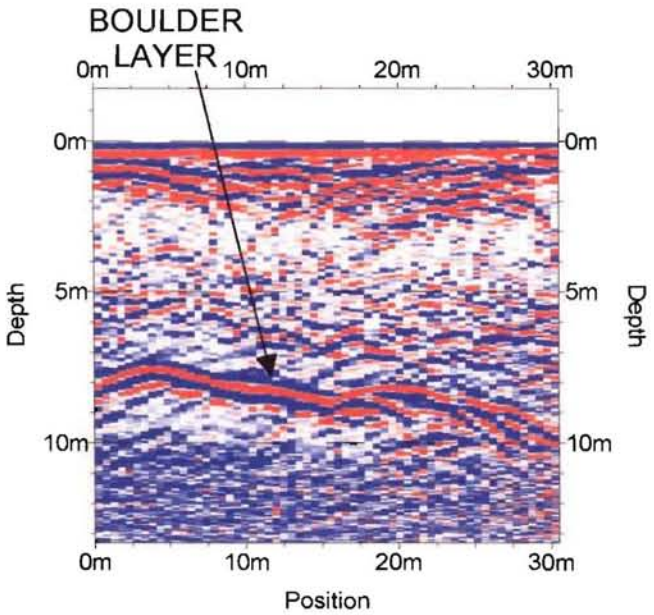

Radar Colour Amplitude Scale

Locally High Positive Radar Reflection Amplitude

Locally High Negative Radar Reflection Amplitude

From:
The Application of Geophysics in Nickel Laterite Resource Evaluation
by Jan Francke
MSc. Thesis - University of Canterbury
New Zealand - 2000

Scale 1:500
4X Vertical Exaggeration

0 10 20 30 40

Chapter 6 - Plate 1
Test Mine
Goro (New Caledonia)

Real Amplitude GPR Data and Interpretation
50 MHz Antennas
150 ns AGC Window

Plate 6.2 – Line 1

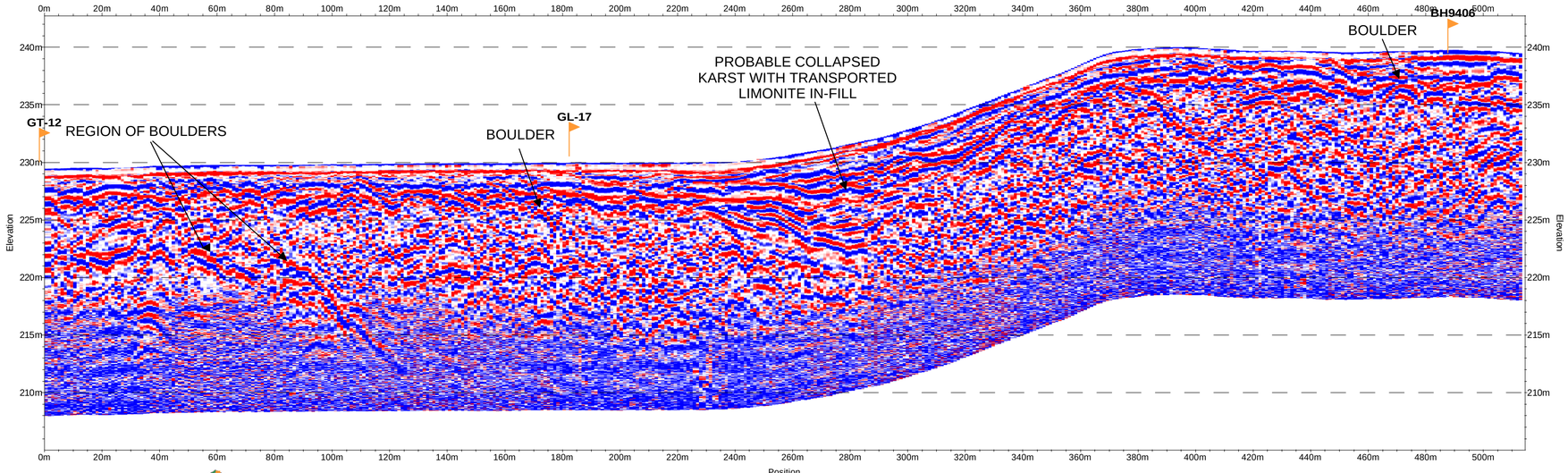

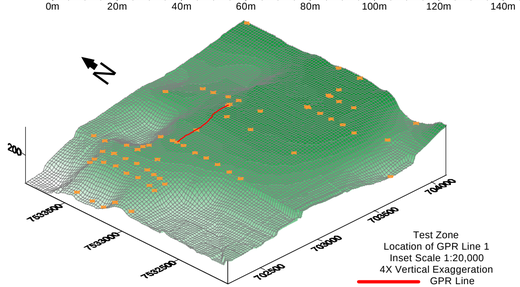

Test Zone
Location of GPR Line 1
Inset Scale 1:20,000
4X Vertical Exaggeration
GPR Line
Borehole Location

Radar Colour Amplitude Scale

Locally High Positive Radar Reflection Amplitude

Locally High Negative Radar Reflection Amplitude

Scale 1:1000
4X Vertical Exaggeration
0 20 40 60 80 100 120

From:
The Application of Geophysics in Nickel Laterite Resource Evaluation
by Jan Francke
MSc. Thesis - University of Canterbury
New Zealand - 2000

Chapter 6 - Plate 2
Line 1
Goro (New Caledonia)

Real Amplitude GPR Data and Interpretation
25 MHz Antennas
150 ns AGC Window

Plate 6.3 – Line 2

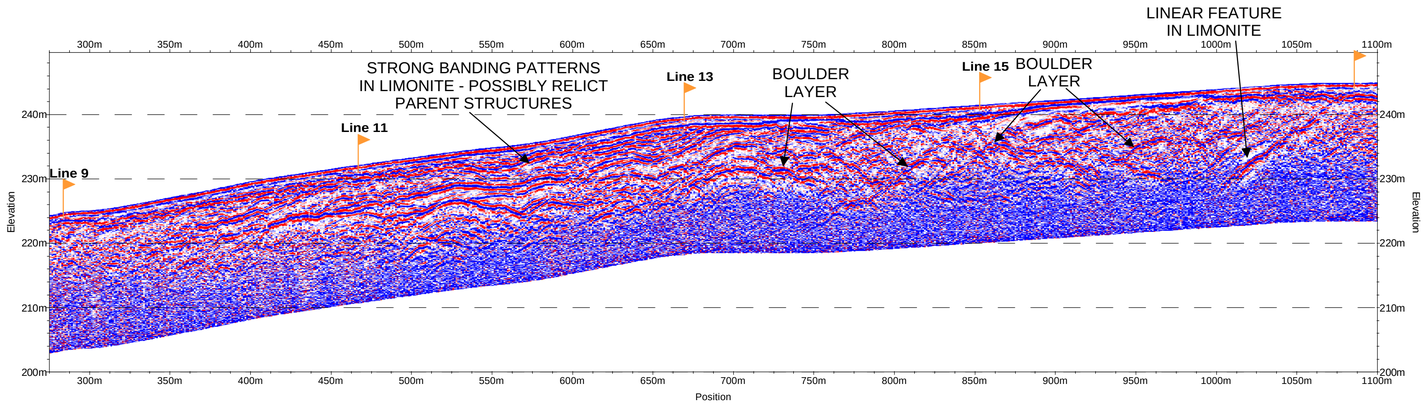

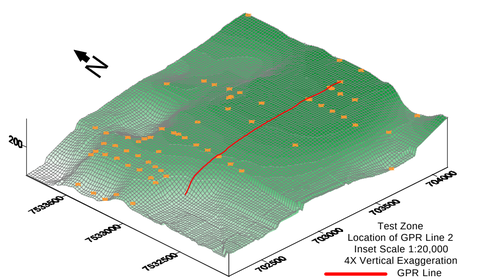

Radar Colour Amplitude Scale

Locally High Positive Radar Reflection Amplitude

Locally High Negative Radar Reflection Amplitude

Scale 1:2000
4X Vertical Exaggeration

0 40 80 120 160 200 240

From:
The Application of Geophysics in Nickel Laterite Resource Evaluation
by Jan Francke
MSc. Thesis - University of Canterbury
New Zealand - 2000

Chapter 6 - Plate 3
Line 2
Goro (New Caledonia)

Real Amplitude GPR Data and Interpretation
25 MHz Antennas
150 ns AGC Window

Plate 6.4 – Line 5

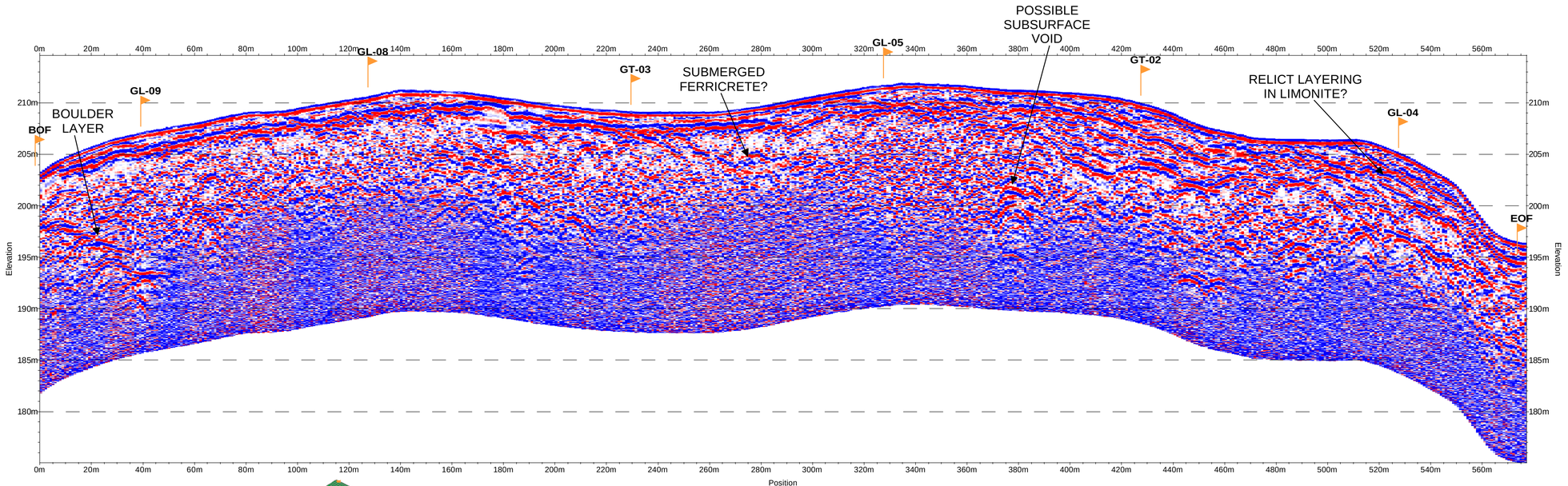

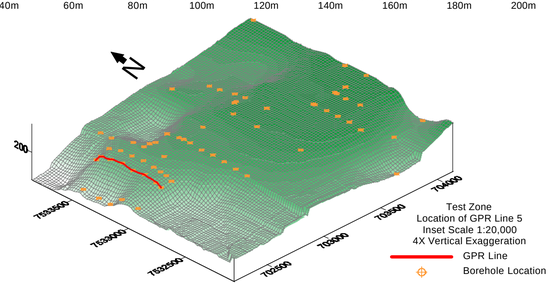

Radar Colour Amplitude Scale

Locally High Positive Radar Reflection Amplitude

Locally High Negative Radar Reflection Amplitude

Scale 1:1000
4X Vertical Exaggeration

0 20 40 60 80 100 120

From:
The Application of Geophysics in Nickel Laterite Resource Evaluation
by Jan Francke
MSc. Thesis - University of Canterbury
New Zealand - 2000

Chapter 6 - Plate 4
Line 5
Goro (New Caledonia)

Real Amplitude GPR Data and Interpretation
25 MHz Antennas
150 ns AGC Window

Plate 6.5 – Line 6

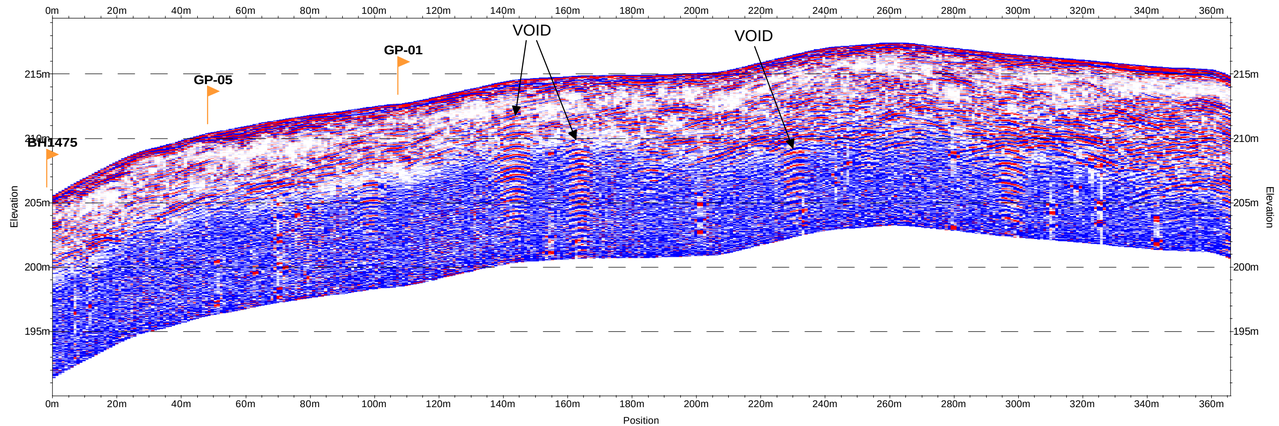

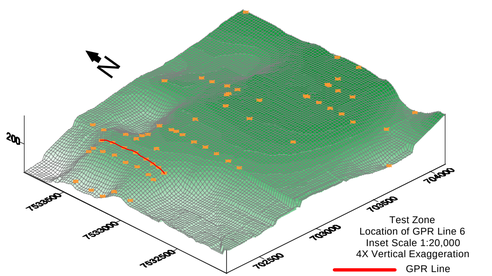

Radar Colour Amplitude Scale

Locally High Positive Radar Reflection Amplitude

Locally High Negative Radar Reflection Amplitude

From:
The Application of Geophysics in Nickel Laterite Resource Evaluation
by Jan Francke
MSc. Thesis - University of Canterbury
New Zealand - 2000

Scale 1:1000
4X Vertical Exaggeration

0 20 40 60 80 100 120

Chapter 6 - Plate 5
Line 6
Goro (New Caledonia)

Real Amplitude GPR Data and Interpretation
200 MHz Antennas
150 ns AGC Window

Plate 6.6 – Line 9

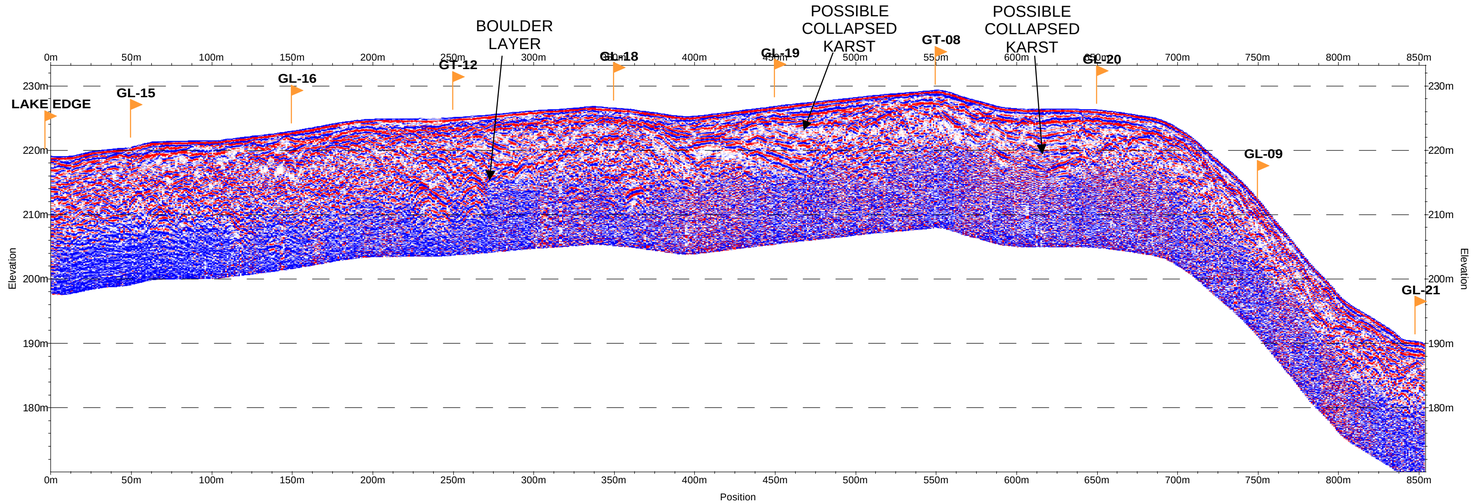

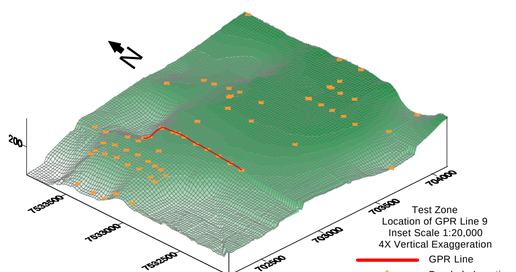

Test Zone
Location of GPR Line 9
Inset Scale 1:20,000
4X Vertical Exaggeration

GPR Line

Borehole Location

Radar Colour Amplitude Scale

Locally High Positive Radar Reflection Amplitude

Locally High Negative Radar Reflection Amplitude

Scale 1:2000
4X Vertical Exaggeration

0 40 80 120 160 200 240

From:
The Application of Geophysics in Nickel Laterite Resource Evaluation
by Jan Francke
MSc. Thesis - University of Canterbury
New Zealand - 2000

Chapter 6 - Plate 6
Line 9
Goro (New Caledonia)

Real Amplitude GPR Data and Interpretation
25 MHz Antennas
150 ns AGC Window

Plate 6.7 – Line 13

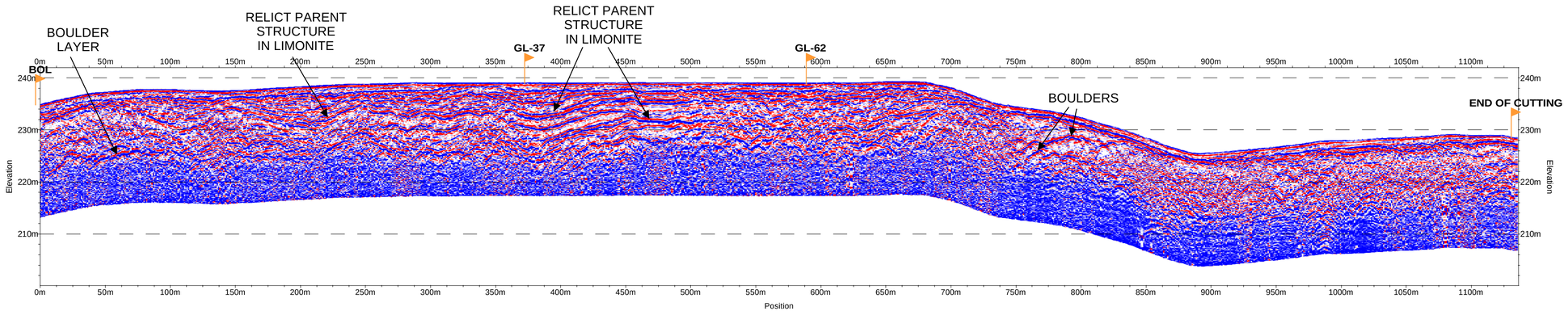

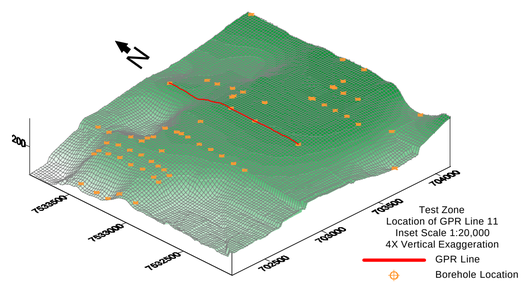

Radar Colour Amplitude Scale

Locally High Positive Radar Reflection Amplitude

Locally High Negative Radar Reflection Amplitude

Scale 1:2000
4X Vertical Exaggeration

0 40 80 120 160 200 240

From:
The Application of Geophysics in Nickel Laterite Resource Evaluation
by Jan Francke
MSc. Thesis - University of Canterbury
New Zealand - 2000

Chapter 6 - Plate 7
Line 13
Goro (New Caledonia)

Real Amplitude GPR Data and Interpretation
25 MHz Antennas
150 ns AGC Window

Plate 6.8 – Line 15

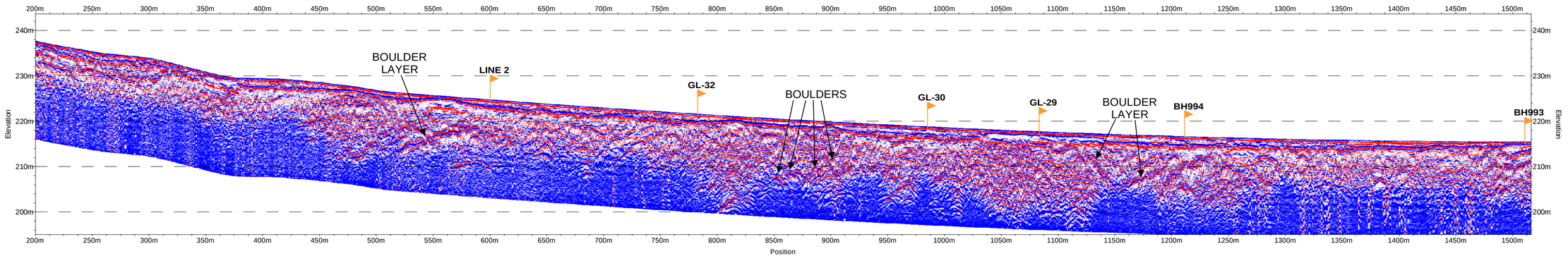

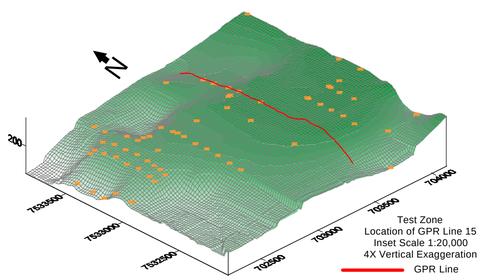

Radar Colour Amplitude Scale

Locally High Positive Radar Reflection Amplitude

Locally High Negative Radar Reflection Amplitude

Scale 1:2000
4X Vertical Exaggeration

0 40 80 120 160 200 240

From:
The Application of Geophysics in Nickel Laterite Resource Evaluation
by Jan Francke
MSc. Thesis - University of Canterbury
New Zealand - 2000

Chapter 6 - Plate 8
Line 15
Goro (New Caledonia)

Real Amplitude GPR Data and Interpretation
25 MHz Antennas
150 ns AGC Window

Plate 6.9 – Line 17 with 25 MHz Antennas

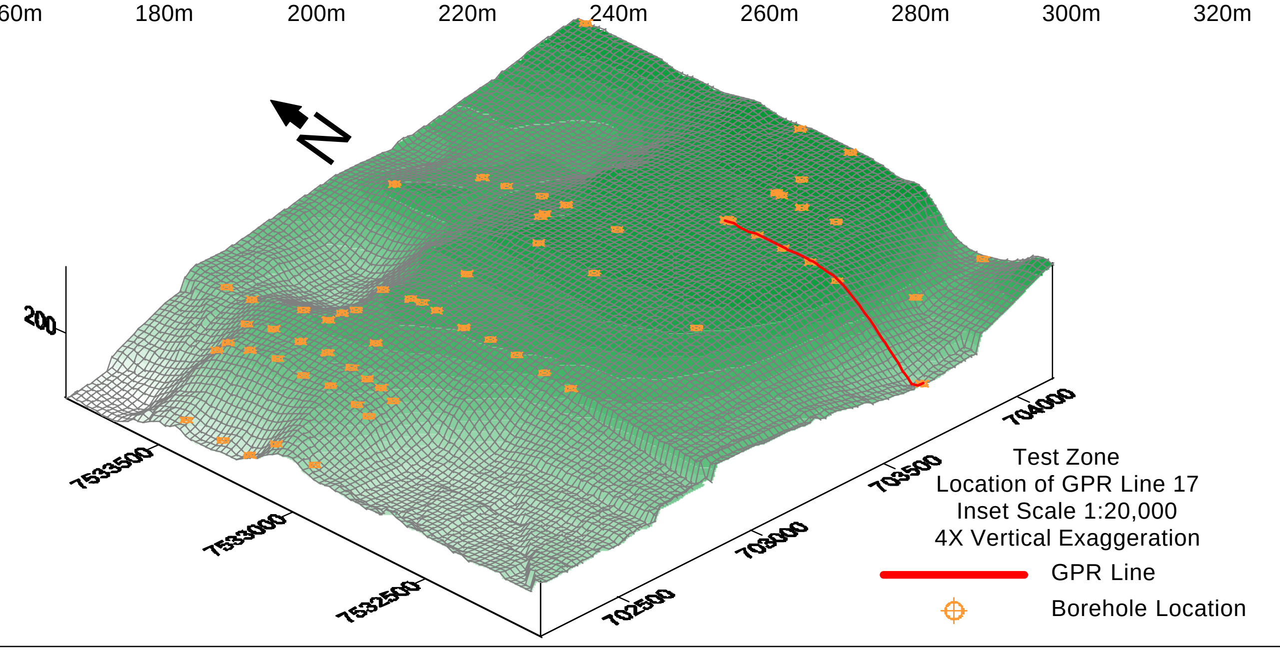

<u>Radar Colour Amplitude Scale</u>

Locally High Positive Radar Reflection Amplitude

Locally High Negative Radar Reflection Amplitude

Scale 1:2000
4X Vertical Exaggeration

0 20 40 60 80 100 120

From:
The Application of Geophysics in Nickel Laterite Resource Evaluation
by Jan Francke
MSc. Thesis - University of Canterbury
New Zealand - 2000

Chapter 6 - Plate 9
Line 17
Goro (New Caledonia)

Real Amplitude GPR Data and Interpretation
25 MHz Antennas
150 ns AGC Window

Plate 6.10 – Line 17 with 50 MHz Antennas (No Topography)

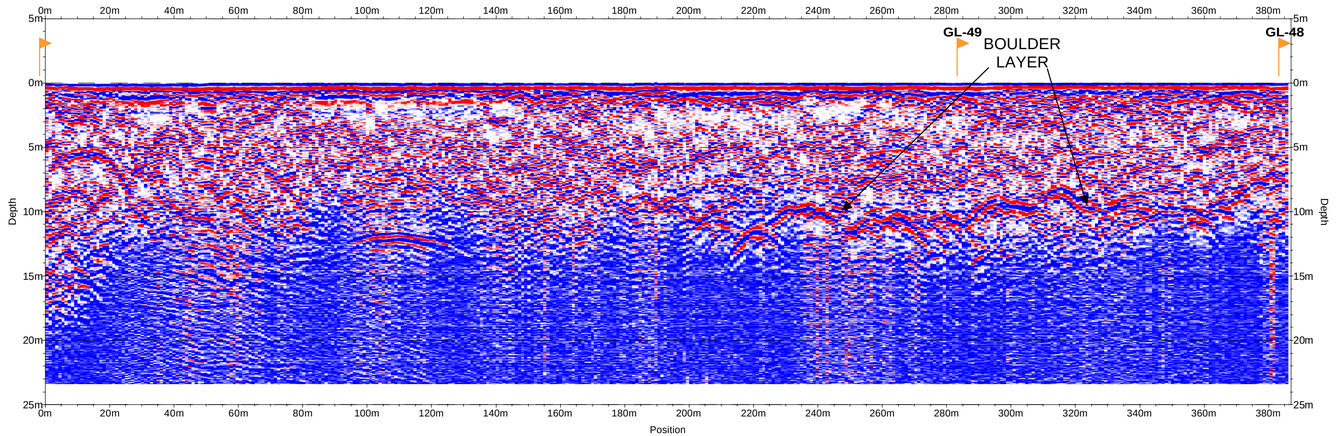

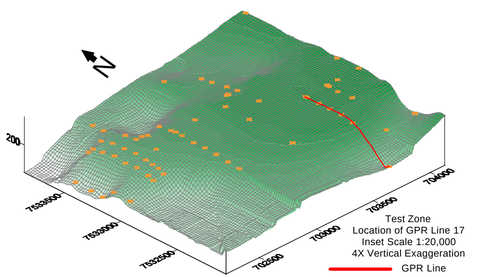

Radar Colour Amplitude Scale

Locally High Positive Radar Reflection Amplitude

Locally High Negative Radar Reflection Amplitude

Scale 1:1000
4X Vertical Exaggeration

0 20 40 60 80 100 120

From:
The Application of Geophysics in Nickel Laterite Resource Evaluation
by Jan Francke
MSc. Thesis - University of Canterbury
New Zealand - 2000

Chapter 6 - Plate 10
Line 17
Goro (New Caledonia)

Real Amplitude GPR Data and Interpretation
50 MHz Antennas
150 ns AGC Window with No Topographic Correction

Plate 6.11 – Line 17 with 50 MHz Antennas

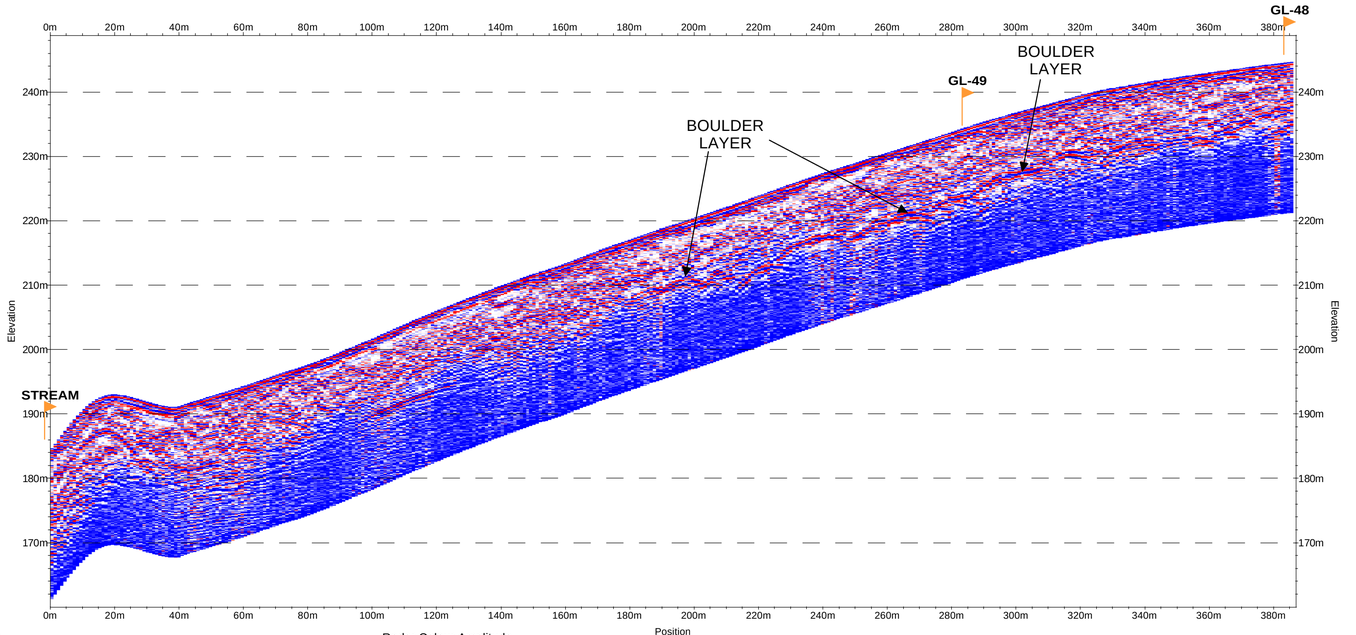

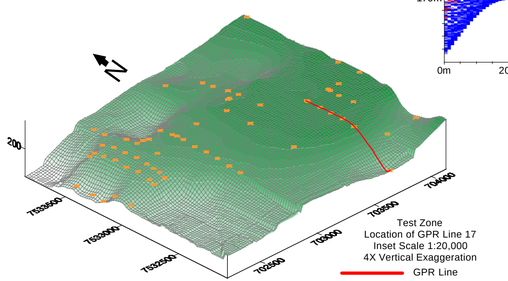

Test Zone
Location of GPR Line 17
Inset Scale 1:20,000
4X Vertical Exaggeration

GPR Line

Borehole Location

Radar Colour Amplitude Scale

Locally High Positive Radar Reflection Amplitude

Locally High Negative Radar Reflection Amplitude

Scale 1:2000
4X Vertical Exaggeration

0 20 40 60 80 100 120

From:
The Application of Geophysics in Nickel Laterite Resource Evaluation
by Jan Francke
MSc. Thesis - University of Canterbury
New Zealand - 2000

Chapter 6 - Plate 11
Line 17
Goro (New Caledonia)

Real Amplitude GPR Data and Interpretation
50 MHz Antennas
150 ns AGC Window

Plate 6.12 – Line 19

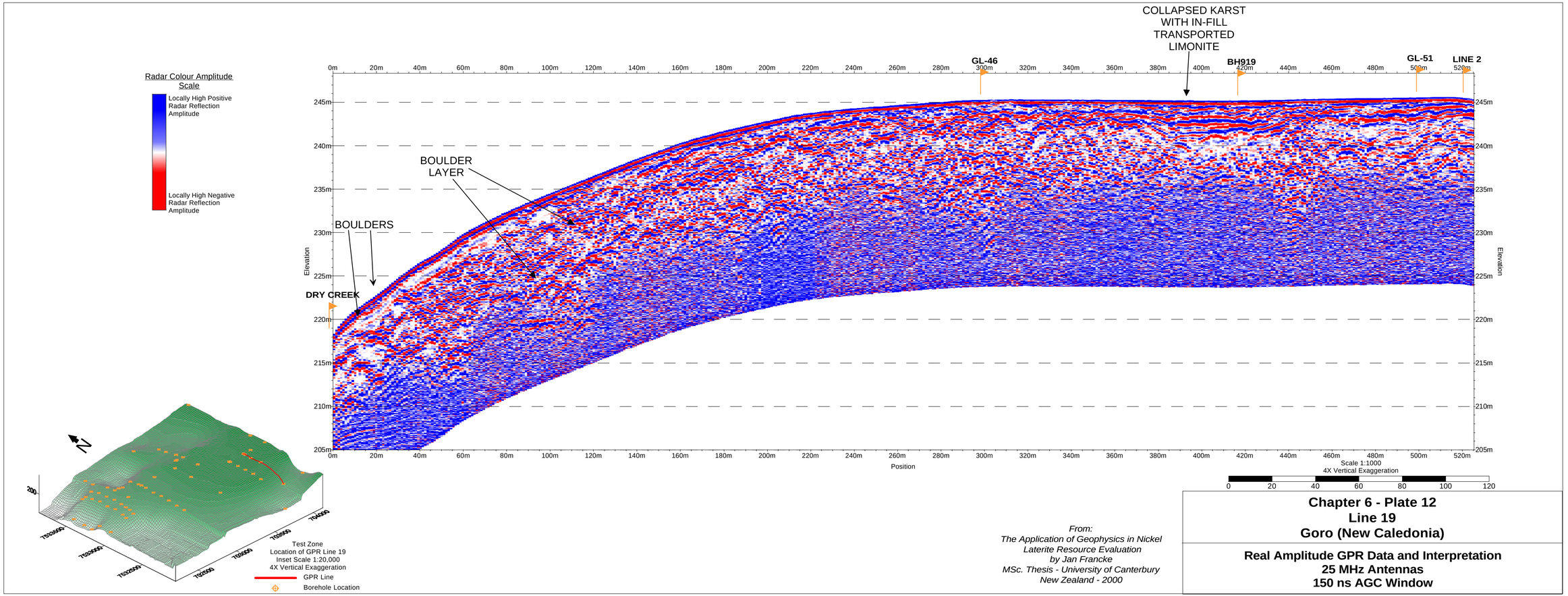

From:
The Application of Geophysics in Nickel Laterite Resource Evaluation
by Jan Francke
MSc. Thesis - University of Canterbury
New Zealand - 2000

Chapter 6 - Plate 12
Line 19
Goro (New Caledonia)

Real Amplitude GPR Data and Interpretation
25 MHz Antennas
150 ns AGC Window

Plate 6.13 – Vertical Radar Profiling Half-Tomograms

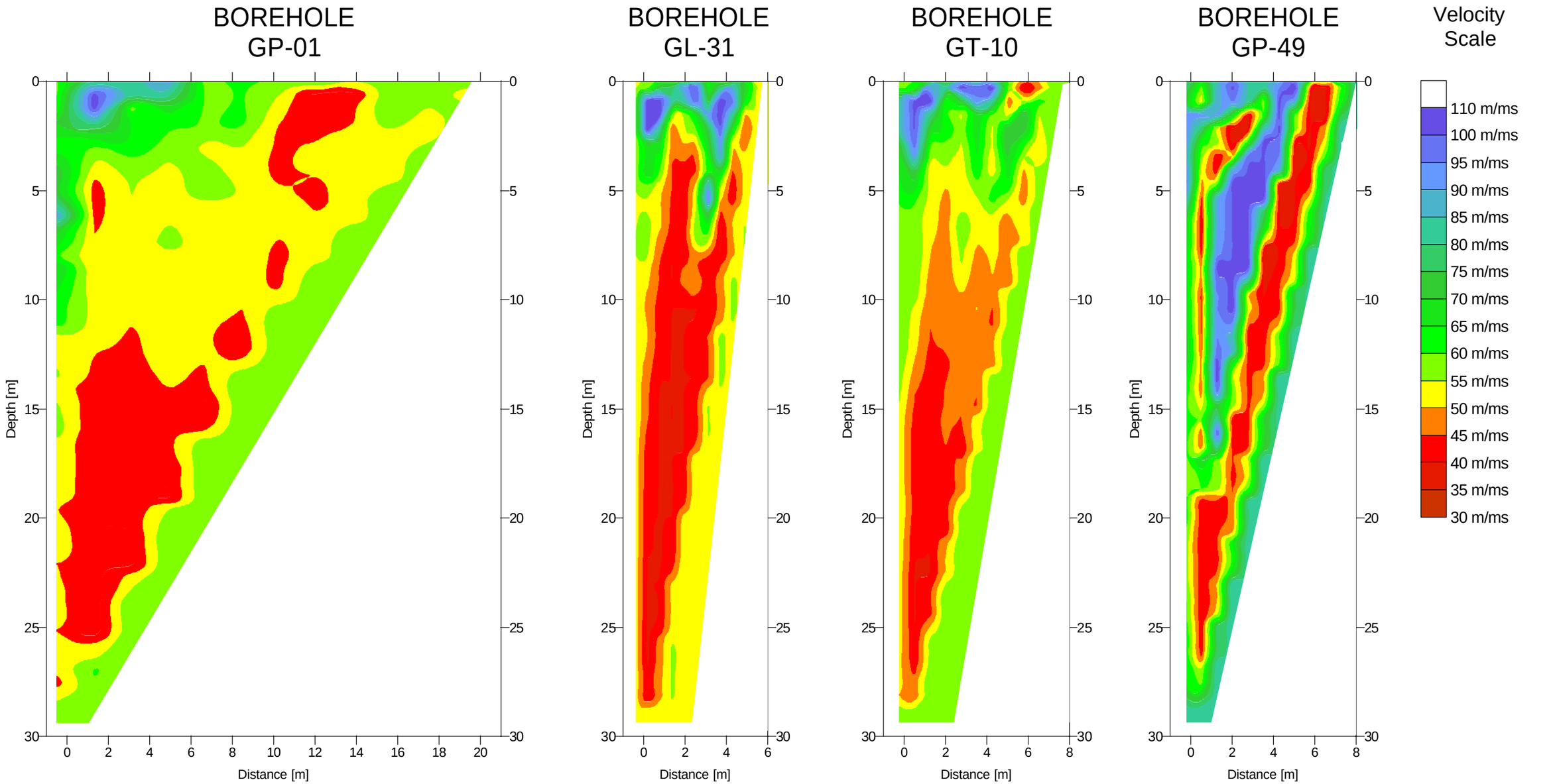

From:
The Application of Geophysics in Nickel Laterite Resource Evaluation
by Jan Francke
MSc. Thesis - University of Canterbury
New Zealand - 2000

Chapter 6 - Plate 13
Velocity Half-Tomograms from Vertical Radar Profiles
Goro (New Caledonia)

VPR Data
50 MHz Surface and Borehole Antennas

Plate 7.1 – Test Zone Line 7

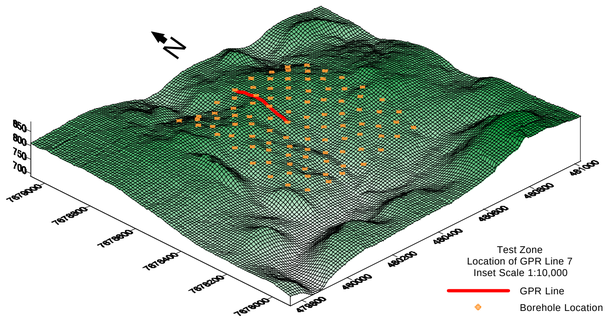

Test Zone
Location of GPR Line 7
Inset Scale 1:10,000

GPR Line

Borehole Location

INSTANTANEOUS FREQUENCY DATASET

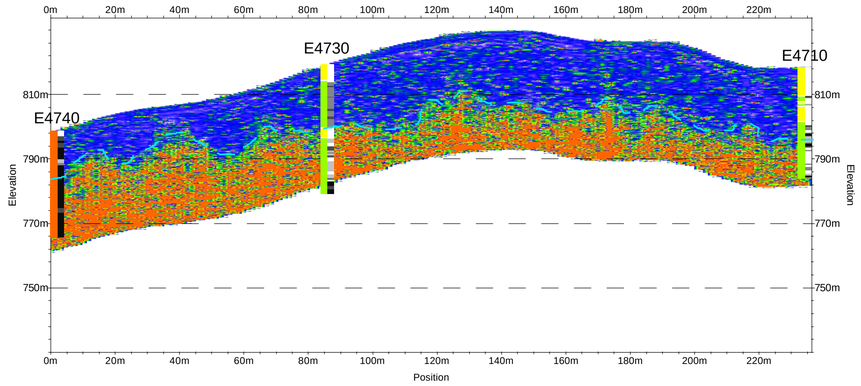

REAL AMPLITUDE DATASET

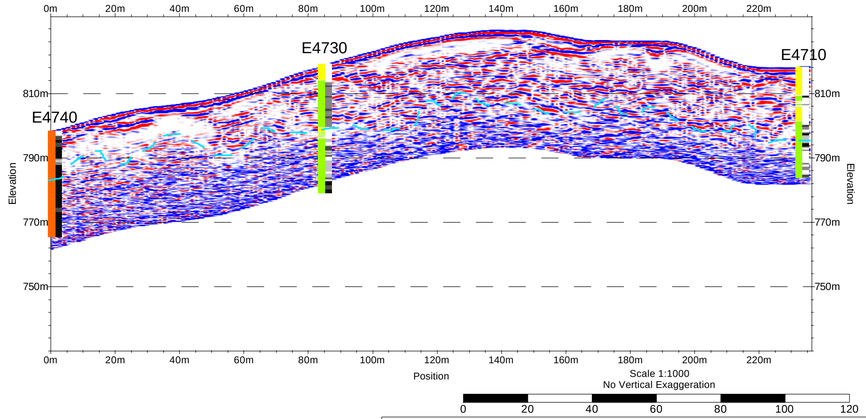

Scale 1:1000
No Vertical Exaggeration

0 20 40 60 80 100 120

Radar Colour Real Amplitude Scale

Local High Amplitude Radar Reflection

Local Low Amplitude Radar Reflection

Radar Colour Instantaneous Frequency Scale

Possible Weathered Laterite / Saprolite Region

Possible Unaltered Bedrock or Corestones

Borehole Legend (from Falconbridge drill logs)

Lithology	Degree of Weathering
Ferricrete	Weathered or Very Soft Weathering with Mineralogy Completely Replaced
Red Laterite	
Yellow Laterite	Deeply Weathered with Preserved Parent Textures
Limonite / Saprolite Transitional Material	
Saprolitic Facies Superior	Thick Weathering with "Onion Skin" Rinds
Saprolitic Facies Intermediate	
Saprolitic Facies Normal	Superficial Weathering Thin Rinds
Saprolitic Facies Basal	
Serpentinite	Unweathered Fresh Rock

Interpretation Legend

Best-Fit GPR Interpretation Based on Instantaneous Frequency to Map Base of Humid Zone

From:
The Application of Geophysics in Nickel Laterite Resource Evaluation
by Jan Francke
MSc. Thesis - University of Canterbury
New Zealand - 2000

Chapter 7 - Plate 1
Test Zone Line 7
Koniambo (New Caledonia)

Instantaneous Frequency and Real Amplitude GPR Data
25 MHz Antennas
225 ns AGC Window Real Amplitude Plot

Plate 7.2 – Test Zone Line 8

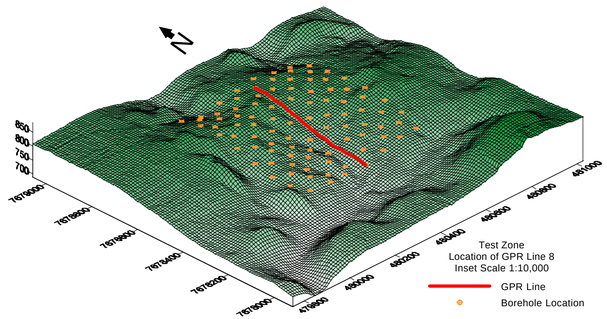

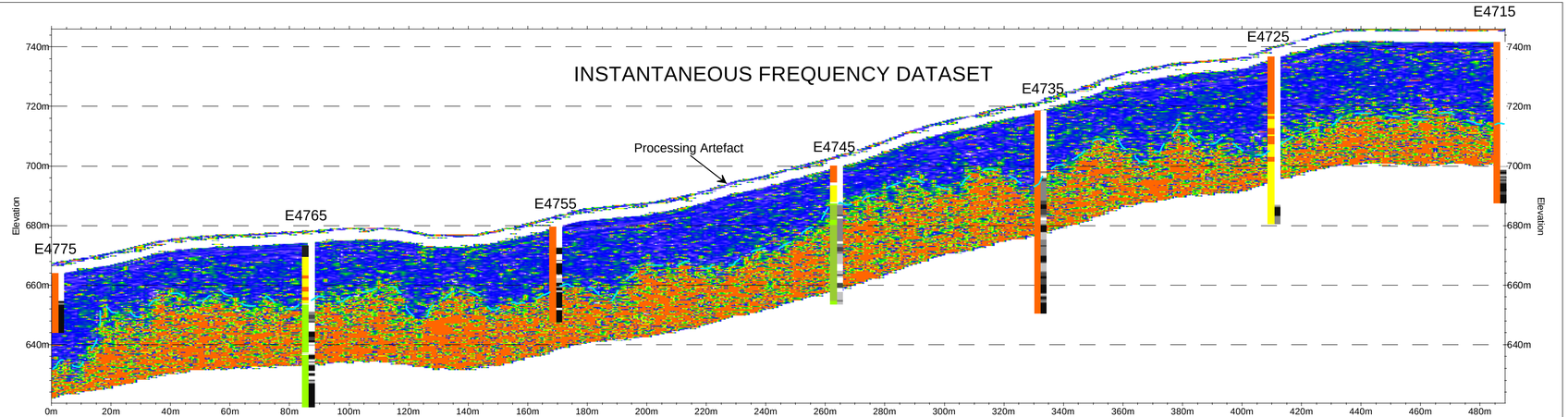

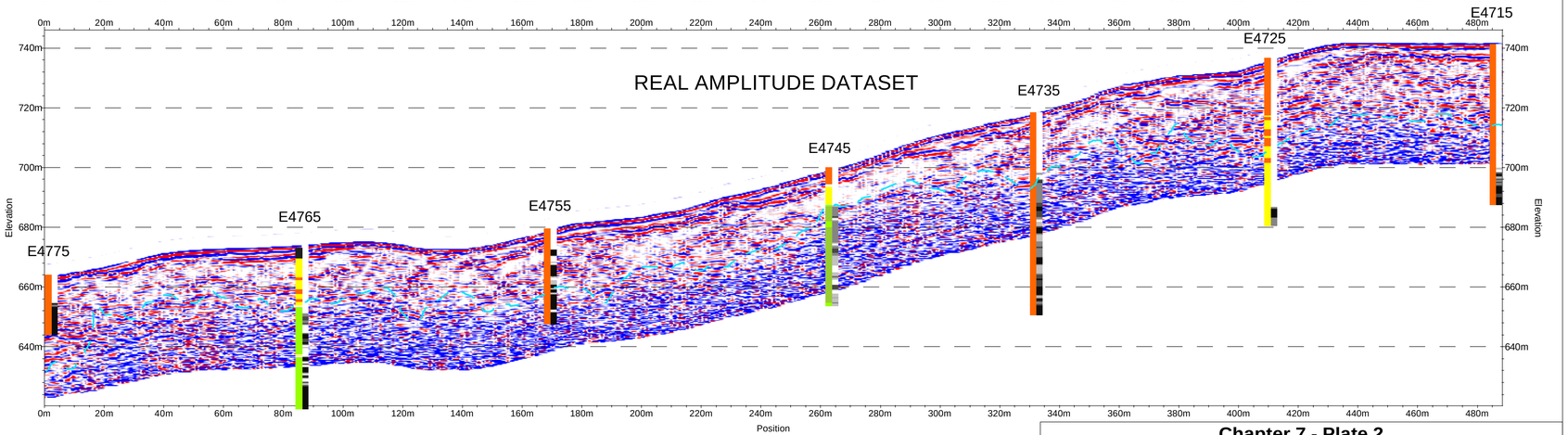

Radar Colour Real Amplitude Scale

- Local High Amplitude Radar Reflection
- Local Low Amplitude Radar Reflection

Radar Colour Instantaneous Frequency Scale

- Possible Weathered Laterite / Saprolite Region
- Possible Unaltered Bedrock or Corestones

Borehole Legend (from Falconbridge drill logs)

Lithology	Degree of Weathering
Ferricrete	Weathered or Very Soft Weathering with Mineralogy Completely Replaced
Red Laterite	Deeply Weathered with Preserved Parent Textures
Yellow Laterite	Thick Weathering with "Onion Skin" Rinds
Limonite / Saprolite Transitional Material	Superficial Weathering Thin Rinds
Saprolitic Facies Superior	Unweathered Fresh Rock
Saprolitic Facies Intermediate	
Saprolitic Facies Normal	
Saprolitic Facies Basal	
Serpentinite	

Interpretation Legend

- Best-Fit GPR Interpretation Based on Instantaneous Frequency to Map Base of Humid Zone

Scale 1:1000
No Vertical Exaggeration
0 20 40 60 80 100 120

From:
The Application of Geophysics in Nickel Laterite Resource Evaluation
by Jan Francke
MSc. Thesis - University of Canterbury
New Zealand - 2000

Chapter 7 - Plate 2
Test Zone Line 8
Koniambo (New Caledonia)

Instantaneous Frequency and Real Amplitude GPR Data
25 MHz Antennas
225 ns AGC Window Real Amplitude Plot

Plate 7.3 – Test Zone Line 9

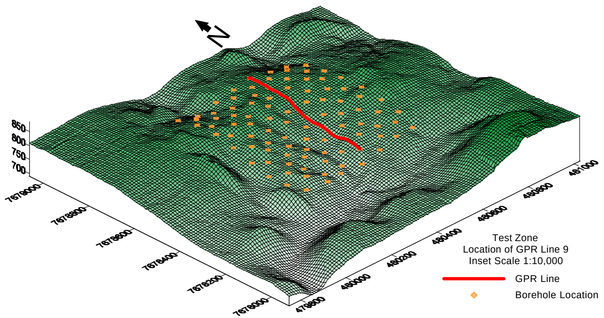

INSTANTANEOUS FREQUENCY DATASET

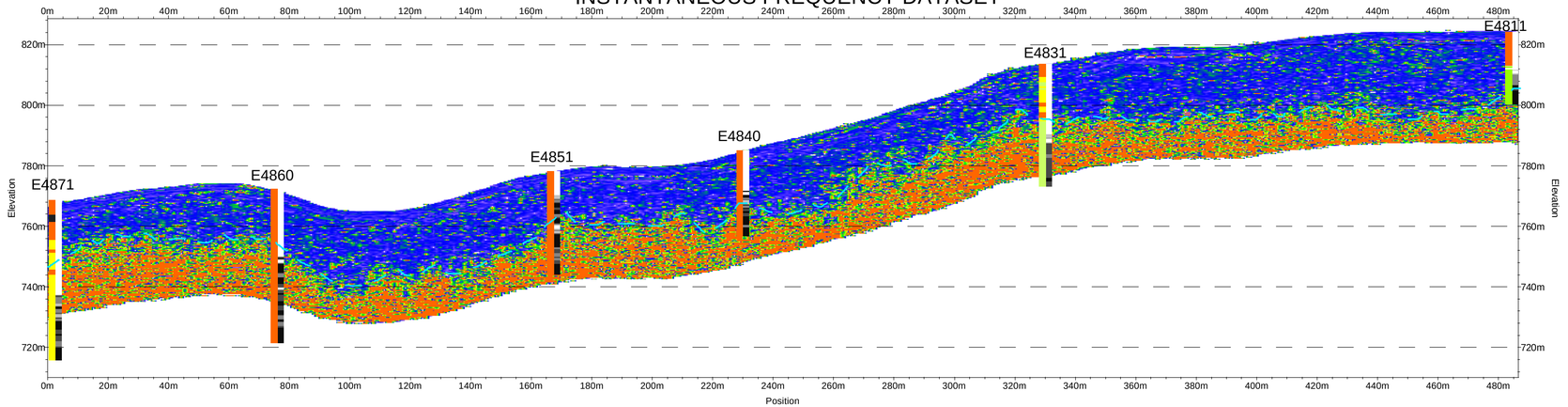

REAL AMPLITUDE DATASET

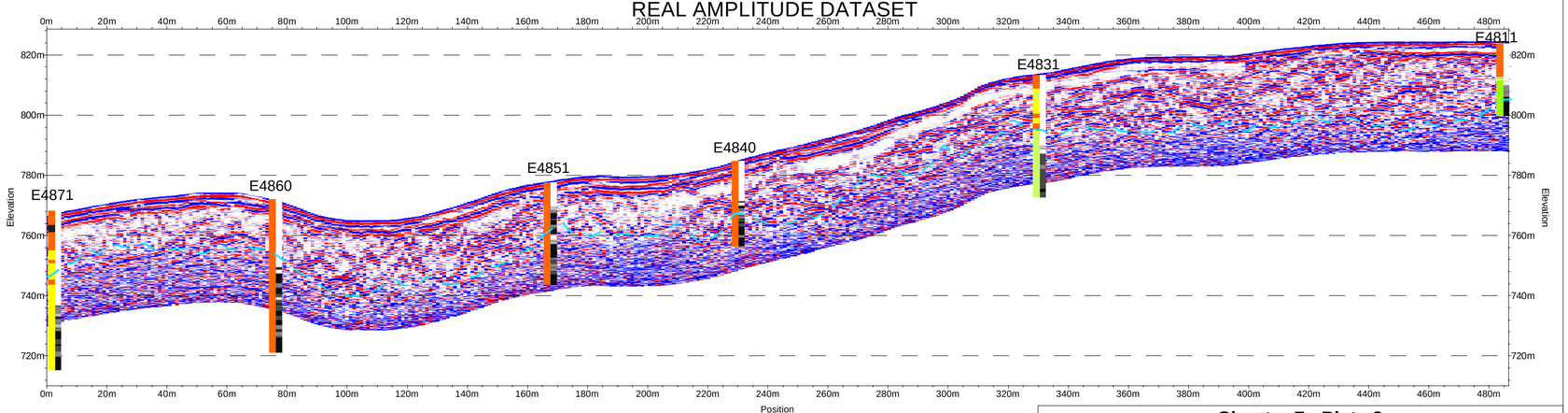

Radar Colour Real Amplitude Scale

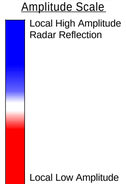

Radar Colour Instantaneous Frequency Scale

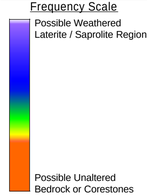

Borehole Legend (from Falconbridge drill logs)

Lithology	Degree of Weathering
Ferricrete	Weathered or Very Soft Weathering with Mineralogy Completely Replaced
Red Laterite	
Yellow Laterite	Deeply Weathered with Preserved Parent Textures
Limonite / Saprolite Transitional Material	
Saprolitic Facies Superior	Thick Weathering with "Onion Skin" Rinds
Saprolitic Facies Intermediate	
Saprolitic Facies Normal	Superficial Weathering Thin Rinds
Saprolitic Facies Basal	
Serpentinite	Unweathered Fresh Rock

Interpretation Legend

Best-Fit GPR Interpretation Based on Instantaneous Frequency to Map Base of Humid Zone

Scale 1:1000
No Vertical Exaggeration

0 20 40 60 80 100 120

From:
The Application of Geophysics in Nickel Laterite Resource Evaluation
by Jan Francke
MSc. Thesis - University of Canterbury
New Zealand - 2000

Chapter 7 - Plate 3
Test Zone Line 9
Koniambo (New Caledonia)

Instantaneous Frequency and Real Amplitude GPR Data
25 MHz Antennas
225 ns AGC Window Real Amplitude Plot

Plate 7.4 – Test Zone Transverse Line 1

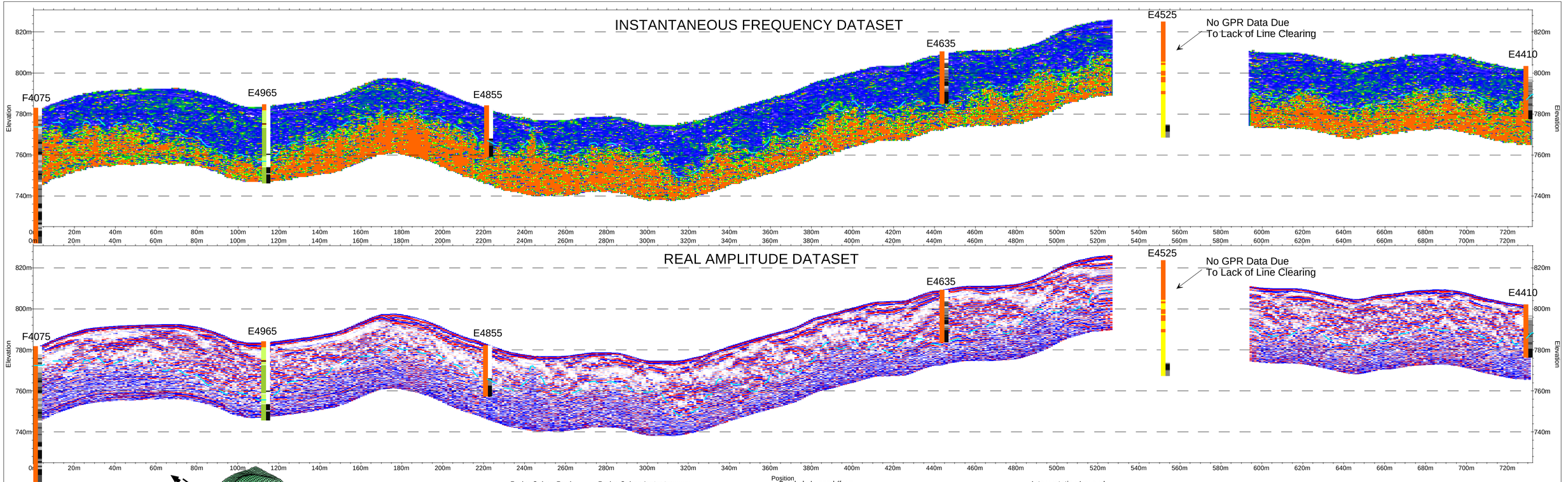

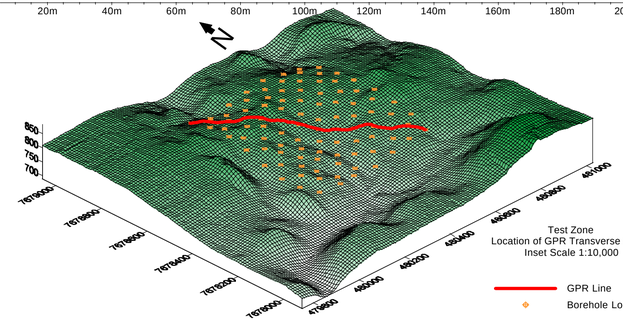

Radar Colour Real Amplitude Scale

- Local High Amplitude Radar Reflection
- Local Low Amplitude Radar Reflection

Radar Colour Instantaneous Frequency Scale

- Possible Weathered Laterite / Saprolite Region
- Possible Unaltered Bedrock or Corestones

Borehole Legend (from Falconbridge drill logs)

Lithology	Degree of Weathering
Ferricrete	Weathered or Very Soft Weathering with Mineralogy Completely Replaced
Red Laterite	Deeply Weathered with Preserved Parent Textures
Yellow Laterite	Thick Weathering with "Onion Skin" Rinds
Limonite / Saprolite Transitional Material	Superficial Weathering Thin Rinds
Saprolitic Facies Superior	Unweathered Fresh Rock
Saprolitic Facies Intermediate	
Saprolitic Facies Normal	
Saprolitic Facies Basal	
Serpentinite	

Interpretation Legend

- Best-Fit GPR Interpretation Based on Instantaneous Frequency to Map Base of Humid Zone

From:
The Application of Geophysics in Nickel Laterite Resource Evaluation
by Jan Francke
MSc. Thesis - University of Canterbury
New Zealand - 2000

Scale 1:1000
No Vertical Exaggeration
0 20 40 60 80 100 120

Chapter 7 - Plate 4
Test Zone Transverse Line 1
Koniambo (New Caledonia)

Instantaneous Frequency and Real Amplitude GPR Data
25 MHz Antennas
225 ns AGC Window Real Amplitude Plot

Plate 7.5 – Test Zone Variogram Cross Lines

VARIOGRAM CROSS LINE 1

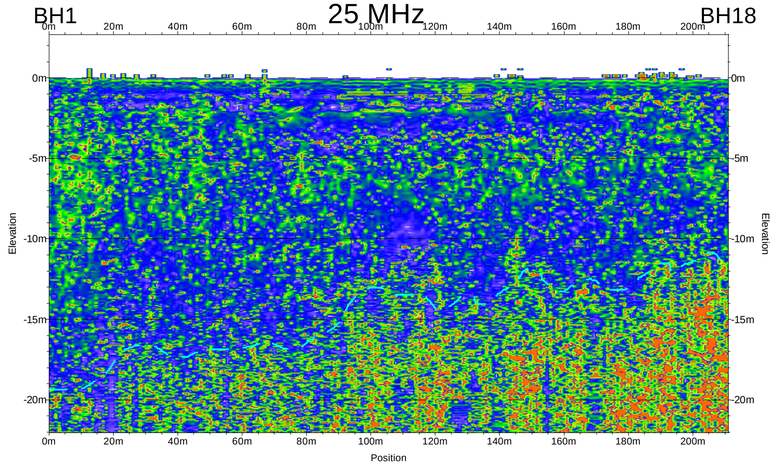

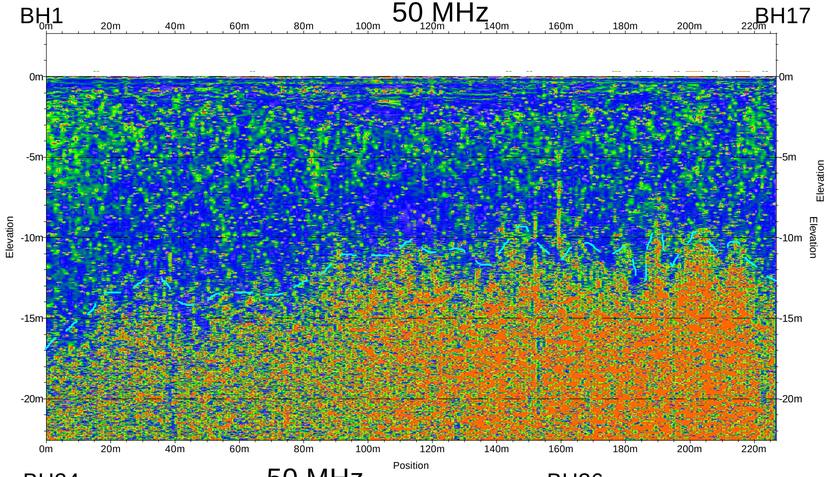

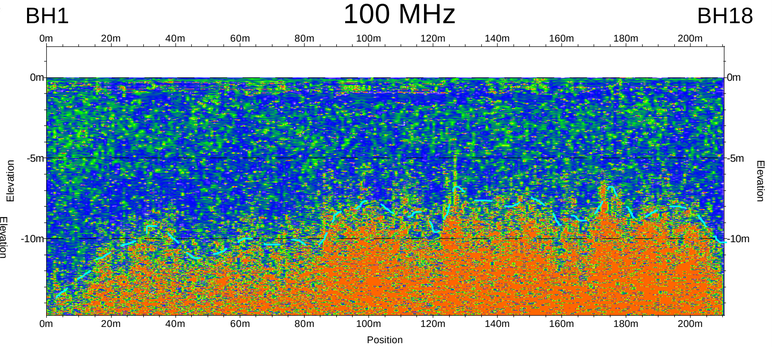

VARIOGRAM CROSS LINE 2

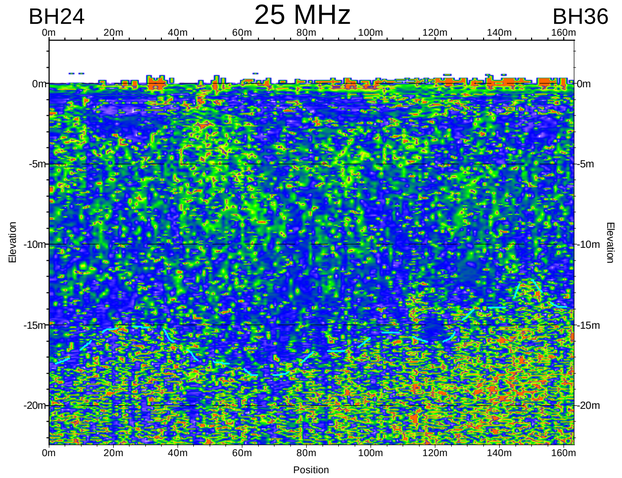

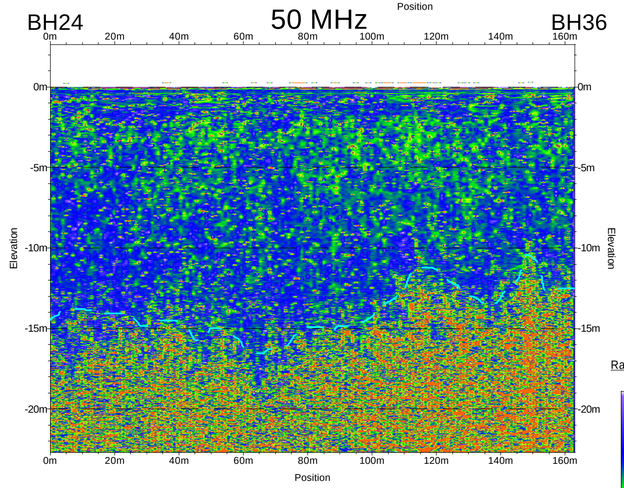

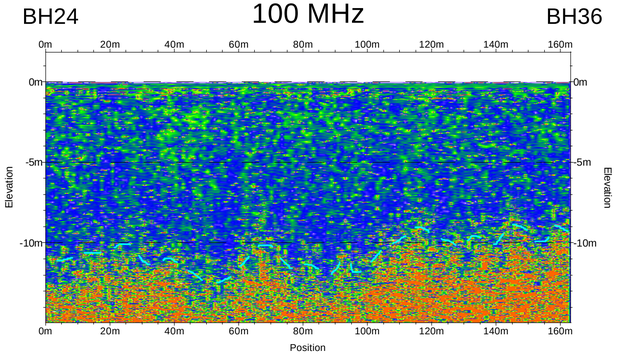

Radar Colour Instantaneous Frequency Scale

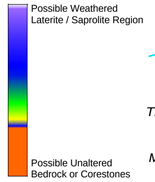

Interpretation Legend

Best-Fit GPR Interpretation Based on Instantaneous Frequency to Map Base of Humid Zone

From:
The Application of Geophysics in Nickel Laterite Resource Evaluation
by Jan Francke
MSc. Thesis - University of Canterbury
New Zealand - 2000

Scale 1:1000
5X Vertical Exaggeration

0 20 40 60 80 100 120

Chapter 7 - Plate 5
Test Zone Variogram Cross Lines
Koniambo (New Caledonia)

Instantaneous Frequency GPR Data and Interpreations
25 MHz, 50 MHz, and 100 MHz Antennas

Plate 7.6 – Trazy Line 1

INSTANTANEOUS FREQUENCY DATASET

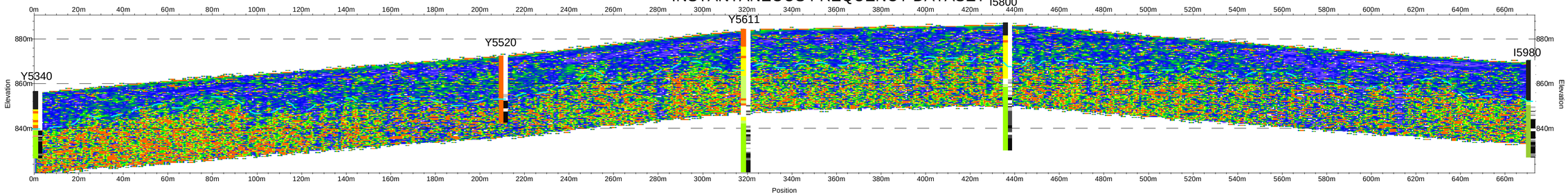

REAL AMPLITUDE DATASET

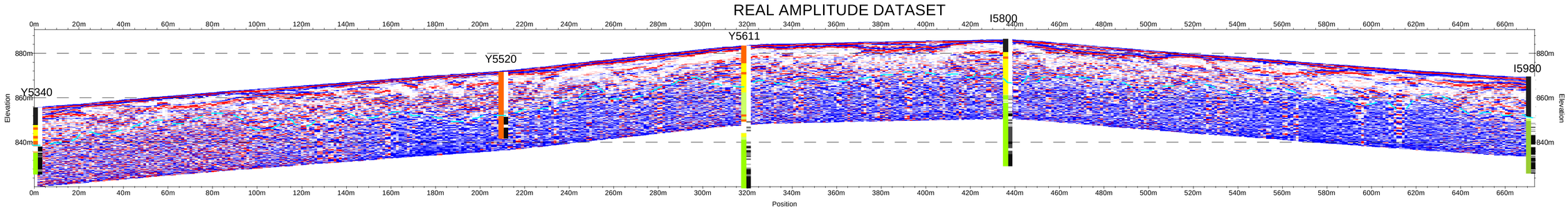

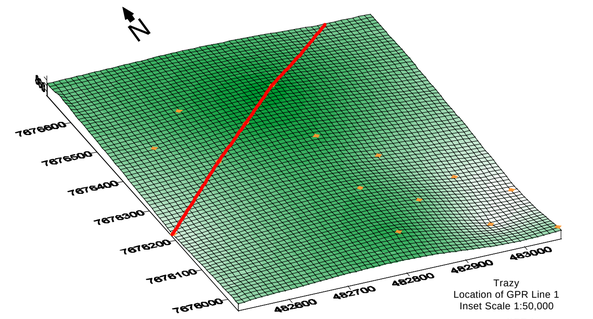

Radar Colour Real Amplitude Scale

- Local High Amplitude Radar Reflection
- Local Low Amplitude Radar Reflection

Radar Colour Instantaneous Frequency Scale

- Possible Weathered Laterite / Saprolite Region
- Possible Unaltered Bedrock or Corestones

Borehole Legend (from Falconbridge drill logs)

Lithology	Degree of Weathering
Ferricrete	Weathered or Very Soft Weathering with Mineralogy Completely Replaced
Red Laterite	Deeply Weathered with Preserved Parent Textures
Yellow Laterite	Thick Weathering with "Onion Skin" Rinds
Limonite / Saprolite Transitional Material	Superficial Weathering Thin Rinds
Saprolitic Facies Superior	Unweathered Fresh Rock
Saprolitic Facies Intermediate	
Saprolitic Facies Normal	
Saprolitic Facies Basal	
Serpentinite	

Interpretation Legend

- Best-Fit GPR Interpretation Based on Instantaneous Frequency to Map Base of Humid Zone

From:
The Application of Geophysics in Nickel Laterite Resource Evaluation
by Jan Francke
MSc. Thesis - University of Canterbury
New Zealand - 2000

Scale 1:1000
No Vertical Exaggeration
0 20 40 60 80 100 120

Chapter 7 - Plate 6
Trazy Line 1
Koniambo (New Caledonia)

Instantaneous Frequency and Real Amplitude GPR Data
25 MHz Antennas
225 ns AGC Window Real Amplitude Plot

Plate 7.7 – Trazy Line 3

INSTANTANEOUS FREQUENCY DATASET

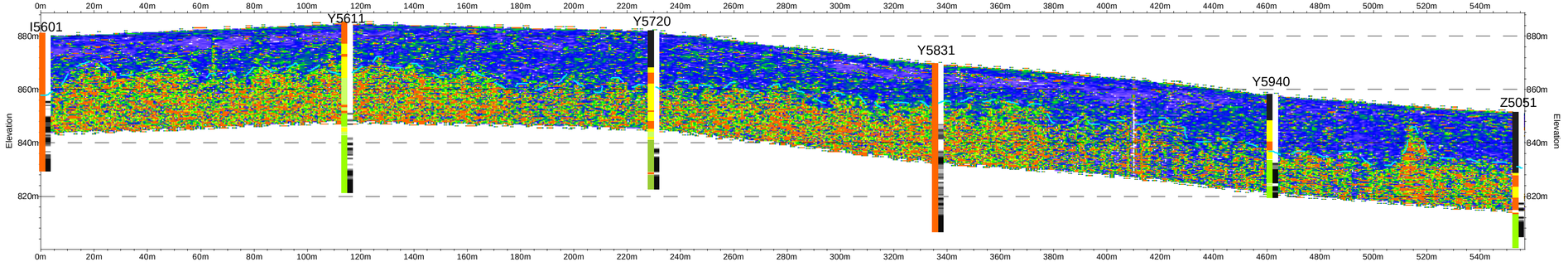

REAL AMPLITUDE DATASET

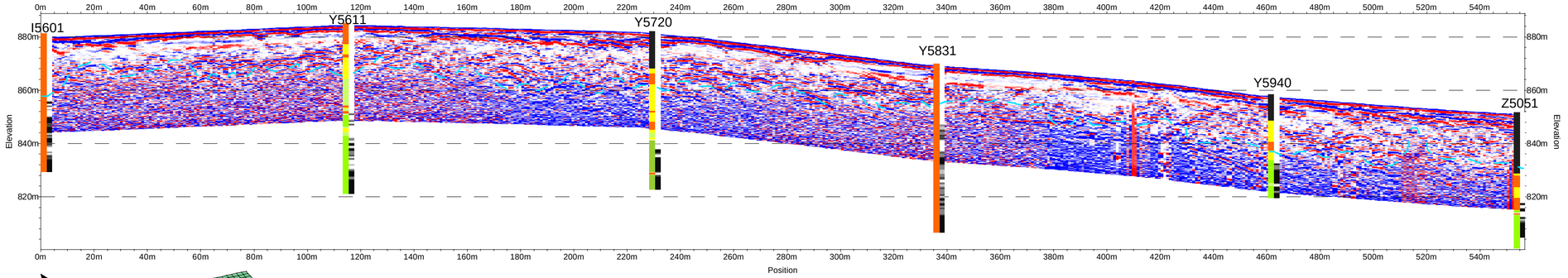

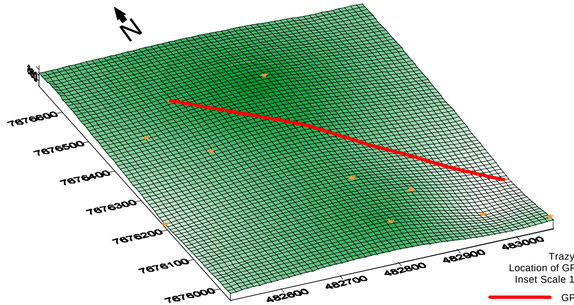

Trazy
Location of GPR Line 3
Inset Scale 1:50,000

GPR Line

Borehole Location

Radar Colour Real Amplitude Scale

Local High Amplitude Radar Reflection

Local Low Amplitude Radar Reflection

Radar Colour Instantaneous Frequency Scale

Possible Weathered Laterite / Saprolite Region

Possible Unaltered Bedrock or Corestones

Borehole Legend (from Falconbridge drill logs)

Lithology	Degree of Weathering
Ferricrete	Weathered or Very Soft Weathering with Mineralogy Completely Replaced
Red Laterite	
Yellow Laterite	Deeply Weathered with Preserved Parent Textures
Limonite / Saprolite Transitional Material	
Saprolitic Facies Superior	Thick Weathering with "Onion Skin" Rinds
Saprolitic Facies Intermediate	
Saprolitic Facies Normal	Superficial Weathering Thin Rinds
Saprolitic Facies Basal	
Serpentinite	Unweathered Fresh Rock

Interpretation Legend

Best-Fit GPR Interpretation Based on Instantaneous Frequency to Map Base of Humid Zone

Scale 1:1000
No Vertical Exaggeration

0 20 40 60 80 100 120

From:
The Application of Geophysics in Nickel Laterite Resource Evaluation
by Jan Francke
MSc. Thesis - University of Canterbury
New Zealand - 2000

Chapter 7 - Plate 7
Trazy Line 3
Koniambo (New Caledonia)

Instantaneous Frequency and Real Amplitude GPR Data
25 MHz Antennas
225 ns AGC Window Real Amplitde Plot